Desilicated ZSM-5 zeolite as catalyst for the dehydration of ethanol

Arlene Ramsaran

A Thesis

in

The Department

of

Chemistry and Biochemistry

Presented in Partial Fulfilment of the Requirements

for the Degree of Doctor of Philosophy at

Concordia University

Montreal, Quebec, Canada

April 1996

ISBN 0-612-10889-9

CONCORDIA UNIVERSITY

School of Graduate Studies

This is to certify that the thesis prepared

By : **Arlene Ramsaran**

Entitled: **Desilicated ZSM-5 zeolite as catalyst for the dehydration of ethanol**

and submitted in partial fulfilment of the requirements of the degree of

Doctor of Philosophy (Chemistry and Biochemistry)

complies with the regulations of this University and meets the accepted standards with respect to originality and quality.

Signed by the final examining committee:

_____ Chair

_____ External Examiner

_____ External to Progam

_____ Examiner

_____ Examiner

_____ Thesis Supervisor

Approved by _____
Chair of Department or Graduate Programme Director

_____ 19____ _____
Dean of Faculty

ABSTRACT

Desilicated ZSM-5 zeolite as catalyst for the dehydration of ethanol.

Arlene RAMSARAN, Ph.D.

Concordia University, 1996

The new desilicated forms of the zeolites X, Y and ZSM-5 were prepared by the selective removal of silicon atoms from the parent zeolites in an aqueous solution of base. This treatment, which decreases the Si/Al ratio while keeping the zeolite framework almost unmodified, enhanced the ion exchange capacities of all the zeolites, a property which can be exploited industrially for the X and Y zeolites since the desilicated forms had higher total ion removal rates of calcium and magnesium ions from hard water.

Similarly, desilication results in a higher density of acid sites as shown in the following. ^{1}H MAS NMR studies were done on anhydrous samples of desilicated ZSM-5 and have detected a signal which was not observed for the parent sample and is believed to arise from the interaction of Bronsted acid sites hydrogen bonded to framework Aluminum atoms. This corresponds to the creation of a second generation of Bronsted Acid Sites (BAS II) distinguishable from the normal bridging hydroxyl BAS (BAS I) associated with tetrahedrally coordinated aluminum in the zeolite framework.

In catalytic testing studies, the desilicated ZSM-5 zeolite was found to display a higher total conversion in the dehydration of absolute ethanol into ethylene, however the

selectivity for ethylene was higher for the parent zeolite at lower reaction temperatures. This was a direct consequence of the higher density of acid sites on the desilicated zeolite, which is comprised of BAS II in the presence of "unusual" Lewis acid sites of type II (LAS II). These Lewis acid sites were also detected by ^{1}H MAS NMR during the rehydration phase and are believed to be produced by dehydroxylation of BAS II which were generated by the " desilication-healing" phenomena. LAS II are distinguishable from LAS I since the latter are easily rehydrated back to the corresponding BAS I. The nature and strength of these different acidic sites on the parent and those created on the desilicated ZSM-5 were also studied in more detail by the techniques of XPS, FTIR, NH_3 TPD, nitrogen and argon adsorption and desorption (BET), DTA/TGA and poison testing using pyridine and 2,6-dimethylpyridine.

Upon steam treatment of the desilicated zeolite, both the total conversion and selectivity for ethylene improved significantly in the dehydration of absolute ethanol. Steaming was capable of rehydrating the LAS II into BAS II, a reconversion which was previously too demanding to be achieved under the conditions of catalytic testing, hence the low selectivity for ethylene at lower reaction temperatures. Further evidence of this reconversion is provided by catalytic testing with aqueous ethanol for which the desilicated zeolite achieved higher total conversions and selectivities for ethylene than the parent at all reaction temperatures, and the selectivity for ethylene was always significantly higher then was achieved with absolute ethanol. This has important implications for the Bioethanol to Ethylene Process.

A cut off temperature was also confirmed for the dehydration of ethanol, at which

the reaction mechanism changed from the two step conversion into diethyl ether and ethylene, into the one step, direct conversion to ethylene. These temperature ranges were determined to be 200-225°C and 225-250°C for absolute and aqueous ethanol respectively.

ACKNOWLEDGEMENTS

I would like to express my sincere gratitude to my thesis supervisor, Dr. R. Le Van Mao, for his guidance and directorship throughout the course of my research and in the preparation of this thesis. He has contributed to my intellectual knowledge enormously.

I would also like to thank the members of my Research Committee, Dr. S.R. Mikkelsen, Dr. R.H. Pallen and Dr. T.J. Adley, who have provided me with many helpful suggestions on my research during the time I spent at Concordia. Special thanks to Dr. Adley for the time and interest he took in reading through the preliminary version of my thesis, and to Dr. O. Tee, for his many helpful suggestions and assistance during my research.

I would like to thank the France-Quebec Cooperation Program for granting me the "stage" in Paris, France, and for financial support during this time. I am especially grateful to the Director, Professor Jacques Fraissard and the members of the Laboratoire de Chemie des Surfaces in Paris for "un temps inoubliable" in their Laboratory in Paris, France : for allowing me the opportunity to learn about and work in their area of research and especially for their assistance and the use of their equipment to analyze my samples.

I am deeply indebted to the technical staff at Concordia University : Ms. Miriam Posner, Mr. Khalil Rahaman, Mr. Franco Nudo, Mr. Christi, Chris, Mr. R. Pisarsky, Mr. R. Allix, Mr. R. Eichhorst, Mr. Kai Lee and Mr. Dimitri Kolokotronis, without whose help I would never have overcome the many breakdowns and repairs of technical

equipment and for their instruction on the use of instruments.

I take the opportunity to thank the Secretaries of the Chemistry Department, Ms. Carole Coutts, Kathy Usas and Donna Gordon, for their assistance always, especially in matters associated with student affairs. Also to all the other faculty members of the Chemistry Department who have always been a constant resource to me during my time at Concordia.

I am especially grateful to and have fond memories of the members of the Catalysis Research Lab : Dr. L. Huang, Dr. S. Xiao and Dr. A. Lavigne, for their helpful suggestions and assistance, and to Dr. J. Yao for her assistance and interest throughout my entire program which she was always so eager to give. To Mr. Bernard Sjariel, special thanks for the technical assistance you imparted, especially during the indoctrination stage of Catalysis Research. And to all the other graduate students at Concordia, who have been so helpful in diverse ways, thank you for your generosity.

Special thanks to Ms. S. Poulin at Ecole Polytechnique and Dr. L. Reven at McGill University for their assistance in performing and data analysis for XPS and ^{27}Al and ^{29}Si NMR experiments.

Finally to my brothers : thank you especially for your understanding and advice; and to my mother : for your continual and selfless support and understanding, for the stability and love I have been fortunate enough to have been blessed with and for you believing in me and encouraging me always to look up : you have given me the greatest gifts I could have ever desired in life, thank you.

In precious memory of my father,

the late, Mr. Kenrick Ramsaran.

TABLE OF CONTENTS

LIST OF FIGURES

CHAPTER 1

CHAPTER 2

CHAPTER 3

CHAPTER 4

CHAPTER 5

CHAPTER 6

Appendix 1

LIST OF TABLES

CHAPTER 1

CHAPTER 2

CHAPTER 3

CHAPTER 4

CHAPTER 5

CHAPTER 6

Appendix 1

Appendix 2

LIST OF ABBREVIATIONS

AES	Auger Electron Spectroscopy
BAS	Bronsted Acid Sites
BET	Brunauer, Emmett and Teller
BETE	Bioethanol to Ethylene
BJH	Barrett, Joyner and Halenda
CEC	Cation Exchange Capacity
CMR	Catalytic Multipass Reactor

DDMI	Direct Dipolar Magnetic Interaction
DME	Dimethyl ether
DEE	Diethyl ether
DTA/TGA	Differential Thermal Analysis/ Thermogravimetric Analysis
Ethy.	Ethylene
FAU	Faujasite structure zeolite
FID	Flame Ionization Detector
FTIR	Fourier Transform Infra Red
HC	Hydrocarbons
HK	Horvath Kawazoe
LAS	Lewis Acid Sites
MAS NMR	Magic Angle Spinning Nuclear Magnetic Resonance
NH_3 TPD	Ammonia Temperature Programmed Desorption
NNN	Next Nearest Neighbours
PBU	Primary Building Units
SBU	Secondary Building Units
TCD	Thermal Conductivity Detector
TFSA	Trifluoro methane sulphonic acid
WHSV	Weight Hourly Space Velocity
XRD	X Ray Diffraction
XPS	X Ray Photoelectron Spectroscopy
ZSM	Zeolite Socony Mobil

CHAPTER 1

INTRODUCTION

1.1 BIOMASS AS FUELS

Approximately 90% of our total energy consumption is based on conventional fossil fuels - coal, petroleum and natural gas. The worldwide energy problem and particularly the depletion of the world's petroleum reserves in the last decade suggested a search for alternative fuels. Natural gas is difficult to mine and coal though abundant is environmentally unacceptable. A viable alternative is the use of cellulosic compounds. Such compounds are referred to collectively as biomass and include all land and water based vegetation such as terrestrial and aquatic plants, grasses and trees, all organic wastes such as municipal solid wastes, sewage, animal wastes and forestry and agricultural residues. Less than 1% of the biomass grown each year in the world is used for energy and this amount fuels 15% of the total primary energy consumption (1).

Oxygenated fuels derived from biomass can replace the fossil fuel sources used for transportation and energy production. Oxygenated fuels contain alcohols and ethers which when added to gasoline increase the oxygen content and boost the octane level. The higher oxygen content decreases the carbon monoxide content without hindering driving performance. In the USA,

Europe, Great Britain and Canada, there is a flourishing market for ethanol in terms of chemical feedstock, fuel and for use as an oxygenated additive to gasoline to produce Reformulated Gasoline (2).

Environmental regulations (Amendments to the Clean Air Act, 1995) (3), have caused the prices of fossil fuels to be elevated by imposing environmental costs, thus there is an incentive to seek and to develop greener fuel technology. Also biomass technology is potentially important to countries like India, Brazil and Trinidad which have a large agricultural base and from which ethanol is generally produced by the fermentation of molasses - a by product of their large sugar industries.

Cellulosic biomass is a complex mixture of carbohydrate polymers derived from plant cell walls. It is comprised of cellulose, hemicellulose, lignin and a smaller amount of other compounds known as extractives. Biomass is converted into aqueous ethanol by acidic or enzymztic hydrolysis of the cellulosic and hemicellulosic compounds, first into glucose followed by fermentation to ethanol. This process is only a small part of the scheme for the conversion of biomass into fuels and other useful by products. Fig 1.1 illustrates the range of end products generated from biomass, ranging from chemicals such as ammonia, synthesis and fuel gas and steam generation to compost and sludge which supports vegetation and landfills.

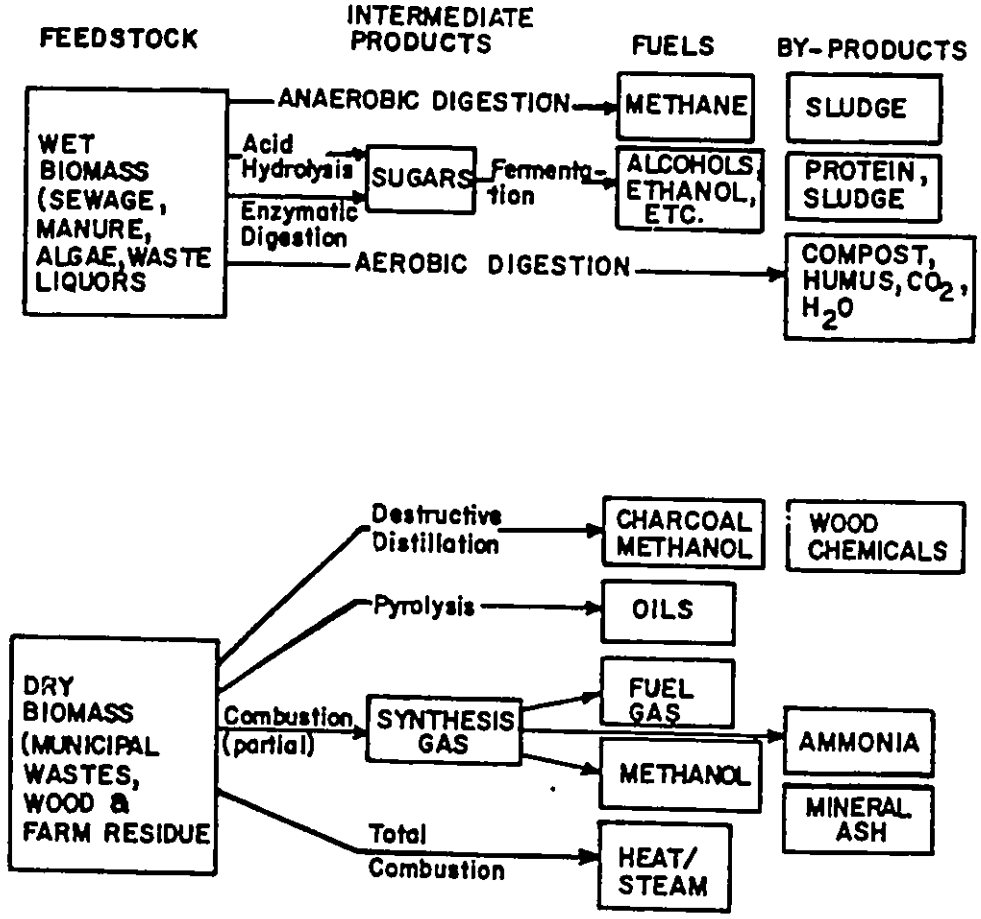

Fig 1.1 Basic processes for the conversion of Biomass into Fuels (from reference (4)

The main source of convertible biomass in the US is corn and even if the entire US corn crop were used for ethanol production, less than 10% of the US oil supply would be replaced by the alcohol fuel. The industry for ethanol production is obviously well established and the production capacity is in excess of its market demand as a fuel and as an additive to fuels. In fact, although promising, ethanol use as a fuel does present some problems. Since it has only two thirds the energy content of gasoline, vehicles must have larger tanks to travel the same distance as a gasoline-fuelled vehicle. Another problem is starting vehicles in cold weather. Ethanol also can be corrosive when used with some conventional engine components. Ethanol-gasoline blends do not pose corrosion problems.

On the other hand the dehydration of ethanol into ethylene is a convenient and viable outlet for any excess supply of ethanol. Ethylene, as the building block of the polyethylene industry has always been in high demand and commands a lucrative market. The industrial activity of many catalysts for the dehydration of ethanol is well known. These include heteropoly acids such as concentrated sulphuric acid at 180°C, phosphoric acid (but this is severely corrosive), sulfonated polymers, metal oxides such as γalumina (13) and acidic and modified zeolites such as phosphorous, manganese, gallium of zinc modified ZSM-5 (14,15,16). Fig 1.2 presents a simplified scheme of a commercial ethanol based, ethylene fixed bed process.

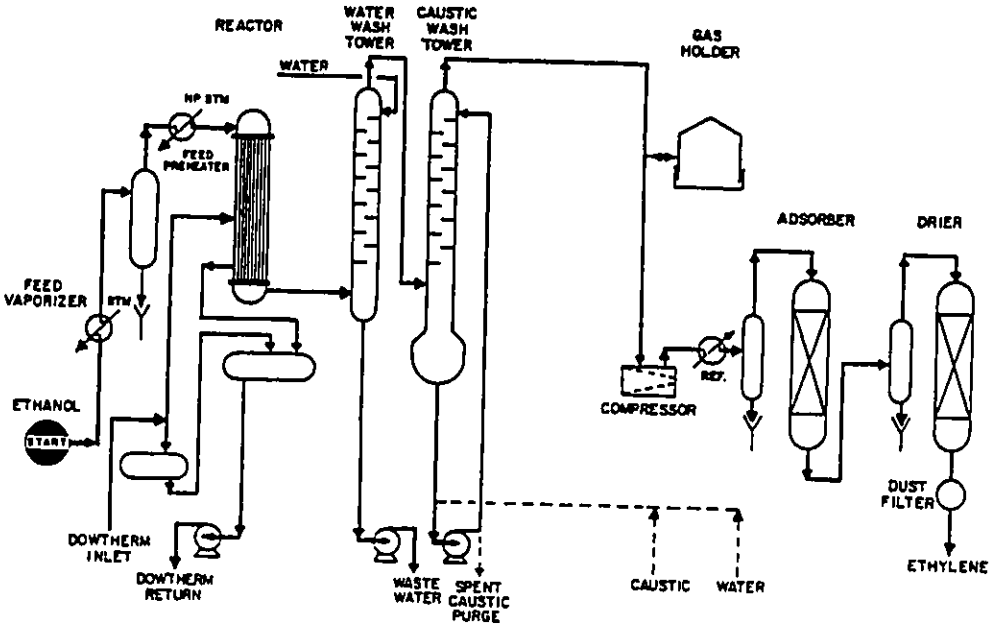

Fig 1.2 Processing scheme of a simplified commercial ethanol to ethylene fixed bed process (from reference 12)

1.2 BIOETHANOL TO ETHYLENE (BETE)

Bioethanol (10-15 wt %), the natural fermentation product derived from biomass, is used in the bioethanol to ethylene process, which has been studied using a fixed bed tubular or plug flow reactor by various groups (5,6) including the Catalysis Laboratory at Concordia University (7-10). This reaction involves the catalytic dehydration of aqueous ethanol into ethylene and other aliphatic hydrocarbons. Depending on the catalyst and the reaction conditions employed (temperature, partial pressure, WHSV as defined by the ratio of flow rate of reactant in g/h to the weight of catalyst in g) the product distribution may vary to include DEE, DME or aromatics. It is a one step process to convert biomass to pure ethylene for which the basic mechanism is acidic dehydration. It has been postulated that this mechanism proceeds by two pathways. One involves the direct conversion into ethylene and the other involves the formation of ether as an intermediate reaction product, depending on the conditions of temperature or contact time (11). The formation of ether is favoured at low temperatures (approximately 230°C) and low contact time while the direct formation of ethylene occurs at higher temperatures (300 to 400°C) and higher contact times with a minimum amount of DEE formed. The conversion of aqueous ethanol into ethylene occurs along pathway II and into diethyl ether along III as illustrated in Fig 1.3. Ethanol first becomes adsorbed onto the BAS in the vicinity of the aluminum atom. This is followed by a rapid proton transfer from the zeolite framework forming a dihydro ethyl oxonium ion, which is very

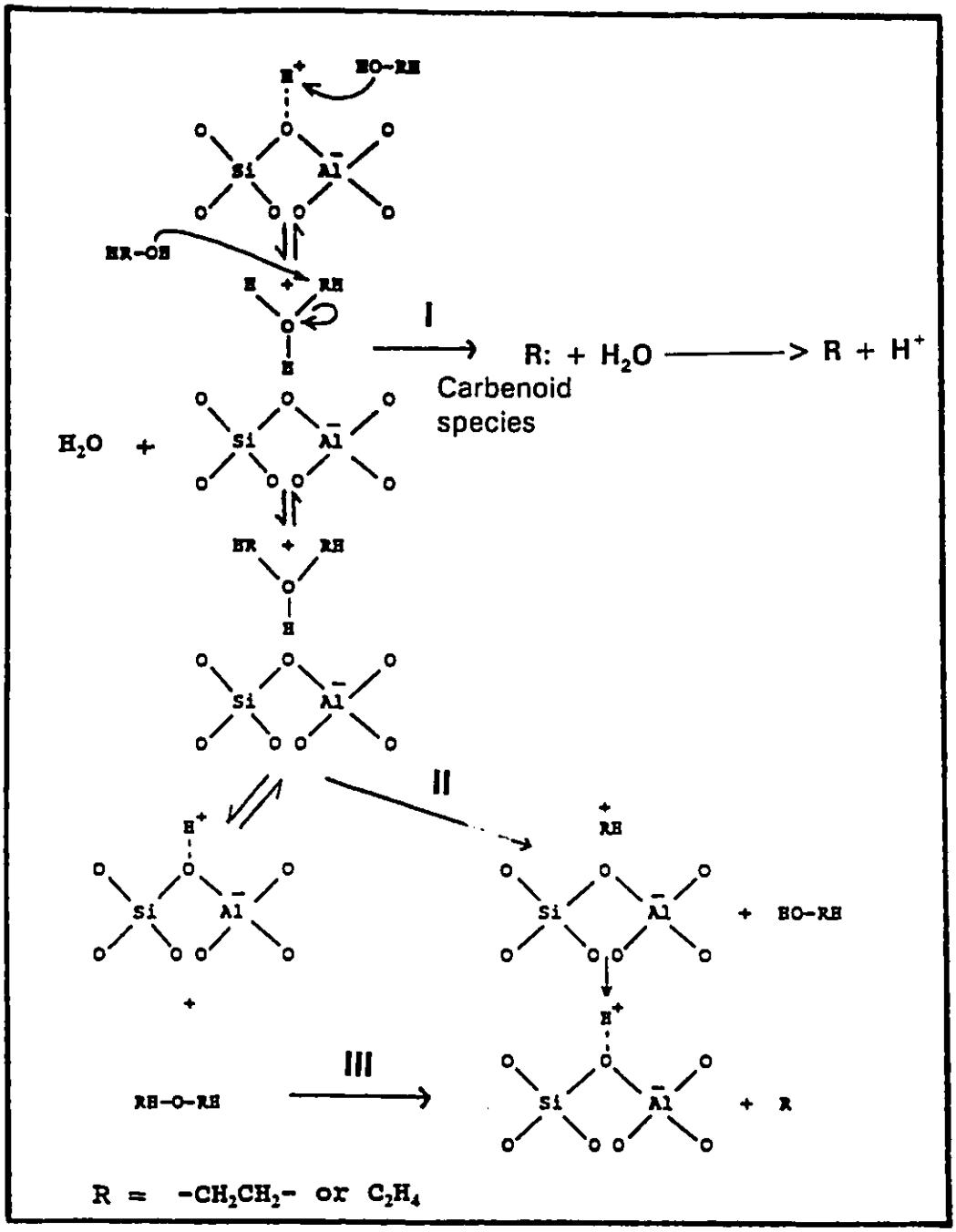

Fig 1.3 Mechanism for the acid catalyzed dehydration of aqueous ethanol into ethylene and diethyl ether on ZSM-5 zeolite (from reference 7 and 183)

unstable and is rapidly attacked by another ethanol molecule to form a more stable hydro diethyl oxonium ion. The rate limiting step is the formation of the ethyl (carbocation) which stabilizes itself by loss of a proton.

Chang (164,183) supported the proposal by Venuto and Landis (184) for the formation of a carbenoid species, as shown in pathway I (Fig 1.3), after initial adsorption of the alcohol on the zeolite. This which then rearranges to form ethylene.

For such low exothermic reactions, isothermal behaviour is assumed for catalytic testing on a laboratory scale. Significant yields of the main dehydration product ethylene have been reported in the Catalysis Laboratory at Concordia University, for which the moderately acidic zeolite HZSM-5 was used at a temperature greater than 275°C and high contact time. However catalytic deactivation rapidly occurs since the high temperature coupled to a large amount of water present in the feed constitute severe hydrothermal conditions and eventually lead to loss in acidity. At lower reaction temperatures diethyl ether is formed in significant amounts. The catalytic activity of modified versions of ZSM-5 of stronger acidity at lower reaction temperatures, such as steam treated HZSM-5 zeolites and asbestos derived zeolites, have also been studied for this reaction (10). The latest version is the superacidic ZSM-5 made by incorporating an organic superacid, trifluoromethanesulfonic acid (TFSA) onto the zeolite and this catalyst was able to achieve high catalytic conversion at temperatures as low as 170°C (17). But the decomposition temperature of

TFSA bound to the zeolite is 245°C, thus the margin between the operational temperature and this limit of thermal stability in the presence of aqueous ethanol is too narrow. Additionally the triflic acid species contributes to undesirable pore blocking.

1.3 HETEROGENOUS CATALYSIS

Catalysts serve to reduce energy barriers associated with a reaction that is thermodynamically feasible by providing an alternative pathway of lower activation energy. They alter the rate to provide a faster reaction rate without affecting the free energy of the reaction since the ratio of the activities of the product and reacting species is unaffected, so that there is a minimum expenditure of energy. Historically, it was thought that these catalysts emerged unchanged after altering the reaction rate, but developments in the ability to observe surfaces at an atomic level have demonstrated that there are changes in the topology and even composition brought about by catalytic activity. Catalysts become sintered, etched, eroded or covered with residues left behind by the interacting molecules (13).

An operational definition of a catalyst is a substance that increases the rate of approach to equilibrium of a chemical reaction without being substantially consumed in the reaction (13). Fig 1.4 shows the changes in energy associated with a simple exothermic reaction. The velocity of a catalyzed reaction for the conversion of reactants A and B into product P may

be expressed as

$$-d[A]/dt = k\,[A]^n\,[B]^m$$

where k = Aexp ($-E_{hom}/RT$) and [A], [B], R, T, n and m are the orders of the reaction with respect to the reactants A and B respectively. E_{hom} is the activation energy for the homogenous reaction, E_{ads} for adsorption of the reactants onto the catalyst , E_{cat} for the formation of the activated complex and E_{des} for the desorption of the products. λ_{ads} is the enthalpy of adsorption of the reactants and is taken to be exothermic, and λ_{des} the enthalpy of desorption of products, taken to be endothermic. The reaction rate at a given temperature will be increased by finding some means of reducing E_{hom} or increasing A. In the presence of a catalyst which might chemisorb A or B or both, the system may follow an alternative reaction path of lower energy of activation E_{cat}. Here the system appears to pass through a new chemisorbed transition state. The overall energy change upon reaction is ΔH and is the same for the two pathways (32).

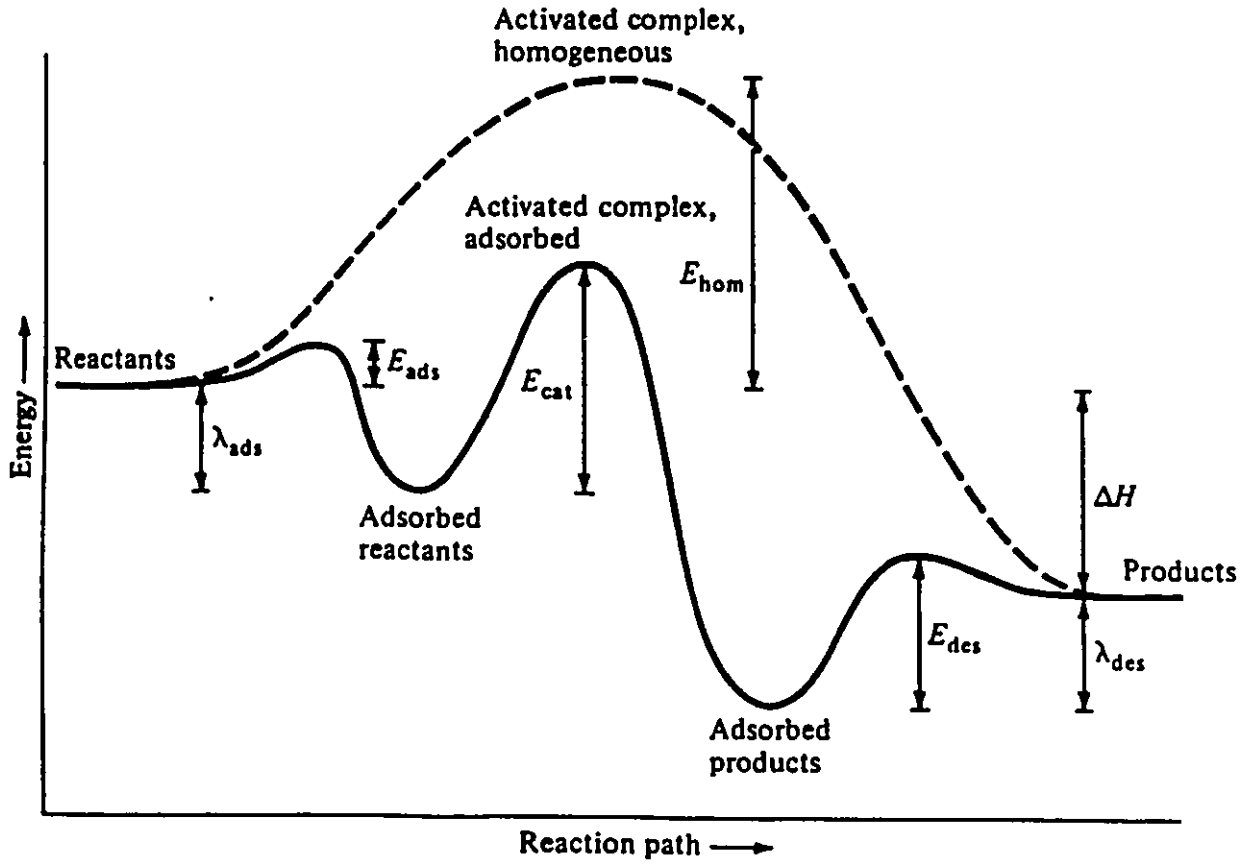

Fig 1.4 Energy changes associated with individual steps of a chemical reaction

1.4 CATALYST TECHNOLOGY :

1.4.1 FROM THE PERSPECTIVE OF PETROLEUM REFINING

Catalytic technology forms the backbone of the chemical and petroleum industries since many of the synthetic and refining processes are catalytically controlled. Thus there is a major thrust to continue technological advancements in the field of catalysis and the progression of catalytic developments continues. The goal of the catalyst researcher is to develop novel catalysts for existing processes, then to optimize the various components in their complementary role with respect to activity and selectivity with emphasis on the minimization of energy consumption and pollution. A synthetic approach must be adopted to develop a catalyst.

It is necessary to understand the processing goal of any catalytic reaction at an atomic level and to discover the mechanism by which catalysis proceeds so that one can design and construct the most efficient catalyst for this particular reaction. The success of a catalyst is gauged by the extent to which it reduces the activation energy barrier for a reaction. An alternative approach is to develop a means of reducing energy consumption to effect the same results of a more efficient catalyst.

With the rapidly emerging progress in computer technology, more sophisticated techniques, such as Molecular Modelling and Computer Aided Design (CAD) have become available and they are now vital diagnostic tools routinely used in predicting and modelling catalytic properties of materials.

Advanced surface analysis techniques are a key element for successfully developing and characterizing catalysts. The advantage of performing analyses in situ is obvious if one considers the possible variations in catalytic behaviour that actual conditions incur compared to empirically optimized reaction conditions. The optimization of each parameter is directly controlled by the operator and can be manipulated in the desired fashion and the effects monitored. Under typical reaction conditions however the extent to which one can exert control over the reaction is limited.

1.4.2 ZEOLITE AS CATALYSTS

The use of zeolites as commercial cracking catalysts was first announced in 1960. By 1976, it was estimated that this development saved the petroleum industry and ultimately the US public more than $3 billion in reduced petroleum and refining costs compared to using the previously used silica-alumina catalysts (18,19). Zeolites are essentially crystalline, hydrated, tectoaluminosilicate, molecular sieves in which the silicon and aluminum tetrahedra are linked by shared apical oxygen atoms.

There may be certain cations delocalized within the framework to compensate for the negative charge associated with tetrahedrally coordinated aluminum atoms (20). Because of their unique structures, pore size distributions and other chemical and physical properties, zeolites have emerged as perhaps the most widely used of the natural and synthetic microporous

solids. One of the most important properties of zeolites is their ability to exhibit shape selective catalysis (21). Their ability to combine molecular sieving properties with unusually high activity for acid catalyzed reactions such as cracking and dehydrations make them especially interesting. Their pore diameters vary between 3 and 8 Å and their pores sizes usually fall within a discreet range with a narrow pore size distribution. Since most catalytic sites are located within the pores of the catalysts, the relative probability of forming product molecules depends on the accessibility of reactant molecules to active sites. Other properties which render them efficient catalysts are their high internal surface area, usually well over 300 m^2/g depending on the zeolite, and because they possess ion-exchangeable cationic sites which allow the introduction of various metal cations with variable catalytic properties. Replacement of a metal cation with a proton (H^+) generates strong acidic sites which are the origin of catalytic activity in solid acidic catalysts (22).

Zeolites have long been used for water softening, utilizing their ion exchange capacities, and for drying. Besides their large scale use as industrial catalysts in petroleum refining and chemical manufacture (Table 1.3), zeolites have evolved as environmental catalysts in auto emissions control (23,24,25), detergent (non-phosphate) builders (26), selective adsorbents, membrane synthesis (27) and as modifiers at electrode surfaces in electrochemical applications (20,28).

1.4.3 ZEOLITE STRUCTURES

The main physical features of a catalyst, essential for controlling its activity in heterogeneously catalyzed reactions are : its structure which is defined by the nature and distribution of atoms or ions in the bulk ; its texture as defined by a detailed geometry of the void space in the catalyst particles and the intragranular voids in the agglomerates ; the pore size distribution at the finest level of resolution ; the shape of the particles and pores and the external and accessible internal surface area (29).

There are many zeolite structures of which some occur in nature, some as synthetic analogues of natural zeolites and some synthetic ones with no natural counterparts. In all there are about 70 structures which are categorized in terms of the number of tetrahedral building units associated to form one, two and three dimensional polyhedra of which about 40 occur in nature (30).

The basic categories can be recognized as small, medium and large pore structures corresponding to 6 or 8, 10 and 12 ringed tetrahedra respectively. A representative example of each class is shown in Fig 1.5

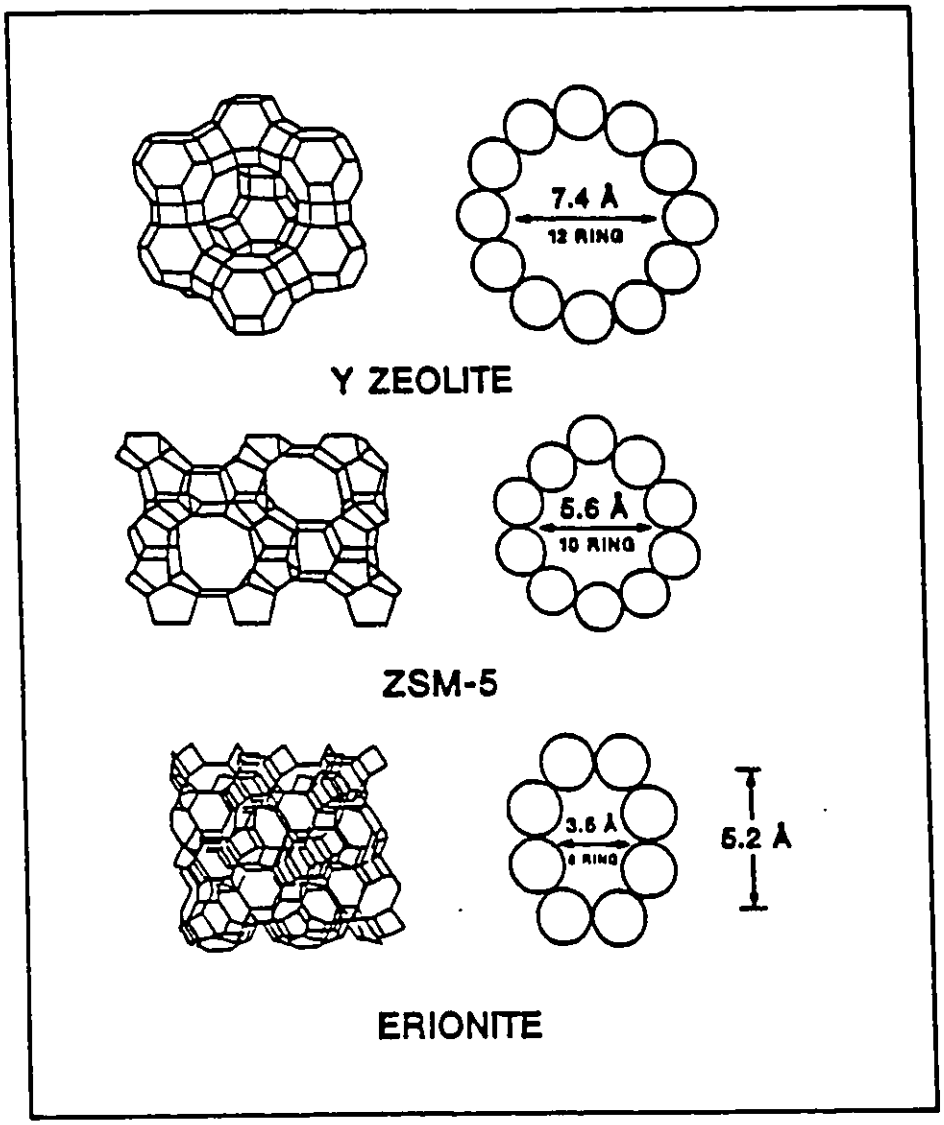

Fig 1.5 Framework Structures and Projection of Zeolites (from reference 18).

1.4.4 FRAMEWORK COMPOSITION

Structurally, the zeolite is a crystalline framework based on an extensive three dimensional network of oxygen ions. Situated within the tetrahedral sites formed by the oxygen can be a Si^{4+} or an Al^{3+} ion. The AlO_4^- tetrahedra in the structure determines the framework charge. This is balanced by cations that occupy nonframework positions. A representative empirical formula for a zeolite is written as:

$$M_{2/n}O \cdot Al_2O_3 \cdot xSiO_2 \cdot yH_2O$$

where M represents the exchangeable cation and *n* represents the cation valence. The value of *x* is greater than or equal to 2 because Al^{3+} does not occupy adjacent tetrahedral sites. The crystalline frameworks contain voids and channels of discrete sizes which contain water molecules and/or the cations which neutralize the negative charge created by the presence of AlO_4^-. Typical cations include Na^+, K^+, Rb^+, Cs^+, Mg^{2+}, Ca^{2+}, NH^{4+}, H_3O^+,TMA^+ (tetramethylammonium) and the rare earth and noble metal ions (28)

The general formula for the HZSM5 zeolite is

$$H_n[Al_nSi_{96-n}O_{192}] \cdot 16\ H_2O$$

where n = number of aluminum atoms/unit cell (31).

The ratio Si/Al is defined as 96-n : n, and this further characterizes zeolites into major classes having different chemical and physical properties. High silica zeolites are typified by the three dimensional pentasil structure such as ZSM-5 and usually have Si/Al ratios in the range 10-500 (18).

1.4.5 HIGH SURFACE AREA

The rate of a catalytic reaction is proportional to its active surface area (32). Because of the high degree of porosity and their multichannel structure, zeolites exhibit extremely large internal surface areas relative to their external surface area, a major factor contributing to their efficiency as catalysts, since it provides a greater accessibility of reactant molecules to active sites where reaction occurs. Occasionally a high surface area at the interface arises when two phases are coupled together under pressure leading to a contact synergy, thereby increasing overall catalytic activity (33,173).

Table 1.1 Typical Surface Areas of common Zeolites

Zeolite	Surface Area (m^2/g)
ZSM-5	300-400
A	650
Beta	400-500
X and Y	700
MCM 41	>1000

1.4.6 DIFFUSION IN ZEOLITES

Pore diameters in molecular sieves usually depend on the number of tetrahedra in the ring. The actual pore size also depends on the type of cation present. Cations occupy positions which block part of the pores and adsorption into the pores cannot occur until the adsorbate molecules are small enough to move freely into and within the pores. Molecular sieve action depends on pore size which controls diffusion rates and transport processes operating within the zeolite pores. A qualitative representation of the diffusion in the pores of solids is shown in Fig 1.6. The Diffusivity, D is shown as a function of pore size. For macropores or at higher pressures, the interactions between the molecules predominate and diffusion is unaffected by the walls of the solid ; for these situations the mode of molecular transport is molecular diffusion (described by Fick's Law). This is also referred to as "Bulk" or "Regular Diffusion," since it is very similar to transport within the bulk fluid phase. In smaller diameter pores or at lower pressures, the diffusion of any species is not controlled by diffusion of any other species or variations in pressure, and interactions with the pore walls predominate. This is referred to as Knudsen Diffusion. Diffusion in zeolites is much more complex than either Knudsen or "Bulk Diffusion", and the activation energy is much greater than either. For pore sizes less than 10 Å as in zeolites when the pore size is of approximately the same dimensions as the critical dimension of the molecule being transported, "Configurational Diffusion" is observed by which the molecules can barely pass into the pores

and the effective diffusion coefficient D depends on the aperture size. A decrease of 0.1 nm can reduce the diffusivity and so transport rate by orders of magnitude (13). Typical reported values of diffusivities at 350°C in ZSM-5 for p-xylene, o-xylene and mesitylene were $>10^{-7}$, 10^{-10} and 10^{-12} cm^2/s respectively (32).

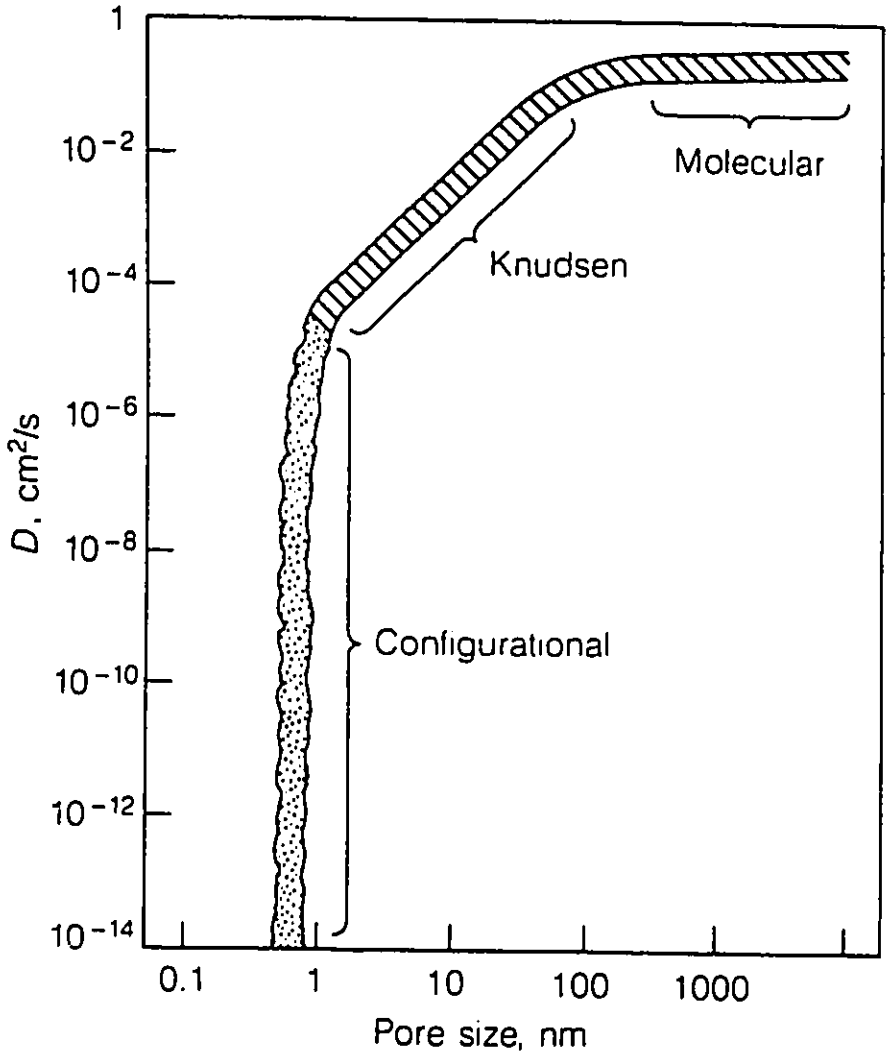

Fig 1.6 Variation of diffusivity with pore size in zeolite (from reference 13)

1.4.7 SHAPE SELECTIVITY

High crystallinity and regular pore structures and sizes are among the properties which render to zeolites their greatest advantages over other catalysts. Because of their specificity and selectivity for certain reactions and their ability to discriminate and exclude undesirable reactions from occurring, they are able to achieve very high yields of particular products. It is possible to distinguish four different types of shape selectivities based on decreased diffusivity of either reactant or product molecules, which ultimately diminishes the reaction rate for the formation of the product. First, certain reacting molecules may be excluded from diffusing into the zeolite pores and are thus unable to gain access to the active sites because of pore size limitations (Fig 1.7.a), a type of molecular exclusion known as reactant selectivity. Alcohol dehydration which requires weak acid sites is a typical case of reactant shape selectivity where secondary alcohols are excluded from the narrow pores of CaA zeolite. Secondly, if the product molecules formed are too bulky to freely diffuse out of the pores and into the surrounding media limiting the formation of certain products, it leads to the phenomena of product selectivity (Fig 1.7.b). The trapped products are either converted into less bulky products by equilibration or they deactivate the catalyst by blocking its pores. An example is the methylation of toluene for which the ortho and meta products are formed depending on the pore size of the catalyst.

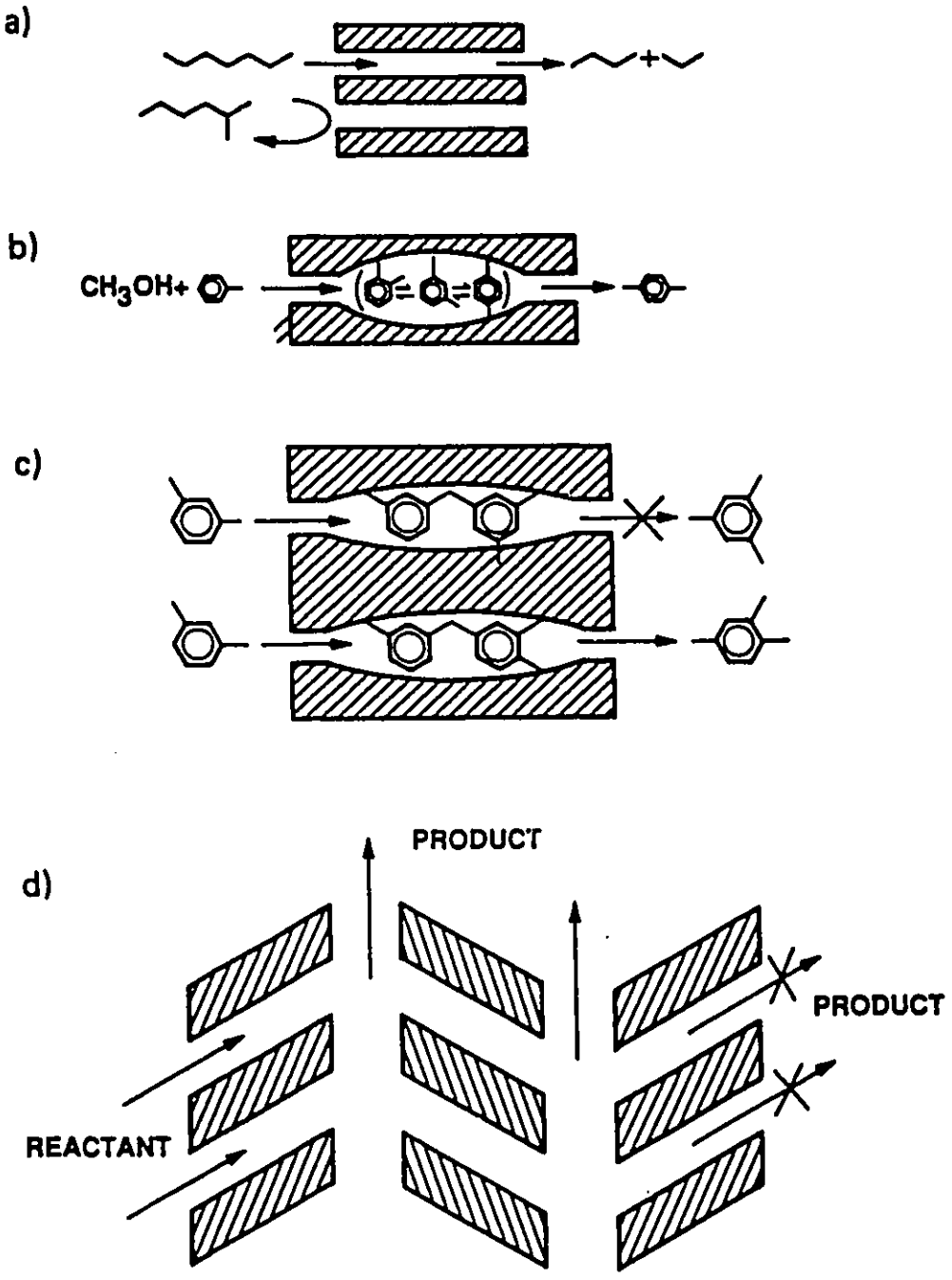

Fig 1.7 Shape selectivity of zeolites (a) (b) (c) and (d)(from reference 35)

The third situation which arises is the formation of transition states which are restricted in movement by the size of the pores of the zeolite. This is a kinetic effect arising because of the local environment around the active site. Since neither reactant nor product molecules are prevented from diffusing through the pores, only the formation of the transition state is hindered. This is termed "restricted transition state selectivity" or "spatioselectivity" (Fig 1.7.c). An interesting example is the acid catalyzed transalkylation of dialkylbenzenes.

The fourth situation is a type of molecular traffic control which may occur in zeolites with more than one type of pore system such as ZSM-5. Reactant molecules may enter through one pore system and product molecules diffuse out through another (Fig 1.7.d). In this way counterdiffusion is minimized. This is illustrated in the alkylation of toluene over modified ZSM-5 zeolites (22).

Fig 1.8 shows the correlation between effective pore size of various zeolites in equilibrium adsorption over temperatures of 77° to 420°K (indicated by ---), with the kinetic diameters of various molecules (from the Lennard Jones potential relation.)

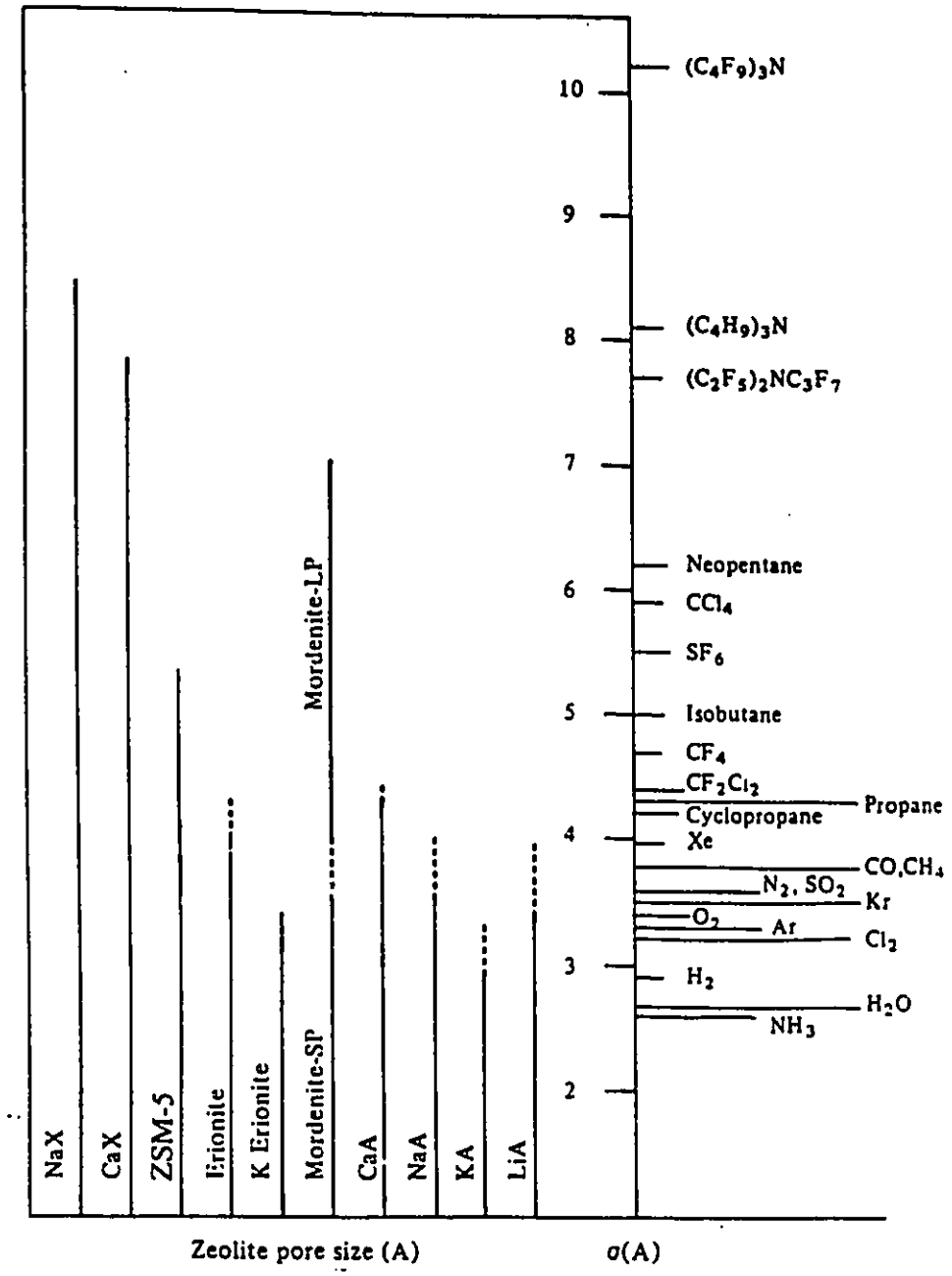

Fig 1.8 Correlation between effective pore size of various zeolites with kinetic diameters of various molecules based on Lennard Jones Relationship (reference 37)

Table 1.2 Kinetic diameters and pore dimensions of some organic molecules and zeolites respectively

Molecule	*Kinetic Diameters (Å)
CO_2	3.30
CH_4	3.80
C_2H_4	3.90
n-C_4H_{10}	4.30
i-C_4H_{10}	5.00
Benzene	5.85
Cyclohexane	6.00
Zeolite	Pore Dimensions(Å)
Chabazite	3.6 x 3.7
Erionite	3.6 X 5.2
A	4.1
ZSM-5	5.4 X 5.6 ; 5.1 X 5.5
ZSM-11	5.1 X 5.5
Mordenite	6.7 X 7.0
X or Y (Faujasite)	7.4

1.4.8 ACIDITY IN ZEOLITES : ROLE OF ALUMINUM

There are two fundamental types of acid sites which classify the active sites in heterogenous catalysts : classical Bronsted and Lewis acid sites. Catalytic activity is defined by the following characteristics:

(i) the strength of acidity

(ii) the concentration and

(iii) the accessibility of the bridging hydroxyl groups which are known to act as Bronsted acid sites (38).

Surface acid sites in zeolites are of two types:

a) those capable of donating protons, as the bridging hydroxyl group in SiO(H)Al which are associated with tetrahedrally coordinated or framework aluminum atoms, or Bronsted Acid Sites, (BAS) or

b) those capable of accepting electron pairs from adsorbed species, like the tricoordinated Al^{3+} or Lewis Acid Sites, (LAS).

These two types of sites are illustrated in Fig 1.9. Acidity on zeolites will be therefore defined by two independent qualities : firstly the "strength" which is defined as the ease of proton transfer from the surface site to the adsorbed base, or of an electron pair transfer from an adsorbed base to a surface site, and secondly by the amount of acid which is given by the concentration (density) of the respective acidic sites assuming no diffusional limitations (73). Bronsted acid strength depends on the electronic charge of those protons associated with the bridging hydroxyl groups of SiO(H)Al in zeolite frameworks.

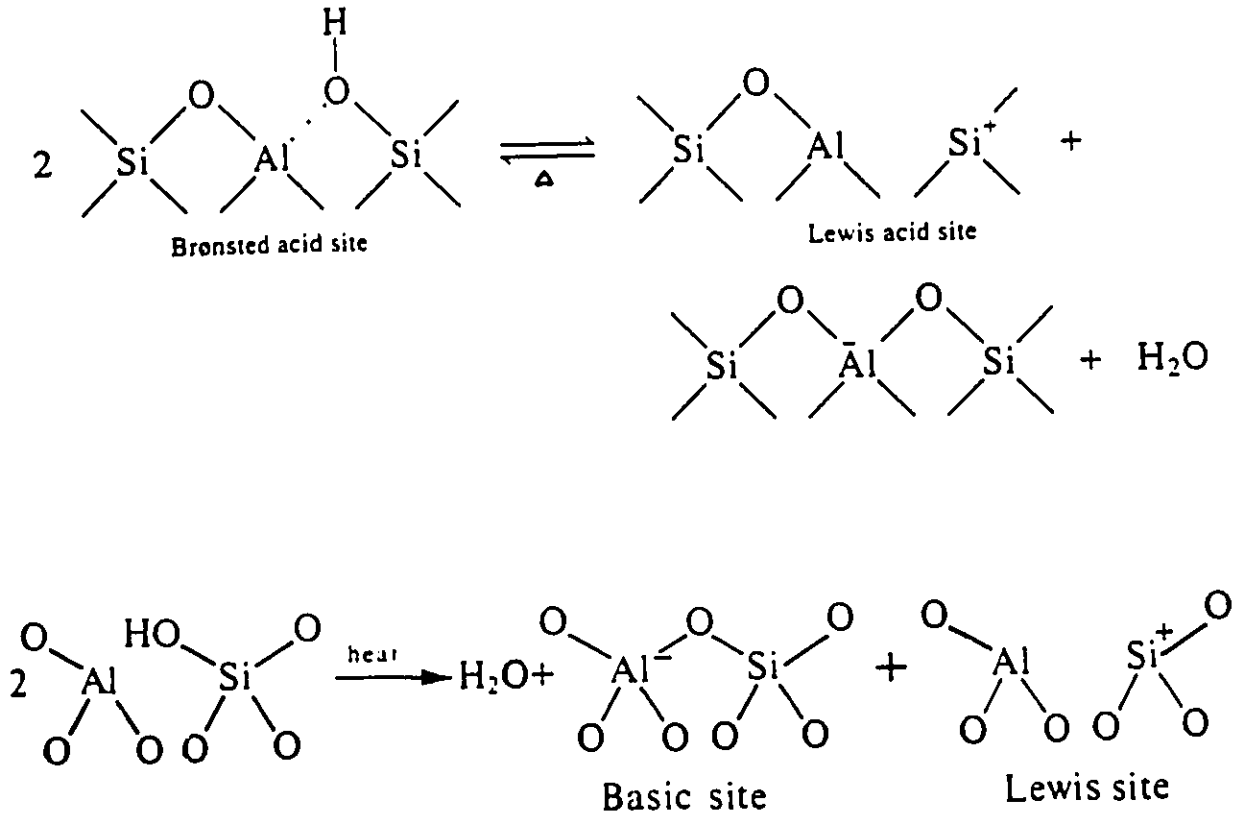

Fig 1.9 Conversion of Bronsted acid site into Lewis centre

Each tetrahedrally coordinated Al atom contributes to one potential Bronsted acid site but since the distribution of aluminum is not uniform there exists a wide distributions of proton strength in zeolites. Using Electronmicroprobe Analysis (EPA) and X Ray photoelectron Spectroscopy (XPS), it was shown that the aluminum in ZSM-5 is distributed non-homogenously, especially in crystallites larger than 5 μm. The surface is

enriched in aluminum as compared to the bulk of the crystal (35,61).

Therefore there are strong, medium strength and weak acidic sites on HZSM-5. The concentration of strong acidic sites depends on the concentration of framework aluminum. An increase in calcination temperature (>500°C) of the zeolite leads to dehydroxylation, resulting in a decrease in Bronsted acidity and an increase in Lewis acidity. Steaming results in a decrease in the concentration of strongly acidic OH groups (Fig 1.9).

According to Lowenstein's Rule (32) for the distribution of aluminum in the tetrahedra of zeolites and aluminosilicates there are no near neighbouring AlO_4^- tetrahedra in zeolites. They are always interspersed with SiO_4 to form an electronically stable structure. Zeolites with higher Si/Al ratios or low densities of proton donor sites have high proton donor strengths (40). Because of the low concentration and specific nature of acidic sites, it is difficult to accurately measure their acidic strength and concentration by conventional methods such as ammonia temperature desorption and IR spectroscopy (13). Recently Doremieux-Morin et al. proposed a scale for measuring the proton acidic strength of solid acids based on a calculated ionization coefficient obtained from simulated Broad-line NMR Spectra. Bronsted acid sites are able to ionize water molecules to form hydroxonium ions (H_3O^+) which can be quantified. Different concentrations of water are adsorbed onto anhydrous zeolite under vacuum and the degree of ionization of water to form hydroxonium ions is directly proportional to the number of acidic sites present (39).

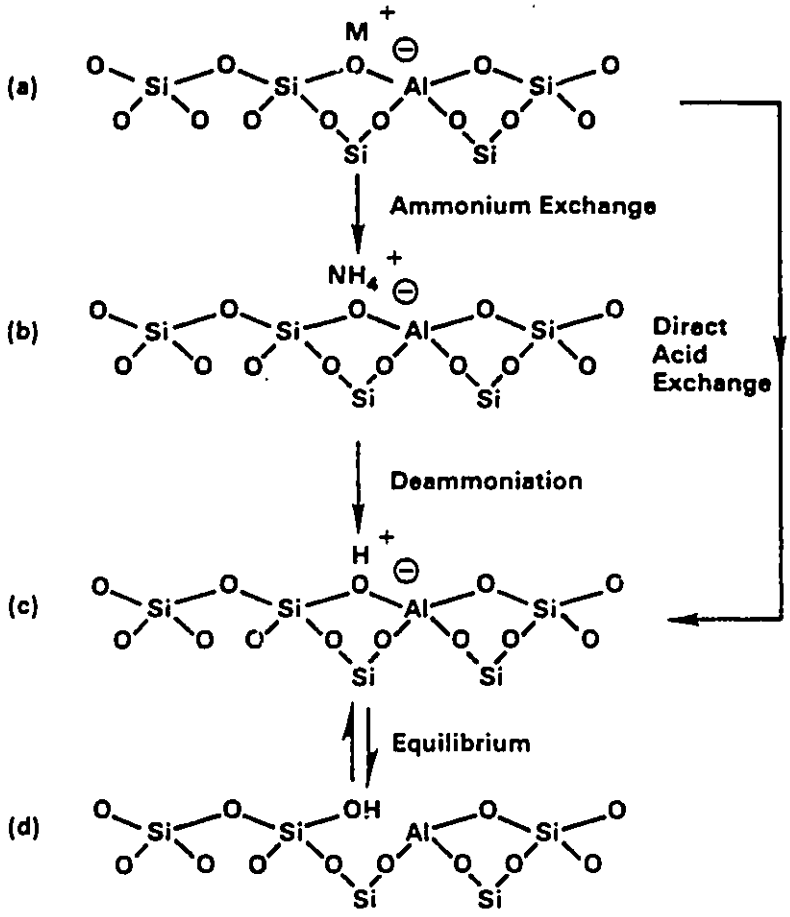

Fig 1.10 shows the typical zeolite framework surface (a) as synthesized, M^+ is either an alkali cation or organic cation. (b) Ammonium ion exchange procedures produce the NH_4^+ form. (c) Thermal treatment (450°C) is used to remove ammonia, producing the H^+ acidic form (d). The acid form in (c) is in thermal equilibrium with the form shown in (d) where there is a silanol group adjacent to a tricoordinate aluminum.

1.4.9 MANIPULATION OF Si/Al RATIO

It is generally known that there is a direct relationship between the chemical composition (Si/Al ratio) and structural stability and purity, and also acidic strength of the bridging hydroxyls of zeolites, in particular for ZSM-5 zeolite that is synthesized. There are three concepts proposed for the defining the lower threshold limit in the Si/Al ratios for different zeolites. The Lowenstein avoidance principle, proposed in the 1950's, states that whenever two aluminum atoms are neighbours to the same oxygen anion, at least one of them must have a coordination number larger than 4, that is 5 or most likely 6 (47). This applies specifically for the A zeolite (Si/Al = 1) which was the only zeolite synthesized at that time, thus according to this theory, it was impossible to synthesize a zeolite with a Si/Al < 1 since all the framework Al of such a zeolite must have a coordination number of 4. This rules explains the maximum substitution of 50% of the silicon in three dimensional framework networks of tetrahedra by aluminum.

During the 1960's, Goldsmith proposed that the crystallization of zeolites is consistent with the "simplexity principle", which related the ease of crystallization to structural "simplexity" (174,181). High structural simplexity is a situation synonymous with high entropy (disorder of a metastable state) and structural simplicity for the primary building units (SiO_4 and AlO_4^- tetrahedra). The growth of zeolites requires the formation of a nucleus. In a system with a high disorder, the principle favours the formation of a smaller

nucleus with the highest simplexity, which may be the nucleus of a crystal of a metastable state (the gel structure is in a state of high simplexity). In zeolites, silicon atoms always exist in 4 fold coordination. Thus the zeolite aluminum atoms which are isomorphous substituents of Si, must assume a 4-coordination with oxygen so that these structures might have a higher ease of crystallization (high simplicity). This contrasts with other aluminosilicates (kaolinite and bentonite clays) in which the aluminum ions are either located in 4-fold coordination or 6-fold coordination with oxygen throughout the structure. These structures are synthesized as thermodynamically stable phases.

The most recent concept for the determining acidic strength of zeolites takes into consideration the nature of the cation occupying the first as well as the second shell of tetrahedra around a Si atom (secondary building units : SBU) and this is related to the topological densities of $A^{t}O_4^-$ tetrahedra. Barthomeuf proposed that the ZSM-5 zeolite cannot be synthesized with a Si/Al ratio lower than 9.5, since firstly, the crystallinity and stability of the structure are severely reduced if there is a higher content of framework aluminum (175). There will be the inevitable introduction of aluminum into extraframework positions during hydrothermal synthesis as octahedral or tricoordinated Al^{3+} and this reduces the purity of the zeolite. Moreover, in accordance with Lowenstein's principle, when two tetrahedra are linked by one oxygen bridge, the centre of only one of them can be occupied by aluminum ; the other centre must be occupied by silicon or some other small ion of valence 4 or more

(Nearest Neighbour). For the structure of faujasite, a given Al atom must have 4 Si atoms in the first surrounding layer (Nearest Neighbour) and 9 Al or Si atoms in the second layer (Next Nearest Neighbours or NNN). For X zeolite, all of these NNN will be Al, by Lowenstein's rule. With increasing Si/Al ratio, some Al will be replaced by Si but at a sufficiently large ratio, all 9 NNN will be replaced with Si and the original Al site will be isolated. The strength of this Al site will depend on the number of NNN Al and will be maximum for 0 NNN Al. According to the model proposed by Barthomeuf using topological densities to include the effects of layers 1 through 5 surrounding the Al atom, the threshold value for the limit to the Si/Al ratio for a highly crystalline ZSM-5 zeolite is 9.5.

1.4.10 ADSORPTION IN ZEOLITES

The usual steps for transport phenomena during heterogenous catalytic activity involves the following sequence :

(i) diffusion of gaseous reactant molecules from bulk phase to the gas/solid interface

(ii) diffusion into the catalyst pores

(iii) adsorption

(iv) reaction at the active sites

(v) desorption of the product molecules away from the latter

(vi) counterdiffusion of product molecules through the catalyst pores

(vii) counterdiffusion to the bulk phase

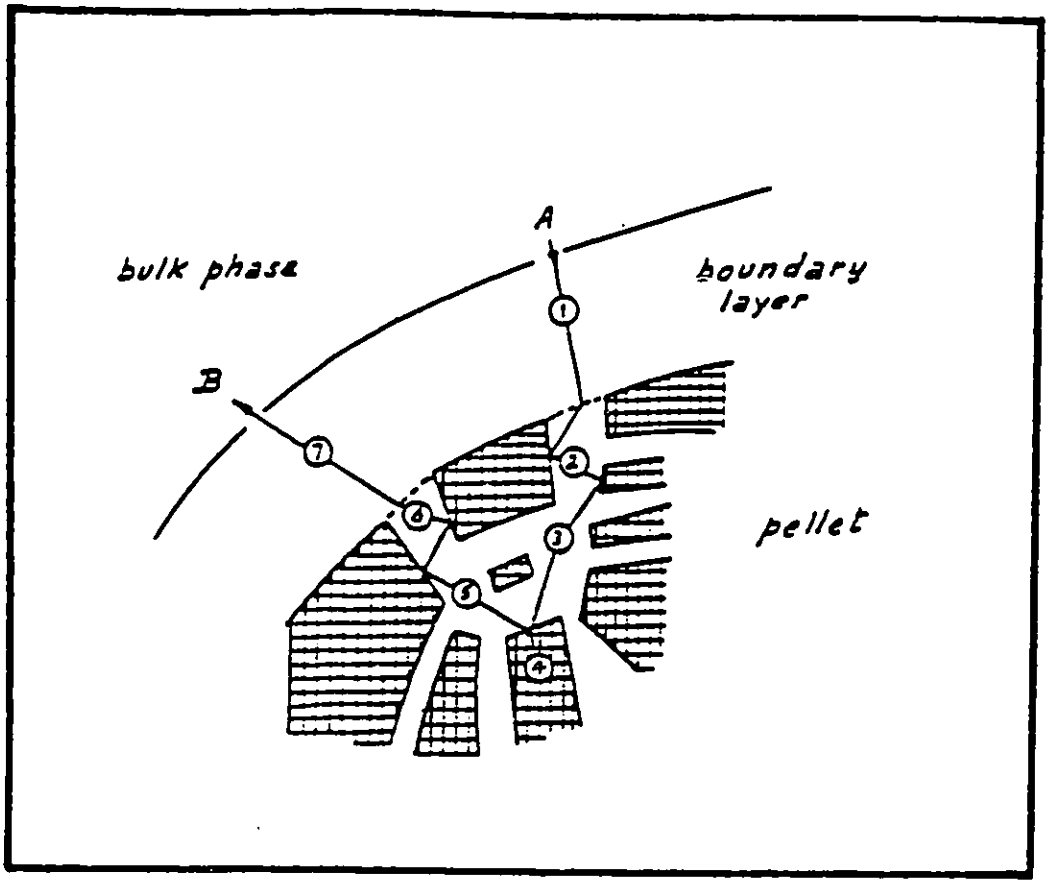

Fig 1.11 Transport phenomena of Heterogenous Catalysis : Physical and Chemical steps (from reference 41)

1- External diffusion

2- Internal diffusion

3- Adsorption of reactant A

4- Chemical reaction

5- Desorption of product B

6- Internal counter diffusion

7- External counter diffusion

Steps (ii) , (iii) and (iv) are usually not distinctly resolved and ideally steps (i) and (vii) should be rapid for reactions that are not diffusion limited. These basic steps are illustrated in Fig 1.11.

1.4.11 ZSM-5 zeolite

This zeolite exhibits a two dimensional network of channels having a structure as illustrated in Fig 1.13. Two pore types exist, intersecting with each other, and both are formed by 10 membered oxygen rings. One pore type varies from 5.1 to 5.5 Å in straight but ellipsoidal rings, the other zig-zags and has circular openings of 5.4 x 5.6 Å. It thus possesses a mean average pore diameter of 5.5 Å with a Si/Al ratio ranging between 10 and 500. Because of its pore structure it exhibits a high degree of shape selective catalysis and has many useful applications in petroleum refining particularly in enhancing gasoline octane when this zeolite is used as a catalyst additive in gas oil cracking.

Many properties of ZSM-5 such as its ion exchange capacity and hydrophobicity are dependent on its chemical composition (Si/Al ratio). Its attractiveness as a catalyst is due to its intrinsic acidity arising from its low aluminum content which can be varied over a large range of concentrations giving rise to catalytic activities that can be predictably changed over many orders of magnitude. ZSM-5 has been shown to be highly active with aluminum contents as low as a few ppm. According to Olson et al, the ion exchange capacity and catalytic activity increase with aluminum content (43).

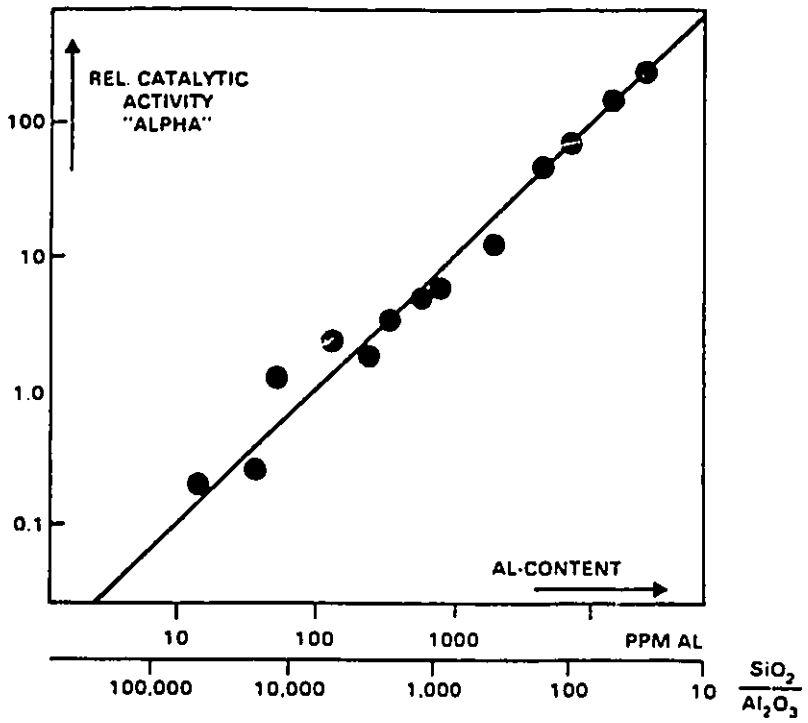

Fig 1.12 Variation of acidic strength (Hexane Cracking) with aluminum content of zeolite (from reference 19)

This is well illustrated by Fig 1.12 which shows the linear relationship between n-hexane cracking activity and aluminum content. On the other hand hydrophobicity increases with decreasing aluminum content.

A lowering of the Si/Al ratio is congruent with an increase in the number of acid sites but according to Barthomeuf et al. as discussed in Section 1.4.8 (40,81) the acidic strength of bridging hydroxyls in SiO(H)Al species increases as the Al content decreases because of the isolated nature of the latter in these

zeolites. From experimental data on the topological densities of isolated AlO_4 tetrahedra in zeolites, Barthomeuf predicted the limiting (lowest) Si/Al ratio for preparing ZSM-5 as 9.5.

The benefits associated with the use of high Silica/low alumina catalysts, particularly in oil refining and organic synthesis include superior efficiency, easier separation and handling, greater stability and environmental factors.

Table 1.3 Large Scale Processes catalyzed by ZSM-5

Petroleum:	
Catalytic Cracking	Distillate Dewaxing
Light Paraffins to Aromatics	Refining
Synthetic Fuels and Chemicals:	
Methanol to Gasoline	Olefins to Gasoline and Distillate
Dehydration of Ethanol	
Chemicals :	
Xylene Isomerization	Toluene Disproportionation
Ethylbenzene Synthesis	

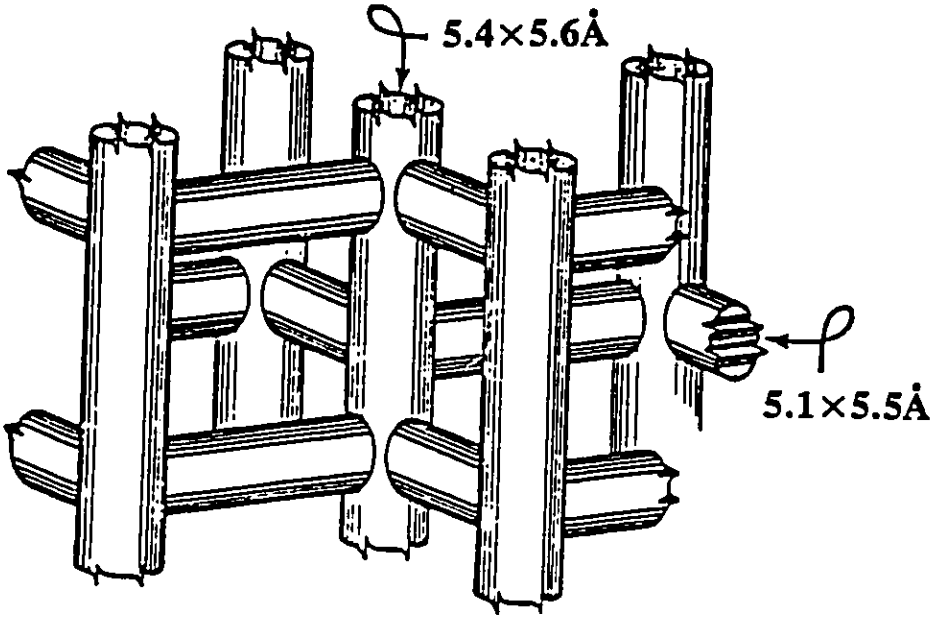

Fig 1.13 Structure of ZSM-5 Zeolite

1.5 OBJECTIVE AND PRESENTATION OF THESIS

Because of the impact on society and industry that an environmentally sound technology provides, while simultaneously satisfying a rapidly expanding market for petrochemical production (particularly the polyethylene to plastic industry), the BETE process was the reaction studied in this work. The primary objective was to develop a catalyst of enhanced acidity which could operate at a lower reaction temperature while still maintaining optimum ethylene yields. An alternative to catalyst development is to develop a reactor which could achieve a high enough yield of the desired product through an alternative technique such as could be achieved through a recycling of the reactant and which would function at a lower reaction temperature.

A good deal of research into catalyst development and optimization for this process (TFSA and Metal loading to increase acidity) has been carried out at the Catalysis Laboratory at Concordia but improved microreactor technology was not examined. The first objective was to develop a catalyst of enhanced acidity (and this resulted in the desilication treatment.) The second objective was to try to improve the reactor technology by the incorporation of a recycle mode of operation and thereafter to combine both technologies by using the reactor for catalytic testing of the newly developed catalyst. However greater emphasis was devoted to the post synthetic development of a novel acidic catalyst, based on the ZSM-5 zeolite.

ZSM-5 is known to possess a large number of medium to weak and a

low number of higher strength acidic sites due to its chemical composition (high Si/Al ratio). Ammonia TPD experiments have also shown the distribution of these sites (54,55,56). The selective removal of silica can provide an indirect route for decreasing the Si/Al ratio of high silica zeolites thereby increasing the amount of tetrahedral aluminum/unit surface area, ion exchange capacity and ultimately improving the acidic properties.

Characterization of the solids formed at every stage of modification is crucial to understanding the nature of the active sites generated and to redirect and improve modifications. Various specific physicochemical techniques such as MAS NMR, XPS and infra red spectroscopy are indispensable for identifying the nature and binding energy of aluminum in modified zeolites. Catalytic activity testing in the dehydration of ethanol to ethylene reaction is the main characterization technique used for assessing the extent of framework insertion of aluminum.

This thesis is presented in 7 chapters. Chapter 1 is a review of the BETE process and a discussion of Zeolites as microporous solids and their properties which make them effective catalysts. Chapter 2 describes the evolution of the desilication treatment to produce desilicated zeolites having a greater number of acidic sites per unit surface area. Chapter 3 is a specific study on the characterization of the nature, concentration and strength of acidity for the desilicated ZSM-5 zeolite of enhanced acidity using ^{1}H MAS and Broad-line NMR. Chapter 4 is the characterization of desilicated ZSM-5 by XPS, ammonia

TPD and poison testing for further correlating the acidic properties. Chapter 5 is the study on the reaction mechanism involved in the dehydration of absolute and aqueous ethanol and a kinetic study of the parent and modified ZSM-5 zeolite from which an apparent activation energy will be calculated and the pre-exponential factor reported. Chapter 6 focuses on the development and optimization of a novel catalytic multipass reactor capable of improving yields in ethylene at temperatures below 180°C. The effect of various reaction conditions such as recycle times, temperature, contact time and partial pressures for the recycle and non recycle modes of operation, the latter corresponding to the adiabatic fixed bed reactor technology, are evaluated in the reaction for the dehydration of ethanol to ethylene.

Chapter 7 discusses the overall conclusions and future projections of this work.

CHAPTER 2

CATALYST DEVELOPMENT AND CHARACTERIZATION

2.0 INTRODUCTION

This chapter describes the development and optimization of the procedure of desilication and the characterization of the desilicated materials formed. The process for silicon removal has been developed as a means of generating solids of enhanced catalytic activities which is a consequence of the higher density of proton sites. Desilication is defined as the selective removal of silicon from highly siliceous materials using a mildly alkaline solution. This invariably decreases the Si/Al ratio in a systematic manner and is a direct means of increasing the cation exchange capacity of the solids (61).

Desilication of commercially available silicalite (165), X, Y and ZSM-5 zeolites is studied for the effect on their textural and chemical properties. Initially the treatment was found to be not reproducible hence, it was necessary to study the effect of temperature fluctuations of ± 10°C on the desilication process. The effect of adjustment of the alkalinity on the reproducibility of the technique was also studied. For economic reasons the volume of solution necessary for treatment was also studied.

The novel desilication treatment, as first developed using an aqueous

solution of sodium carbonate (57) and optimum conditions (58) will be described. A non catalytic application of the desilicated materials, to remove calcium and magnesium ions, as potential detergent builders will then be discussed (63).

2.1 DESILICATION

The application of a strongly alkali solution medium on the one hand represents the conditions of the zeolite synthesis, but on the other hand silicates can be dissolved by alkali (59). The removal of silicon atoms from highly siliceous zeolites (Si/Al > 1) using hot alkaline solutions of either sodium carbonate which hydrolyzes to sodium hydroxide or sodium hydroxide directly results in severe structural collapse (60,61). In addition there is the possibility of other species recrystallizing from the solution especially during the treatment of zeolites with high aluminum content (62). Recently Le Van Mao et. al. developed a technique whereby silicalite and other silica rich zeolites such as NaZSM5, and lower Si/Al ratio zeolites such as X and Y zeolites, were treated with mildly alkali solutions of sodium carbonate in such a way to effect the selective removal of silicon atoms from these structures (57). Silicalite, a pure silica, structural analogue of the ZSM-5 zeolite was first studied to assess the effect of silica removal from high silica materials. These results are only briefly reported in this thesis.

2.2 EXPERIMENTAL

2.2.1 SAMPLE PREPARATION

The ZSM-5 zeolite initially used was the form synthesized according to the method of Argauer and Landolt (52). The details of this synthesis are given in Appendix 1, section A 1.2.7. This sample is hereafter referred to as NaZ. Na-Y (LZY52) and Na-X (13 X) were purchased from Aldrich and Linde respectively. Silicalite was purchased from Union Carbide as S-115 and from UOP as MHZ 420. All samples were used in their powdered, Na forms and were activated at 550°C prior to treatment.

2.2.2 DESILICATION

(a) SILICALITE

Silicalite was treated with a basic solution of 0.8 M sodium carbonate (1g zeolite/30 ml solution) for 4 hours at 80° C with mild stirring. The mixture was allowed to settle and the supernatant decanted and fresh solution added. Subsequent treatments were each performed for 4 hours and repeated until the total time of treatment of the material was 16 hours. The resulting desilicated material was dried at 120°C and characterized after each treatment by atomic absorption for chemical composition, X-Ray diffraction for crystallinity and BET measurements for textural properties of surface area and pore size distribution. These characterization data are reported in Table 2.1.

(b) X, Y and ZSM-5 ZEOLITE

Each sample of activated zeolite was treated for desilication with sodium carbonate (pH = 11.8) as described above. This procedure was repeated 3 times with fresh solution each time for a total exposure time of 12 hours. (Based on the preliminary experiments using silicalite, a total exposure time of 12 hours was chosen, since this resulted in the preservation of the crystallinity of the desilicated materials). The solid was filtered and washed several times on the filter with distilled water. Samples of these solids were dried at 120°C and denoted NaDY, NaDX and NaDZ respectively. The desilicated zeolites were then washed at 80° C with stirring in distilled water (1g/30 ml) for 6 hours to complete the removal of silica as sodium silicate from the medium, changing the wash water after 3 hrs. The samples were dried at 120°C and are hereafter referred to as NaDWX, NaDWY and NaDWZ. Each of these samples was characterized by atomic absorption analysis for chemical composition, X-Ray diffraction for structural identification and crystallinity, and by nitrogen and argon adsorption and desorption measurements for BET and Langmuir surface area and mesopore and micropore size distribution. Table 2.2 and 2.3 report this data. The solids were degassed at 350°C under vacuum at 10^{-3} Torr for at least 12 hours prior to nitrogen and argon adsorption/ desorption measurements. Further characterization techniques including the limit of thermal stability by DTA/TGA analysis and ^{29}Si and ^{27}Al NMR for the configuration of aluminum in the zeolite framework for both parent and

desilicated zeolites were performed.

The experimental details of these various techniques used for physicochemical characterization of all the parent and modified zeolites are described in Appendix 1.

2.2.3 OPTIMIZATION OF DESILICATION PROCEDURE

As a potential means of adjusting the pH of the sodium carbonate solution, sodium hydroxide, of various concentrations was added to the sodium carbonate solution as shown in Table 2.4 and the desilication treatment performed on each zeolite in the way described in 2.2.2(b) (48). The ZSM-5 zeolite used was the commercially available form obtained from Chemie Uetikon (Switzerland) and was activated at a maximum temperature of 450°C. The desilication was also repeated for Y zeolites using higher concentrations of sodium hydroxide (74). Desilication of silicalite (S-115) was also performed but without sodium hydroxide addition. These samples were dried at 120°C and then characterized by similar techniques to those used earlier but also included FTIR. This experimental technique is described in Appendix 1.

Other parameters which might affect the Si/Al ratio of the desilicated zeolite including temperature and volume of the treatment solution were varied independently of each other as follows. Desilication of ZSM-5 and Y zeolites was performed at higher and also lower temperatures (± 10°C), all other parameters were maintained as before and the effect on the Si/Al ratio

determined from atomic absorption. A lower volume (1g zeolite/20 ml solution) of treatment solution was then investigated in the same way (49). These data are not reported in this thesis but a summary is reported in the discussion of the optimized conditions for desilication.

2.2.4.1 CALCIUM AND MAGNESIUM ION EXCHANGE TESTING

The selectivity for calcium and magnesium removal was studied by ion exchange capacity testing as described below and the initial rates of ion exchange of the zeolite samples NaA, NaY and NaX at temperatures ranging from 25 to 60°C were calculated. Then the ion exchange capacities of desilicated X and Y zeolites (prepared as described to produce NaDWX and NaDWY respectively) was investigated.

The ion exchange testing was performed in the schematic shown in Fig 2.1. The experimental set up was designed to simulate the actual working conditicns for detergent powders in washing machines. Hard water (700 ml) was placed in a flask containing a strong stirring bar. The flask was placed in a water bath which was heated at a constant temperature by a hot plate equipped with a magnetic stirrer which achieved a strong and constant stirring action throughout the experiment. The of homogeniety of the exchange media was a key factor for reproducibility of the data. At the specific temperature of the solution, 1.0 g of the zeolite sample was rapidly poured into the flask. This was taken as time zero, after which a 2 ml fraction was removed from the

flask using a fraction collector. Water was added from a reservoir to replace the solution removed in order to compensate for the volume loss. The experiment was terminated after 16 mins corresponding to the residence time of the detergent in the washing machine. A blank test was performed according to the same procedure but without adding zeolite to the solution. The concentrations of Ca and Mg ions remaining in each sample were determined by atomic absorption using external standards and the concentrations were reported in ppm (63). The results reported were average values obtained from two sets of data with not more than 3 % variation.

2.2.4.2 TREATMENT OF DATA

The techniques for data computation are given as follows The concentrations of calcium and magnesium ions respectively (C_{Ca} and C_{Mg}) were plotted against time and a second order polynomial function of the following form was used to fit the data:

$$C_{Ca} = y = a + bt + ct^2$$

The calcium ion removal was expressed as :

$$IR_{Ca}(\%) = [C^i_{Ca} - C^f_{Ca}]/C^i_{Ca} \times 100$$

where C^i_{Ca} and C^f_{Ca} were the initial and final concentrations of Ca ions expressed in ppm. C^f_{Ca} was calculated from the curve by replacing t in the previous equation by 16 (mins). Magnesium ion removal (IR_{Mg}) was determined in a similar way. The total ion removal was expressed as :

$$IR_{tot} \text{ (equiv. based \%)} = [1 - (C^f_{Ca} + C^f_{Mg})/(C^i_{Ca} + C^i_{Mg})] \times 100$$

where all the concentrations were based in ion equivalents. The rate of calcium ion removal (in ppm /min) is equal to the first derivative of the function y :

$$r_{Ca} = dy/dt = b + 2ct$$

The initial rate of calcium removal was determined by taking t = 0. Thus:

$$[r_{Ca}]^\circ = b \text{ (ppm/min)}$$

The rate and initial rate of magnesium removal (r_{Mg} and $[r_{Mg}]^\circ$) were determined in the same way.

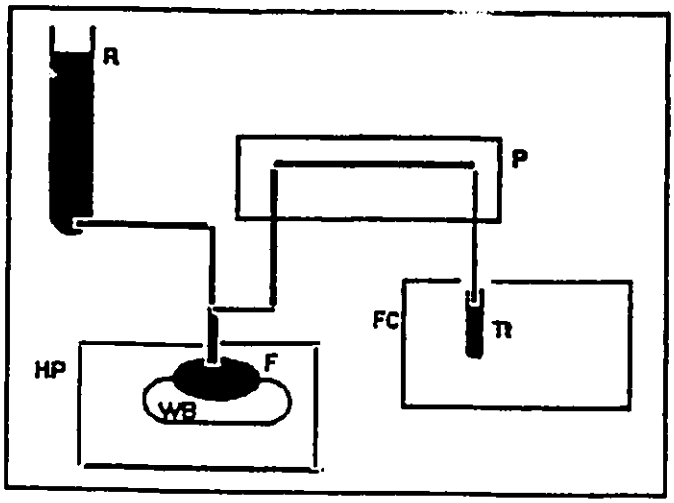

Fig 2.1 Experimental set up for Ca and Mg ion removal from hard water using zeolite powders. R = distilled water reservoir ; P = Peristaltic pump ; FC = fraction collector; Tt = test tubes ; F = ion exchange flask ; WB = water bath ; HP = hot plate

2.3 RESULTS AND DISCUSSION

2.3.1 THE EFFECT OF DESILICATION OF SILICALITE

Silicalite, an almost pure silica (SiO_2) analogue of the ZSM-5 zeolite but having infinitesimal quantities of Aluminum, was treated for desilication. Table 2.1 summarizes the treatment conditions used and physicochemical characterization data. These preliminary findings indicated a significant reduction in the Si/Al ratio of the parent without significantly decreasing the degree of crystallinity or the surface area despite the fact that framework Silicon was being removed. Moreover mesopores are created by this treatment as indicated by the increase in the total volume of Nitrogen adsorbed.

Table 2.1

Treatment conditions and physicochemical characterization data for silicalite.

Sample	Time hrs	% Rec.	DC[a] %	SA[b] (m^2/g)	Vol. N_2 adsorb. Total(cm^3/g)	Si/Al
Silicalite	4		100	405	0.104	125
Silicalite	4x2	65	87	406	0.661	38.4
Silicalite	4x4	74	70	418	0.693	18.2

[a] DC : Degree of Crystallinity ; [b] SA : BET Surface area

Table 2.2 reports the chemical composition of the parent zeolite samples that were studied, the zeolites modified by desilication treatment only and then when the latter were washed in distilled water. It is obvious that this chemical treatment decreased the Si/Al ratio more significantly with the highly siliceous zeolites as follows : ZSM-5 (48%)> Na-Y (46%)> > Na-X (19%).

Table 2.2

Chemical composition of parent and modified zeolites (in % wt/wt on the dry oxide basis)

Sample	% SiO_2	%Na_2O	%Al_2O_3	Si/Al	Na/Al
NaZ	92.2	2.8	5.0	15.7	0.9
NaDZ	81.1	10.5	8.4	8.2	2.1
NaDWZ	86.0	5.4	8.6	8.5	1.0
NaY	63.7	13.6	22.7	2.39	1.0
NaDY	48.7	19.5	31.8	1.30	1.0
NaDWY	50.0	17.2	32.8	1.30	0.9
NaX	47.7	19.6	32.7	1.24	1.0
NaDWX	43.0	20.5	36.5	1.00	0.9

2.3.2 ZSM-5 Zeolite

The Si/Al ratio of ZSM-5 decreased from 15.7 to 8.2. Such a decrease is congruent with the removal of silicon from the framework. When such a sample was washed with distilled water, it was possible to reduce the Na/Al ratio to 1.0 without altering the Si/Al ratio significantly. Presumably, the resulting NaDWZ was fully ion exchanged with sodium. The XRD patterns of the NaZ and NaDZ, from which the degree of crystallinity was calculated, are shown in Figures 2.2 (A) and (B) respectively. From these patterns, the ZSM-5 structure is maintained by the desilicated NaDZ sample and thus the possibility of conversion of the ZSM-5 zeolite into another species is eliminated (62). Table 2.3 reports the textural and adsorptive properties of the parent zeolites studied, as well as crystallinity data after modification. The degree of crystallinity of all the desilicated materials was very close to that of the parent zeolite although the Si/Al ratio decreased by almost 50 % (Table 2.2).

Si^{28} and Al^{27} NMR are also used to study acidity in zeolites. Individual Si atoms adopt geometries consistent with the crystal structures and the number of nearby aluminum atoms, and produces a typical spectrum for ^{29}Si with five peaks corresponding to Silicon atoms with 0 to 4 nearest aluminum atoms in structures with Si/Al ratio > 1. The peaks correspond to Si(0Al), Si(1Al), Si(2Al), Si(3Al) and Si(4Al) indicating the number of Al atoms associated with the framework respectively. From this data the Si/Al ratio may be calculated. Aluminum NMR has been used primarily to observe the presence of

tetrahedrally coordinated (framework) aluminum atoms in zeolites. A non framework aluminum atom produces a signal at approximately 60 ppm. The ^{27}Al NMR spectra reported in Fig 2.3 A-1 and A-2 for NaZ and NaDWZ show that all the aluminum in the desilicated sample remain in the tetrahedral configuration (peak II) since peak I which corresponds to octahedral aluminum (45,46) was not detected in the treated sample. On the other hand, the ratio of I/O peaks from the ^{29}Si NMR spectrum, Fig 2.3 B-1 and B-2 (for which the I and O peaks are associated with Si atoms having 1 [Si(1)Al] and 0 [Si(0)Al] aluminum atoms adjacent in the zeolite framework respectively (45,46), increased significantly, indicating that the framework was enriched with aluminum upon desilication.

There was also some loss in micropore surface area as reported in Table 2.3. Fig 2.4 (b) and Table 2.3 show a slight narrowing of the micropores of NaZ that occurs upon treatment by desilication. However, upon activation at 550°C there was a rearrangement of the pore system as shown in Fig 2.4 (c). On the other hand, there was some enlargement of the existing mesopores as depicted by a broadening of the hysteresis loop of the nitrogen adsorption desorption isotherm for NaDZ as illustrated in Fig 2.5 (b) as compared to that of the parent in Fig 2.5 (a). These isotherm plots for parent and desilicated ZSM-5 zeolite correspond to that of an isotherm type 1, according to the general classification of physical isotherms proposed by Brunauer (29,a), produced by mesoporous solids containing a large amount of micropores.

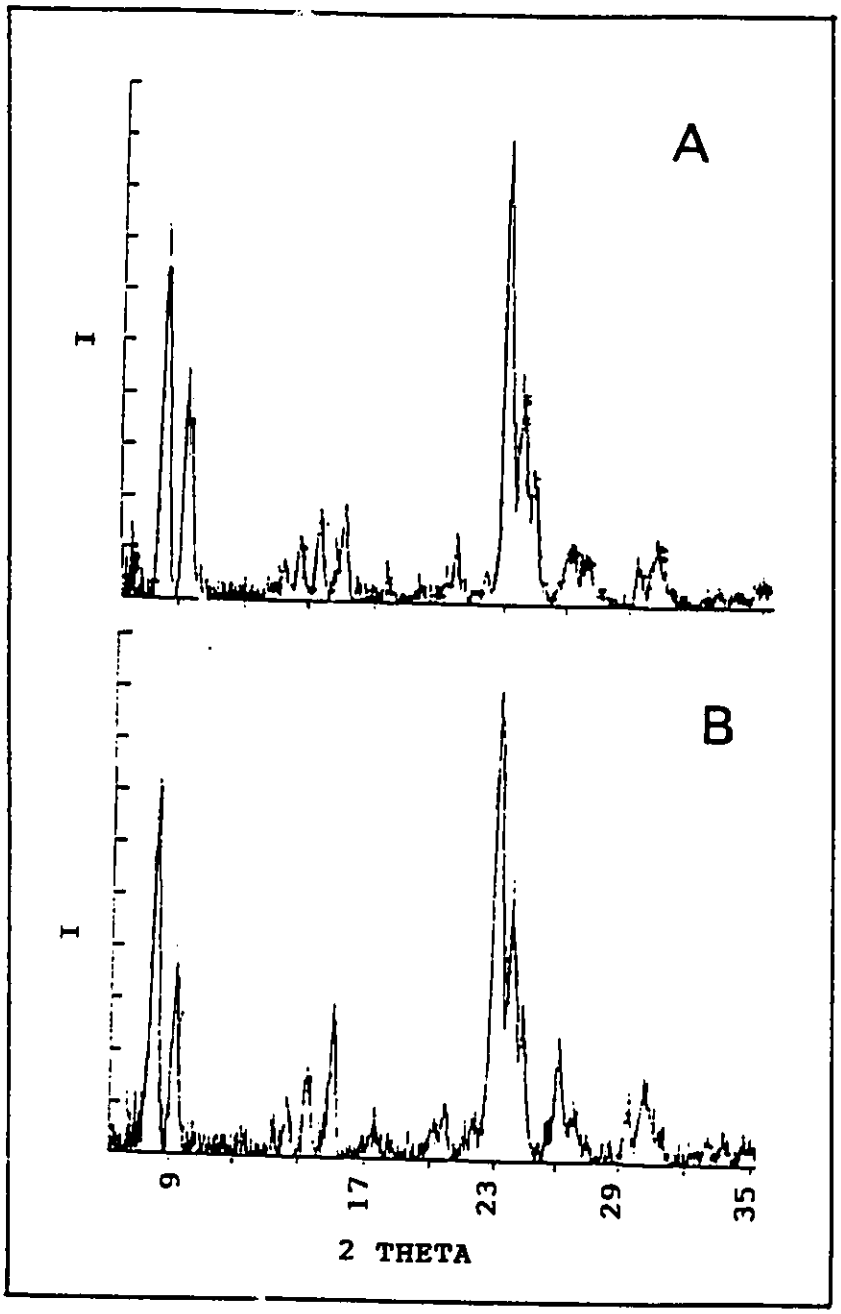

Fig 2.2 X-ray powder diffraction patterns of parent NaZ (A) and NaDZ (B) where I is the intensity in counts per second (cps) vs 2θ in degrees

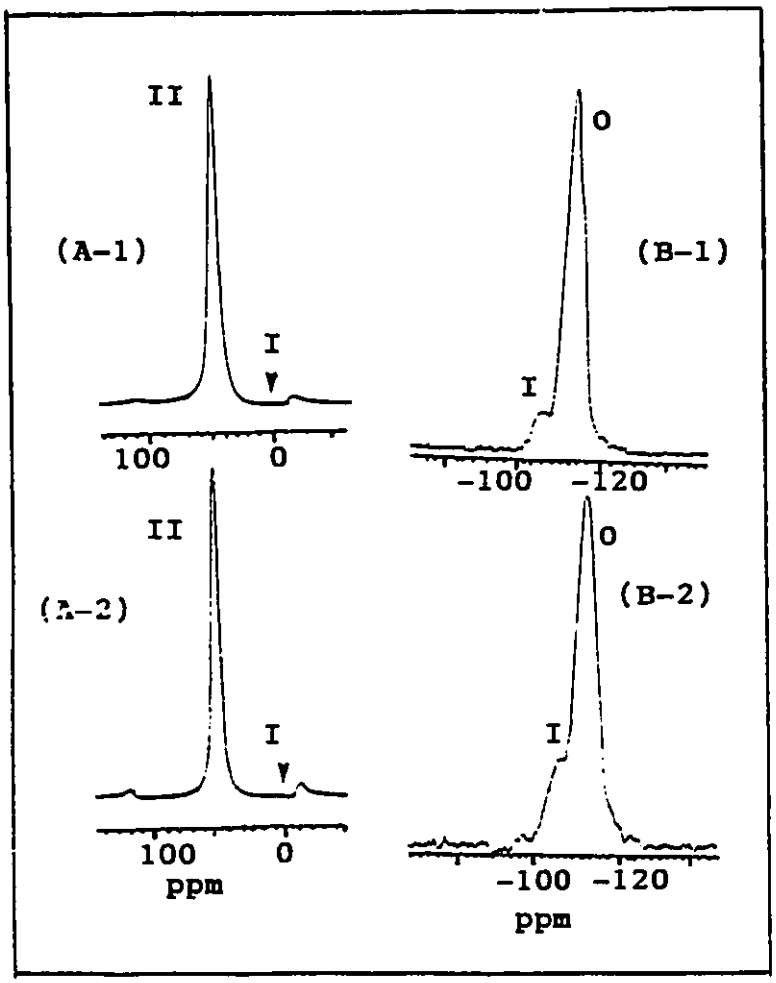

Fig 2.3 ^{27}Al NMR spectra NaZ (A-1) and NaDWZ (A-2) zeolites respectively and ^{29}Si NMR spectra of NaZ (B-1) and NaDWZ (B-2)respectively.

The ordinate axis is in arbitrary units of intensity.

Table 2.3 Textural and sorptive properties of zeolite samples studied.

		NaZ	NaWDZ	NaY	NaDWY	NaX	NaDWX
DC[a] (%)		100	92(90[c])	100	88(95[c])	100	99
BET SA[b] (m^2/g)	N_2	333	338(361[c])	742	701(659[c])	617	675
	Ar	387	404(343[c])	823	792(702[c])	709	805
Langmuir SA[b] (m^2/g)	N_2	450	449(406[c])	996	940(863[c])	833	908
	Ar	425	453(387[c])	929	892(792[c])	794	901
Vol. N_2 adsorbed		0.211	0.359	0.365	0.353	0.314	0.343
(cm^3/g)			0.359[c]		0.319[c]		
Vol. Ar adsorbed		0.187	0.436	0.308	0.296	0.264	0.300
(cm^3/g)			0.357[c]		0.263[c]		
micropores [b,d] (%)		80	64	97	96	96	96
			67[c]		97[c]		
pore size : micropores([e])		0.41	0.40	0.57	0.52	0.52	0.51
			0.39[c]		0.52[c]		
mesopores([f])		5.7	8.0	4.1	5.6	5.3	5.5
			7.9[c]		4.8[c]		

DC[a] : Degree of crystallinity ; SA[b] : Surface Area ; [c] : sample degassed at 550°C for > 12 hours prior to adsorption ; [d] : based on SA N_2 adsorption ; ([e]) and ([f]) average value (nm) from Ar and N_2 adsorption respectively.

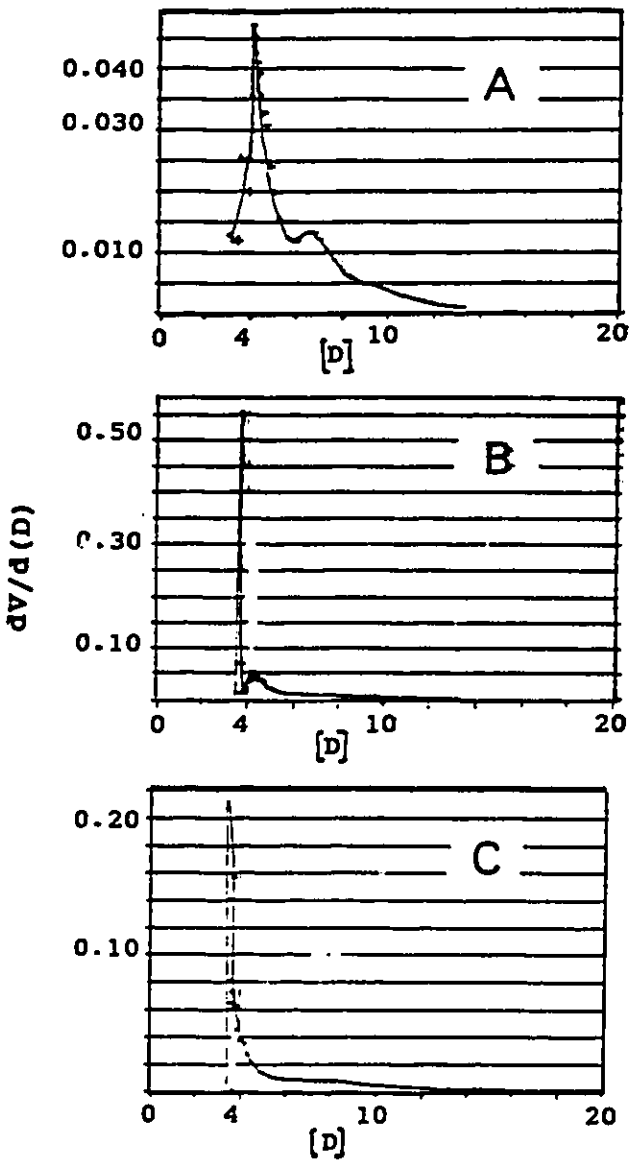

Fig 2.4 Micropore size distribution, dV/d(D) (V = pore volume in cm^3/g of argon adsorbed) vs D (Diameter of pore (Å)) determined by Horvath Kawazoe method. (A) NaZ parent (B) NaDWZ and (C) NaDWZ (activated at 550°C)

The mesopores are slit shape based on the type of hysteresis loop (H4) according to the classification of hysteresis loops proposed by de Boer (29,b). Further experimental evidence of the distribution of pores in both parent and desilicated zeolites is provided by the high percentage (80%) of the total surface area attributed to micropores (Table 2.3).

2.3.3 Na-Y

There was no significant change in the structure and degree of crystallinity of the Y zeolite upon desilication as shown in the X-ray diffractogram of both parent and desilicated Y zeolite (Fig 2.6 and Table 2.3). From the ^{27}Al spectra of both NaY and NaDWY shown in Fig 2.7 A-1 and A-2 respectively, it can also be concluded that all the aluminum remained in the tetrahedral configuration within the zeolite framework of the desilicated sample (45,46), despite the fact that the Si/Al ratio decreased by almost 50% (reported in Table 2.2). On the other hand, the peak IV in the ^{29}Si NMR spectrum corresponding to Si(4)Al, shown also in Fig 2.7 B-1 and B-2 for NaY and NaDY respectively, increased dramatically, obviously at the expense of the other existing configurations of silicon (Si(3)Al, Si(2)Al and Si(1)Al associated with peaks III, II and I respectively) present in the zeolite. This indicates that selective removal of silicon led to a steep increase in the number of silicon atoms having framework aluminum atoms adjacent. As was observed with the ZSM-5 zeolite, desilication generated NaDWY, having micropores which were

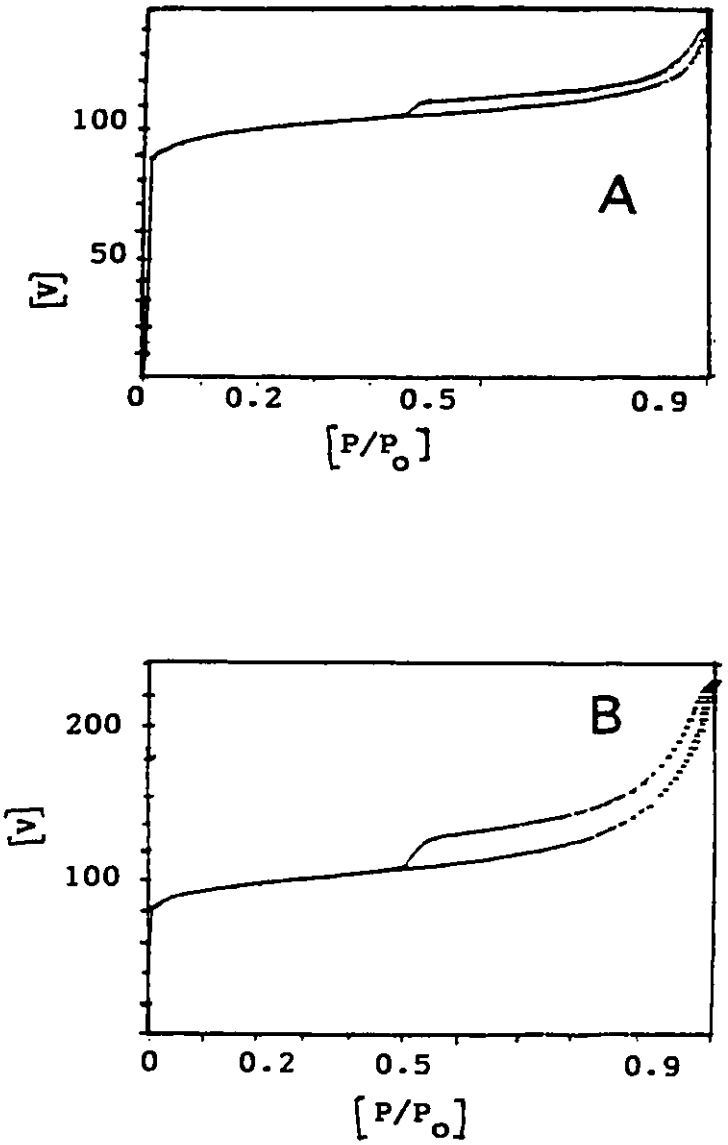

Fig 2.5 Nitrogen adsorption-desorption isotherms for NaZ (A) and NaDWZ (B) showing hysteresis loop. [V] : volume of nitrogen in cm^3/g vs P/P_o : relative pressure

slightly narrower than those of the parent NaY zeolite as shown in Fig 2.8 (a) and (b), and which underwent a similar rearrangement upon activation at 550°C as illustrated in Fig 2.8 (c).

The nitrogen adsorption-desorption isotherms demonstrated for NaY and NaDWY are shown in Fig 2.9 (a) and (b) respectively. The isotherm for NaDWY corresponds to the shape of the Langmuir isotherm and there was no hysteresis loop. It is also apparent that the adsorption and desorption isotherms were almost coincident. This provides direct experimental evidence for the selectivity of silicon removal since the micropore system is well preserved although the density of the aluminum sites was almost doubled with the removal of silicon.

2.3.4 NaX

From the textural and adsorptive data reported in Table 2.3 and other data which show the same trends observed for the NaY zeolite, including X-ray diffractogram, nitrogen adsorption-desorption data and micropore size distribution (50), it can be concluded that the NaX zeolite behaved in a similar way to the NaY zeolite when subjected to desilication. The ^{27}Al and ^{28}Si NMR spectra for the parent and desilicated NaX zeolite (Fig 2.10 A-1 and A-2 ; B-1 and B-2 respectively) confirms an enrichment of framework aluminum after the selective removal of silicon. There was however a less dramatic decrease in the Si/Al ratio than observed for the other zeolites, probably as a result of a lower initial value in this ratio. Thus the effect of silicon removal is less obvious.

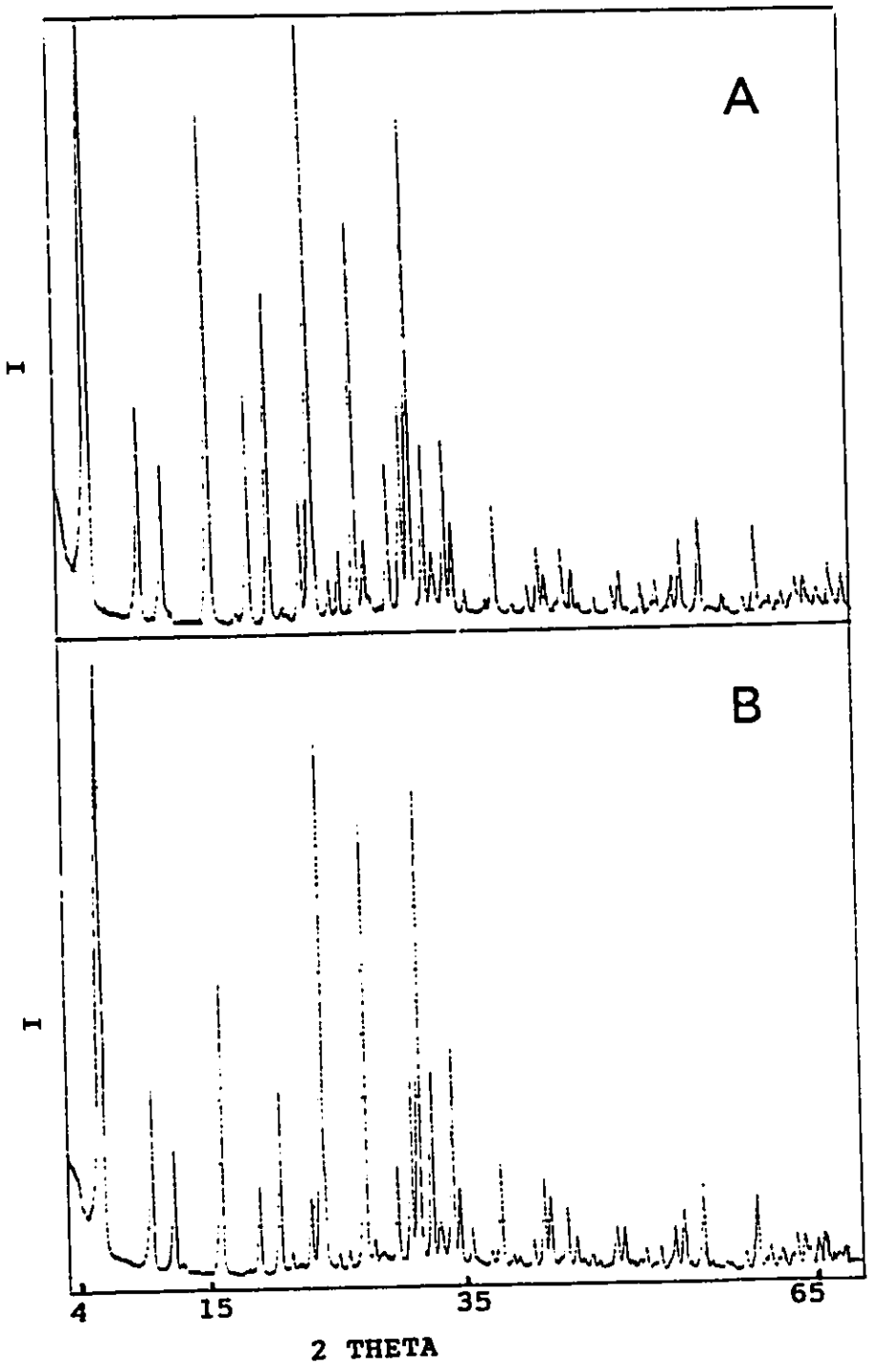

Fig 2.6 X-ray diffractogram of NaY (A) and NaDWY (B). I = Intensity in cpi vs 2θ in degrees.

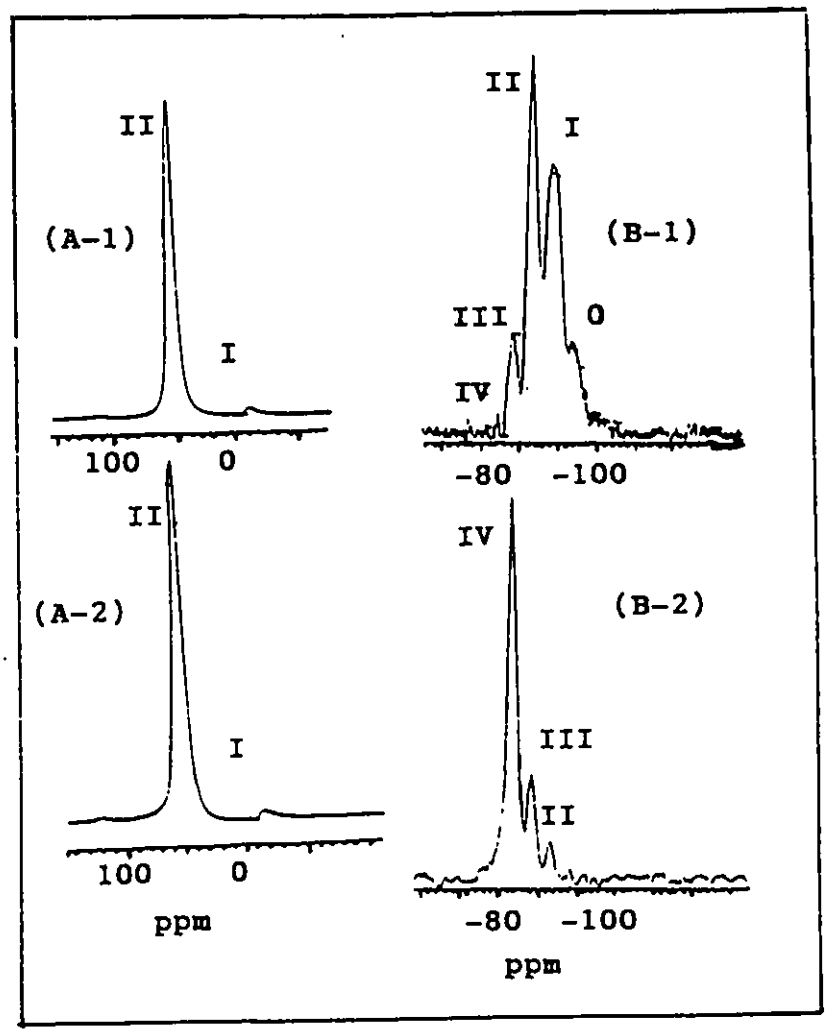

Fig 2.7 ^{27}Al NMR for NaY (A-1) and NaDWY (A-2) and ^{29}Si NMR for NaY (B-1) and NaDWY (B-2). The ordinate axis is in arbitrary units of intensity.

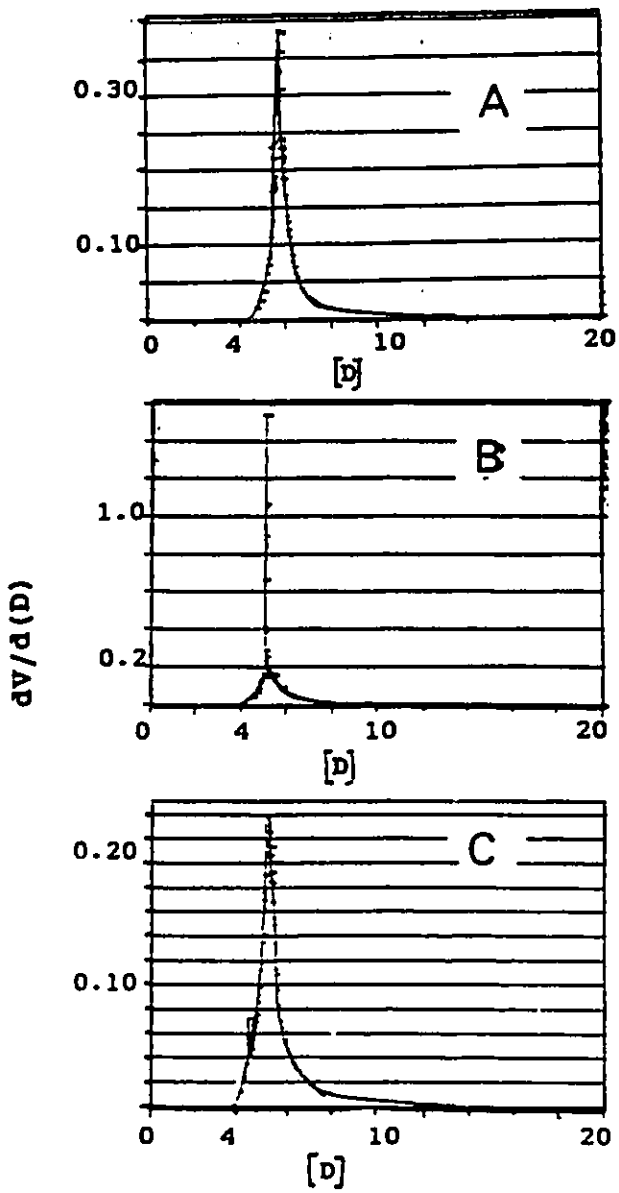

Fig 2.8 Micropore size distribution, dV/d(D) (V = pore volume in cm^3/g of argon adsorbed) vs D (Diameter of pore (Å)) determined by Horvath Kawazoe method for NaY (A), NaDWY (B) and NaDWY activated at 550°C for 12 hrs (C).

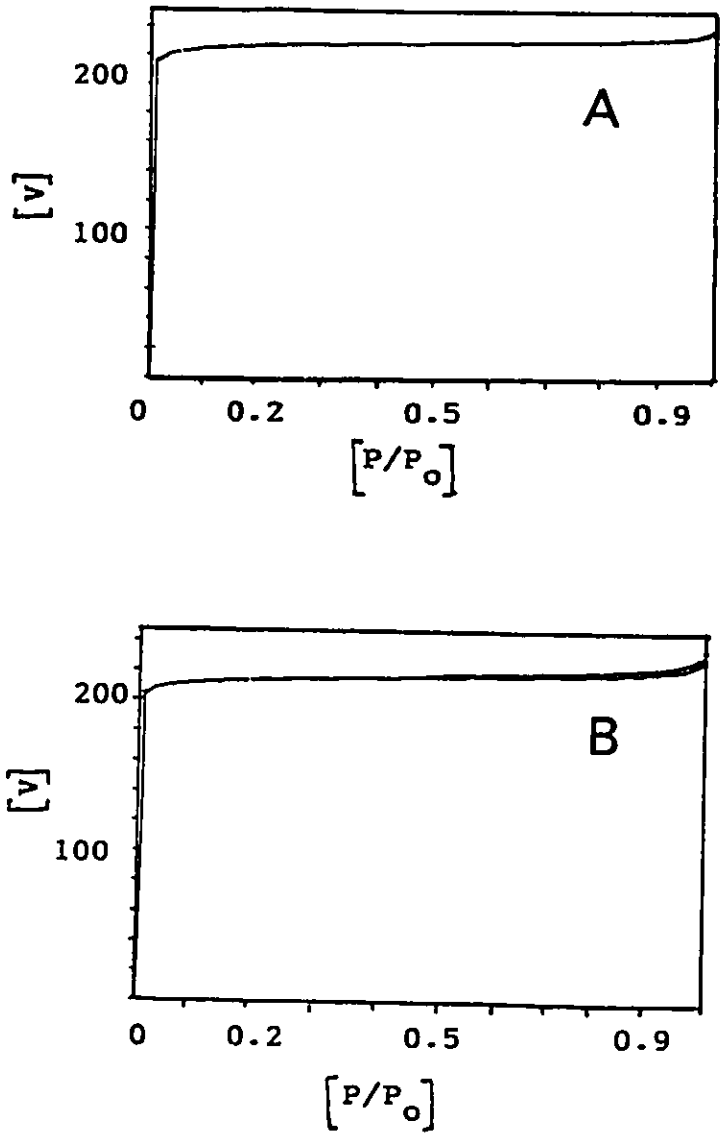

Fig 2.9 Nitrogen adsorption-desorption isotherms for NaY (A) and NaDWY (B).

[V] : volume of nitrogen in cm^3/g vs P/P_o : relative pressure

As already noted, there was some decrease in the size of the micropores upon desilication (Table 2.3 and Fig 2.4 and 2.8) indicative of the formation of some new micropores in all the zeolites studied. This might be attributed to a healing process which occured within the zeolite's framework after the removal of Silicon by base. This verifies that the removal of silicon is sufficiently selective so as not to cause significant structural collapse to the zeolite and decrease surface area, and may actually lead to the creation of new microporosity.

DTA/TGA studies have revealed that the desilicated Y and X zeolites exhibited thermal stabilities as high as the parent forms. This is seen in Fig 2.11 (A) and (B) corresponding to the NaY and NaDWY respectively for which the DTA exotherms were located at approximately 847 and 997°C.

Furthermore the desilicated sample which was activated at 550°C exhibited a degree of crystallinity as high as that of the unactivated sample and the sorptive properties of the activated sample were only slightly lower than the unactivated one (Table 2.3).

However the desilicated ZSM-5 zeolite, in which the DTA exotherms were located at 527 and 697°C, was stable up to *circa* 527°C as shown in Fig 2.12 (B). Available evidence (Table 2.3) indicated that this material only underwent some minor changes in the degree of crystallinity and textural properties when heated at 550°C. It must be mentioned that the desilication treatment does not yield good results when applied to the A type zeolite.

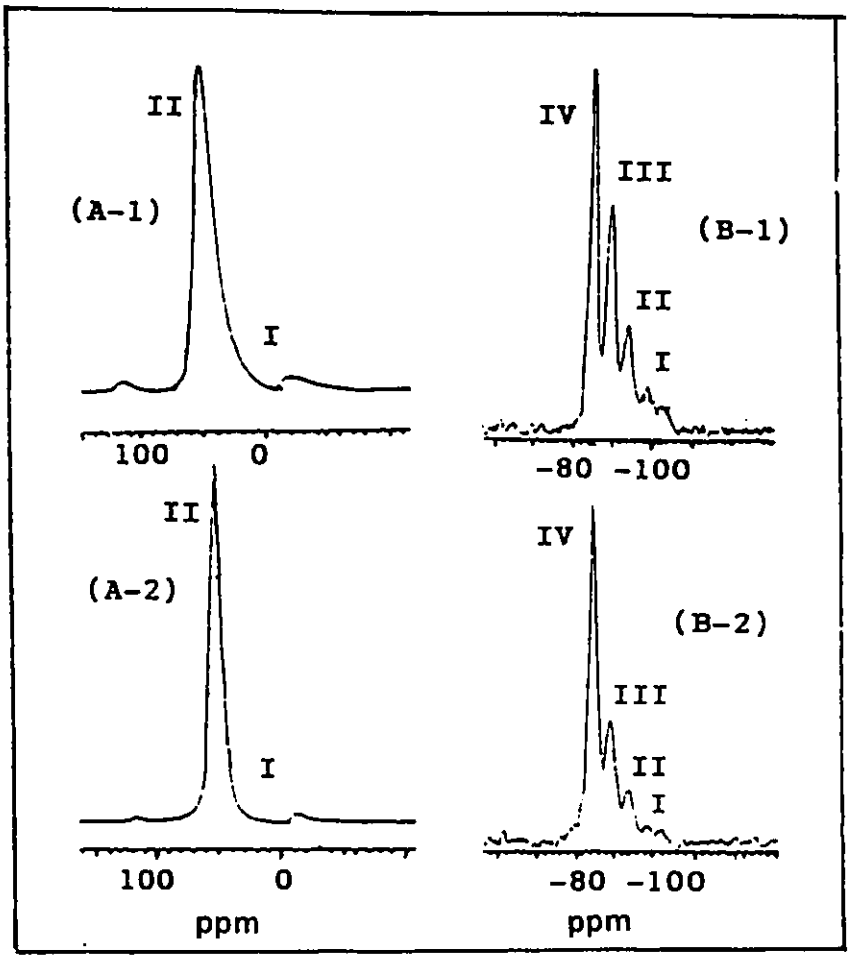

Fig 2.10 ^{27}Al NMR for NaX (A-1) and NaDWX (A-2) and ^{29}Si NMR for NaX (B-1) and NaDWX (B-2). Ordinate axis in arbitrary units of intensity.

Presumably, the lowest value for the Si/Al ratio of materials suitable to the application of desilication is limited to 1.0 (NaA zeolite) which complies with the Lowenstein avoidance principle for aluminum (174).

2.3.5 EFFECT OF pH OF THE SODIUM CARBONATE SOLUTION USED FOR DESILICATION OF ZEOLITES

The use of sodium carbonate solutions to effect desilication, resulted in data which was not very reproducible (48), particularly when X and Y zeolites were treated with sodium carbonate obtained from suppliers other than Fisher Scientific. The aqueous solution of sodium carbonate (anhydrous, Fisher, certified ACS reagent grade) containing the solid to be treated exhibited a pH of 11.5 when measured at room temperature. When this suspension was heated, the sodium carbonate was gradually hydrolyzed and the solution became more alkaline. But the "alkalinity" was consumed by the desilication reaction and the final pH was lower than the initial one. In fact, a lowering of 1 pH unit was observed after desilication of silicalite in a 0.8M sodium carbonate solution for 4 hours.

It should be noted that the pH of the suspension after desilication depended on the type of zeolite to be treated and its Si/Al ratio as well as the extent of desilication. In order to carry out the desilication in a reproducible manner it was necessary to make the sodium carbonate solution more alkaline by adding NaOH (48,58).

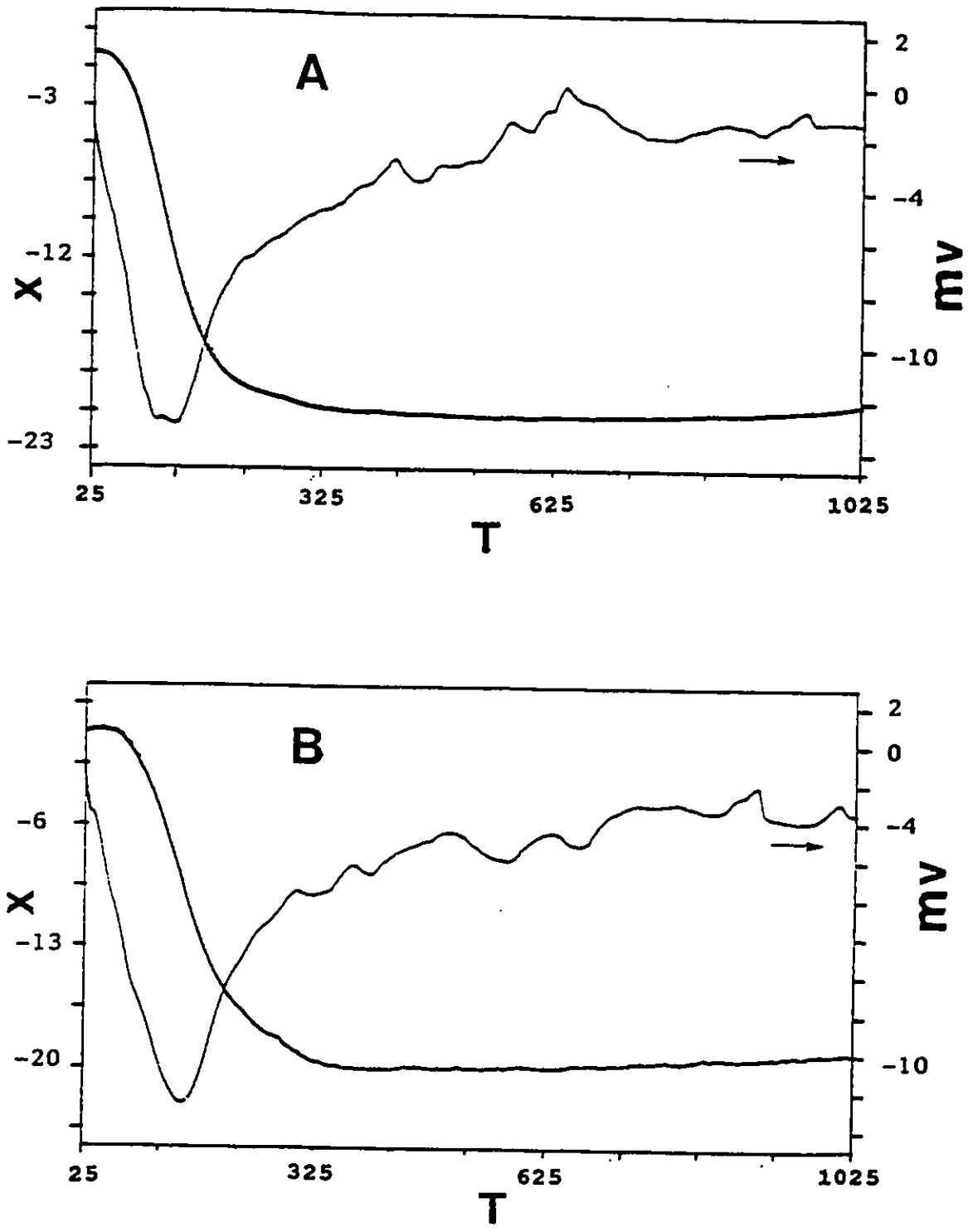

Fig 2.11 DTA/TGA thermograms of parent NaY (A) and desilicated zeolite NaDWY (B) where X = weight loss in % and mv in millivolts vs T = Temperature in °C

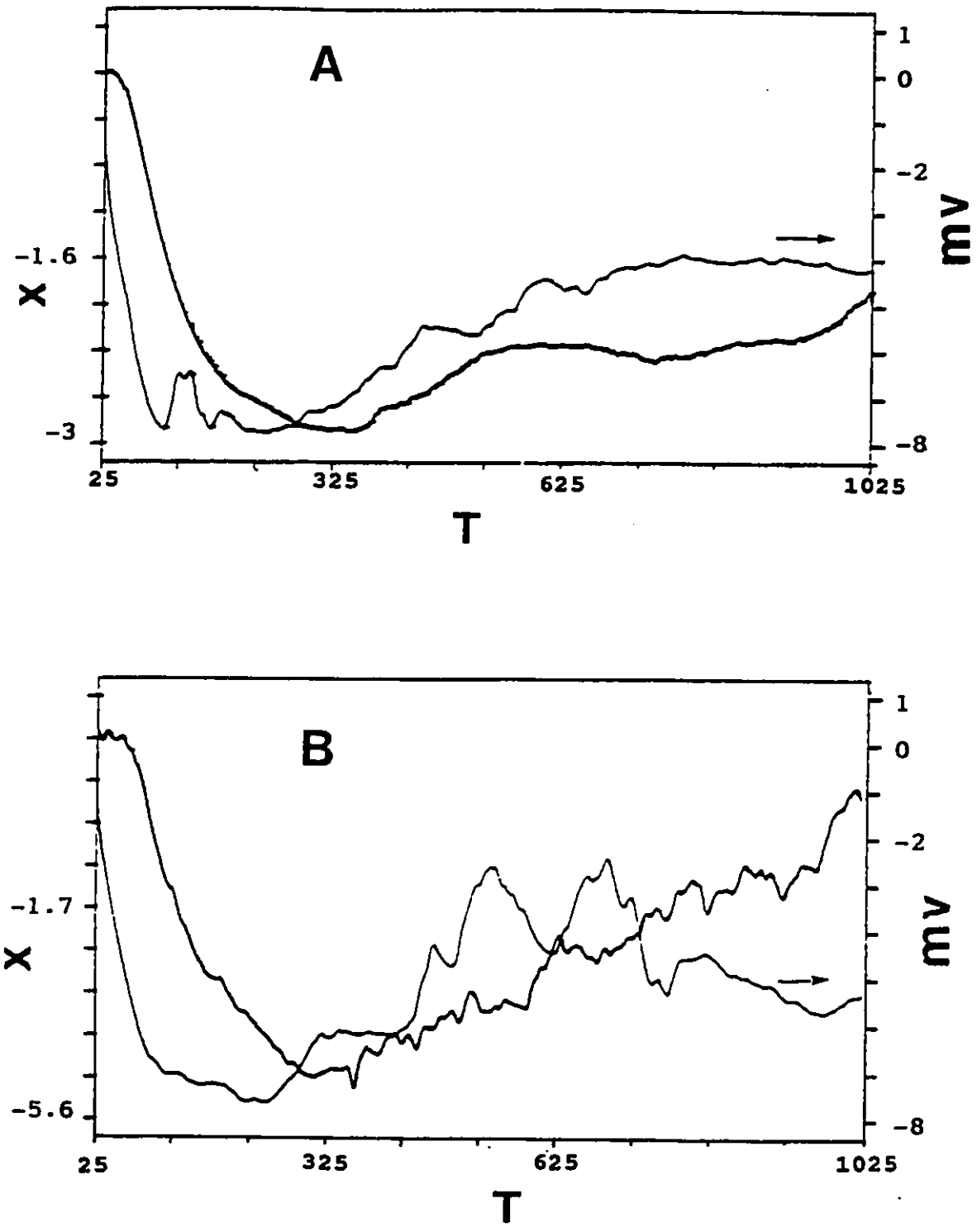

Fig 2.12 DTA/TGA thermograms for parent NaZ (A) and desilicated zeolite NaDWZ (B) where X = weight loss in % and mv in millivolts vs T = Temperature in °C

As a general rule the higher Si/Al ratio materials required a lower pH of the starting desilication solution. With the ZSM-5 zeolite, the best range for the concentration of sodium hydroxide was 0.005 to 0.02 mol dm^{-3} (pH of the starting desilication solutions was 11.7 to 12.1). With the Y zeolites the best range for the concentration of sodium hydroxide added was in the range of 0.1 to 0.5 mol dm^{-3} (pH of the treatment solution was 12.5 to 13.1). Since the Y zeolite has a lower Si/Al ratio, harsher conditions are required to bring about desilication. Silicalite, which has a very high Si/Al ratio did not require the addition of sodium hydroxide for adjustment of the pH of the treatment solution. Table 2.4 shows the influence of pH on the Si/Al ratio and crystallinity of the zeolites after the desilication operation. Table 2.5 reports the adsorption and textural properties of the parent and desilicated zeolites for which the pH was adjusted. All parent zeolites contain some mesopores which are somewhat enlarged by the desilication process. The data indicates that the volume of nitrogen adsorbed by the ZSM-5 zeolite increased significantly while that for the Y zeolite does not change noticeably after desilication although the measured surface areas of both zeolites remains effectively constant. With silicalite which is a ZSM-5 zeolite having a high content of silica, new micropores, of sizes varying between 0.8 to 2 nm, are created by desilication, although the size distribution of these micropores is not as sharp as that of the parent silicalite (50). This is also obvious from the dramatic increase in surface area corresponding to the formation of new micropores. It can be concluded

that desilication of high silica materials can lead to the formation of new microporous materials. It is also possible to prepare a zeolite with a chemical composition similar to that of an X zeolite by desilication of a Y zeolite. In this way one can achieve a lower Si/Al ratio species while maintaining the main textural properties of the starting material.

Fig 2.13 and 2.14 show the FTIR spectra of the parent ZSM-5 (NaZ) and desilicated ZSM-5 (NaDZ) zeolites. The samples were dried at 120°C prior to recording the spectra. Two bands can be distinguished at 970-1100 and 750-820 cm^{-1}, which were assigned by Flanigen and Khatami (79) to the asymmetric stretching and symmetric stretching vibrations of the principal T-O bonds respectively (T denotes Si or Al). It was assumed that these two bands were sensitive to variations in the density of the framework Al sites. In particular, the asymmetric stretching band of the T-O bond shifted to a lower frequency when the content of the framework Al sites increased. A linear dependence of the frequency of this band on the atomic fraction of aluminum in the framework has also been reported (79). A similar relationship between the frequencies of these stretching bands and the Si/Al ratio of desilicated ZSM-5 and Y zeolites was observed and is reported in Table 2.6.

This Table shows the frequency shifts for the main FTIR stretching bands of the T-O bonds recorded for the parent X, Y and ZSM-5 zeolites and for the desilicated ZSM-5 and Y zeolites within the region 400-1400 cm^{-1} (58).

Table 2.4 Physicochemical characterization data after pH adjustment of the Na_2CO_3 desilication solution with NaOH

Sample	C_{NaOH}(M)	[a]pH	% Rec.	% DC	Si/Al
NaZ		11.5		100	19.5
NaDZ1	0.005	11.7	68	84	12.7
NaDZ2	0.01	11.9	68	84	12.2
NaDZ3	0.02	12.1	66	89	11.6
NaDZ4	0.10	12.8	30	43	4.1
NaY				100	2.5
NaDY1	0.10	12.5	67	93	2.2
NaDY2	0.20	12.9	67	91	2.0
NaDY3	0.50	13.1	52	90	1.6
Sil				100	125
Sil-1	0.0	11.5	57	81	30

[a]pH measured at room temperature

[b]DC : Degree of Crystallinity calculated with reference to the parent zeolite

Sil : Silicalite ; Sil-1 Desilicated Silicalite

Table 2.5

Adsorption and Textural properties of parent and desilicated zeolites.

	N_2 adsorbed (cm^3/g)		BET SA (m^2/g)		[a]Pore Size (nm)	
	Total	micropores	Total	micropores	MP	BJH
NaZ	0.348	0.118	359	255	0.58	7.7
NaDWZ1	0.599	0.091	370	194	0.63	9.3
NaDWZ2	0.549	0.116	397	250	0.52	9.4
NaDWZ3	0.625	0.111	396	241	0.58	9.5
NaY	0.365	0.309	742	700	0.74	4.4
NaDWY1	0.414	0.339	765	716	0.73	9.2
NaDWY2	0.347	0.257	684	678	0.73	6.5
NaDWY3	0.395	0.327	755	731	0.72	8.0
NaX[b]	0.274	0.247	571	531	0.74	4.5
Sil	0.104	0.049	405	116	0.62	3.8
Sil-1	0.434	0.105	381	224	0.61	6.7

[a] Micropore (MP) size determined by argon adsorption according to the HK method and BJH is the mesopore size determined by BJH nitrogen desorption method. [b] Commercial NaX zeolite obtained from Linde ; Si/Al ratio = 1.24

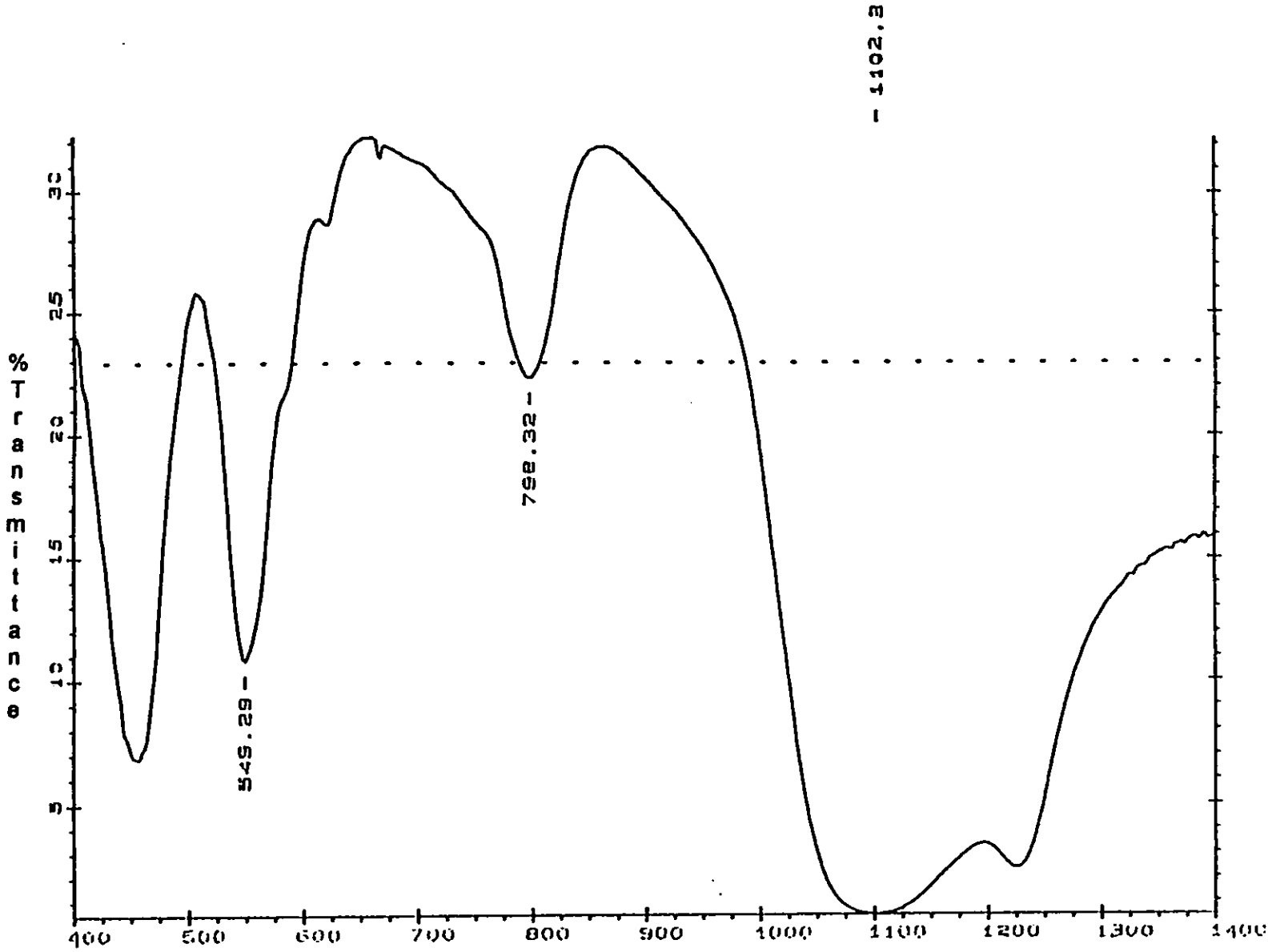

Fig 2.13 FTIR Spectrum of NaZ

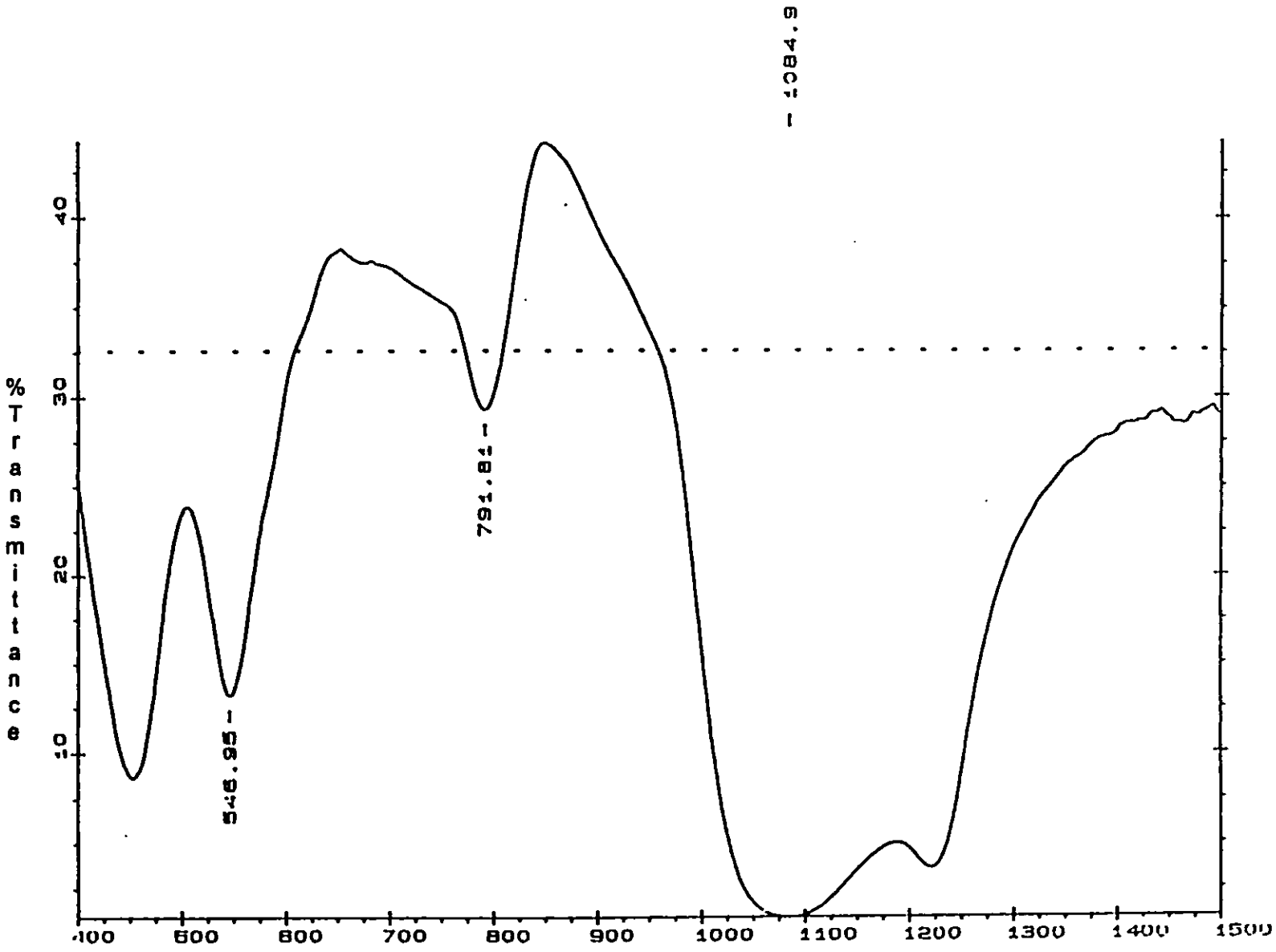

Fig 2.14 FTIR spectrum of NaDZ

Table 2.6 Frequency shifts for the main FTIR stretching bands of the T-O bonds recorded for the parent X, Y and ZSM-5 zeolites and for the desilicated ZSM-5 and Y zeolites[a] within the region 400-1400 cm^{-1}.

Sample	Si/Al	ν_{asym}/cm^{-1}	$\Delta\nu^{b}/cm^{-1}$	ν_{sym}/cm^{-1}	$\Delta\nu^{b}/cm^{-1}$
NaZ	19.5	1102	-	798	-
NaDWZ2	12.2	1085	-17	792	-6
NaDWZ3	11.6	1087	-15	791	-7
NaY	2.5	1011	-	792	-
NaDWY2	1.9	1004	-7	787	-5
NaDWY3	1.6	1000	-11	784	-8
NaDWY4[c]	1.3	989	-22	757	-35
NaX	1.24	985	-26[d]	756	-36[d]

[a] The frequency values in this Table are averaged values obtained with at least two analyses (exhibiting differences not exceeding 3 cm^{-1}) carried out with different pellets (Zeolite + KBR). [b] $\Delta\nu$ = variation of frequency with respect to that of the ZSM-5 or Y zeolite (parent zeolites used as references). [c] Sample prepared under the same conditions as Y3, except for the time of exposure (24 hrs instead of 12 hrs). [d] With respect to the Y parent zeolite.

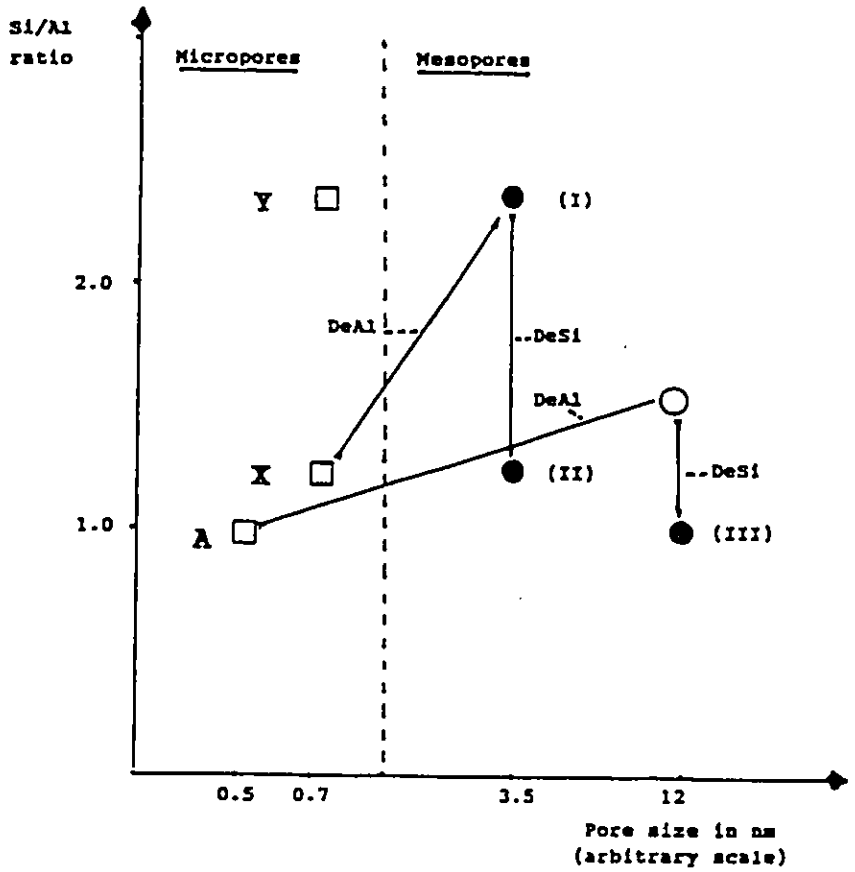

Fig 2.15 Mesoporous homologues of zeolites, I, II and III for the Y, X and A zeolites respectively. DeAl : Dealumination, DeSi : Desilication.

These results for the Y zeolite suggests a possibility of preparing mesoporous homologues of zeolites, by carrying out a sequential treatment as follows :

(a) enlargement of the zeolite micropores by dealumination developed by Le Van Mao et al for alumina rich zeolites (105,106).

(b) adjustment of the Si/Al ratio by desilication of the resulting mesoporous solid.

As depicted in Fig 2.15, mesoporous homologues of X, Y and A zeolites can be prepared for which the main difference between these zeolites and their homologues is the sizes of their pores.

Subsequent studies on the effect of temperature and the volume of treatment solution on the efficiency of desilication, primarily when ZSM-5 and Y zeolites were to be treated, led to the following conclusions. While a 10°C increase in treatment temperature lowered the Si/Al ratio of the desilicated product further, there was a more serious loss in crystallinity as indicated by a lower percent recovery of desilicated product. On the other hand a temperature decrease of 10°C resulted in a lower degree of desilication. It was however possible to lower the volume of treatment solution to 1 g zeolite in 20 ml solution without having any significant affect on the extent of desilication (49). As was demonstrated earlier if the pH of the treatment solution is too high there is severe structural collapse due to the highly corrosive nature of the strongly alkaline media. Additionally, deviations from the optimum conditions

can lead to undesired transformations such as recrystallization into another crystalline form (51) or dealumination and then reinsertion of aluminum into the framework (59).

2.4 APPLICATIONS OF DESILICATION

2.4.1 CATALYTIC APPLICATIONS

The utility of such a treatment is understood from the perspective of the properties of the tetrahedral aluminum site located in the framework of the zeolite. Each tetrahedral aluminum site corresponds to a proton or cationic exchange site, thus an increased framework aluminum content will be congruent with an increase in the ion exchange capacity or (proton) acid density of the desilicated materials. This in turn will confer improved catalytic properties (43,72). Data on the cation exchange capacity (in milliequivalents/g dehydrated zeolite) calculated from the aluminum content and the information obtained from the ^{27}Al MAS NMR is reported in Table 2.7. The maximum temperature of activation without any significant affect on the degree of crystallinity or textural properties of the solids are given in column 3 of Table 2.7.

Table 2.7 Thermal stability and Cation Exchange Capacity (CEC) of zeolites studied.

Sample	CEC(millieq./g)	Temperature of Activation/°C
NaZ	0.98	550-600
NaDWZ	1.69	550-600
NaY	4.45	830-850
NaDWY	6.43	830-850
NaX	6.41	800-850
NaDWX	7.16	800-850

2.4.2 NON CATALYTIC APPLICATIONS

Phosphates are necessary for detergent action since they remove calcium and magnesium ions from washing water. This allows the removal of surfactants to occur during washing, by the processes of solubilization, emulsification and suspension (109). However because of the harmful effects to the environment associated with phosphates in water, there is a need to develop phosphate free detergents.

Zeolites are being widely used as detergent builders, since they are less harmful to aquatic plant life compared to the phosphate builders used in detergents (62,107,108). Other benefits associated with their use include their low cost, their capacity for removal of magnesium and calcium ions which otherwise impede detergent action during washing, and their efficiency of manganese and iron removal from water, which if present can stain fabrics. Thus zeolites are fast evolving as the preferred alternatives to phosphate detergent builders. Zeolite derived phosphate builders may be able to achieve improved performance if their improved ion exchange properties, arising from desilication, could be exploited. The following section discusses the ion exchange capabilities of the modified (desilicated) zeolites.

The enhanced cation exchange capacity of the desilicated zeolite NaDWX is herein demonstrated to be an important property, rendering it even more effective in the removal of calcium and magnesium ions from wash water than the NaA zeolite commercially used in detergent powders (110).

Table 2.8 Ion removal and summary of some physicochemical properties of NaA, NaX and NaY zeolites (given earlier)

	NaA			NaX			NaY		
Si/Al	1.00			1.24			2.39		
CEC[a]	7.16			6.41			4.45		
Pore size[b](nm)	0.42			0.74			0.74		
BET SA (m^2/g)	531[c]			571			742		
Langmuir SA (m^2/g)	716[c]			750			977		
T/°C	IR_{Tot}	IR_{Ca}	IR_{Mg}	IR_{Tot}	IR_{Ca}	IR_{Mg}	IR_{Tot}	IR_{Ca}	IR_{Mg}
25	69.8	92.5	24.3	65.0	71.8	52.5	61.7	69.6	46.0
45	69.7	74.9	59.2	73.2	75.0	69.7	67.7	68.2	66.8
65	81.2	80.2	83.4	80.7	81.0	80.0	66.3	68.0	63.0

CEC[a] Cation Exchange Capacity expressed in millieq./g zeolite assuming that all aluminum sites correspond to cation exchange sites

[b] taken from reference 175

[c] measured on the CaA zeolite.

Although NaA is known to be a highly efficient insoluble ion exchanger capable of removing calcium ions, its removal efficiency for magnesium ions is low (110) particularly at ambient temperature when its exchange rate is low (62). Zeolite X exchanges magnesium rapidly, however, its total ion exchange capacity is low. Mixtures of zeolites X and A have been claimed to exhibit synergistic effects in the removal of Ca^{2+} and Mg^{2+} from hard water (111). The data in Table 2.8 and Fig 2.16 to 2.19 can be summarized as follows :

(i) the total ion removal increases with increasing temperature

(ii) at ambient temperature, the total ion removal depends strongly on the Si/Al ratio and therefore on the CEC of the zeolite for which the following sequence of effectiveness can be discerned : NaA > NaX > NaY. However there was a strong tendency for an increase in IR_{Tot} for the NaX zeolite at higher temperatures. In particular the following sequence was obtained at 65°C : NaA = NaX > NaY.

(iii) At ambient temperature, the Ca^{2+} removal exhibited the following sequence: NaA >> NaX > NaY, which is parallel to the CEC values . However the sequence for Mg^{2+} removal is as follows : NaA << NaY < NaX. This phenomena might arise as a result of pore size of the zeolites as discussed in the following section. Nevertheless, the Na A zeolite became more effective in the elimination of Mg ions at higher temperatures, mainly at or above 65°C.

(iv) The values determined for initial rates (Table 2.9) confirm the trends previously observed.

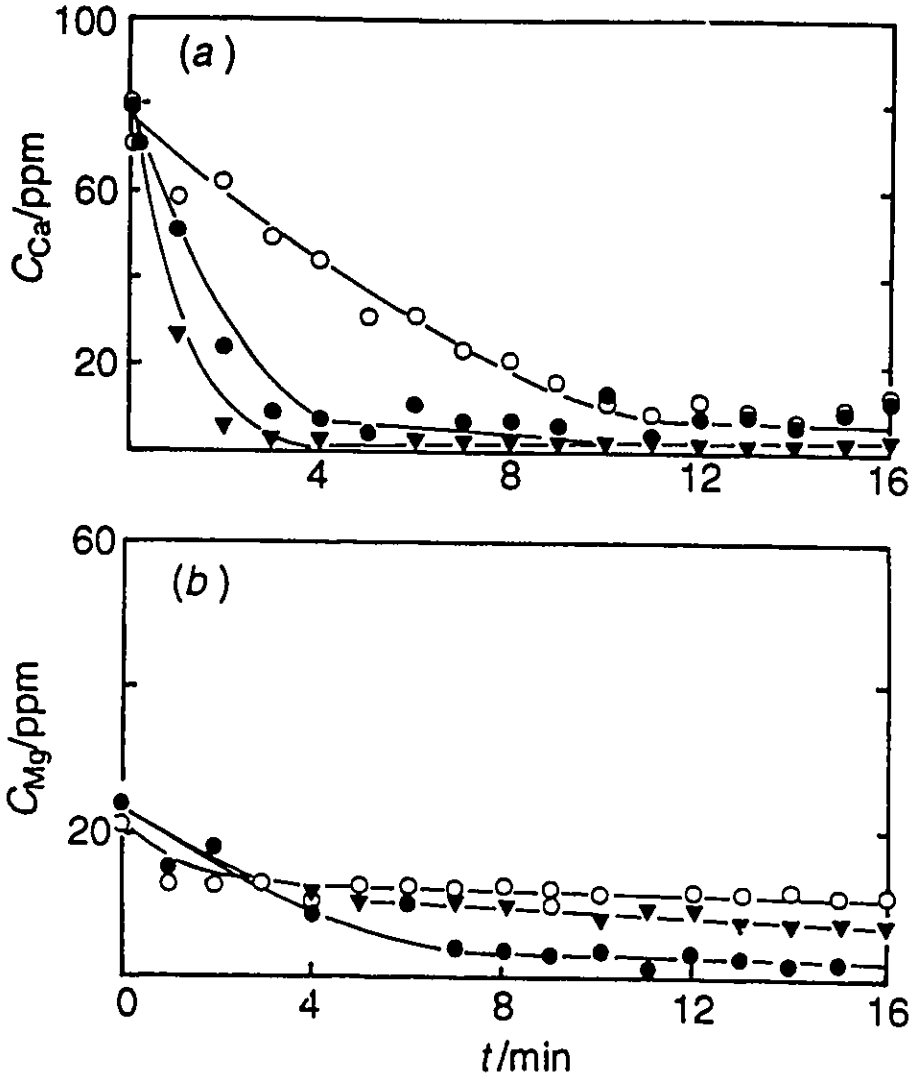

Fig 2.16 Graphs of the concentration of Ca, C_{Ca}, curve (a) and Mg, C_{Mg}, curve (b) expressed in ppm versus time of contact with the solution, t, expressed in min for parent NaA zeolite at different temperatures. (○) : T= 25°C ; (▾) : T= 45°C and (●): T= 65°C.

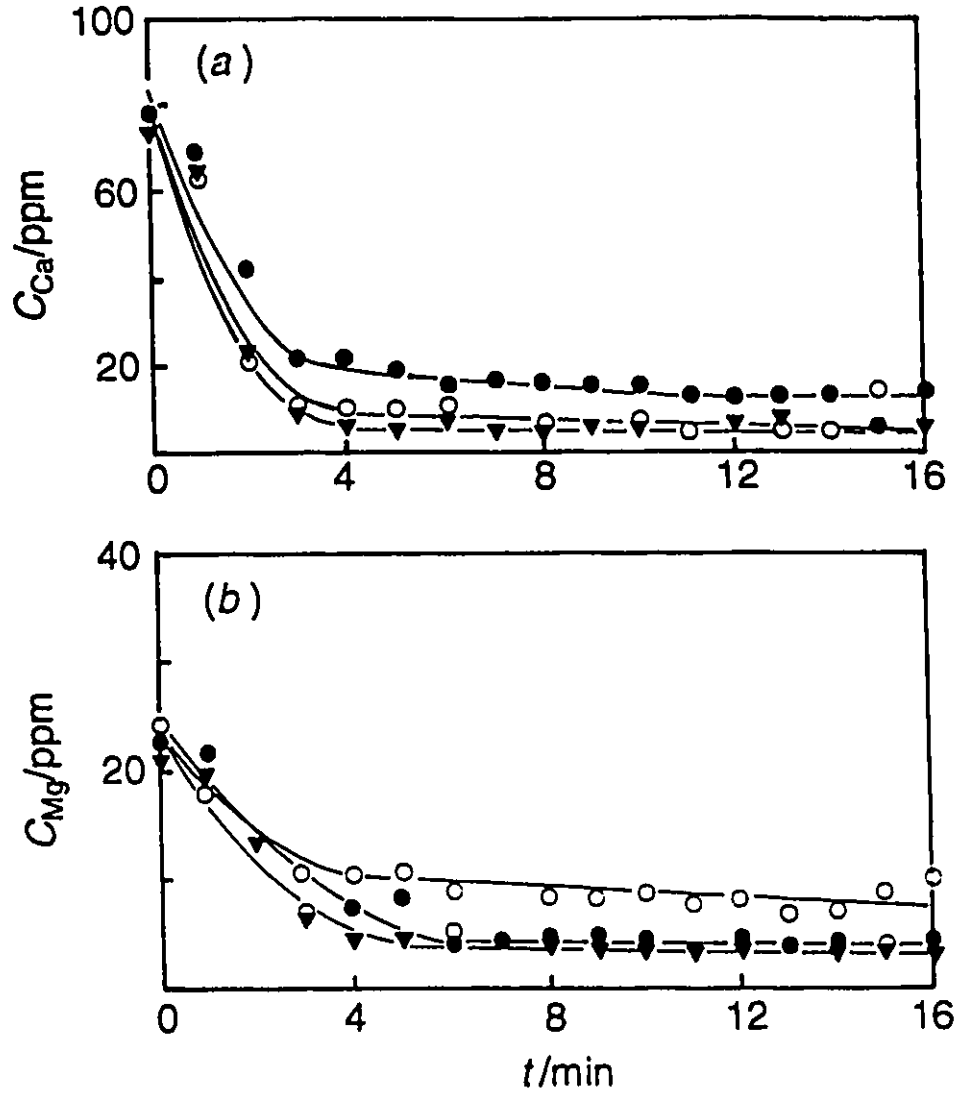

Fig 2.17 Graphs of the concentration of Ca, C_{Ca}, curve (a) and Mg, C_{Mg}, curve (b) expressed in ppm versus time of contact with the solution, t, expressed in min for parent NaX zeolite at different temperatures. (○) : T = 25°C ; (▾) : T = 45°C and (●): T = 65°C.

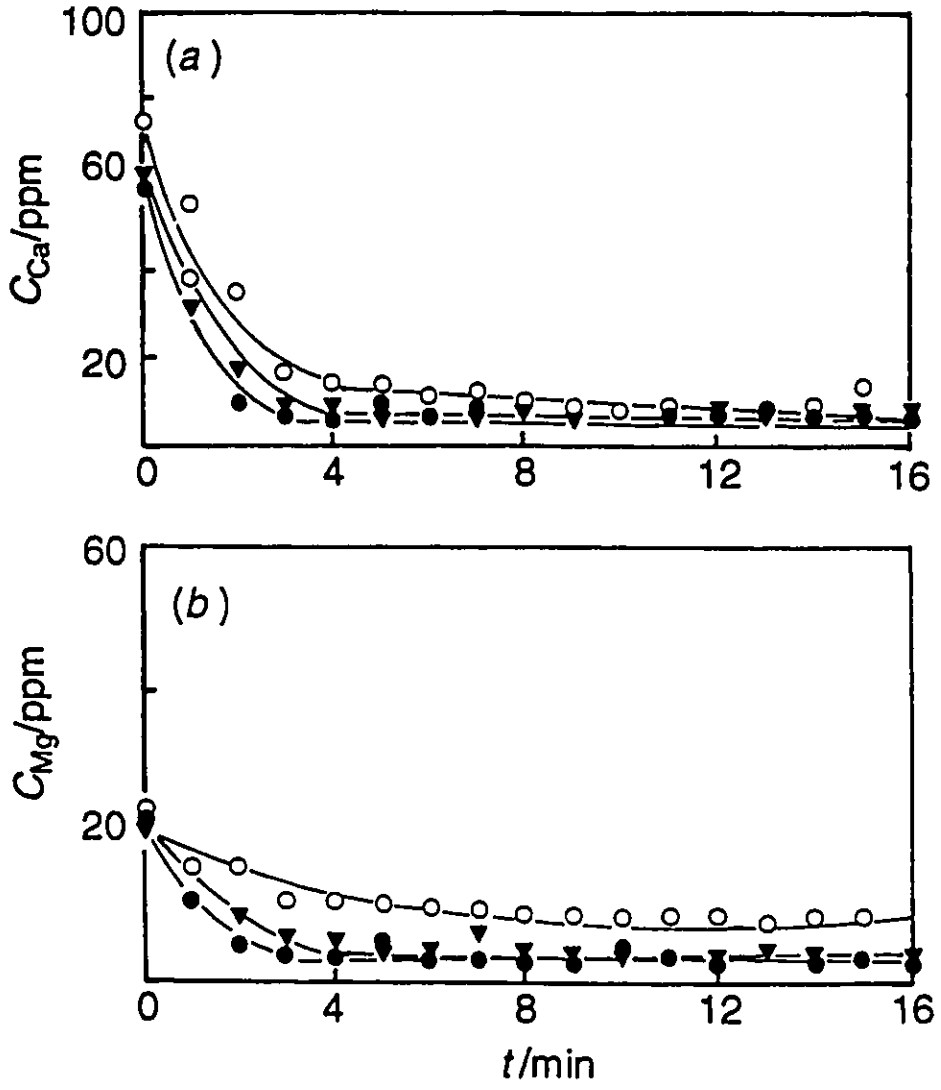

Fig 2.18 Graphs of the concentration of Ca, C_{Ca}, curve (a) and Mg, C_{Mg}, curve (b) expressed in ppm versus time of contact with the solution, t, expressed in min for parent NaY zeolite at different temperatures. (○) : T = 25°C ; (▾) : T = 45°C and (●): T = 65°C.

Table 2.9 Initial rates (in ppm/min) of ion removal for NaA, NaX and NaY zeolites.

	NaA		NaX		NaY	
T/°C	$[r_{Ca}]^{\circ}$	$[r_{Mg}]^{\circ}$	$[r_{Ca}]^{\circ}$	$[r_{Mg}]^{\circ}$	$[r_{Ca}]^{\circ}$	$[r_{Mg}]^{\circ}$
25	-8.1	-0.5	-12.0	-2.9	-10.1	-1.9
45	-10.0	-1.7	-12.0	-3.2	-8.1	-2.7
65	-13.5	-4.1	-11.6	-3.5	-8.2	-2.6

One can readily see that the initial rates of Ca and Mg removal at ambient temperatures, for the larger pore zeolites X and Y, were much higher than those obtained with the smaller pore zeolite NaA.

The initial rate of removal of Mg ions did not change significantly with temperature for the NaX and NaY zeolites. However with the NaA zeolite, this rate was observed to increase dramatically with increase in temperature. This indicates some dependency of the Mg ion exchange rate on the diffusion rate of these ions through the narrow pores of the NaA zeolite (Table 2.8). At ambient temperatures, such diffusion limitations experienced by the NaA zeolites were due to the strong solvation tendency of Mg ions, which have a

high propensity for forming bulky complexes with water molecules (113). However at higher temperatures there was an improvement in the diffusion rates of Mg (and to a smaller extent of Ca ions) through the pore system of NaA, which was reflected in an overall improvement in the total ion removal rate. This may have significant implications in the utility of NaA zeolite as a water softening agent under the warmer temperatures encountered in washing machines. In contrast, the X and Y zeolites, which possess the same open pore structure but different CEC (Table 2.8), exhibited slightly different values for the total ion removal.

Fig 2.19 shows the concentration of Ca and Mg ions remaining in solution versus the time of contact, t, when the NaX zeolite modified by desilication, NaDWX, was used at ambient temperature in ion exchange testing. This zeolite appeared initially to have the same Ca ion removal capacity as the parent NaA zeolite, (Tables 2.8 and 2.10). However it also had a tendency to eliminate Ca at a higher rate at the beginning of the process (at ambient temperature and t=4 mins, C_{Ca} = 30 ppm and 43 ppm for the NaDWX and NaA zeolites respectively see Fig 2.16 (a) and 2.19).

With the modified zeolites, the total ion removal was increased significantly, which is a direct consequence of the increase in CEC (Table 2.8 and 2.10). In particular the NaDWX behaved even better than the NaA in terms of IR_{tot} and IR_{Mg} (almost the same IR_{Ca}). This was due to the fact that the NaDWX had the same CEC as the NaA but a larger pore size.

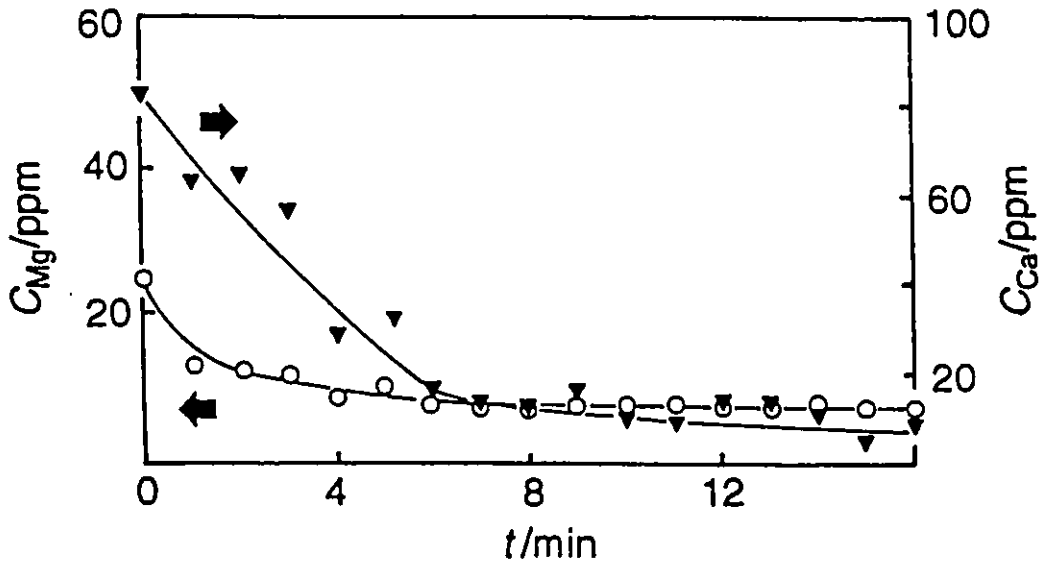

Fig 2.19 Graph of the concentration of Ca, C_{Ca}, and Mg, C_{Mg}, expressed in ppm versus time of contact with the solution, t, expressed in min for modified NaX zeolite at T = 25°C where (▾) denotes C_{Ca} and (○) C_{Mg}.

Table 2.10 Ion Removal properties of desilicated zeolites at ambient temperature.

	Si/Al (CEC) (meq/g)	Pore size (nm[a])	BET LANG[d] (m^2/g)	IR_{Tot} (%)	IR_{Ca} (%)	IR_{Mg} (%)	[c]$[r_{Ca}]^\circ$	[c]$[r_{Mg}]^\circ$
NaDWX	1.00	0.73	595	71.5	85.7	43.1	-10.0	-1.0
	(7.16)	0.72[b]	781[d]					
NaDWY	1.30	0.68	611	65.0	80.4	34.1	-11.3	-0.9
	(6.43)	0.67[b]	802[d]					

[a] average values obtained using HK method

[b] samples activated at 550°C overnight prior to micropore size measurements

[c] initial rates of ion removal are in ppm/min

[d] Langmuir Surface Area

This conclusion is in agreement with the findings by Kuhl and Sherry (113) who found that their low silica NaX type zeolite had the same Ca removing property as NaA zeolite and a much higher aptitude for the elimination of Mg ions. Moreover our desilicated NaX sample had much higher initial rates of removal of both Ca and Mg ions than the NaA at ambient temperatures (Tables 2.9 and 2.10). This can be taken as indirect experimental evidence that the aluminum atoms present in the desilicated NaX zeolite have a tetrahedral configuration, and are responsible for the generation of ion exchange sites, which complements the earlier findings from ^{27}Al MAS (Fig 2.10).

In contrast the NaDWY zeolite exhibited the same total ion removal capacity as the NaX zeolite because of the similar CEC of both materials (Table 2.8 and 2.10). The slight decrease in the IR_{Mg} could be attributed to the pore narrowing of the X and Y zeolites upon desilication (Tables 2.8 and 2.10).

Fig. 2.20 (a) and (b) illustrate the pore size distribution of the parent NaX and modified NaX zeolite respectively and Fig 2.21 (a), (b) and (c) the same parameter for the parent and modified NaY zeolite, and modified NaY zeolite activated at 550°C respectively. In spite of the pore narrowing, there were sharp and symmetrical pore size distribution peaks for both parent and modified zeolites, suggesting a pore system for the desilicated zeolites, which was as homogenous as that of the untreated parent zeolites. Using the new Interaction Parameters (obtained using zeolite standards as described in Appendix 1) for calculation of the micropore size distribution using argon it can be concluded:

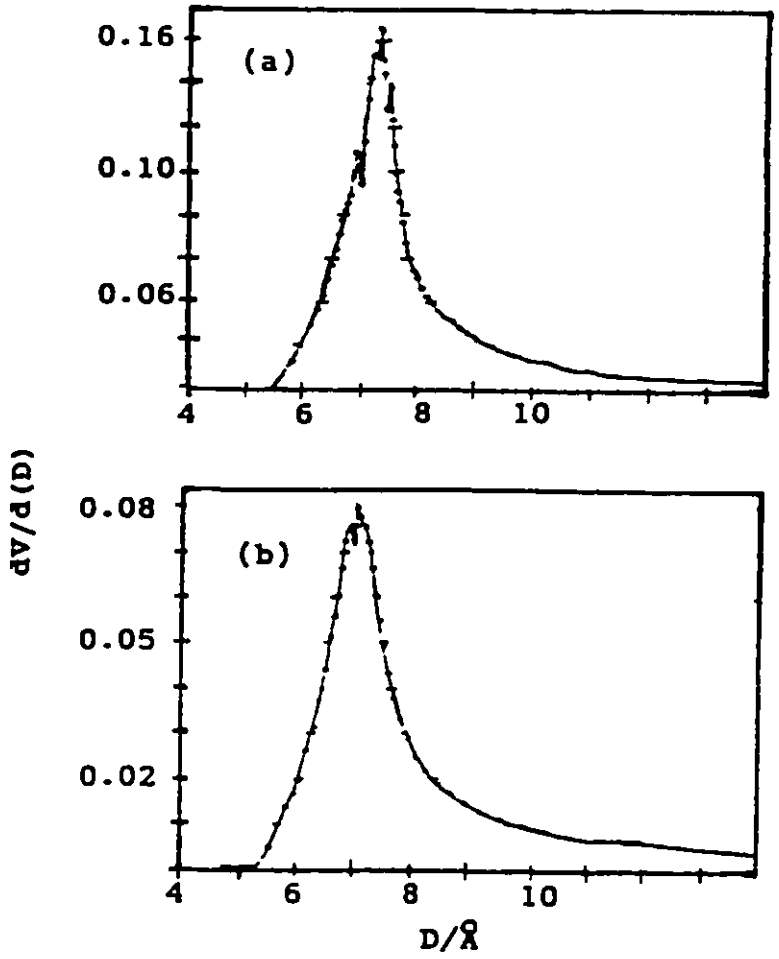

Fig 2.20 Micropore size distribution of parent NaX (a) and modified sample NaDWX (b). dV/d(D) (Pore volume, V, in cm^3/g of argon adsorbed) vs Pore Diameter, D (Å)

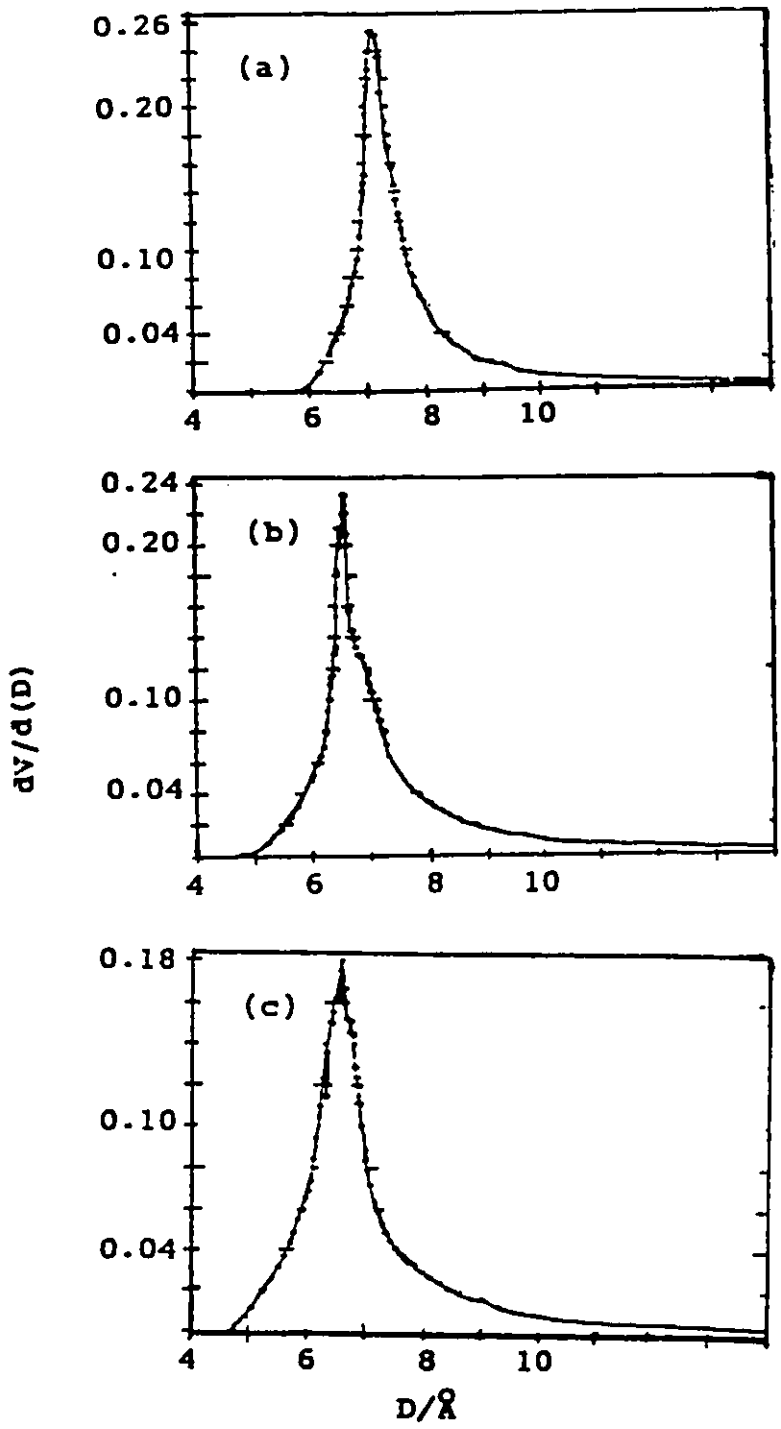

Fig 2.21 Micropore size distribution of parent NaY (a) modified sample NaDWY dried at 150°C (b) this latter sample activated at 550°C (c). dV/d(D) (Pore volume V, in cm^3/g of argon adsorbed) vs Pore Diameter, D, (Å).

(i) there was a significant change in the shape of the peaks for the pore size distribution of NaDWX and NaDWY upon activation at 550°C (Fig 2.21 c), which did not occur when the corresponding parent was subjected to a similar activation under the same conditions. This indicated that there was some rearrangement in the framework of the modified zeolite upon activation at high temperatures, although the average sizes of these micropores did not vary significantly (Table 2.10).

(ii) the NaDWX and NaDWY have the same basic FAU structure as shown from the X-ray diffraction patterns (Fig 2.6); however they both exhibited average pore sizes which were smaller than that of the parent zeolites (0.74 nm). This decrease could be dependent on the extent of Si removal(114).

2.5 CONCLUSIONS

It can be concluded from these studies that desilication of zeolites NaX, NaY and NaZ by treatment with an aqueous solution of sodium carbonate, to which sodium hydroxide is added for pH adjustment, under precisely controlled conditions, results in a selective removal of framework silicon. This results in an increase in the aluminum content without significantly altering the structure and textural properties of the zeolite. The cation exchange capacity and the density of surface Bronsted acid sites increased as the Si/Al ratio decreased. No extraction of aluminum atoms from the zeolite frameworks was detected in this work.

CHAPTER 3

BRONSTED ACIDITY OF A NOVEL ACIDIC SITE FORMED BY DESILICATION OF HZSM-5 ZEOLITE

3.0 INTRODUCTION : CHARACTERIZATION OF ACIDITY : GENERAL

The study of surface sites capable of donating protons (Bronsted acid sites) or accepting electrons (Lewis acid sites) from adsorbed molecules is essential for evaluating the strength and concentration of acid sites in heterogeneous catalysis. The quantitation of acid sites is accomplished by chemical and physico-chemical methods of analysis (87). However the determination of the strength of such sites presents a greater challenge to physical chemists. Moreover it is not known what is the true nature of the species responsible for Lewis acidity.

Cracking of n-hexane by the catalytic test (alpha) reaction gives information on the nature and density of acidic sites (43). It was developed by Mobil researchers to characterize the catalytic activity of zeolites. It compares the cracking first order rate constant for a given catalyst to that of an equal volume of standard amorphous silica-alumina catalyst. Olson et al (43) obtained data on the acidic activity of a series of HZSM-5 zeolites for the cracking of n-hexane at 100°C, showing that the catalytic activity is a linear function of

(protonated) tetrahedral aluminum content even over a four hundred fold increase in aluminum content for Si/Al > 5 (Fig 1.12). Separate experiments have shown that extraframework aluminum has no activity for hexane cracking under these reaction conditions. Tanabe 1970, (80) gave a more detailed discussion on correlations between acid-base properties and catalyst activity and selectivity in zeolites. Hammet indicator methods are traditionally used to give information on the strength of solid acidic sites (86) but because of their bulky size, their use for zeolites is limited because of accessibility limitations, except when one is interested in acidic properties of the external surface of the zeolite particles. Acidic catalysts are characterized by the negative value of H_o, the most negative value corresponding to the strongest acidity. H_o represents the tendency of a site to donate a proton to an indicator (123). Infra red spectroscopy studies in the region 200-1500 cm^{-1} are a sensitive tool for indicating structural features and acidic properties of zeolites. After adsorption of basic probe molecules, like pyridine, changes in the IR spectrum occur. The classical spectrum of coordinately bonded pyridine is very different from that of the pyridinium ion formed by proton transfer from a Bronsted acid site. Depending on the strength of the acid site, the presence of H bonded pyridine shows up as a band at 1400-1447 cm^{-1}, coordinately bonded pyridine as a band at 1447-1460 cm^{-1} or the pyridinium ion which appears at 1485-1500 cm^{-1}. This technique permits a distinction between Bronsted and Lewis acid sites and also gives an assessment of their relative quantities. It must be noted

however that the technique is limited by the capacity to emulate actual reaction conditions, since this may vary immensely from the conditions of spectroscopic studies, especially for the presence of water vapour under one set of conditions and not for the other (87).

Since the acidic strength depends on the electronic charge of the hydrogen atom of a bridging hydroxyl group, it can be measured by NMR. ^{1}H NMR at 300K allows detection of the nature of acidic sites on the zeolite surface (81,87,115,116), and provides quantitative information on Bronsted acidity, structural defects, and also on realumination and dealumination of zeolites, since in the H form of zeolites, the number of framework aluminum atoms is equal to the number of acidic OH groups (158). Broad line NMR at 4K provides a means for measurement of the strength of various acidic sites (39,84,91,117). Simulated spectra, fitted to experimentally determined half derivative absorption spectra of samples, onto which different amounts of water are adsorbed, allows the calculation of an ionization coefficient.

3.1 THEORETICAL BASIS FOR CHARACTERIZING ACIDITY BY ^{1}H MAS AND 4K NMR.

High resolution ^{1}H MAS NMR provides qualitative information on the local environment and geometric relationships of protons as the isotropic chemical shift for which the direct dipolar interactions are averaged to zero. The number of Bronsted acidic sites/unit cell can be estimated from a simulated

MAS NMR spectrum of the anhydrous sample and the different types of acidic sites detected from their respective chemical shift values.

Experimentally determined and simulated broad line ^1H spectra of solid acids at 4K, has been demonstrated to depend on the interaction of their Bronsted acid sites with adsorbed water, and the weighted contributions of each of the possible oxygen-protonated species formed can be calculated. These species are represented by different magnetic configurations of protons possessing specific geometries, such as H_3O^+, $H_2O...HOZ$, H_2O and ZOH where Z is zeolite and OH corresponds to the hydroxyl group of silanol (Figure 3.1), which are theoretically formed through the interaction of adsorbed water and zeolite according to the following equilibrium :

$$ZOH + H_2O \rightleftharpoons Z\text{-}OH\cdots OH_2 \rightleftharpoons ZO^- + H_3O^+$$

These magnetic configurations of spin 1/2 are identified on the basis of the Direct Dipolar Magnetic Interaction between two protons separated by a distance r.

$$DDMI = \text{constant } (1\text{-}3\cos^2\theta)\, r^{-3}$$

Fig 3.1 illustrates the geometries of the various oxygen protonated species formed through the interaction of the acidic surface with adsorbed water. The

protons on H_2O are represented by the two spin configuration of water molecules remaining which do not interact with OH groups, and also for some OH groups. Hydroxonium ions, H_3O^+ are represented by a three spin species at the apices of an equilateral triangle. The three spins at the apices of an isosceles triangle represents groups formed from a water molecule hydrogen bonded to an OH or for hydroxonium ions hydrogen bonded to oxygen atoms of SiOH in the framework. A Gaussian function is used to describe the resonance of a set of OH groups and a Lorentzian function represents some particular sets of diluted OH (64,180). The parameter of each Gaussian, R is the shortest H-H distances of distinct configurations. r is the intra-configuration H-H distance parameter of H_2O and H_3O^+ (Fig 3.1), (157). The acid strength is evaluated through simulation of the broad line spectra for a series of concentrations of water adsorbed onto the zeolite. This is achieved by curve fitting the experimental spectrum, from which the weighted contribution of the different proton species is calculated. The ionization coefficient, defined as the number of hydroxonium ions (H_3O^+) per unit cell, formed when the number of water molecules adsorbed is equal to the number of BAS per unit cell of the zeolite, is calculated as a means of ranking the acid strength. It is also possible to estimate the hydrogen bond lengths ($\pm$ 5 pm) in each distinct configuration based on the direct dipolar interaction between their protons (39). This gives an estimate of bond strength. The acidic properties of the parent and desilicated zeolite, HZ and HDZ respectively, were studied by this technique.

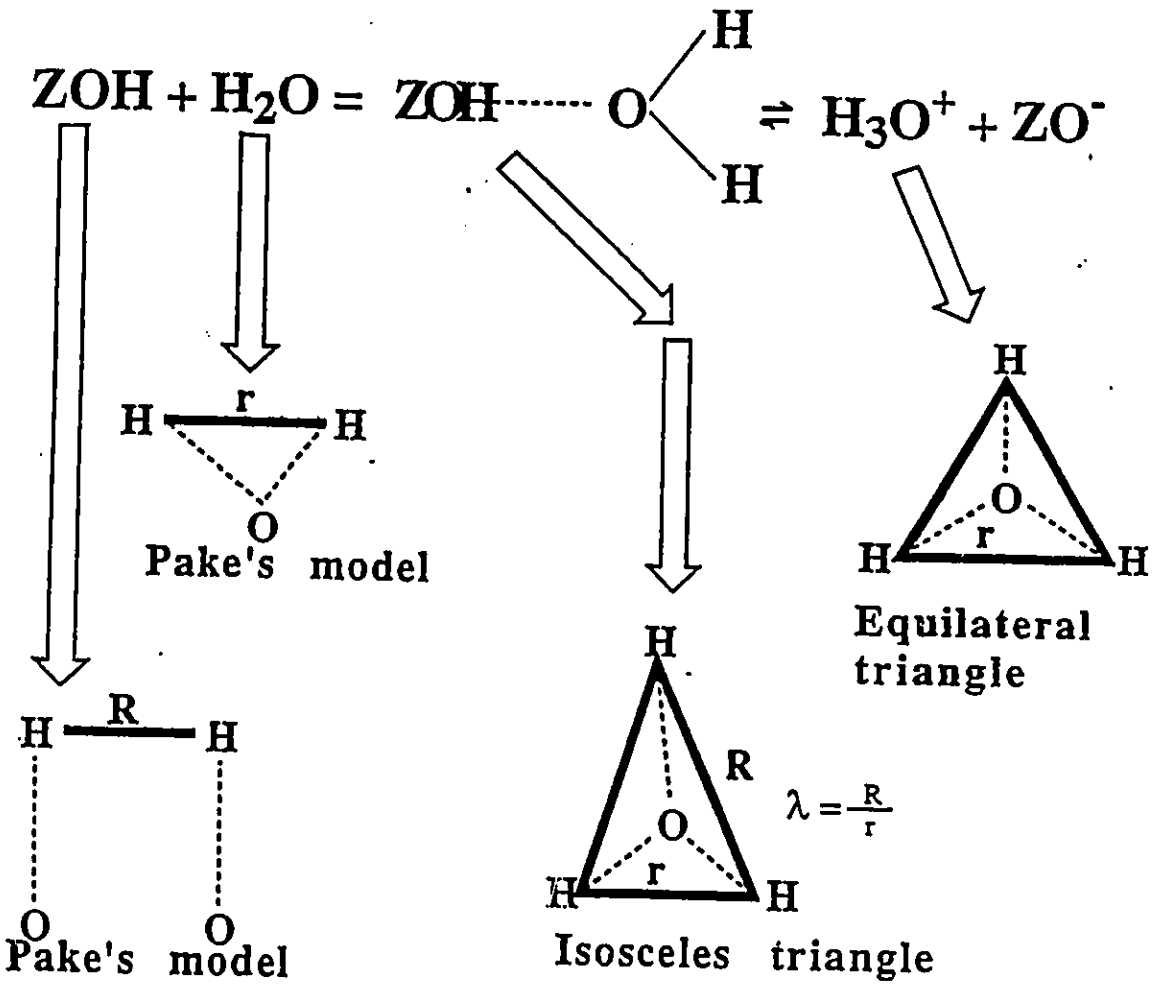

Figure 3.1 Magnetic configurations of oxygen protonated species

3.2 EXPERIMENTAL

3.2.1 SAMPLE PREPARATION

Commercially available samples of the ZSM-5 zeolite suffer from the many drawbacks associated with mass production, such as a high degree of inhomogeneity in the pore sizes and shapes. This results in a large pore size distribution, a lower crystallinity resulting from the increased amount of amorphous phase present and a lower thermal stability. ZSM-5 is less availabile commercially, and is inevitably higher priced. A typical laboratory synthesis according to Argauer's and Landolt's patent requires 10 days (52) and the relatively small batch (100 g) of NaZSM-5 synthesized using the autoclave facilities at Concordia University were factors contributing to the use of commercially available zeolite.

3.2.1.1 PRETREATMENT OF THE COMMERCIAL ZSM-5

The commercially available NaZSM-5 zeolite was obtained from Chemie Uetikon, Switzerland. The optimum temperature used for activation in air was determined from DTA/TGA thermograms performed on the unactivated zeolite and was further investigated by BET analyses. The activated sample is hereafter referred to as NaZ. BET analyses were also performed on all forms of this zeolite (NaZ, HZ, NaDZ and HDZ) activated at various temperatures to ascertain their limits of thermal stability (Table 3.1). The experimental details of these techniques used for characterization are described in Appendix 1.

3.2.1.2 ACIDIC FORM OF ZEOLITES

The acidic forms of both zeolites were prepared by repeated ion exchange with a 5 wt % solution of ammonium chloride at 80 °C with stirring. Each treatment lasted for 1 hour after which the spent solution was decanted and fresh solution added (1g zeolite in 10 ml solution). The procedure was repeated for 7-8 times, after which the solid was washed on the filter several times with double deionized water and dried at 120 °C (53). The final form was generated by activation at 450 °C overnight in flowing air, as previously described (53). A sample of the desilicated zeolite prepared as described in Chapter 2 using 0.8 M sodium carbonate solution and dried overnight at 120°C was also transformed into the acidic form as described above and activated at 450°C. These zeolites are hereafter referred to as H-Z and H-DZ respectively. These samples were characterized by atomic absorption, XRD and BET measurements. Table 3.2 gives the chemical composition and textural properties of the parent zeolite HZ and the modified form HDZ.

3.2.2 ^{1}H MAS and Broad-line NMR

0.5g of each sample was pretreated in a cell of a particular configuration and dimensions for use in this work (Fig 3.2). The pretreatment consisted of gradual heating (12^{0} C/hr) under vacuum (10^{-2} Pa) to 400°C under "shallow bed" conditions and this temperature was maintained for at least 12 hrs. "Shallow bed" conditions represent a physical configuration of the catalyst for

which limited hydrothermal reaction can occur and is essentially the use of a narrow layer of zeolite (4 mm or less). It is believed that this preserves the original structure of the zeolite. The loss in sample weight is determined to an accuracy of $+/-10^{-4}$g. Water was then adsorbed onto the dry sample in a stepwise manner at low pressure and ambient temperature. The adsorbed water was monitored gravimetrically, and the distribution was homogenized by heating sample cell with sample at 100°C overnight. The sample ampoules were then carefully sealed under vacuum in such a way to fit into the sample probe for NMR measurements.

The Si/Al ratio was determined by both atomic absorption and NMR, and the similarity of the values indicated that these samples did not contain extraframework aluminum. This ratio could be used to calculate the number of aluminum atoms per unit cell in the zeolite according to the basic formula for ZSM-5 ($Na_n[Al_nSi_{96-n}O_{192}]$ 16 H_2O). However after desilication, although the Si/Al ratio had decreased significantly the number of aluminum atoms/unit cell remains the same, and the above formula is no longer valid.

The fact that the BET surface area of the desilicated ZSM-5 zeolite does not differ vastly from that of the parent (Table 3.2) provides an opportunity to express the concentration of aluminum sites as the number of aluminum per unit surface area since the latter parameter remains unchanged. This unit conveniently relates data obtained to the properties of materials involved in surface contact phenomena (catalysis or ion exchange).

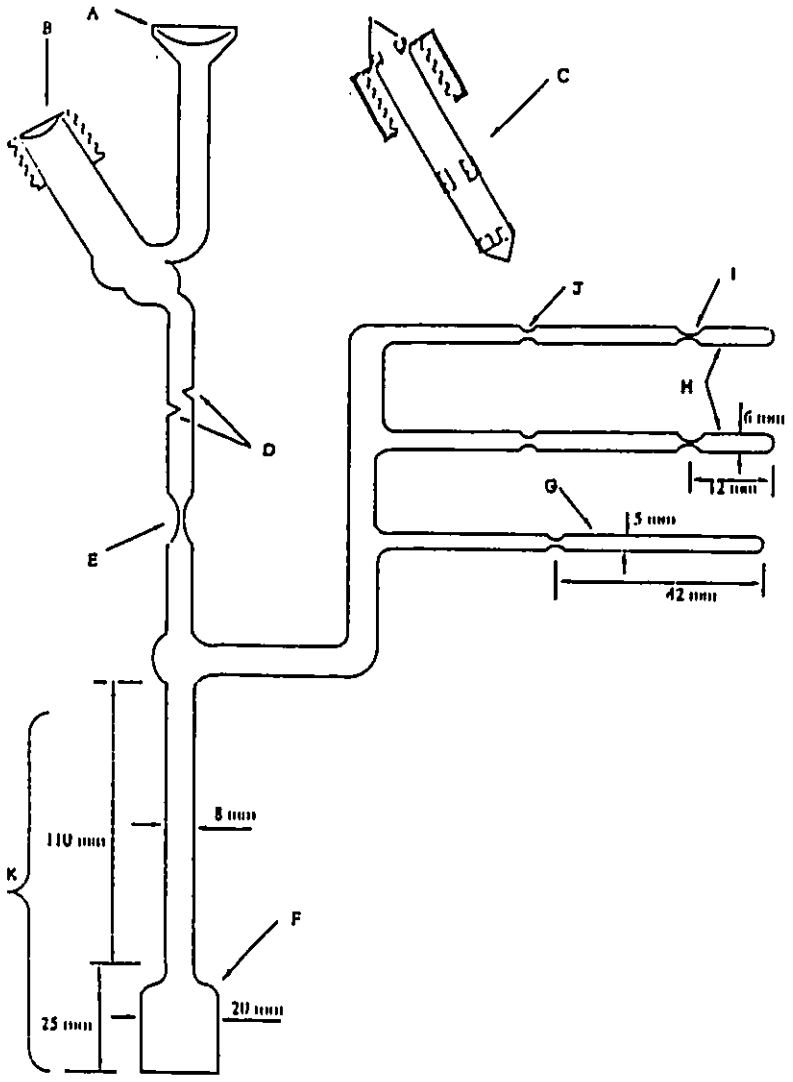

Fig 3.2 Diagram of sample cell used for pretreating zeolite for water adsorption A : female joint (for connecting to the adsorption ramp) ; B : Tap entrance ; C : Tap; D : Region for holding glass wool ; E : Glass tubing used to close off the main portion; F : Region reserved for sample ; G : Small glass tube used for rigid conditions of experiment ; H : Small glass tube for NMR experiments ; I : Glass tubing to seal the NMR sample ampoules ; J : Glass tube for sealing off ; H ; Ampoules for NMR

Hence acidity will hereafter be expressed in units of moles per m^2.

(i) ^1H MAS NMR were run on an MSL 400 MHz Bruker Spectrometer with a 3KHz spinning rate at the University of Pierre and Marie Curie, Paris. Spectra were recorded for anhydrous samples of HZ and HDZ and those samples onto which various different water concentrations were adsorbed, including one concentration with the same number of water molecules as Bronsted acid sites (see Table 3.4). Chemical shifts of protons are given relative to liquid TMS as external reference without susceptibility correction. The repetition time was between 5 and 100 s. MAS NMR spectra of the anhydrous samples HZ and HDZ were simulated in order to calculate the quantity of H^+/unit cell and the relative distribution of hydroxyl protons from SiOH, AlOH and bridging Si(OH)Al after taking into consideration the spinning side bands arising from each peak.

(ii) Broad line NMR (4K) on each of the samples for all concentrations of adsorbed water were collected on a 60 MHz Spectrometer using a home made probe operating at the temperature of liquid helium (4K). Half derivative adsorption spectra were obtained and then simulated using a method developed by Doremieux Morin (91) from which the concentrations of the various oxygen protonated species, contributing to the shape of the spectra were calculated.

3.3 RESULTS AND DISCUSSION

3.3.1 Stability of ZSM-5 zeolite as a function of temperature.

There is an optimum temperature range within which the pore structure of ZSM-5 was preserved, beyond which structural collapse begins. This temperature limit is shown in the DTA/TGA temperature profile thermogram of NaZ corresponding to the region of the endotherm where ther is a change in shape. This occurs at around 450°C, corresponding to a change in phase of the material. Thus the commercially available sample was thermally less stable than the synthesized sample and it was necessary to use a lower temperature (450°C) for activation than is normally used for ZSM-5 zeolite.

Further evidence of this lower limit of thermal stability is provided by the BET and Langmuir surface areas of the parent zeolite (sodium and acidic form) activated at increasing temperatures (Table 3.1). According to the variation of surface area, all forms of the zeolites were stable up to 450°C after which a decrease in surface area indicates destruction of porosity or framework. The maximum surface areas (BET and Langmuir) possessed by all the samples were obtained when the calcination temperature did not exceed 450°C. This temperature was chosen as the highest temperature to which the parent or modified zeolite was activated. The effect of the variation in BET and Langmuir surface areas of NaZ, HZ, NaDZ and HDZ with increasing calcination temperature are given in Table 3.1

Moreover there was a noticeable difference in the meso and micropore

size distribution between the commercially available and synthetic ZSM-5 zeolite activated at 450 and 550° respectively. The former sample was seen to possess a broader distribution of mesopores, veryifying that the commercially available sample was less homogenous (49).

Table 3.1 BET and Langmuir Surface Area for NaZ, NaDZ, HZ and HDZ zeolites calcined at various temperatures

Temperature(°C)	BET SA[1] (m^2/g)				Langmuir SA[1] (m^2/g)			
	NaZ	HZ	NaDZ	HDZ	NaZ	HZ	NaDZ	HDZ
450	370	402	366	406	496	499	496	545
500	334	357	366	397	443	478	490	533
550	342	361	369	380	457	481	495	511
600	339	347	354	383	453	463	474	512
650	339	344	348	380	453	458	467	509
700	337	346	345	380	447	460	463	509

[1] SA : surface area

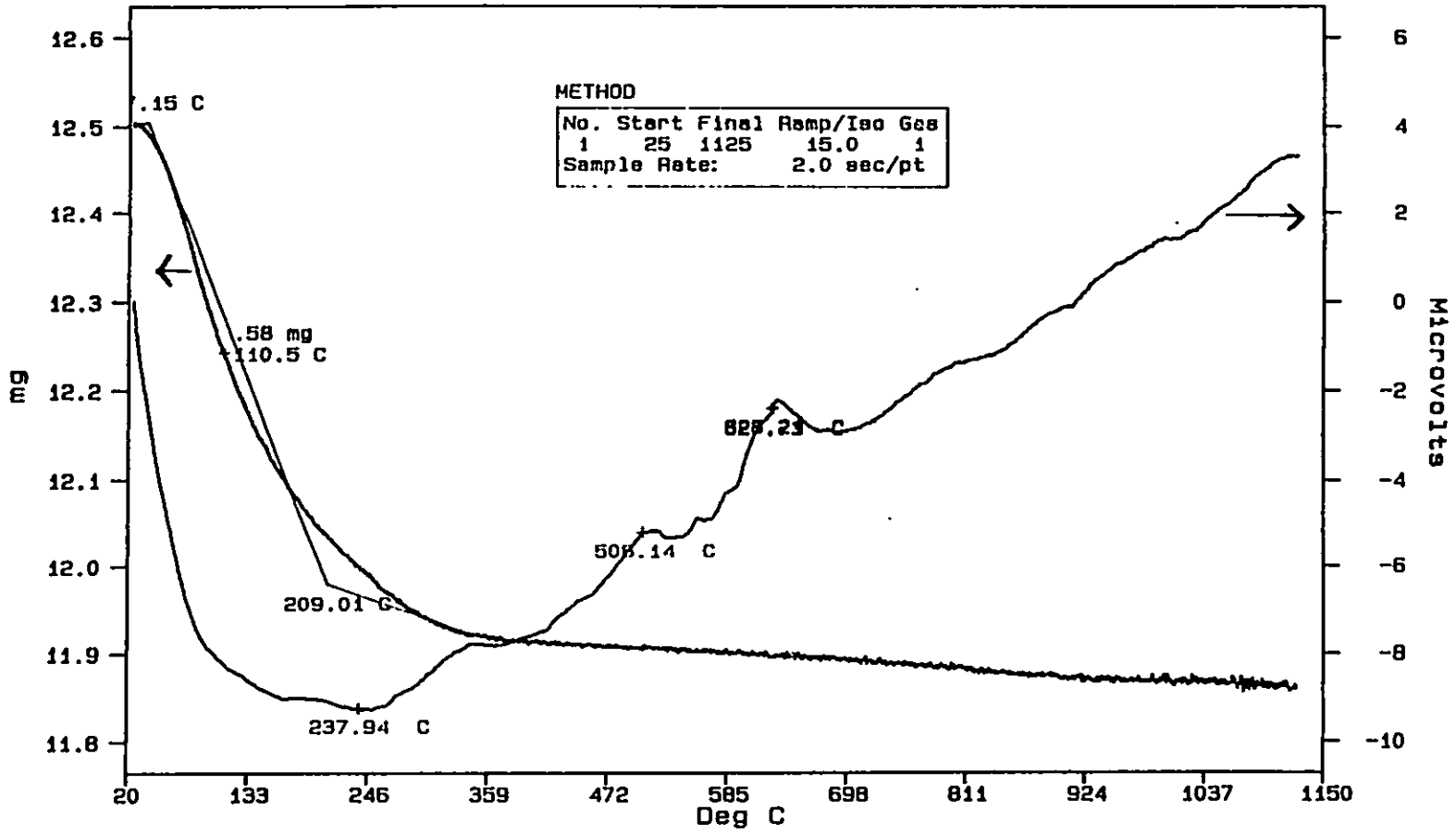

Fig 3.3 DTA/TGA thermogram of NaZ from Chemie Uetikon dried at 120°C overnight.

Table 3.2 Physicochemical properties of HZ and HDZ

	DC[a]	BET SA[b] (m^2/g)	Vol. N_2[c] Total	MP	Chemical Composition[d] % Na_2O	%Al_2O_3	Si/Al[e]
HZ	100	402	.321	.108	0.35	4.5	18.0
HDZ	89	406	.418	.105	0.33	7.3	10.7

[a] Degree of crystallinity, expressed in %

[b] BET Surface area

[c] Volume of nitrogen adsorbed, expressed in cm^3/g.

[d] Expressed in wt %, dried oxide basis [e] Atomic ratio

3.3.2 ^{1}H MAS and Broad-line NMR

Fig 3.4 and 3.5 show the experimentally obtained ^{1}H MAS spectra for the anhydrous parent HZSM-5 (HZ) and the desilicated HDZSM-5 (HDZ) respectively, on which are superimposed their respective deconvoluted spectra. In both spectra, a shoulder was present on the low field edge of the 3.9-4.3 ppm signal, as described by Beck et al. (118). The signal, which arises from the characteristic bridging hydroxyl of Si(O)HAl (Bronsted acid sites), generally referred to as ZOH, is located at 4.2 ppm whereas the signal of OH from silanol (SiOH) is located at *circa* 2 ppm for pentasil zeolites (85). It has been shown

by Brunner et al. (38,82) that such a shoulder or a broad signal at 3.9-4.3 ppm was narrowed when the temperature of the sample was lowered to 125 K, resulting in an approximately 400 Hz wide signal at 6.7-7.0 ppm. A similar peak could be discerned in the ^1H MAS spectra for HDZ obtained at room temperature (Fig 3.5). However this signal was practically negligible for the parent HZ zeolite (Fig 3.4). The assignment of this signal has recently been under much discussion (38,82,119-121). It presumably corresponds to Bronsted acid sites hydrogen bonded to framework oxygen atoms, denoted as type II Bronsted acid sites (those of type I resonating at 4 ppm) (82).

Zholobenko et. al (83) have observed a broad band at 3250 cm^{-1} in addition to the silanol OH and bridged acidic OH at 3610 and 3740 cm^{-1} respectively in IR diffuse reflectance experiments performed on HZSM-5 zeolites. They have also assigned this band as arising from a complex formed between acidic OH groups and a neighbouring oxygen atom of the lattice. This is further supported by the large width and low frequency of this band, which are not characteristic of isolated OH groups.

The signal observed at 6.7-7.0 ppm cannot be confused with the one at 6.5 ppm assigned to molecular water on Lewis acid sites (120), since no NMR signal characteristic of molecular water was detected on Broad Line spectra at 4 K (no doublet for a two spin configuration). Type II Bronsted acid sites (BAS) will hereafter be referred to as ZOH^* for convenience in distinguishing them from type I BAS. The presence of this signal at *circa 6.8 ppm* in the spectrum

of the anhydrous HDZ, and its absence from that of HZ, shows that the whole process of desilication, including the subsequent healing, is responsible for the creation of $ZOH^{\bullet}$ sites, which were presumed to be hydrogen bonded to the lattice oxygens. The formation of hydrogen bonds in these $ZOH^{\bullet}$ sites may be favored by the presence of structural defects on the zeolite that would occur in a dealuminated or desilicated zeolite. It can be inferred that silicon removal may occur from two possible locations in the sodium form of the zeolite framework as illustrated in Fig 3.6.

(a) In a zone rich in silicon, several terminal SiOH groups are formed with the departure of a silicon atom. Those silanol groups do not normally exhibit significant acidic strength. For this situation, the healing must create the more or less deformed siloxane bonds. This does not involve all the newly formed silanol (SiOH) groups, thus contributing to an increase in the number of these silanols from 1.10×10^{-6} to 1.30×10^{-6} mol/m^2 (Table 3.3).

(b) If the silicon atom to be removed is part of an anionic ZO^- site (Fig 3.6 (b)), first the ZO^- is destroyed, then in the Na^+ aqueous environment, most of the Al atoms become Al^- tetrahedrally coordinated by oxygen atoms. Such a reinsertion of Al species into the zeolite framework is probably promoted by the presence of Na^+ ions and water (steam) (59). Healing goes to completion when the desilicated sample is heated to high temperatures ($> 250°C$) (57,63). Thus, ZO^- groups are regenerated from the tetracoordinated Al^- through a healing process which will be discussed further in the next chapter.

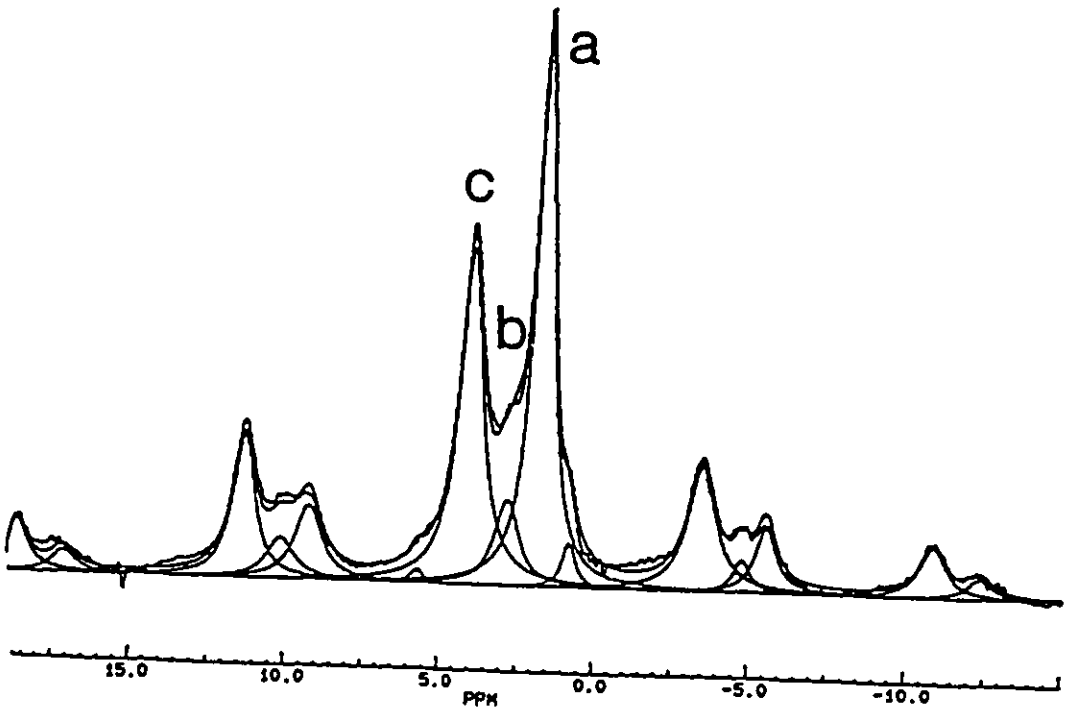

Fig 3.4 ^{1}H MAS spectra for anhydrous form of HZ zeolite and the corresponding decomposition curves. Peaks a, b and c are assigned to Si-OH groups, the AlOH and Z-OH acid sites respectively.

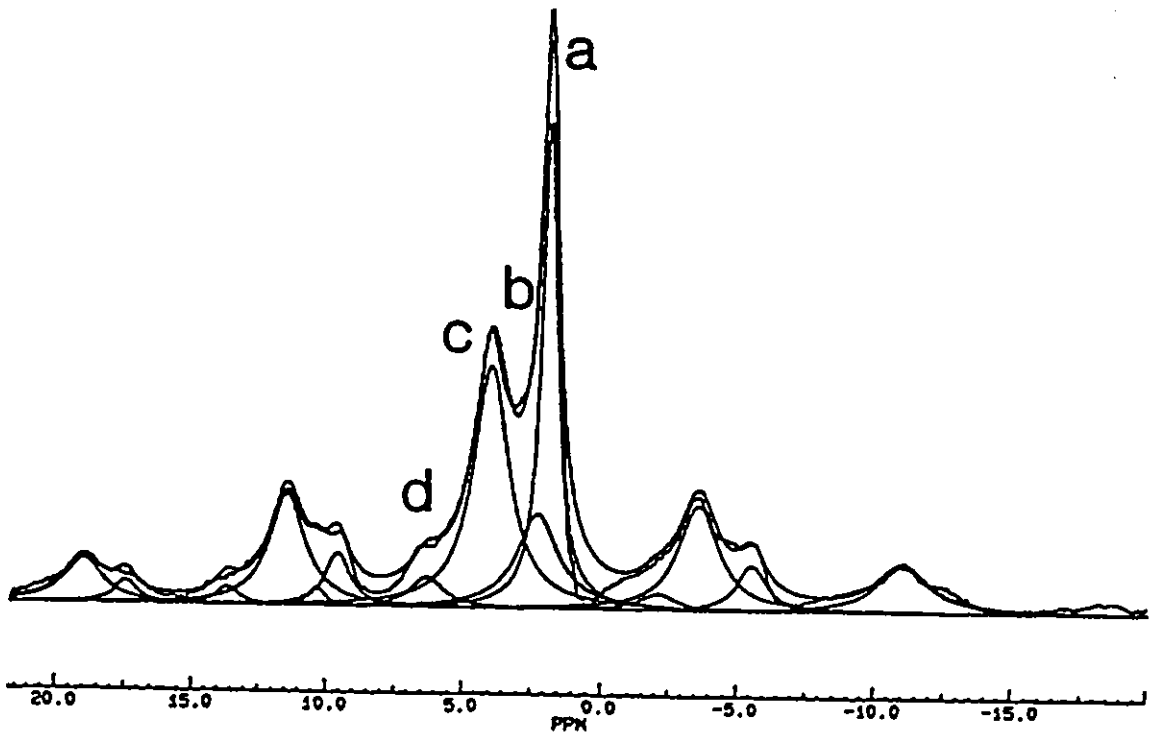

Fig 3.5 ^{1}H MAS spectra for anhydrous form of HDZ zeolite and the corresponding decomposition curves. Peaks a, b, c and d are assigned to Si-OH groups, the AlOH, Z-OH and Z-OH* acid sites respectively.

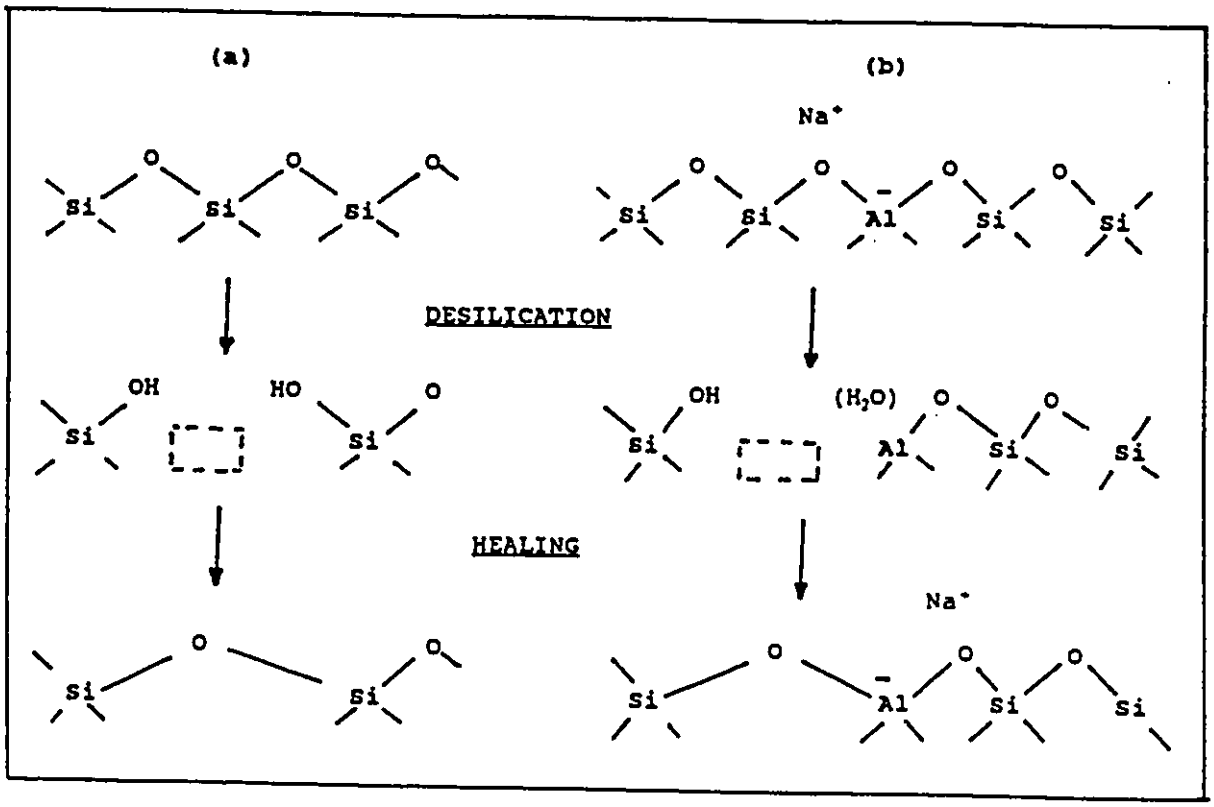

Fig 3.6 Proposed mechanism for desilication and the subsequent healing of HZ

Table 3.3 ^{1}H MAS NMR data : distribution of oxygen protonated species groups of anhydrous zeolite samples (HZ and HDZ) expressed in units of 10^{-6} moles/m^2.

Sample	HZ	HDZ
Al atoms	2.19 ± 0.20	2.19 ± 0.20
SiOH	1.10 ± 0.08	1.30 ± 0.10
AlOH	0.73 ± 0.10	0.26 ± 0.05
ZOH	1.47 ± 0.10	1.50 ± 0.10
ZOH*	negligible	0.43 ± 0.050
Total OH	3.30	3.49
acidic OH	1.47 ± 0.10	1.93 ± 0.30

ZOH* probably has the following configuration : ZOH ...O_z (O_z being a framework oxygen atom (38,82,119)).

Table 3.3 shows that the initial concentration of Al(OH) in HZ is 0.73 x 10^{-6} mol/m^2, which is approximately equal to the sum of the Al(OH) concentration (0.26 x 10^{-6} mol/m^2) and that of the ZOH^+ created (0.43 x 10^{-6} mol/m^2) in HDZ. This result appears to be consistent with the idea that the overall process (desilication + healing), concerns mainly the environment of the Al(OH) defects, transforming them into bridged Al(O)HSi sites. Whatever the exact mechanism, the concentration of acid sites is greater in HDZ than in HZ. These results explain why desilicated Y and X zeolites exhibit enhanced cation exchange capacities (63) as discussed in Chapter 2. They also support other indications mentioned in Chapter 2, that no framework aluminum atoms are extracted during desilication using sodium carbonate solution (57,63).

When water was loaded onto the anhydrous zeolite samples (according to equation A), the forced interaction between the water molecules and the OH groups on the zeolite may result in the formation of varying quantities of the oxygen protonated species. It has been recently shown by neutron diffraction and infrared spectroscopic studies by Cheetham's and Thomas' groups, that water binds to microporous solids in two ways. The researchers located two types of acid sites : one associated with hydrogen bonded water molecules and the other with hydroxonium ions (178,179). The concentrations of these species depend firstly on the acidic properties of the solid, in particular the acidic strength, and secondly on the amount of water loaded. Table 3.4 gives a summary of the data obtained from simulation of the average half derivative

absorption spectra for samples with different concentrations of water adsorbed onto the anhydrous zeolite. The following features stand out :

- When the concentration of adsorbed water is less than or equal to that of ZOH (the number of Bronsted acid sites per unit surface area), all these acid sites interact with the adsorbed water molecules, either by hydrogen bonding or by forming H_3O^+. This is in agreement with results obtained for other zeolites (117). The dissociation coefficient of these OH groups is 0.2 when the number of water molecules adsorbed is equal to the number of ZOH groups.

- "Free water" molecules (ie water molecules which did not interact with the OH groups of the zeolite) can be detected when the water concentration is greater than that of OH.

- There was a difference in the ionization behaviour for parent and desilicated zeolites with different concentrations of adsorbed water. In fact a linear increase in the number of H_3O^+ species formed with the degree of hydration per unit Bronsted acid site (H_3O^+ formed/Bronsted acid site vs H_2O adsorbed/Bronsted acid site) was observed for the parent zeolite, whereas a similar plot for the treated sample shows that the quantity of ionic species (H_3O^+) formed by the adsorption of water was greater for the first two different loadings of adsorbed water. Thereafter a plateau was observed at the third concentration of adsorbed water (4.1×10^{-6} molecules of water/m^2 adsorbed).

A similar plateau at $n(ZOH) < n(H_2O) < 2n(ZOH)$ followed by a linear

increase has been observed for mordenite samples in which Lewis acid sites have been detected. It has been proposed that for a given amount of water adsorbed, there are important quantitative differences in the way the Bronsted acid sites of the various species of zeolites ionize (85). It was not possible to study the effect of further adsorbed water concentrations ; this investigation is now underway.

In contrast with what was observed with the parent zeolite HZ, the signal at 6.8 ppm in the ^{1}H MAS NMR spectrum for HDZ (Fig 3.7), indicates that a few water molecules are bonded to Lewis acid sites from the start of adsorption. This is supported by broad line NMR at 4 K, which demonstrates that there are water molecules not interacting with the OH groups from the start of adsorption. Fig 3.8 shows the experimental and simulated broad line spectra for HDZ when the number of water molecules equals the number of Bronsted acid sites/unit surface area).

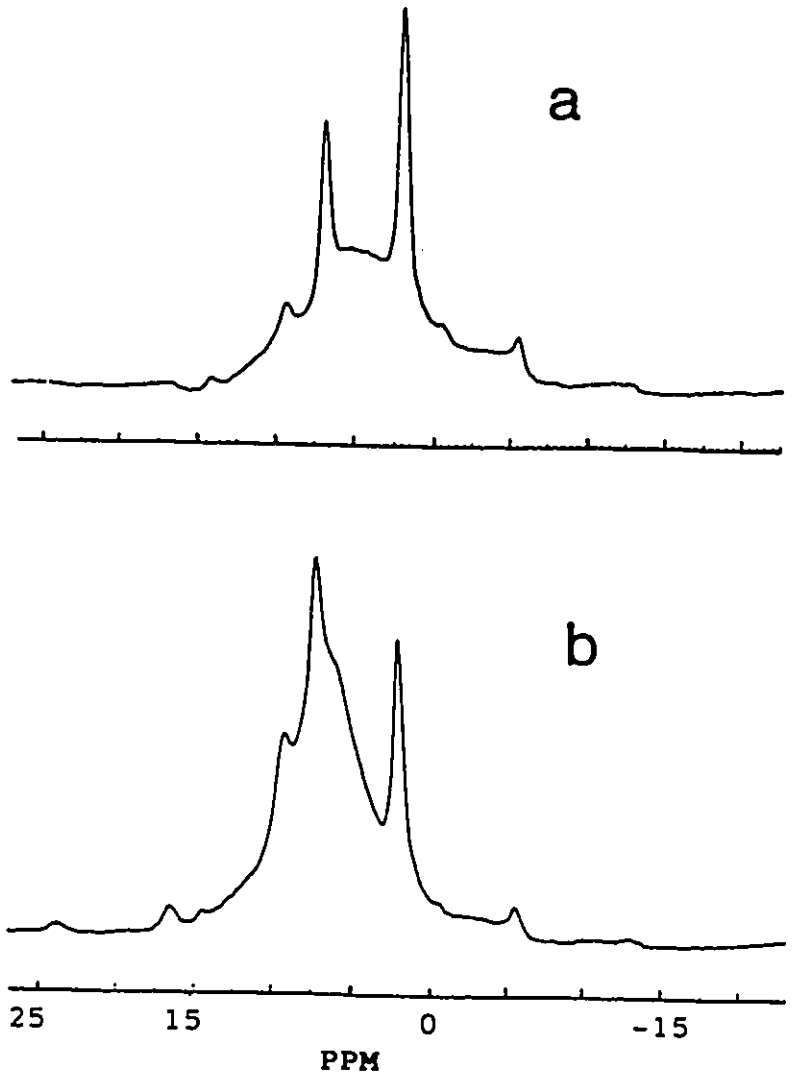

Fig 3.7 ^{1}H MAS NMR spectra of HDZ zeolite with two different (high) water concentrations loaded (a) 3.6×10^{-6} mol/m^2 and (b) 6.6×10^{-6} mol/m^2

Table 3.4 Broad Line ^1H NMR data : distribution of oxygen protonated species groups (data expressed in 10^{-6} mol/m^2) of zeolite after adsorption of water.

No. H_2O[a] adsorbed	n H_3O^+[a]	n H_2O...HOZ[a,b] groups	n free OH[a] groups	n H_2O[a]	IC[c]
HZ zeolite					
1.1	0.33	1.33	0.50	0	
1.4	0.20	1.22	1.84	0	
2.2	0.38	1.82	1.08	0	0.2[d]
4.5	0.74	1.66	1.24	2.0	
HDZ zeolite					
1.0	0.19	0.80	2.26	0.2	
2.2	0.42	1.54	1.75	0.2	0.2[d]
4.1	0.43	1.68	1.75	1.8	

[a] Accuracy according to reference 39 for : adsorbed water at water loadings similar to those used in this work = ± 5% ; H_3O^+ ions = ± 10% ; H_2O...HOZ groups = ± 10% ; free H_2O molecules = ± 10%

[b] ZOH : includes ZOH and eventually ZOH* ; [d] Estimated accuracy = ± 20 %

[c] Ionization coefficient = H_3O^+ per initial acidic OH group

These molecules represent about 10 % of the water molecules adsorbed and about 2 % of the total number of atoms in the sample, when the number of water molecules adsorbed is 2.2×10^{-6} mol/m^2, ie slightly higher than the total number of Bronsted acid sites (1.93×10^{-6} mol/m^2). These concentrations are in fair agreement with those deduced from MAS NMR.

It is believed that a few aluminum atoms coordinately bound to water are created during the desilication process (Fig 3.6 (b)), resulting in these Lewis acid sites during the "shallow bed" pretreatment (117). Remy et al. also found such three coordinated Aluminum atoms in dealuminated mordenites by XPS (122).

For the special situation when the number of water molecules loaded is equal to the number of Bronsted acid sites in the zeolite material, the number of free water molecules present in the sample is either nil (HZ) or very low for Lewis acid sites (HDZ). The ionization coefficient (IC), which was found to be practical in the setting up of an acidity scale for solid acids (39), was calculated according to the following formula when the number of water molecules adsorbed is equal to the number of acidic OH :

$$IC = \text{No. } H_3O^+ \text{ formed/No } H_2O \text{ adsorbed}$$

This value was lower than some values obtained for HZSM-5 and H-Mordenite type zeolites (85) for which it has been found to be equal to 0.3.

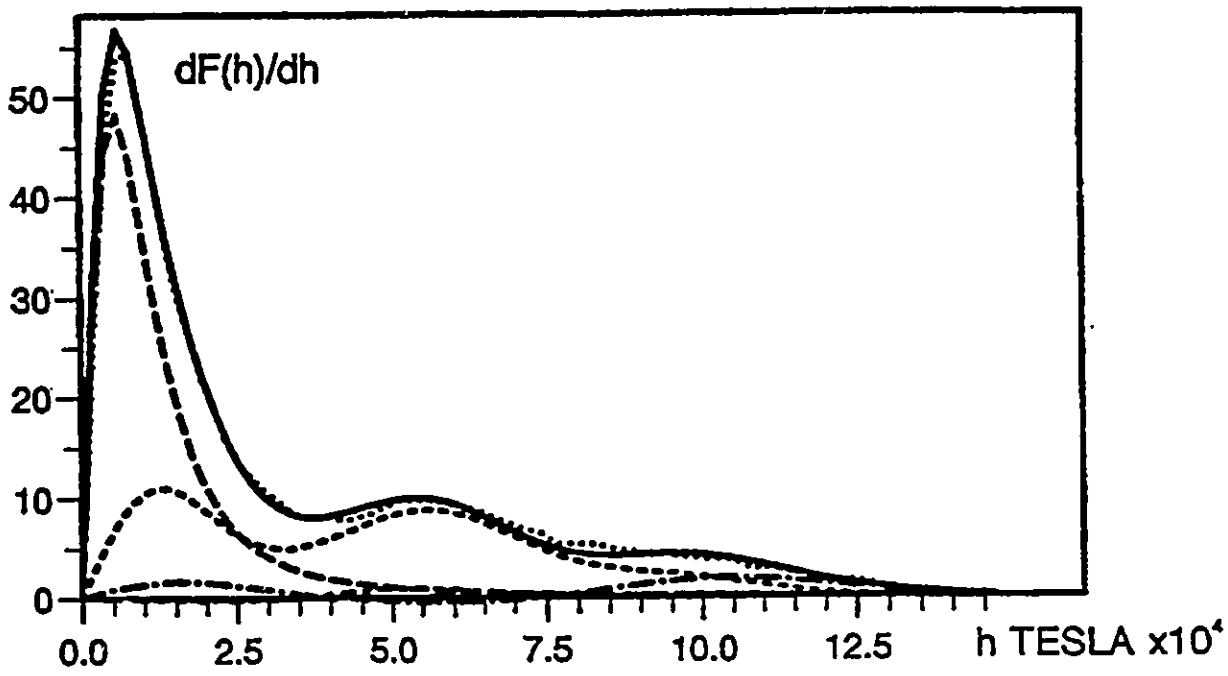

Fig 3.8 Simulated broad line spectra of HDZ when the number of adsorbed water molecules equals the number of BAS /unit cell (———) : calculated ; (•••••) : experimental; (– –) : Lorentzian function ; (- - -) : Isosceles ; (–•–) : equilateral

This is a small change in the value which can be attributed to the fact that the ZOH* sites identified in the "anhydrous" form of the desilicated zeolite are easily converted back to the bridged ZOH sites during the rehydration phase.

3.4 CONCLUSIONS

The results of this study show that ^1H MAS NMR and Broad Line NMR are very useful techniques for the study of acidity. In particular it was possible to show that the selective removal of silicon from the zeolite ZSM-5 results in a few more silanol groups (more structural defects) and more Bronsted acid sites per unit surface area. It was also possible to determine the strength of the acid sites present on the desilicated zeolite ZSM-5, since the strength of these sites as determined by the ionization coefficient, does not differ significantly from that of the normal bridging Bronsted acid sites present in zeolites. Some Lewis acid sites, produced by the desilication treatment were detected by ^1H MAS NMR during the rehydration phase. More detailed studies on acidity, which are discussed in Chapter 4, have been carried out using more conventional techniques for characterization such as Ammonia Temperature Programmed Desorption (NH_3 TPD), X Ray Photoelectron Spectroscopy (XPS), Catalytic testing and Poison testing with pyridine and 2,6-dimethylpyridine, in addition to IR Spectroscopy (123,124,117).

CHAPTER 4

OTHER EVIDENCE OF MODIFICATION OF ACID SITES BY XPS, FTIR, NH_3 TPD, ^{27}Al, ^{29}Si AND XENON NMR, AND ON STREAM POISON TESTING

4.0 INTRODUCTION

The objective of this work was to further compare the acidic and main physico-chemical properties of the desilicated ZSM-5 material with the parent zeolite, including the catalytic activity and product selectivity. Techniques such as XPS, ^{27}Al and ^{29}Si MAS-NMR, FT-IR and ammonia temperature programmed desorption (TPD), as well as $^{129}Xenon$ NMR were used. The poison testing of acid sites of HZ and HDZ was investigated using the dehydration of absolute ethanol as a model reaction.

4.1 THEORETICAL BASIS OF TECHNIQUES USED

4.1.1 X RAY PHOTOELECTRON SPECTROSCOPY (XPS)

Surface analysis by X Ray Photoelectron Spectroscopy (XPS) is accomplished by irradiating the sample with monoenergetic soft X-rays such as Mg Kα of energy 1253.6 eV or Al Kα of energy 1486.6 eV. The photons

penetrate the surface layers (60 Å depth) and interact with surface atoms within this region by the photoelectric effect, causing electrons to be emitted. The emitted electrons have kinetic energies defined by :

$$KE = h\nu - \text{Binding Energy(BE)} - \Phi$$

where $h\nu$ is the energy of the incident photon, BE is the binding energy of the atomic orbital from which the electron originates, and Φ is the work function of the spectrometer. The BE may be regarded as an ionization energy of the atom for the particular shell involved. XPS is used for observing shifts in the binding energies to lower values, corresponding to decreased Si/Al ratio of materials as a direct consequence of different coordination and ionicity/covalency of oxygen bonded to aluminum and silicon.

Photoionization usually leads to two types of emitted electrons, a photoelectron and an Auger electron. Auger electrons are emitted due to relaxation of the energetic ions left after photoemission.

Primary Process :

Photoionization

$$A + h\nu \longrightarrow A^{+\cdot} + e^{-} \text{ (photoelectron of discrete energy)}$$

$$E \text{ (kinetic)} = E \text{ (photon)} - E \text{ (binding)}$$

This photoelectron emitted is measured in XPS and its energy is the difference between the energy of the incident photon and the binding energy of the

electron.

Secondary Process :

In the Auger process an outer electron falls into an inner orbital vacancy and a second electron is emitted, carrying with it the excess energy. In competition with Auger electron emission is the process of X-ray fluorescence by which the excited ion may relax by emission of a photon. The Auger electron thus possesses kinetic energy equal to the difference between that of the initial ion and the energy of the doubly charged ion, and is independent of the mode of the initial ionization (89).

(i) Auger electron emission

$$A^{+\cdot} \longrightarrow A^{++} + e^{-} \text{ (Auger electron of discrete energy)}$$

(ii) X Ray Flucrescence

$$A^{+\cdot} \longrightarrow A^{+} + h\nu'$$

These processes are illustrated in Fig 4.1. The XPS process is shown on the left of the diagram whereby a 1s electron is ejected from the atom by an incident photon. The middle figure illustrates the emission of a photon of energy which occurs when an electron from the 2p orbital drops into the vacant 1s hole left after photo ionization. The right figure illustrates Auger electron emission in which an Auger electron (2p) is emitted when a 2s electron falls to the vacant 1s orbital left from photoionization.

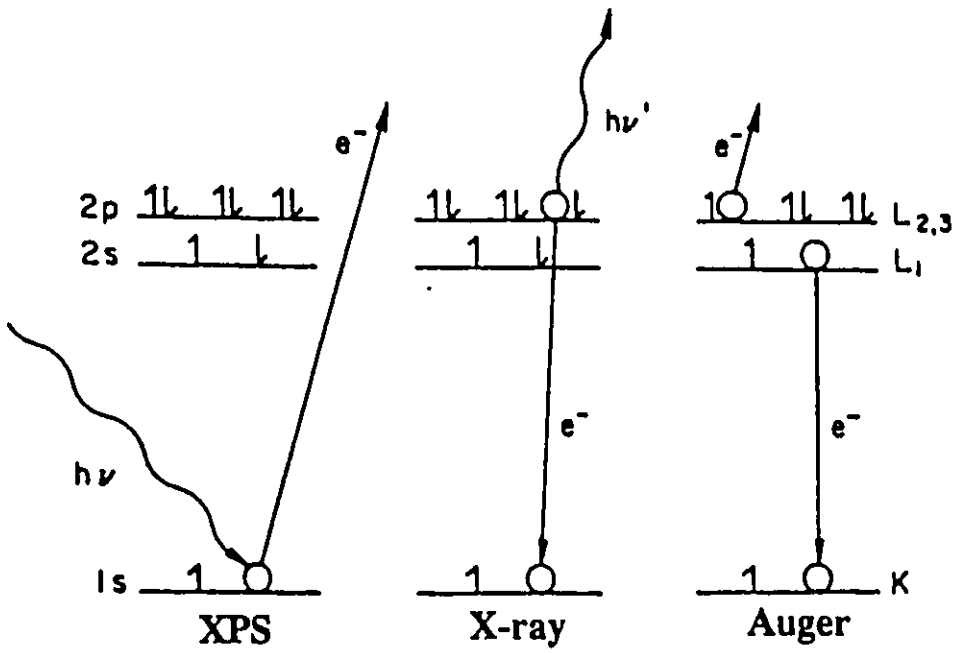

Fig 4.1 Diagram of ESCA, X Ray and Auger emission processes.

4.1.2 NH_3 TPD

Temperature programmed desorption of gaseous basic probe molecules such as ammonia or pyridine adsorbed onto the acidic sites in solid acids provides a convenient and fairly good characterization technique for estimating the total number of acidic sites and the strength and distribution of these acid sites (9,55). This technique exploits the temperature dependent adsorptive properties of the chemisorbed base since the higher the temperature required for desorption the stronger the acidity of the active site. Ammonia is chosen for its small kinetic diameter (2.62 Å) and with a lone pair of electrons it can reach practically all acid sites even those within a zeolite pore having a six membered ring.

The theory of this experiment is adapted from the flash filament experiment used in surface science and makes the following assumptions for which all desorbing molecules should have the same activation energy : firstly, that no readsorption of ammonia occurs during desorption and secondly that the ammonia becomes adsorbed onto a homogenous surface with minimum interactions between the adsorbed molecules (56). Attention should be directed to removing physisorbed ammonia before the temperature programmed desorption, since this leads to erroneously high quantities of base titrating (desorbing) at lower temperatures.

NH_3 TPD was used for quantitation and characterization (the strength) of acidic sites in the parent and desilicated zeolite.

4.1.3 CATALYTIC ACTIVITY STUDIES

Dehydration of ethanol to ethylene over zeolite catalysts requires acid sites of a fairly significant strength (8-10,16,17,125). Under normal conditions of testing, the catalyst performance is closely related to the Si/Al ratio of the ZSM-5 zeolite (9,127).

As already mentioned low Si/Al ratio ZSM-5 (lower than 9.5) cannot be obtained by direct synthesis without having some non-framework Al species in the synthetic preparation. The latter species which probably exists in 6 fold coordination as in alumina, is not as active and selective as protonic sites. In fact, compared to the ZSM-5 zeolite (9,125,126) or other acidic compounds such as the heteropolyacids (127), the performance of alumina appears fairly poor for the production of ethylene (128) probably owing to its weaker acid sites.

It was already shown that it was possible to increase the Al content of a ZSM-5 zeolite by a (controlled) desilication (57,58). ^{1}H Broad-line and MAS-NMR studies (64) showed that desilication of ZSM-5 zeolite (and then ion-exchange with protons) resulted in more Bronsted acid sites per unit weight or per unit surface area. Catalytic testing, in the dehydration of ethanol to ethylene, is therefore a good index for demonstrating Bronsted acidity.

4.1.4 POISON TESTING

In order to study the effect of a poison on the nature of the acid sites,

pyridine and 2,6-lutidine (2,6-dimethylpyridine) were co-fed with ethanol into the reactor during catalytic testing operations. These tests were expected to reveal the presence of Lewis acid sites with the Al(III) coordination.

Pyridine can poison all types of acid sites present in the zeolite (the Bronsted, Lewis and all other sites of varying acidic strengths). This occurs because pyridine molecules can freely access Bronsted acid sites [Fig 4.2 (a)] or Lewis acid sites [Fig 4.2 (b)] both located inside the zeolite micropores. This is a reference reaction for the adsorption of an unhindered amine on the zeolite being studied. On the other hand, 2,6-dimethylpyridine, because of its sterically hindered molecular configuration, is selectively adsorbed onto very accessible acid sites, and is thus a very useful index of Bronsted acid catalytic activity. Because of the nature of the BAS which is represented as a proton of a bridging hydroxyl group attached to silica and aluminum tetrahedra, 2,6-dimethylpyridine can access BAS, but not the less accessible LAS site. Hence the LAS remain active in the presence of 2,6-dimethylpyridine (74,90,99).

4.1.5 ^{28}Si and ^{27}Al NMR

^{27}Al and ^{29}Si NMR will be used to determine the environment of silicon atoms and detect changes in the zeolite framework and in this way distinguish between framework and non-framework aluminum in the parent and desilicated zeolites.

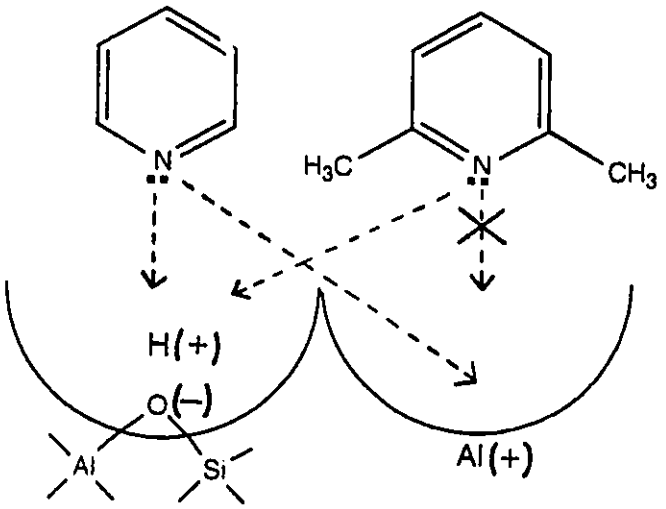

(a) (b)

Fig 4.2 (a) and (b) Molecular configuration of pyridine and 2,6-dimethylpyridine relative to BAS and LAS in zeolite micropores

4.1.6 POROSITY OF ZSM-5 Zeolites by Xenon adsorption and ^{129}Xenon NMR

Xenon NMR spectroscopy has been used to study the porosity of the parent and modified zeolites by first constructing isotherms for various pressures of xenon adsorbed at low temperature. The effect of pressure of

xenon adsorbed, on chemical shifts, was measured on the acidic forms of the parent and modified zeolites at ambient temperature. Properties such as dimensions of cavities and channels, void space, structural properties (short range crystallinity, porosity) which are difficult to detect by classical physicochemical methods, and the location, distribution and size of extra lattice species (cations) too small to be detected by electron microscopy, can be detected by xenon NMR. The adsorbed xenon NMR spectrum is very sensitive to the chemical environment of xenon within the zeolite. Xe is thus an ideal probe since it is inert, its kinetic diameter is 4.4 Å, it is monatomic, and its large electron cloud transmits any distortion directly to the Xe nucleus causing significant changes in the NMR chemical shift (93-97). The chemical shift (δ) for Xe adsorbed on a zeolite has been shown to be the sum of the following terms corresponding to the various perturbations to which this probe is subjected (98).

$$\delta = \delta_o + \delta_{Xe\text{-}Xe} \times {}_{Xe} + \delta_{Xe\text{-}zeolite} + \delta_E$$

where δ_o = reference chemical shift of xenon ; $\delta_{Xe\text{-}Xe}$ = chemical shift associated to Xe-Xe interactions ; ${}_{Xe}$ = density of xenon ; $\delta_{Xe\text{-}zeolite}$ = chemical shift associated to collisions of Xe with walls of zeolite pores which is characteristic of each particular zeolite structure ; δ_E = chemical shift due to electric field within zeolite pores. In this study the technique has been utilized for the determination of changes in porosity and adsorption capacity of parent and desilicated zeolites.

4.2 EXPERIMENTAL

4.2.1 PREPARATION OF THE ZEOLITE MATERIALS

The parent zeolite used was the commercially available Na-ZSM-5 zeolite (obtained as Zeocat PZ 2/30 Na-form, powder, from Chemie Uetikon, Switzerland) activated at 450 °C overnight. This zeolite is referred to as Na-Z. The desilicated zeolite was prepared as described before in Chapter 3 using 0.8 M sodium carbonate and 0.01 M sodium hydroxide solution and the acidic forms of the parent and desilicated zeolite were prepared by repeated ion exchange with a 5 wt % solution of ammonium chloride at 80 °C, (57,58), then drying at 120 °C and activating at 450 °C overnight in a stream of air, as described previously for HZ and HDZ.

4.2.2 PREPARATION OF THE FINAL CATALYSTS

The final form of these catalysts was prepared (53) by mixing the zeolite with bentonite clay (Anachemia, USP, 10 wt %) with the dropwise addition of water to form a malleable paste (1 g zeolite/ 2-4 ml of water) and then extruding the paste into "spaghettis" (1 mm O.D.) which were dried at 120 ° C overnight and then activated at 450 ° C for 12 h.

4.2.3 CHARACTERIZATION

4.2.3.1 PHYSICOCHEMICAL

The original and modified samples were first characterized by atomic

absorption spectrophotometry (chemical composition) and X-ray powder diffraction (structural identification and measurement of the degree of crystallinity (DC), using the parent Na-ZSM-5 zeolite as external reference (57). BET total surface area and distributions of mesopore and micropore sizes were determined by nitrogen and argon adsorption /desorption.

Fourier transform infra red spectra (Nicolet Magna IR spectrometer 500, resolution: 1 cm^{-1}) were recorded in the region 400 - 1400 cm^{-1} using the transmission mode, for identification of the T-O bonds (where T stands for Si or Al) associated with the tetrahedral units (58) for both parent and desilicated samples in both the sodium and protonic forms.

4.2.3.2 X Ray Photo Electron Spectroscopy

XPS studies were performed on a VG ESCALAB 3 MK II instrument. A sample of *circa* 0.1 g was pressed onto a copper sample holder (1 cm in diameter) and degassed under vacuum overnight. The residual pressure in the analysis chamber was 1-5 x 10^{-8} torr. The samples were analysed at room temperature, using Mg Kα X-rays at 1253.6 eV, 280 watts to cause the photoemission of electrons from core levels of the surface atoms. For a detector perpendicular to the surface, a depth of *circa* 60 angstroms is probed. The surface analysed was 2 x 3 mm. The analyzer pass energy of 20 eV permitted a peak resolution of 1.2 eV, measured on the silver $3d_{5/2}$ peak. The error margin on peak positions was 0.05 eV. All peak positions were corrected

for adventitious carbon, at binding energy of 285.0 eV, to adjust for charging effects. This is particularly important for the high silica zeolites where adventitious carbon can lead to inexplicably high values in the Si_{2s} and O_{1s} binding energies. A Shirley-type nonlinear background subtraction was utilized (129), and a nonlinear least squares program was used to obtain individual peaks. The Si_{2s}, O_{1s} and Al_{2p} peaks were co-added over 16 scans to increase the signal-to-noise ratio.

4.2.3.3 NH_3 TPD

Dried powdered samples in the protonic form were compressed into pellets and passed through a 60 mesh sieve. Approximately 0.6 g were loaded into the U shaped quartz reactor and placed into a temperature programmable furnace (Micromeretics Oven Controller). The sample was pretreated in helium flowing at 20 ml/min at 450°C for at least 12 hours and then cooled to 100°C Ammonia gas (Linde, high purity) predried with 3A molecular sieves, was passed through the sample at 100°C for 45 mins to saturate it completely. Helium was then flushed through the reactor containing the sample at 20 ml/min for 60 mins at the same temperature in order to remove physically adsorbed ammonia. Initially TPD is performed from 100 to 750°C using a heating rate of 288 K/min. The measurement of the acid density was carried out during these ammonia TPD experiments by using a 0.01 mol dm^{-3} HCl solution which was then back-titrated with a 0.01 mol dm^{-3} NaOH solution.

Helium was used as carrier gas flowing at 20 ml/min and the desorbed ammonia was detected by a GC equipped with a TCD detector. The trace profile of the ammonia desorption was recorded on an integrator (HP3390) interfaced to a SRI 8610 student GC.

Thereafter the technique of deconvolution of the ammonia desorption peaks which was developed earlier (130), was used to obtain a rough estimation of the number of acid sites of the ZSM-5 zeolite according to their strength. The desorption was carried out as follows. The sample was heated at 15°C/min from 100 to 220°C, isothermal at 220°C for 30 mins, heating to 350°C at 15°C/min, isothermal for 30 mins, heating to 500°C, maintained at this temperature for a further 30 mins and finally heating to 550°C and maintained at this temperature for 30 mins.

This technique consisted of a combined TPD and stepwise heating procedure with temperature plateaux occurring at 206°C, 342°C and 496°C. The resulting desorption peaks were assigned to W (weak), M (medium) and S (strong) acid sites, respectively (130). Fig 4.3 is a profile of the stepwise heating program used for deconvolution of the ammonia desorption peaks. Fig 4.4 is a schematic representation of the experimental setup for pretreating the sample and ammonia adsorption and desorption. Fig 4.12 shows the profiles generated for ammonia desorption for HZ and HDZ.

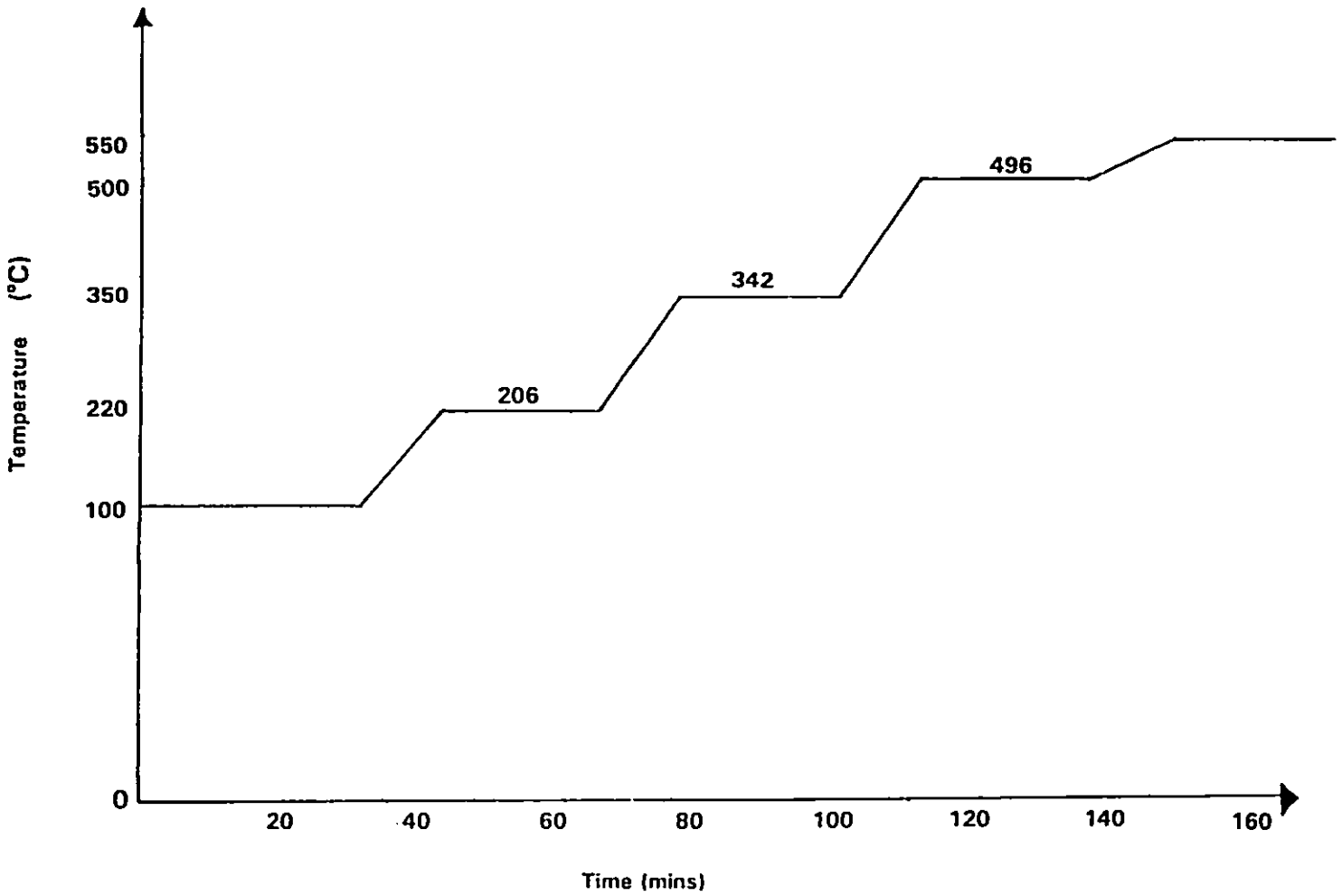

Fig 4.3 Stepwise heating program used for deconvolution of ammonia desorption peaks.

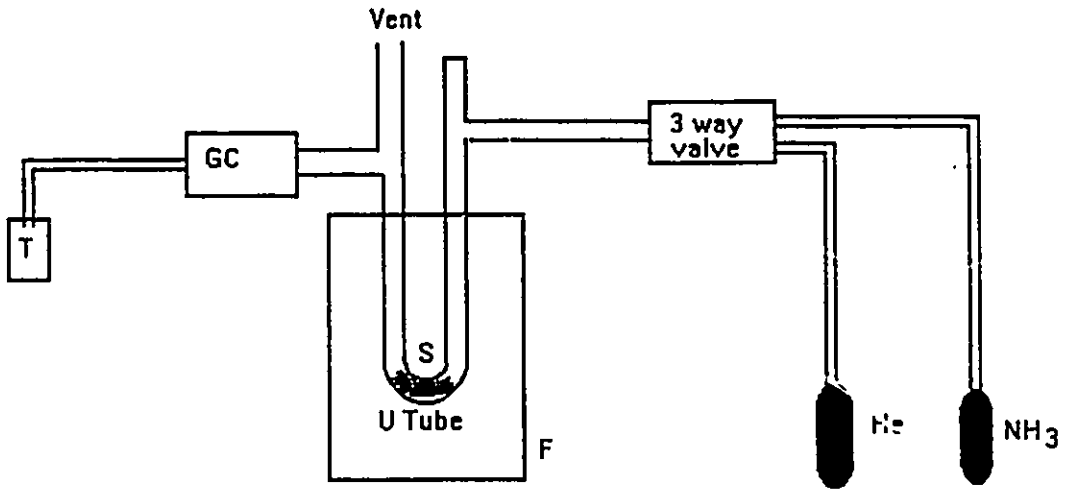

Fig 4.4 Experimental setup for ammonia TPD testing

He : Helium ; S : Sample ; T : Solution of HCL for titration of desorbed ammonia ; F : Furnace (Programmable) ; GC : Gas Chromatograph

4.2.2.4 CATALYTIC TESTING

Catalytic testing was performed in a fixed bed reactor set up as illustrated in Fig 4.5. This set up is similar to that used for previous catalytic testing in the BETE process (16). However, the dimensions of the horizontal fixed bed reactor were altered to 39.5 cm in length and outer diameter 1.5 cm. Ethanol was injected into a vaporization flask maintained at 120 ° C (using a syringe on an infusion pump).

The catalytic runs lasting typically for 3 hours, were carried out with 100 wt % ethanol during which time the aqueous reaction products were collected in a sample flask maintained at approximately 5°C, and were analyzed after the run on a Hewlett Packard 5790 GC equipped with a flame ionization detector (FID) and 50 m PONA capillary column. The aqueous reaction products that formed when 100 % ethanol was used were diluted by a 1/10 dilution factor before analysis by GC. Samples of the gaseous reaction products, taken periodically from a gas sampling bulb, were analyzed on a Shimadzu Mini 3 GC (FID) and a 2.5m packed column of 15 wt % squalene coated Chromosorb P. 2,2-dimethylbutane (DMB) was used as internal standard for the gaseous sample analysis. The reaction conditions used for this series of experiments were as follows : Temperature = 200-250°C (+/-3°) ; catalyst weight = 0.800(+/-0.005g) ; total length of catalyst bed = 2.2 cm ; cross sectional diameter of catalyst bed = 1.3 cm ; pressure = 1 atm ; inert gas (nitrogen) flow rate = 12 ml/min : WHSV = 8.2 hr^{-1} ; duration of run = 3 hrs. The

Space Velocity (WHSV) is expressed as follows:

$$WHSV = F/W\ (hr^{-1})$$

where F is the flow of reactant in g/hr and W is the weight of the catalyst bed.

The contact time, t (hr) with respect to ethanol is defined as :

$$t = 1/WHSV$$

The reported conversion and product selectivities are average values obtained during each run and are calculated as follows :

The total conversion of the reaction is calculated in carbon atom % by:

$$CVT\ (C\ atom\ \%) = \frac{(EtOH)_f - (ETOH)_p * 100}{(ETOH)_f}$$

where $(ETOH)_f$ and $(ETOH)_p$ are the number of carbon atoms of ethanol in the feed and recovered in the product respectively.

Product selectivity is given by :

$$S_i\ (C\ atom\ \%) = 100 \times P_i/(EtOH_f - EtOH_p)$$

where P_i is the number of carbon atoms of product i.

The yield of each component Y_i is defined as

$$Y_i = S_i * CVT/100$$

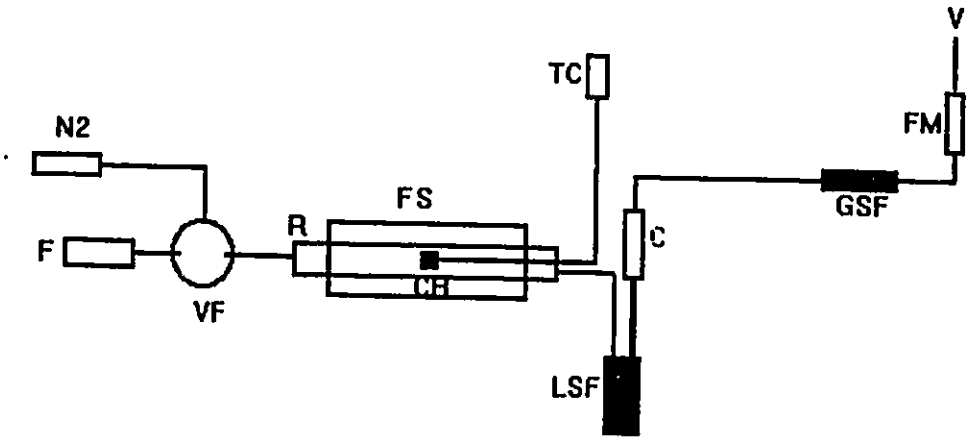

Fig 4.5 Experimental set up of reactor for catalytic testing.

N_2 : Nitrogen ; F : Feed ; VF : Vaporization Flask ; CB : Catalyst bed ; R : Reactor ; FS : Furnace ; C : Condenser ; LSF : Liquid Sample Flask ; V : Vent; TC : Thermocouple with meter ; GSF : Gas Sampling Flask ; FM : Flow meter

4.2.3.5 POISON TESTING

The poison tests were performed for both HZ and HDZ catalysts at 225°C using a contact time of 0.12 hr for the dehydration of absolute ethanol to ethylene using the above described catalytic reactor. Each poison, which varied in concentration from 0.025 to 0.3 mol %, was co-fed with absolute ethanol into the vaporization flask, by means of a syringe mounted on an infusion pump. The total conversions and product selectivities were calculated as before and the effect of the accumulated poison on the total conversion with mol % poison injected for both catalysts is reported in Fig 4.11.

4.2.3.6 ^{27}Al and ^{29}Si MAS NMR

^{27}Al and ^{29}Si experiments were carried out on Chemagnetics CMX 270 and CMW 300 spectrometers, respectively. All ^{29}Si and ^{27}Al chemical shifts were referred to tetramethylsilane $[Si(CH_3)_4]$ and $[Al(H_2O)_6]^{3+}$, respectively. The following parameters were used.

Table 4.1

Parameters	^{27}Al	^{28}Si
Resonance Frequency(MHz)	78.069	53.660
Spin Rate (Hz)	4	3
Pulse Width (μsecs)	1.6	3.5
No of Acquisitions	500	1600

4.2.3.7 XENON NMR

The following samples were analyzed : HZ, NaZ, NaDZ and HDZ NaDZ450 (NaDZ activated at 450°C). The samples were pretreated by heating approximately 0.5 g of zeolite powder in a sample cell to 450° C at a rate of 12° C/hr under a pressure of 10^{-2} Pa. These conditions were maintained for 16 hrs. The sample cells were isolated and different pressures of xenon were admitted and allowed to equilibrate. Isotherms of N (number of xenon atoms adsorbed/g zeolite) vs Pressure (Torr) have been plotted for each of the samples (Fig 4.13). NMR spectra were obtained at room temperature (26°C), for samples for which different pressures of xenon was adsorbed, using an MSL 100 Fourier Transform Spectrometer operating at 24.9 MHz. The recycle delay was 0.5 s, spectral width was 10 KHz and the number of scans varied between 1000 to 250000. Chemical shifts are measured relative to xenon gas extrapolated to zero pressure. A plot of the chemical shifts that were obtained for the samples HZ and HDZ is given in Fig 4.14.

4.3 RESULTS AND DISCUSSION

Table 4.2 reports some chemical and physical properties, including the textural characteristics, of Na-Z, H-Z, Na-DZ and H-DZ. It can be seen that desilication increased the volume of mesopores (Tables 2.5 and 4.2) ; however, despite the importance of the Si removal (as shown by the quite large variation of the Si/Al ratio), the healing process that occurs during the activation of the desilicated material succeeded in: i) preserving the ZSM-5 structure, ii) limiting the loss of the crystallinity, and iii) homogenizing the distribution of the micropore size which was still in the 6 Å region (Figure 4.6). In fact, while the parent ZSM-5 zeolite displayed a micropore distribution with two peaks corresponding to two sizes (and shapes) of channel (31), the desilicated material showed only one peak corresponding to *circa* 6 Å.

The data in Table 4.2 also shows that the incorporation of protons into the desilicated zeolite (Na-DZ) by ion-exchange with NH_4^+ and activation at high temperature to provide the acid form (H-DZ) did not significantly change the main characteristics of the material. Thus, "proton attack" which was so damaging for the structure of the Al rich zeolites (87,114), was not actually detrimental for the H-DZ sample owing to the still fairly high Si/Al ratio of this material. This also confirms that almost all the tetrahedral Al (IV) sites of the H-DZ, which had been modified by the desilication and subsequently regenerated by the healing process (64), were quite resistant to the "proton attack".

Table 4.2 Some chemical and physical properties of the zeolites studied

ZEOLITE	Si/Al[1]	DC[2]	BET[3]	Volume N_2 adsorbed		Acid density
				Mes[4]	Mic[5]	μmol/g
Na-Z	19.5	100	359	0.216	0.120	no[6]
H-Z	20.3	100	373	0.241	0.104	229
Na-DZ	13.2	89	389	0.423	0.108	no[6]
H-DZ	13.6	87	406	0.407	0.103	357

[1] atomic ratio, determined by chemical analysis

[2] degree of crystallinity (%); a 100 % DC was assigned to the Na-Z only for convenience

[3] BET surface area (m^2/g)

[4] adsorbed by the mesopores (cm^3/g)

[5] adsorbed by the micropores (cm^3/g)

[6] no acidity

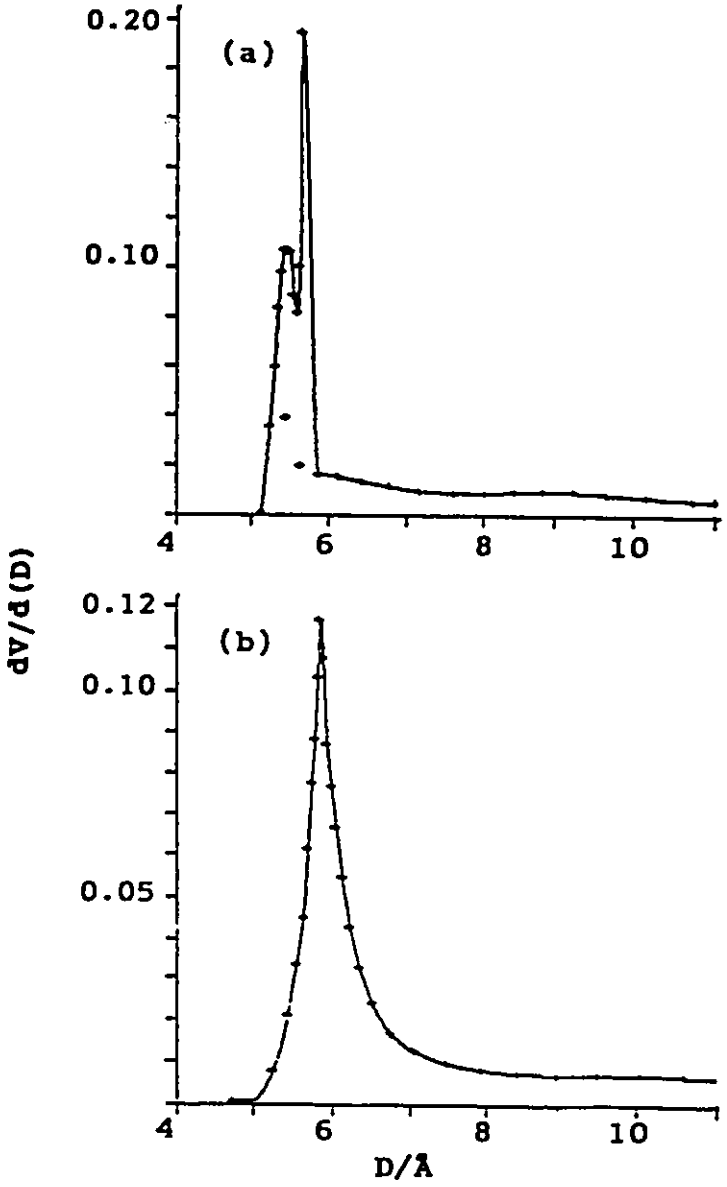

Fig 4.6 Micropore size distribution dV/d(D) (pore volume, V, cm^3/g argon adsorbed) versus pore diameter (D): a) parent ZSM-5 (Na-Z) and b) desilicated ZSM-5 (Na-DZ).

Rabo et al (87) and Okamoto et al (131) have proposed that Al (IV) sites which can be considered as resulting from the acid-base interaction of a terminal silanol with an Al Lewis site, are the form in equilibrium with the tetrahedral Al configuration.

Nevertheless, some of these sites in the H-DZ sample were converted, upon activation at high temperatures, into Lewis acid sites having the Al (III) configuration. The latter are not as easily rehydrated as the "normal" Lewis acid sites obtained by dehydroxylation of "normal" Bronsted acid sites (37). The almost complete integrity of the Al (IV) sites in the H-DZ sample was also confirmed by the ^{27}Al MAS-NMR data (Fig. 4.7 (a) and (c)) which show that the amount of octahedral Al (extra-framework Al (VI), δ = ca 0 ppm) was very small when compared to the Al with tetrahedral configuration (δ = ca 60 ppm). On the other hand, the ^{29}Si MAS-NMR spectra (Fig. 4.7 (b) and (c)) show peaks at δ = - 114 ppm assigned to Si(0Al) and δ = - 106 assigned to Si(1Al) (132). It is seen that the ratio of the peak intensities, Si(1Al)/Si(0Al) (Fig. 4.6 (b) and (c)) increased noticeably upon the desilication/healing of the HZ while there was a significant decrease of the overall Si/Al ratio of such a sample (Table 4.2). This suggests that the Si environment of the desilicated zeolite, represented by the Si(1Al)/Si(0Al) ratio, was now richer in Al than that of the parent zeolite.

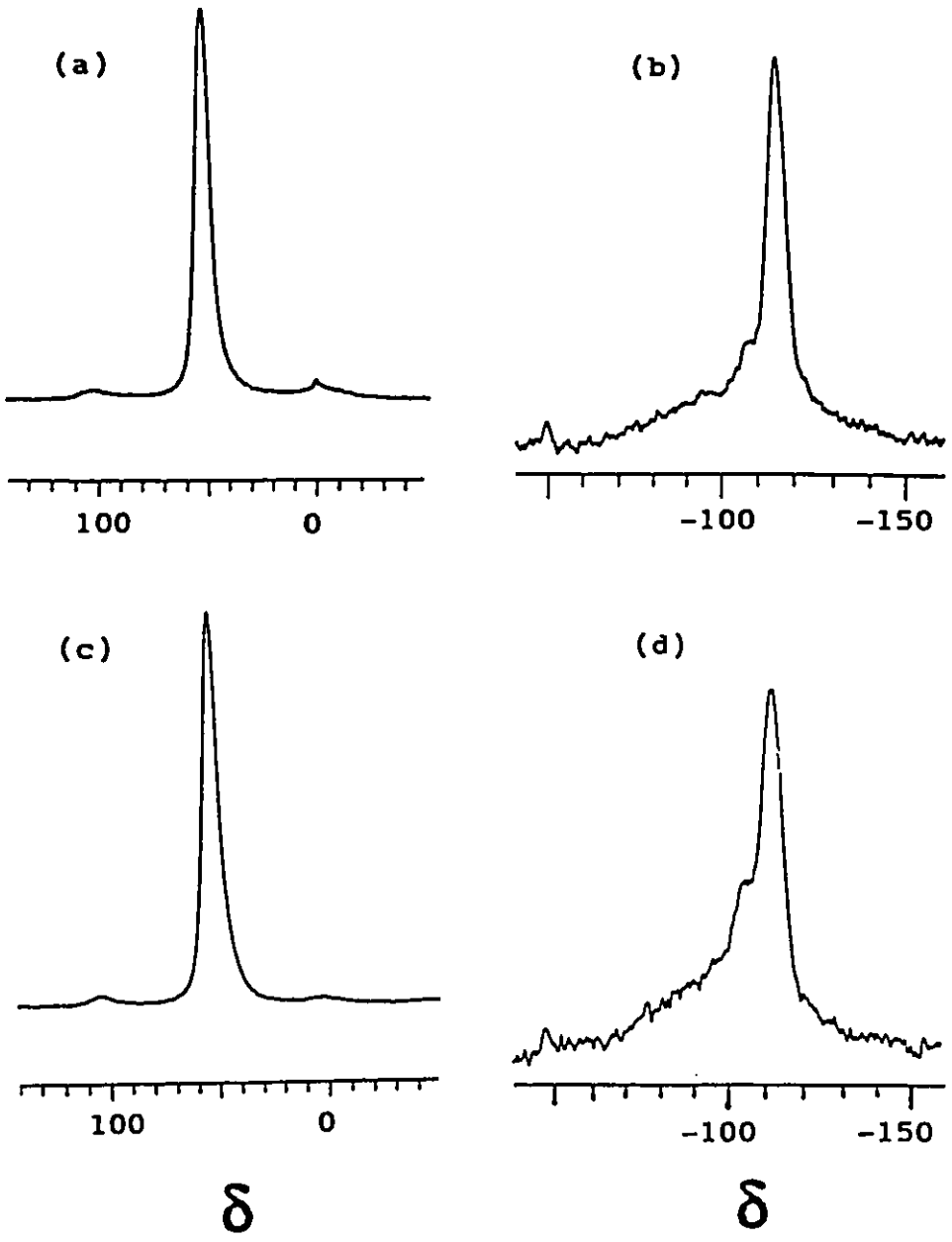

Fig 4.7 ^{27}Al MAS-NMR spectra [chemical shift with respect to $Al(OH)_6^{3+}$] of: a) Na-Z (parent ZSM-5) and (c) Na-DZ (desilicated ZSM-5); and ^{29}Si MAS-NMR spectra [chemical shift δ in ppm with respect to TMS] of: (b) Na-Z and (d) Na-DZ. Ordinate axis in arbitrary units of intensity.

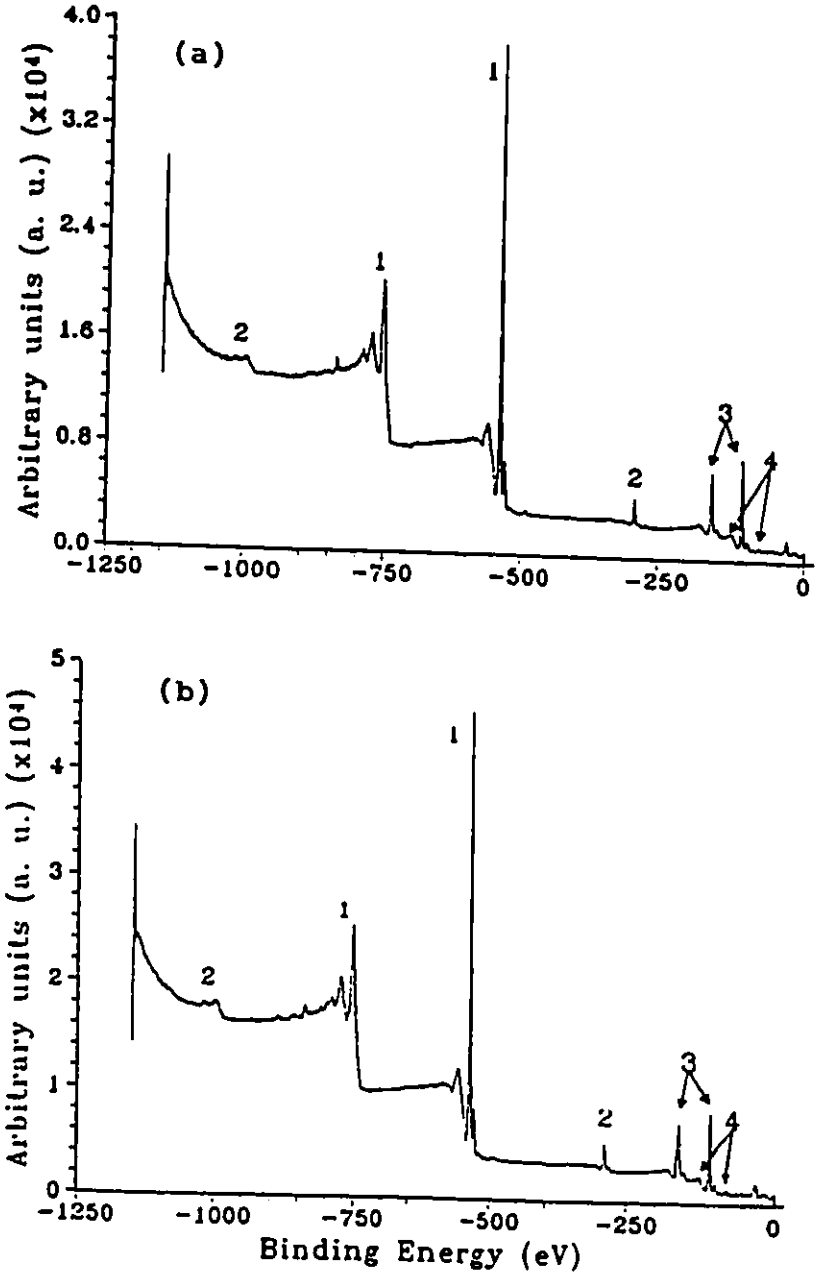

Fig. 4.8 XPS survey spectra of : (a) H-Z (acid form of parent ZSM-5) and (b) H-DZ (acid form of desilicated ZSM-5). Peaks 1, 2, 3 and 4 are related to O, C, Si and Al, respectively.

Table 4.3 Frequency shift of the FTIR stretching bands of the T-O bond in the desilicated ZSM-5 zeolite (resolution: 1 cm^{-1})

Sample	Si/Al	ν_{asym}/cm^{-1}	ν_{sym}/cm^{-1}
Na-Z	19.5	1102	798
H-Z	20.3	1102	798
Na-DZ	13.2	1094	793
H-DZ	13.6	1096	795

Table 4.3 reports the results obtained with the FT-IR technique, which are in agreement with results of reference (58) ie. that upon desilication the stretching bands of the framework (Si-O or Al-O) bond shifted towards lower frequencies owing to the decrease of the Si/Al ratio.

Table 4.4 and Fig. 4.8 show the results obtained with the XPS technique on the H-Z and H-DZ. Table 4.4 reports the binding energies (BE), obtained from curve fitting, for the O_{1s}, Si_{2p} and Al_{2p}. The values of the Si_{2p} BE of the HZ are slightly higher than those of the Na-Z in agreement with the data reported in the literature (92). This was due to the replacement of the Na^+ by H^+, the latter species being less ionic than the former. The increased ionicity of the Na-O bond as compared to the H-O correlates with increased covalency of the

adjacent Si-O and Al-O bonds. This causes a shift in the binding energies to slightly lower values for the Si_{2s} and Al_{2p} electrons if the Na form dominates in the zeolite.

Slightly higher binding energies of the Si_{2s} and Al_{2p} peaks were obtained in this work for both parent, HZ and desilicated ZSM-5 zeolite, HDZ. The increased acidic character of HDZ is depicted as on averall decrease in average binding energies of the Al_{2p} and Si_{2s} peaks. This correlates with an increased covalency of the Al-O and Si-O bonds and an increased ionicity (acidity) of the H-O bond.

Fig 4.9 (a) and (b) show the deconvolution curves for the Al_{2p} peaks indicating the relative amounts of aluminum in different coordination in HZ and HDZ. The two peaks of Al_{2p} correspond to the two configurations of the Al, Al (IV) and Al (III). The latter coordination is commonly observed when high Si zeolites are activated at high temperatures (122,123), as in the case of the H-Z and H-DZ samples. As observed by Remy et al. (122), the XPS Al (IV) peak is also associated with extra-framework Al (VI). However, since the amounts of octahedral Al in both samples, according to the previous ^{27}Al MAS-NMR results were very small, the XPS Al_{2p} peak with lower BE may be considered as corresponding essentially to the Al (IV) whereas the second Al_{2p} peak may be due to the presence of Al in a coordination state which is neither IV nor VI, i.e. III (122).

Table 4.4 XPS Binding Energies (BE) for the zeolites studied.

Zeolite	Binding energies[1] [][2]		Si/Al[3]	
	Si_{2p}	Al_{2p}	Bulk[4]	Surface[5]
H-Z	103.4 [25.5]	74.6 [0.8]	20.3	17.8
	104.6 [3.0]	75.7 [0.8]		
H-DZ	102.8 [16.4]	74.2 [1.3]	13.6	11.7
	103.5 [10.6]	75.4 [1.0]		

[1] in eV (+/- 0.05 eV), referenced to C_{1s} = 285.0 eV

[2] concentration in (%) (normalized to elemental composition obtained by XPS)

[3] atomic ratio

[4] obtained by chemical analysis

[5] obtained by XPS

Nevertheless, the increase of the total amounts of the Al species upon desilication was clearly shown by XPS analysis. Table 4.4 shows the sums of the normalized concentrations corresponding to all Al_{2p} peaks: 1.6 % for H-Z and 2.3 % for H-DZ).

Since two values of BE were found for Si_{2p} for all the samples, the species having the higher BE should correspond to the Si-O bond of the Si-O-H bridge. Since the O-H bond of the silanol group is predominantly covalent (the amount of acidic SiOH groups in both samples, HZ and H-DZ, being very small), the Si-O bond of such a group is also predominantly covalent. This results in a BE value (104.6 eV or 103.5 eV, Table 4.4) for the Si of the silanol group which is higher than the BE value of the Si of the Si-O-Si bridge (103.4 eV or 102.8 eV, Table 4.4).

Since desilication leaves a Si vacancy with 4 silanol groups for each Si atom removed (64), the amount of Si species related to silanol groups increases steadily with this treatment (Table 4.5). In addition, the Si removal resulted in an enhanced ionic character for the zeolite framework (or a decreased covalency (92) by "increasing" the content of the Al-O bonds, thus causing a general decrease of the values of the binding energy for both Si_{2p} and Al_{2p} (Table 4.4). A decrease in Si/Al ratio is accompanied by a decrease in average binding energies (87).

Finally, all the values of the surface Si/Al ratio determined by XPS were significantly lower than those of the bulk Si/Al ratio determined by atomic

absorption spectroscopy. This suggests an aluminum zoning in both the ZSM-5 and desilicated zeolite particles (i.e. the external surface is richer in Al than the bulk) as already observed by Dessau et al (61). Dehydroxylation of the "healed" Bronsted acid sites of the H-DZ sample (by activation at high temperature) resulted in Lewis acid sites (LAS of type II, Figure 4.10) whose reverse-conversion (rehydration) to the Bronsted acid configuration (BAS of type II, Figure 4.10) was "more demanding" than with the normal "Lewis" acid sites (LAS of type I giving the BAS of type I upon rehydration, Figure 4.10) of the parent H-Z zeolite.

Table 4.5 Assumption of the nature of Si-O bond based on the XPS results

Sample	Si/Al	Binding energy (eV)	Relative amt[1] (%)	Assumed nature of Si-O bond
H-Z	20.3	103.4	90	Si-O-Si
		104.6	10	Si-O-H
H-DZ	13.6	102.8	61	Si-O-Si
		103.5	39	Si-O-H

[1] calculated using the values of normalized concentrations of Table 4.4

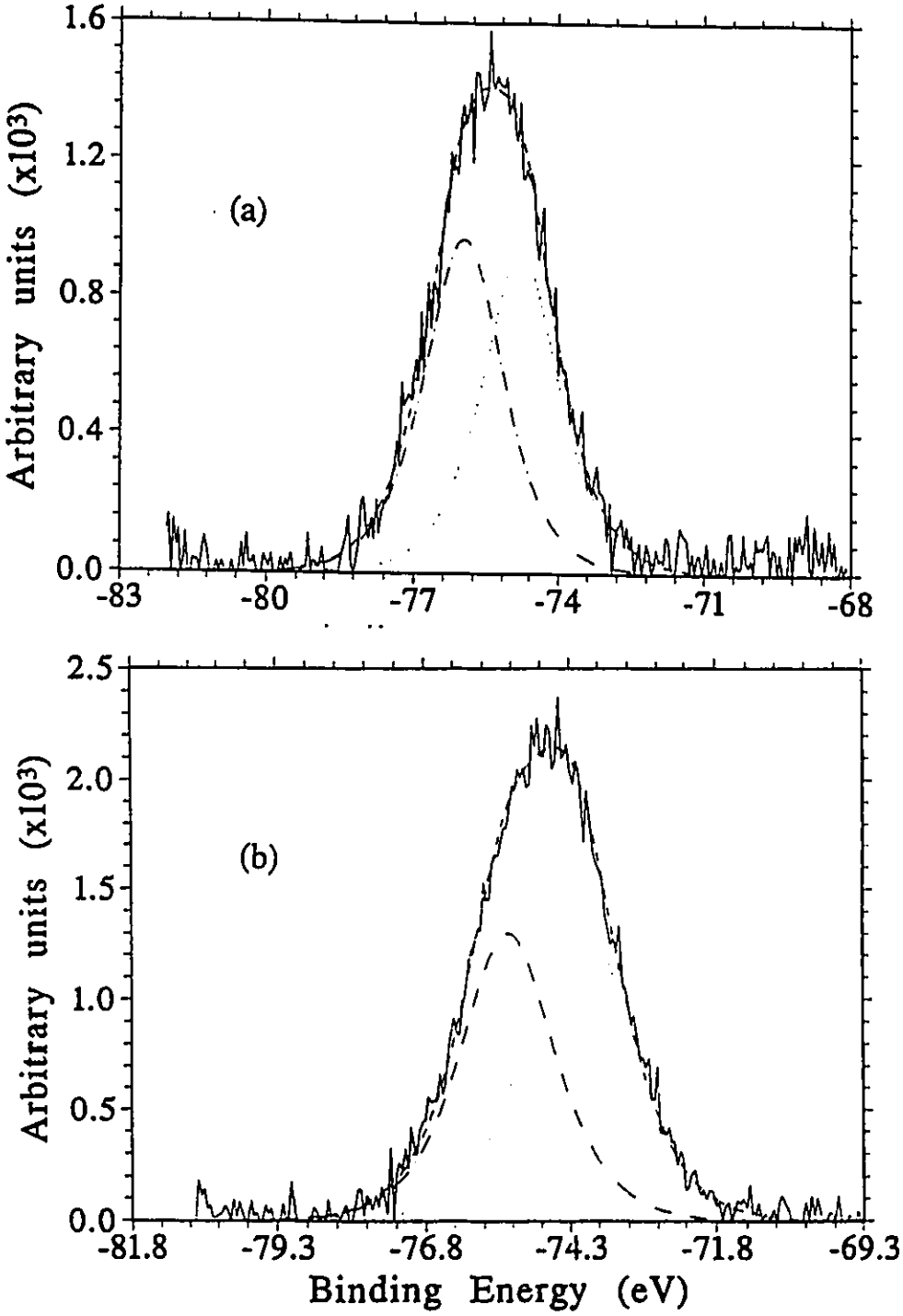

Fig 4.9 Curve fitting (XPS) for Al_{2p} peaks for (a) HZ and (b) HDZ

In fact, there were several indications of such a difference :

i) some "unusual" Lewis acid sites were detected by MAS-NMR as discussed in Chapter 3, in the partially rehydrated H-DZ (desilicated ZSM-5) while there was no significant amount of such an acidity in the partially rehydrated H-Z (parent ZSM-5) (64);

ii) dehydration of (absolute) ethanol produces water (9,10):

a) by a two-step conversion :

$$2\ C_2H_5OH \rightleftharpoons (C_2H_5)_2O + H_2O \rightleftharpoons 2C_2H_4 + H_2O$$

b) direct conversion :

$$C_2H_5OH \longrightarrow C_2H_4 + H_2O$$

Thus, after a few minutes on stream, the "normal" Lewis sites (LAS I) of the H-Z would be fully rehydrated into Bronsted acid sites (BAS I) by water produced by the dehydration of ethanol reaction, so that injection of poisons such as pyridine and 2,6-dimethylpyridine affected the catalyst activity in the same manner (Figure 4.11). However, the poison testing curves for HDZ shows that this catalyst has a higher activity using 2,6-dimethylpyridine compared to pyridine, which could be ascribed to the presence of these "less reversible" Lewis acid sites (LAS II). Presumably, the rehydration of LAS II into the more easily poisoned corresponding BAS II does not occur under the conditions used for the dehydration of ethanol reaction, and the LAS II remain active.

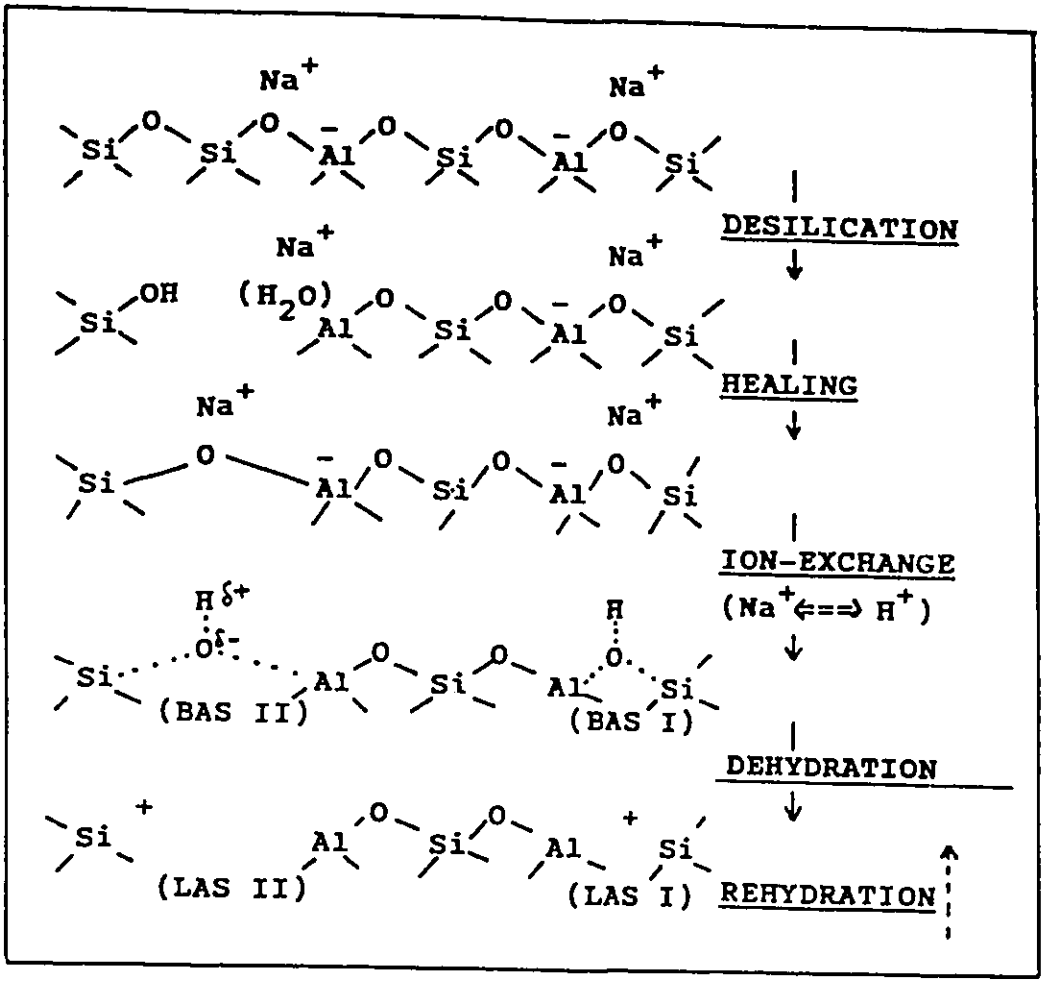

Fig 4.10 Schematic representation of the Bronsted acid sites (BAS) and the Lewis acid sites (LAS) of the H-DZ sample. (I) and (II) = "normal" and "desilication/healing-derived" types, respectively.

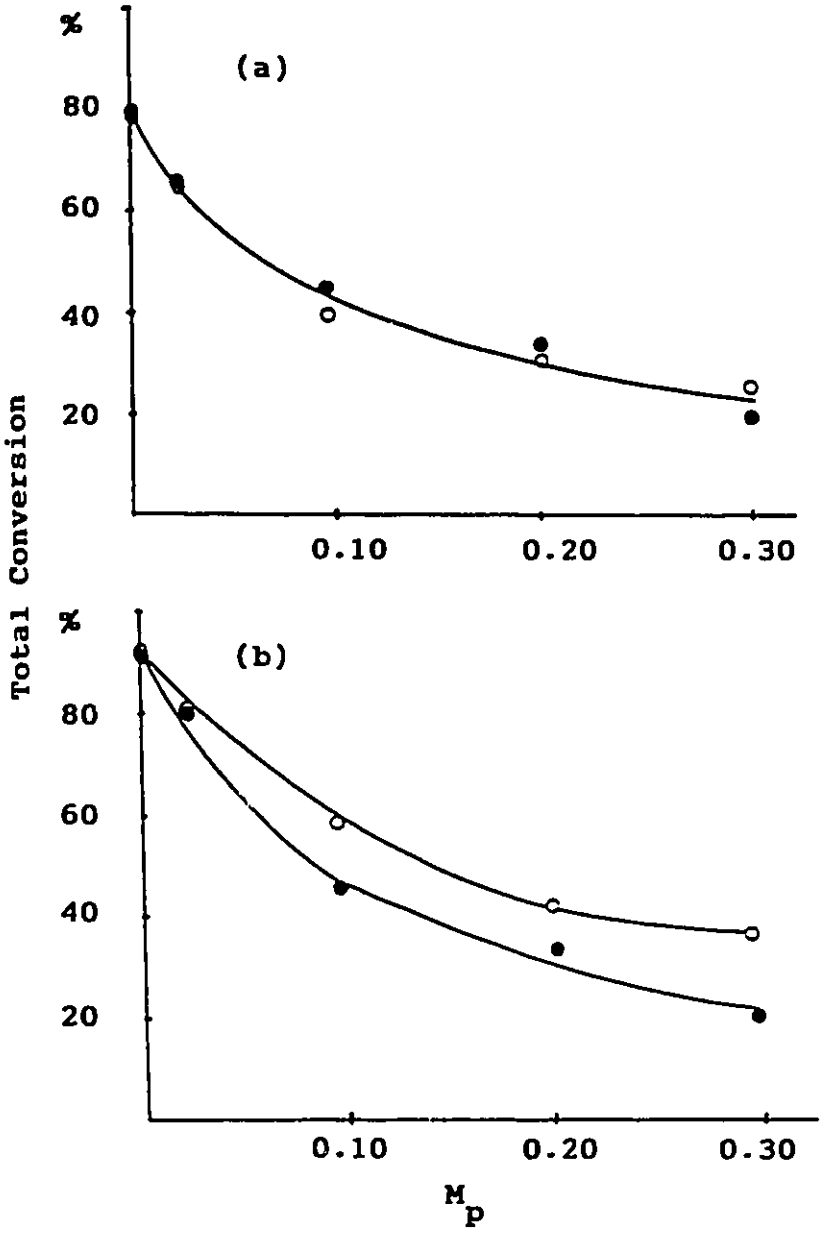

Fig 4.11 Poisoning testing over: (a) H-Z and (b) H-DZ catalysts. (●) = pyridine and (○) = 2,6-dimethylpyridine. Total conversion of ethanol (C_t) versus moles of poison injected/moles of injected ethanol (M_p, %).

Table 4.6 Results of the catalytic testing in the conversion of ethanol.

Sample	Temperature (° C)	Total conversion (C atom %)	Product Selectivities[1] S_{DEE}	S_{et}	S_{OHC}
H-Z	200	66.9	89.4	10.4	0.2
	225	79.6	11.6	87.2	1.2
	250	91.5	2.9	93.6	3.5
H-DZ	200	78.2	93.8	6.2	0.0
	225	89.7	15.1	84.4	0.5
	250	98.6	0.3	95.0	4.7

[1] DEE = diethylether; et = ethylene and OHC = other hydrocarbons

Table 4.6 reports the results of the conversion of absolute ethanol over the H-Z and H-DZ catalysts at 200 - 250 °C. When compared to the parent ZSM-5 zeolite H-Z, the desilicated zeolite H-DZ showed a higher conversion of ethanol for all reaction temperatures (Table 4.6). This is readily understandable because the H-DZ catalyst had a higher density of acid sites (Table 4.2). Moreover, at low reaction temperatures, the H-DZ sample was slightly less selective for ethylene and higher hydrocarbons (comparison at equal conversions) suggesting that there were fewer strong acid sites in the H-DZ than in the parent H-Z. (It is generally known that stronger (Bronsted) acid sites are required for the direct one step conversion of ethanol into ethylene (10)).

This was confirmed by the profile of the ammonia TPD curves of the two zeolites (Figure 4.12) showing that in H-Z the number of strong acid sites was slightly higher than in H-DZ. The technique of peak deconvolution gave the following results (+/- 1 %):

i) H-Z: W = 36 % ; M = 30 % and S = 34 %

ii) H-DZ: W = 39 % ; M = 32 % and S = 29 %

Where W, M and S refer to weak, medium and strong acid sites.

This slight decrease in the number of "strong" acid sites in the H-DZ might at first be ascribed to the higher Si/Al ratio of the H-Z sample since it is known that higher strength is obtained with more isolated Bronsted acid sites displaying higher topological densities (87,134).

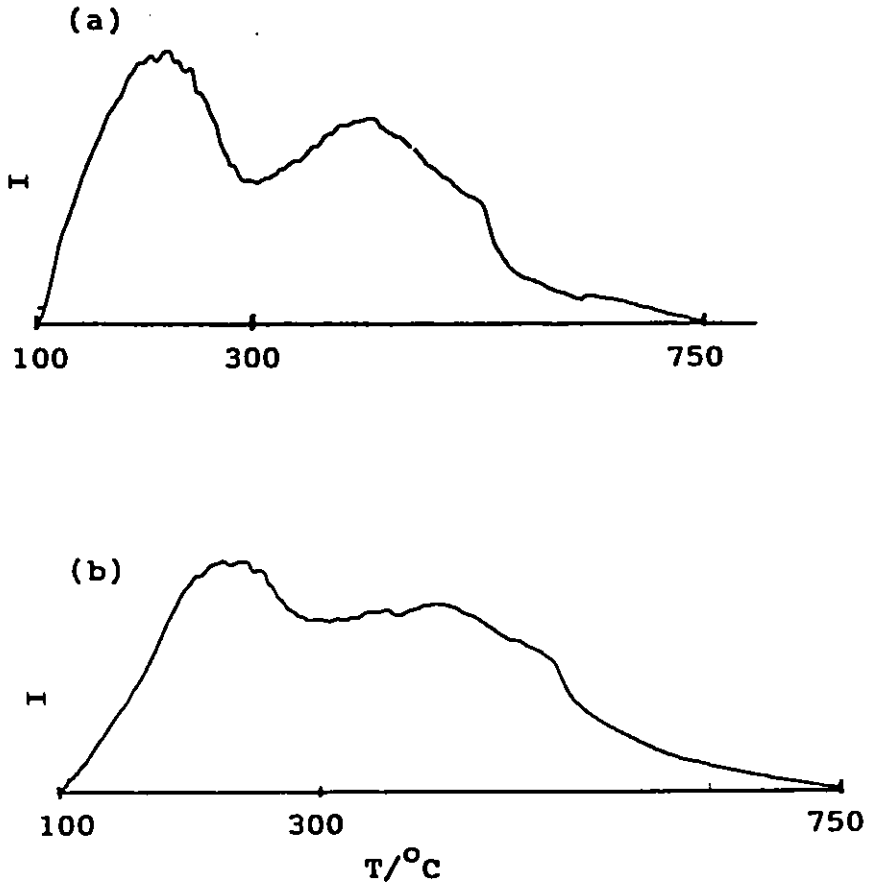

Fig 4.12 Ammonia TPD profiles of: (a) H-Z and (b) H-DZ catalysts. I is the response of the GC thermal detector in arb. units.

However, since both zeolites had a Si/Al higher than the threshold (Si/Al = 9.5) defined for the MFI structure (134), the slight difference in the acid strength between the "healed" BAS (type II, Fig 4.10 (b)) and the normal BAS (type I, Fig 4.10 (a)) should be taken into account in further investigations.

Fig 4.13 is a plot of the xenon isotherms for parent and desilicated ZSM-5 zeolite and the desilicated zeolite activated at 450°C showing their relative adsorption capacities. From the isotherm plot of N(Xe atoms adsorbed/g) vs P(torr) shown in Fig 4.12, the desilicated zeolite and parent were seen to have similar xenon adsorption capacities although the desilicated sample had a slightly higher adsorption capacity at higher xenon pressures. This is in agreement with the slight enlargement of the existing mesopores through desilication as was observed (57) in Chapter 2. Activation of the desilicated ZSM-5 at 450°C resulted in an increase in adsorption capacity which is attributed to the removal of extraporous material generated during desilication in combination with the "healing effect" (Fig 4.13 in which NaDZ450 displayed the highest adsorption capacity of all the samples).

A plot of the chemical shift (ppm) from ^{129}Xenon NMR vs N(Xenon atoms adsorbed/g) for HZ and HDZ shows higher average chemical shifts for the modified sample compared to the parent (Fig 4.14). An increase in slope was also obtained for increasing pressures of xenon adsorbed on the zeolite. This is characteristic of ZSM-5 zeolites, since their adsorption capacity changes at higher xenon pressures due to their channel structure (31,98).

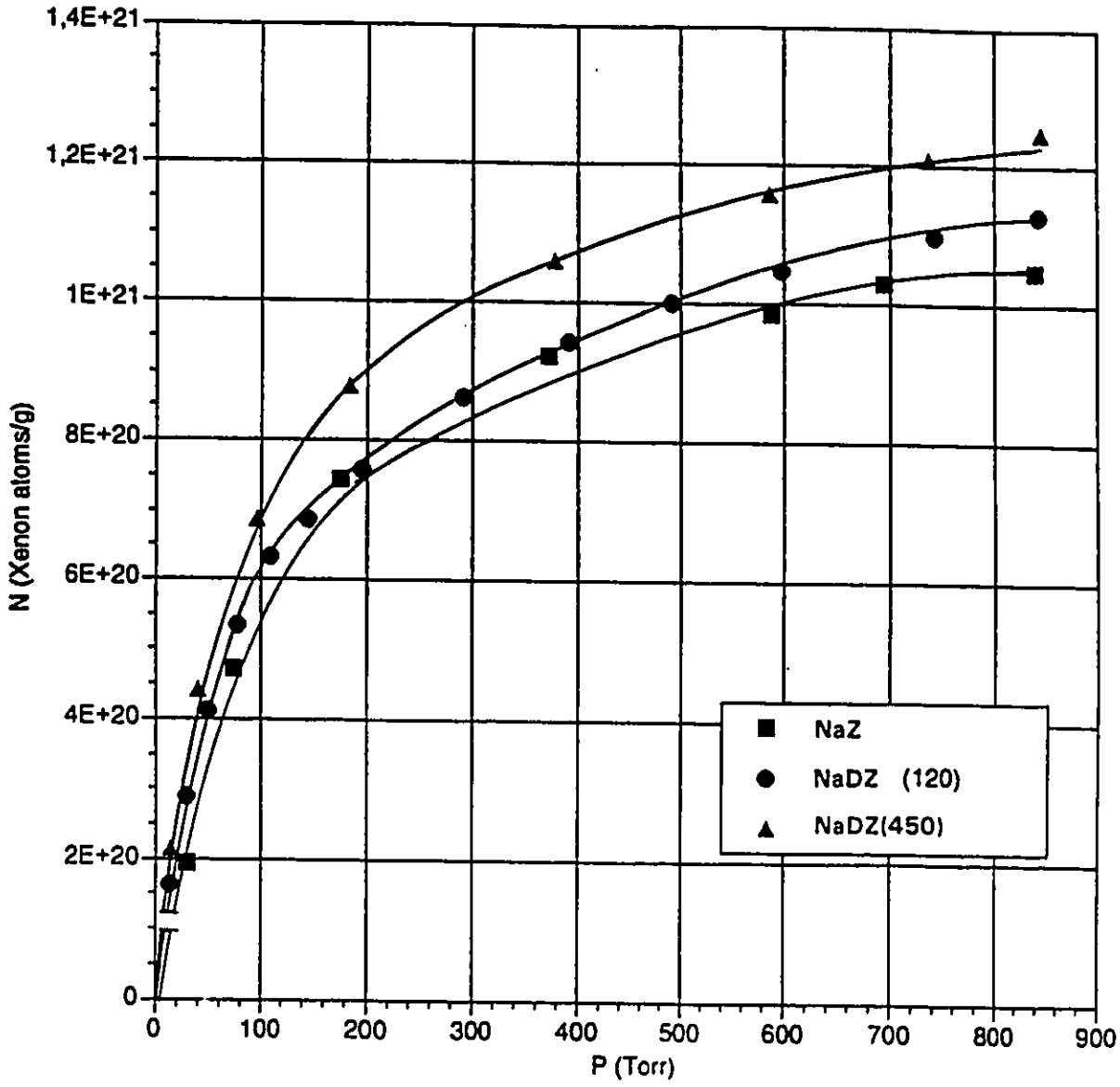

Fig 4.13 Xenon isotherms (Number of xenon atoms adsorbed/g zeolite with increasing pressure (Torr)) for NaZ, NaDZ and NaDZ450.

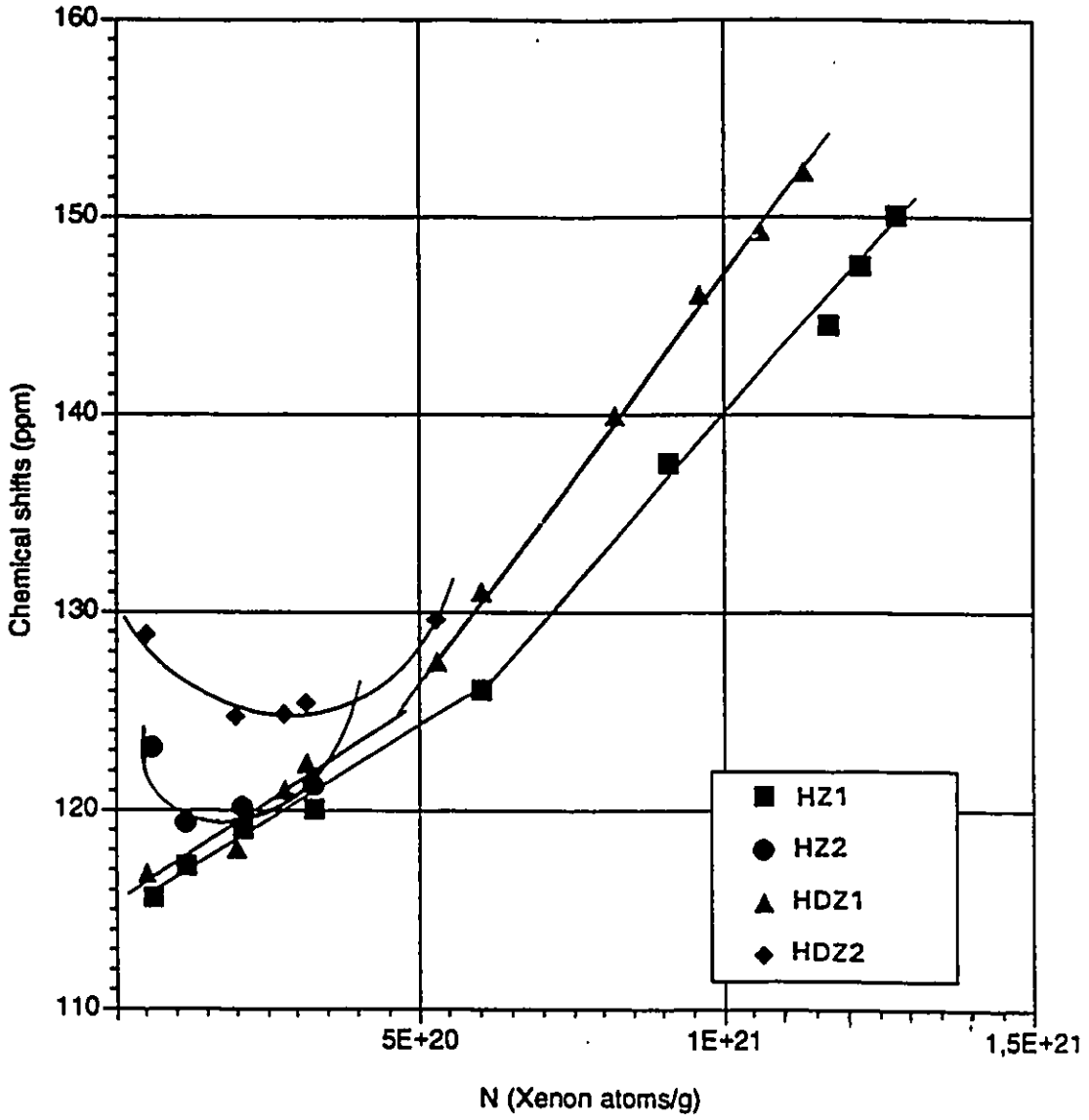

Fig 4.14 Plot of ^{129} Xenon chemical shifts (ppm) vs N (number of xenon atoms adsorbed/g zeolite) for parent (HZ) and desilicated zeolite (HDZ); HZ1 and HDZ1 are main and HZ2 and HDZ2 are second signals in ^{129}Xenon NMR respectively.

An increase in chemical shifts is associated with the presence of Strong Adsorption Sites (SAS), such as occurs in the presence of highly polarizable cations eg. extra framework Al^{3+} in the zeolite, or as diffusion of xenon becomes more difficult which occurs when Xe-Xe interactions within the zeolite become more significant. Comparison of the slopes of the chemical shifts vs N (Xenon atoms/g) at high Xenon pressures shows a higher value for the treated sample ($3.29x\ 10^{-20}$) compared to the parent (2.18×10^{-20} in Table 4.6). The value obtained for HZ is in agreement with those obtained for ZSM-5 by Alexander et al. ($2.6 \pm 0.4 \times 10^{-20}$ ppm/atom g^{-1}) (95). The increase in slope may be due to a lower crystallinity of the modified zeolite (88%) or an increase in SAS content, which is in agreement with a significant increase in the quantity of Al^{3+} (as LAS) in the modified sample (98). At low adsorbed xenon pressures the signals for both samples are coincident. The chemical shift when no xenon is adsorbed on the zeolite, (115 ppm) agrees with values obtained by Springer-Huet for ZSM-5 zeolite with a similar Si/Al ratio (98). The most outstanding feature however, is the presence of a second signal at low adsorbed xenon pressures for both parent and modified zeolite. The modified form also displayed higher average chemical shifts than the parent form for this second signal. This signal which is more significant in the modified sample is attributed to the presence of other Al species produced by desilication followed by healing. Gedeon et al. (136) have detected the second signal for zeolite samples known to have framework defects as Al^{3+}.

Table 4.7 Slopes of Plots of chemical shifts vs N (Xe/g) at high Xe pressures

Sample	Slope (pprn/atom g^{-1})
HZ	2.18×10^{-20}
HDZ	3.29×10^{-20}

The signal disappeared when the samples were leached with concentrated HNO_3 which served to remove the Al^{3+}. Further work is to be done on HZ and HDZ to study the effect of acid leaching on the second signal at low xenon adsorbed pressures.

4.4 CONCLUSIONS

Desilicated ZSM-5 zeolite (HDZ) showed a higher conversion of ethanol to ethylene when compared to the parent zeolite. This is due to the enhancement of the density of acid sites per weight unit resulting from the partial removal of framework Si in generating the H-DZ sample. Therefore, (controlled) desilication of ZSM-5 and other silica rich zeolites is an elegant method for post-synthetic adjustment of the Si/Al ratio. Desilicated zeolites can also be used as precursors for the preparation of special zeolites bearing acidic or redox species which are incorporated into the vacancies created by the removal of Si during the desilication operation (135).

CHAPTER 5

DEHYDRATION OF ETHANOL AND AQUEOUS ETHANOL OVER DESILICATED ZSM-5 ZEOLITE

5.0 INTRODUCTION

Kinetic investigations are important for the design of large scale reactors and they are usually performed in laboratory scale microreactors prior to upscale for commercial utility. In kinetic experiments, the measured reaction rates should not be disguised by mass and/or heat transfer resistances and the concentrations and temperatures at which the reactions occur must be accurately known. Proper mixing of the reaction solution with the catalyst (by turbulence) allows rapid transfer of material and the measured reaction rate is the actual rate. In such a situation both internal and external diffusion effects can be neglected. Thus high gas velocity around the particles is required to avoid interparticulate transport limitations.

In a perfectly mixed reactor, concentrations and temperatures are uniform and can be easily determined. The interpretation of experimental data in a gradientless reactor such as the one used in this work is simple, because no temperature or concentration profiles have to be interpreted as in an integral reactor type.

The parent and desilicated ZSM-5 zeolite were tested under similar

conditions of temperature and contact times and their total conversions in the dehydration of absolute ethanol compared. Their apparent activation energies were calculated for comparison of the similarity in the mechanisms of reaction for both catalysts. This approach is used in the present study in which the role of water in the reaction mechanism is elucidated by conducting dehydration reactions with aqueous and absolute ethanol at different temperatures.

5.1 EXPERIMENTAL

5.1.1 EXTERNAL DIFFUSIONAL EFFECTS

Prior to kinetic studies for the reactions catalyzed by HZ and HDZ, it was necessary to ensure that the reaction was not limited by external and internal diffusional and mass transfer effects, which if significant, may affect the physical and chemical processes of heterogenous catalytic reactions (Chapter 1). Internal diffusional effects can be considered as included in the rate measurements for zeolites due to the small particle sizes(142). External diffusional effects were studied in order to verify the constancy of catalytic activity in a flow system. This was accomplished by diagnostic tests in which the catalyst weight was varied from 6.00 to 1.53 g while the flow rate of reactant was simultaneously varied in such a way as to maintain the same WHSV. These tests were performed in the preliminary stages of the study of the dehydration of 10 % (wt) aqueous ethanol over steam treated HZSM-5 zeolite catalyst (7). Table 5.1 shows that the conversions to hydrocarbons and

ethylene was practically unchanged under these conditions, thus confirming that internal diffusional effects were insignificant in this reaction.

Table 5.1 Conversion of 10 wt % ethanol over steamed HZ(21) at 300°C and WHSV 3.2 hr^{-1} (from reference 10)

Feed (g/hr) Ethanol	Mass (g) Catalyst	Conv. HC(%)	Product Selectivity (%) Ethylene	C_3^+ Olefins
19.20	6.00	99.64	99.38	0.62
12.80	4.00	99.55	99.36	0.64
8.10	2.53	99.57	99.42	0.58
4.90	1.53	99.63	99.41	0.59

5.1.2 REPRODUCIBILITY OF EXPERIMENTAL DATA

Experiments were carried out in order to estimate the reproducibility of the data obtained for experiments for catalytic testing in the fixed bed horizontal microreactor. The catalyst used was a sample of HDZ prepared by treatment of NaZ with an aqueous solution of 0.8 M sodium carbonate and 0.01 N sodium hydroxide, subsequently ion exchanged with ammonium

chloride, dried and activated at 450°C to produce the acidic form of the zeolite with a Si/Al ratio = 14.2. The conditions used for these tests were as follows: mass of catalyst used = 0.8 g ; temperature = 225 ° C ; WHSV = 0.12 hr^{-1}; nitrogen flow rate = 12 ml/min ; feed reactant was absolute ethanol. The reaction data is reported in Table 5.2. The data was reasonably reproducible with an experimental error of ± 1.5 % for the values of total conversion and ± 3 % for the selectivity for ethylene.

Table 5.2

Run Number	Total Conversion (% C atoms)	Product Selectivity (C atom %)		
		Ethylene	DEE	*OHC
1	85.07	83.4	16.0	0.6
2	86.57	84.2	15.3	0.6
3	84.14	80.7	18.3	1.0
Average	85.26	82.7	16.5	0.73

* OHC : other hydrocarbons

5.1.3 TREATMENT OF KINETIC DATA

For heterogenous catalysis, the reaction rate, r, for a gas phase reaction in which reactant A is converted into product B is expressed as:

$$r = -d[A]/d\tau = k\,[A]^n$$

$$= -1/RT \times d[P]/d\tau = k/(RT)^n \times P^n$$

[A] is the concentration of A, τ is the contact time, k is the rate constant, n is the order of the reaction and P is the partial pressure of the reactant.

In the dehydration of ethanol to ethylene, C_t is the % total conversion of ethanol for a given contact time, t, and P_o is the initial partial pressure of ethanol. The partial presssure of ethanol P is given by

$$P = [(100-C_t)/100] \times P_o$$

and $$d[P]/d\tau = -dC_t/d\tau \times P_o/100$$

The general form of the rate equation is defined as the reaction rate ,

$$r = (P_o/100RT) \times dC_t/d\tau$$

and the initial rate r_o is given by

$$r_o = (r)_{\tau=0} = P_o/100RT\ (dC_t/d\tau)_{\tau=0}$$

$$= \text{constant 1} \times [dC_t/d\tau]_{\tau=0} \qquad (1)$$

where constant 1 = $P_o/100RT$

but $r_o = k \times P_o^n/[RT]^n$

$= k \times \text{constant 2}$ (2)

where constant 2 $= P_o^n/[RT]^n$ and k is expressed by the Arrhenius equation :

$$k = A \times e^{-Ea/RT}$$

in which A is the pre-exponential factor, E_a is the apparent activation energy, R is the molar gas constant and T is the absolute temperature. From (2)

$$r_o = A \times e^{-Ea/RT} \times \text{constant 2} \qquad (3)$$

A series of total % conversions (C_t) is obtained for the dehydration using absolute ethanol by varying the contact time at different temperatures. These temperatures were chosen to be within the range which permitted the conversion of ethanol into diethyl ether : 150, 160, 175 and 180°C. For each catalyst and each reaction temperature, the experimental data for total conversion were fitted to a function, f (τ), of the contact time, τ, by using a non-linear regression algorithm generated by the software "Slidewrite" (176). A third-order polynomial function was found to provide a good correlation factor (Cor), as follows:

$$C_t = a\tau + b\tau^2 + c\tau^3$$

In order to calculate the apparent activation energy, it was necessary to determine the initial rates of the reaction ie. when the contact time between reactant and catalyst is zero. The initial reaction rate, r_o, is obtained therefore by taking the derivative of the function f(t) at zero contact time ie.

$$[df(\tau)/d\tau]_{\tau=0} = (dC_t/d\tau)_{\tau=0}$$

$$(dC_t/d\tau)_{\tau=0} = a$$

From (1) r_o = constant 1 x $(dC_t/d\tau)_{\tau=0}$

= constant 1 x a (4)

From (2), (3) and (4)

$$a = (\text{constant 2/constant 1}) \times A\, e^{-Ea/RT}$$

$$a = \text{constant 3} \times A\, e^{-Ea/RT}$$

where constant 3 = $P_o^n/[RT]^n/P_o/100RT$

= $1/100(P_o/RT)^{n-1}$

$$\ln a = \ln A' - E_a/RT$$

where A' = constant 3 x A . The values of the apparent activation energy were determined from a plot of ln a vs $10^3/T$.

5.1.4.1 PREPARATION OF THE CATALYSTS

H-Z, was obtained by ion-exchange of the commercially available Na-ZSM-5 zeolite (Chemie Uetikon) with ammonium ions and then activated at 450 °C, as previously described. HDZ, also prepared as before by desilication of the Na-ZSM-5 and then transformed into the acid form by the same method of ion-exchange as that used for the HZ. The final forms of the zeolite catalysts, also referred to as H-Z and H-DZ, were prepared by extrusion with bentonite clay.

5.1.4.2 CHARACTERIZATION

H-Z and H-DZ samples were characterized by the following techniques: atomic absorption (chemical composition); X-ray diffraction (structural identification and measurement of the degree of crystallinity); BET surface area by adsorption of nitrogen and ammonia adsorption and TPD desorption (acid density). The results are reported in Table 5.3.

5.1.5 CATALYTIC TESTING

Catalytic test runs were performed in an experimental set up similar to that shown in Fig 4.4. Each run, typically lasting for 3 hours, was carried out with 100 wt % ethanol and 15 wt % ethanol in water (referred to as abs-ethanol and aqueous ethanol, respectively). The procedures for catalyst testing and product analysis were very similar to those already described. The reaction

conditions used were as follows: temperatures = 150-275 °C; contact time, τ (grams of catalyst per grams of ethanol injected per hour) = 0.06-0.4 h; flow-rate of nitrogen (used as carried gas) = 12 ml/min except for the kinetic study where this flow-rate was adjusted to keep the partial pressure of ethanol almost constant. The reported conversions and product selectivities calculated as before were average values.

5.2 RESULTS AND DISCUSSION

5.2.1 CHARACTERIZATION

As reported in Table 5.3, desilication of the ZSM-5 zeolite resulted in a lower Si/Al ratio. There was some decrease in the degree of crystallinity; however, the ZSM-5 structure was not destroyed and there was even some increase in the BET surface area, as reported earlier in this thesis. Healing phenomena were hypothesized to explain the full preservation of the framework Al atoms (64). In fact, when referred to a weight or surface area unit, there were significant increases in the cation exchange capacity (57,63) and in the density of acid sites (Table 5.3).

Table 5.3 Physico-chemical characteristics of the zeolites studied

Sample	Si/Al[1]	Na_2O[2]	Na/Al	DC[3]	BET[4]	Acid density[5]
H-Z	20.3	0.3	.08	100	373	229
H-DZ	13.6	0.1	.02	87	406	357

[1] atomic ratio; [2] in wt %; [3] degree of crystallinity (%); a 100 % DC was assigned to the H-Z only for convenience; [4] BET surface area in m^2/g; [5] in μmol/g

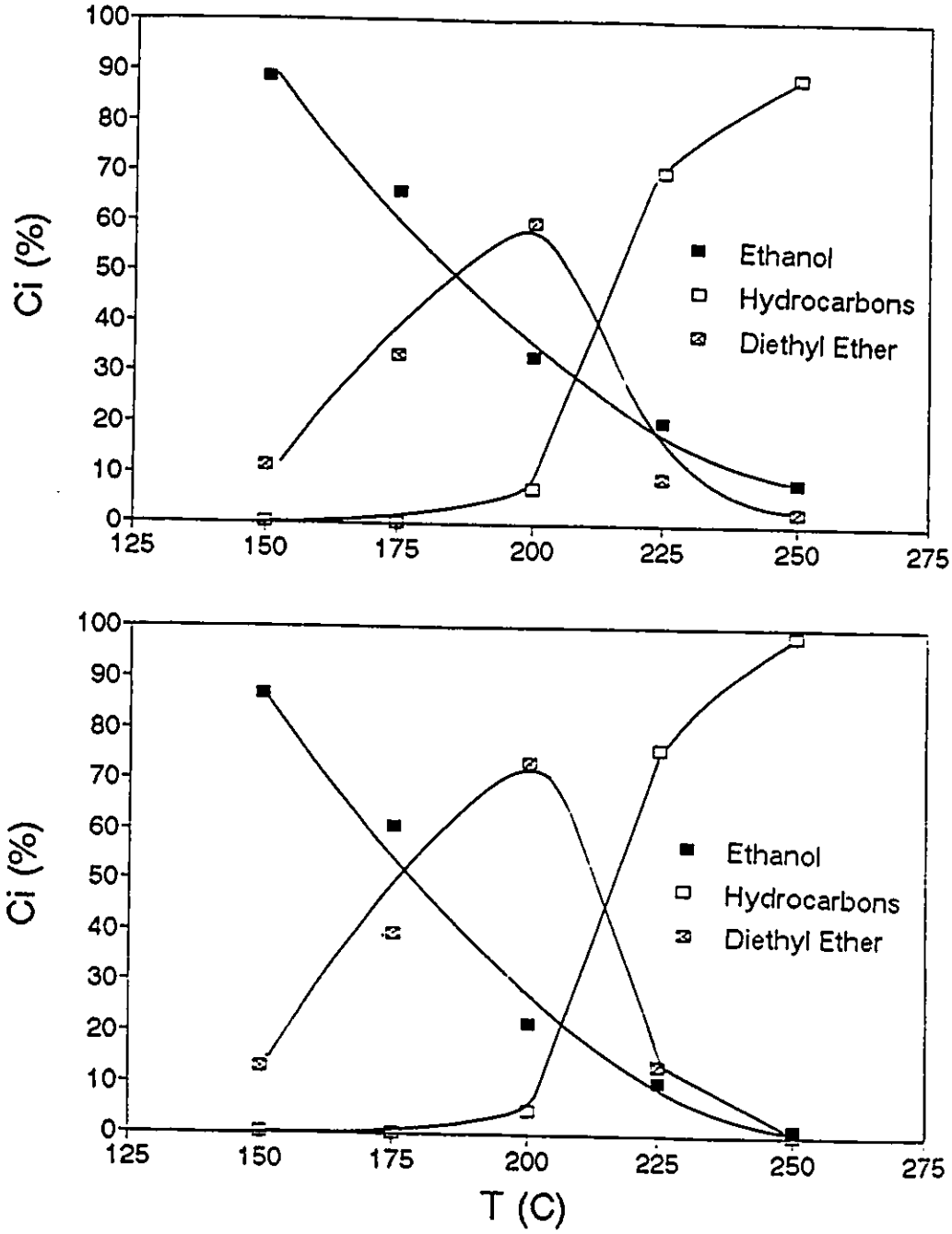

Fig 5.1 Composition of the reactor outstream (C_i) in % versus reaction temperature, T, (°C) for HZ (top) and HDZ (bottom) in the dehydration of absolute ethanol (□) hydrocarbons (□) diethyl ether (■) ethanol

5.2.2 DEHYDRATION OF ABSOLUTE ETHANOL

It is known that in the dehydration of an alcohol over alumina, both an intermolecular and an intramolecular dehydration may occur. These result in an ether and an alkene, respectively (138). Dehydration of two alcohol molecules to form an ether has a lower activation energy than the intramolecular dehydration to produce alkenes. Van Hooft et al.(5), Moser et al. (126), and Le Van Mao et al. (9,10) showed that over the ZSM-5 catalysts, the one step pathway (direct conversion to ethylene) coexisted with the normal two step one when the reaction temperature reached a relatively high value. It was also reported that over steam and asbestos derived ZSM-5 zeolites (9,10), such a "cut off point" occurred at 250-270°C. In order to determine whether such a cut off point existed we report in Figure 5.1 (a) and (b) data corresponding to the reactor outstream compositions obtained with the H-Z and H-DZ, for the dehydration of absolute ethanol using the same contact time (0.12 h) and varying the temperature from 150 °C to 250 °C. In both cases, there was indeed a cut-off point for the reaction mechanism when the reaction temperature was increased from 200 °C to 225 °C at which point there was a dramatic increase in the ethylene production from a few % to 70 -80 %. From Table 5.4 it can be seen that even the use of higher reaction contact times at 200 °C, which resulted in total conversions comparable to those obtained at 225 °C, provided ethylene selectivities which were extremely low when compared to those of 225 °C.

Table 5.4 Catalytic results for H-Z and H-DZ catalysts near cut-off point using absolute ethanol

Sample	Temperature T(°C)	Contact Time τ (h)	C_t (C atom %)	Product selectivities[1] S_{Et}	S_{DEE}	S_{OHC}
H-Z	150	0.12	11.4	0.1	99.9	0.0
	175	0.12	33.9	1.0	99.0	0.0
	200	0.12	66.9	10.4	89.4	0.2
	200	0.18	77.9	19.8	80.2	0.0
	225	0.12	79.6	87.2	11.6	1.2
	250	0.12	91.5	93.6	2.9	3.5
H-DZ	150	0.12	13.2	0.1	99.9	0.0
	175	0.12	39.3	0.3	99.7	0.0
	200	0.12	78.2	6.2	93.8	0.0
	200	0.18	81.6	17.0	83.0	0.0
	225	0.12	89.7	84.4	15.1	0.5
	250	0.12	98.6	95.0	0.3	4.7

[1] expressed in C atom %; Et = Ethylene; DEE = diethylether and OHC = hydrocarbons higher than ethylene

5.2.3 CALCULATION OF APPARENT ACTIVATION ENERGY

In terms of activation energy, the values reported in the literature are summarized as follows:

i) two-step pathway (predominating at low reaction temperatures):

ethanol $\rightleftharpoons$ (1) $\rightleftharpoons$ diethyl ether $\rightleftharpoons$ (2) $\rightleftharpoons$ ethylene

Apparent activation energies reported in the literature:

step (1) = 56 KJ/mol (steamed ZSM-5 and asbestos-derived ZSM-5 zeolites) (10).

step (2) = 79-80 KJ/mol (10) and 92 KJ/mol (5).

ii) direct conversion (effective only at high temperatures):

ethanol $\rightleftharpoons$ ethylene [5,126]

Apparent activation energies reported in the literature: 119-123 KJ/mol (10) and 122 KJ/mol (5).

The "cut off point" can be defined as the temperature range in which both pathways for the conversion of ethanol into ethylene coexist.

Table 5.5 (a) Determination of the initial rates r_o (Feed = abs-ethanol) for HZ

Sample	T (°C)/(K)	τ (h)	C_t (C atm %)	r_o [1]	Cor[2]
H-Z	150/423	0.24	16.9		
		0.17	13.9		
		0.15	12.5	152.5	0.99
		0.12	11.4		
		0.09	9.8		
		0.06	7.1		
	160/433	0.24	23.0		
		0.17	19.2		
		0.15	17.2	158.6	0.99
		0.12	14.6		
		0.09	11.9		
	175/448	0.24	49.8		
		0.17	42.6		
		0.15	35.6	313.6	0.93
		0.12	33.9		
		0.09	26.7		
		0.06	17.2		
	183/456	0.24	63.6		
		0.15	41.3	498.3	0.99
		0.09	29.7		
		0.06	22.7		

[1] expressed in mol/mol.h x 100
[2] correlation factor

Table 5.5 (b) Determination of the initial rates r_o (Feed = abs-ethanol) for HDZ

Sample	T (°C)/(K)	τ (h)	C_t (C atm %)	r_o [1]	Cor[2]
H-DZ	150/423	0.24	20.4		
		0.17	15.9		
		0.12	13.2	249.7	0.96
		0.09	10.6		
		0.06	10.4		
	160/433	0.24	24.7		
		0.15	20.4	267.6	0.99
		0.09	15.7		
		0.06	11.4		
	175/448	0.15	45.6		
		0.12	39.3	509.5	0.99
		0.09	31.1		
		0.06	23.6		
	183/456	0.12	44.8		
		0.09	37.7	968.9	0.99
		0.06	32.0		

[1] expressed in mol/mol.h x 100
[2] correlation factor

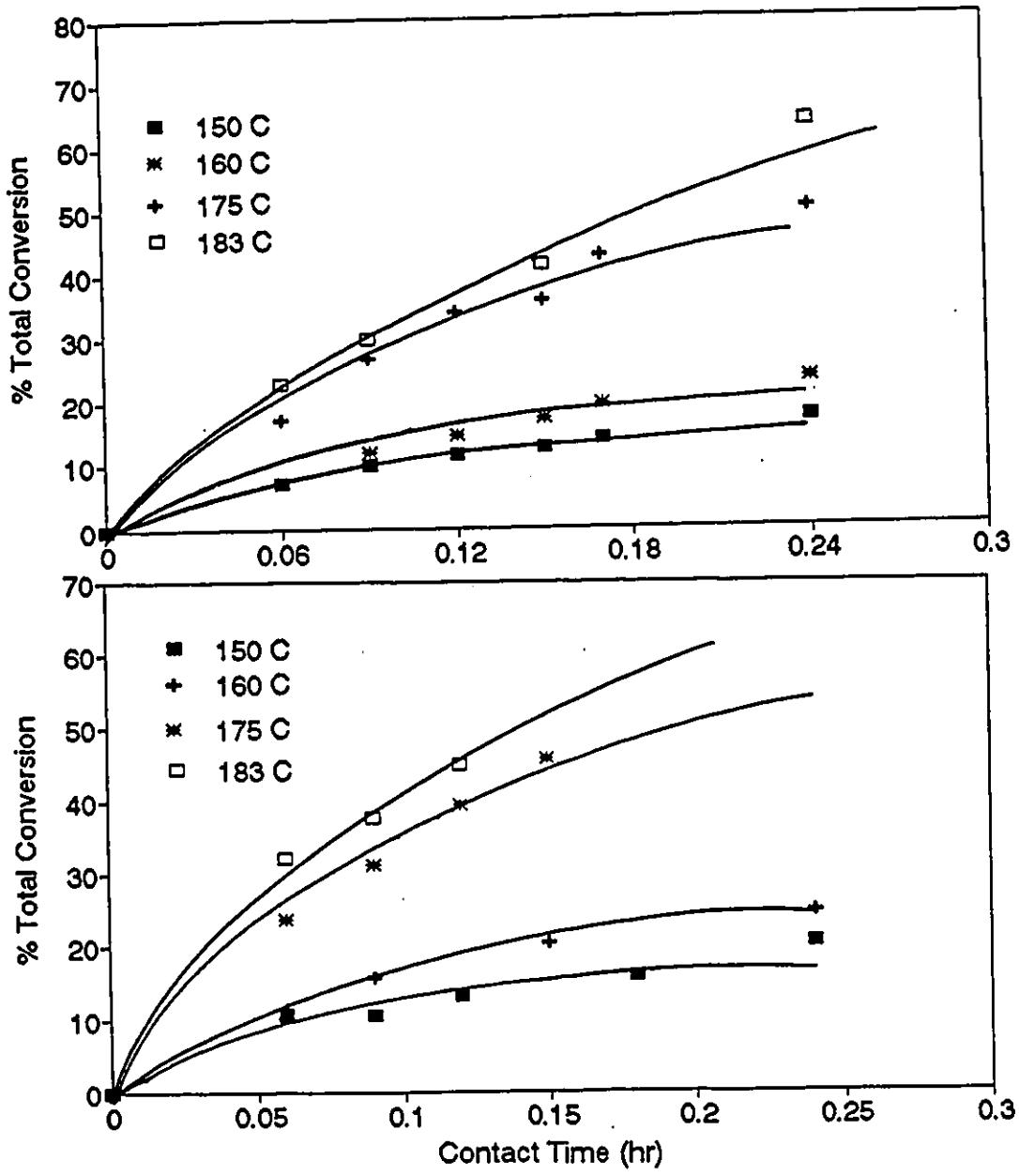

Fig 5.2 Variation of % total conversion with contact time at various temperatures for HZ (top) and HDZ (bottom)

Tables 5.5 (a) and (b) report the catalytic data which permitted calculation of the initial rates. Since these rates were determined within the 150 - 183 °C range, i.e. the temperature range where the two-step pathway prevailed, these initial data corresponded to the conversion of ethanol-to-diethylether. Fig 5.2 (a) and (b) show the variation of the total conversion with contact times at the various temperatures for HZ and HDZ respectively. Fig 5.5 shows the corresponding Arrhenius curves which resulted in the following values of the apparent activation energy:

i) for the H-Z sample, ΔE^a = 59 KJ/mol with a correlation factor of 0.96.

ii) for the H-DZ sample, ΔE^a = 65 KJ/mol with a correlation factor of 0.95.

Thus, these values are comparable to those reported in the literature for step (1) of the two-step pathway using the same ZSM-5 zeolite structure (ΔE^a = 56 KJ/mol (10) .

Table 5.6 Apparent activation energies calculated for HZ and HDZ

Catalyst	ΔE^a KJ/mol	A (Pre-exponential factor)
HZ	59	2.7×10^9
HDZ	65	2.4×10^{10}

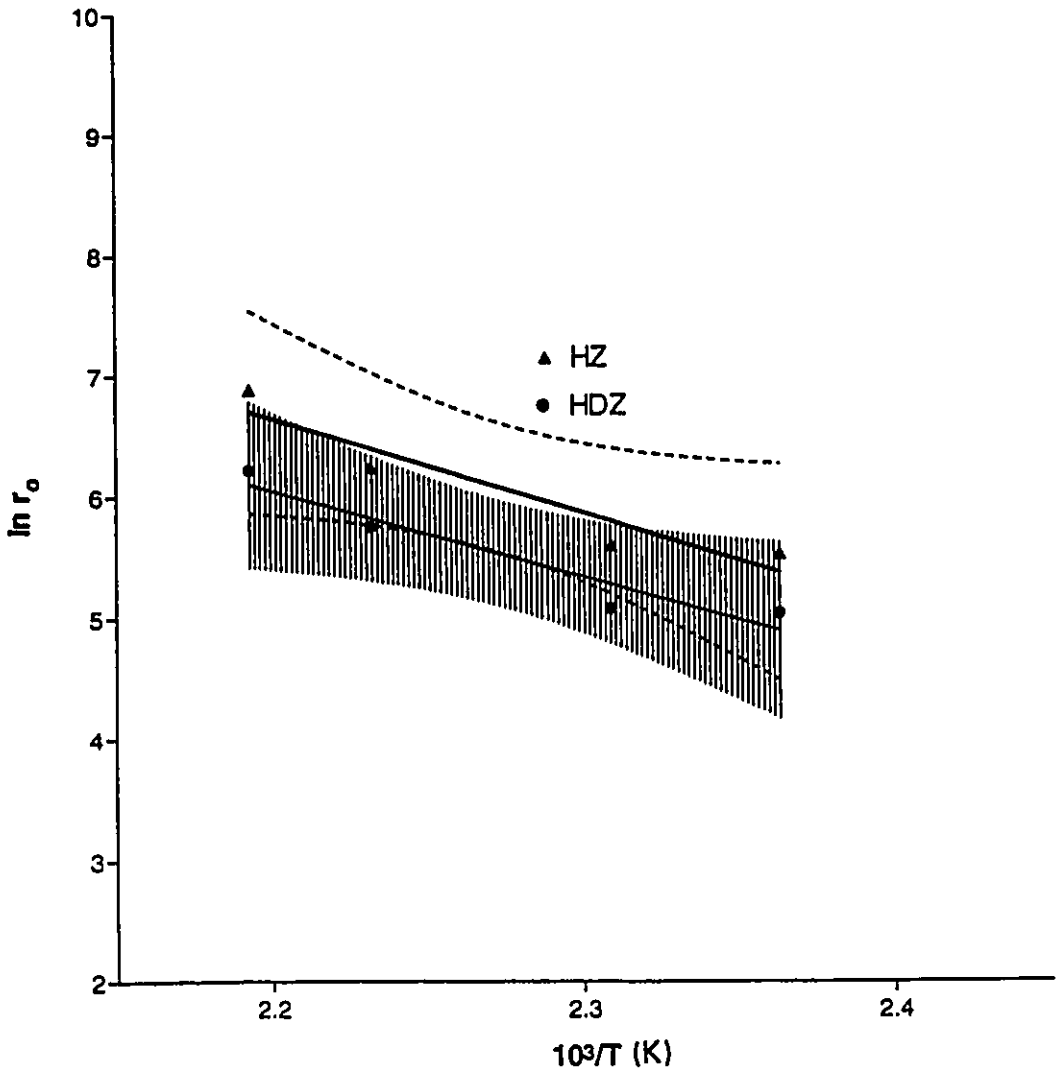

Fig 5.3 Arrhenius plot for the log of the initial rate of conversion of absolute ethanol (r_o) vs 1000/T(K) for HZ and HDZ.

------ : 95 % Confidence zone for HZ

: 95 % Confidence zone for HDZ

Generally speaking, the values of total ethanol conversion obtained with the desilicated zeolite (H-DZ sample) were significantly higher than those obtained with the parent zeolite (H-Z sample) (Table 5.4). As already reported in Chapter 4 (137), this was due to the high density of acid sites of the H-DZ in comparison with that of the H-Z (Table 5.3). However, at low reaction temperatures, the selectivity to ethylene obtained with the H-Z was slightly higher than that obtained with the H-DZ (Table 5.4), owing to the presence of "unusual" Lewis acid sites of type II (LAS II), formed by calcination of the desilicated zeolite, H-DZ. In fact, these LAS II were produced by dehydroxylation of the Bronsted acid sites of type II (BAS II) generated by the "desilication-healing" phenomena (137). These LAS II were not easily rehydrated to the corresponding Bronsted acid sites, as in the case of the normal Lewis acid sites (called LAS I) obtained by dehydroxylation of the parent ZSM-5 zeolite (137).

5.2.4 DEHYDRATION OF AQUEOUS ETHANOL

Table 5.7 reports the catalytic results obtained with the H-Z and the H-DZ using aqueous ethanol (15 wt %) as feed. It can be seen that:

i) for both catalysts, there was a cut-off point based on the ethylene yield which was located between 225 and 250 °C (Figure 5.4 (a) and (b), i.e. 25 °C higher than that obtained with absolute ethanol. It is worth mentioning that by using an aqueous solution of 10 wt % over other types of ZSM-5 zeolites as

mentioned earlier, a cut-off point between 250 and 270 ° C was obtained (9). Therefore, water dilution is also an important factor in terms of the reaction path followed.

ii) with both catalysts, the massive presence of water in the feed resulted in lower total conversions of ethanol (Tables 5.4 and 5.7). However, the product selectivity for ethylene obtained with the aqueous ethanol was significantly higher than with the absolute ethanol even if the reaction temperature was below the cut-off point (Table 5.7). This is an important result for the BETE process in which large amounts of water are present in the feed (8,17).

iii) the total conversion of (aqueous) ethanol over the H-DZ was significantly higher than over the H-Z (Table 5.7). On the other hand, in contrast with the results obtained with absolute ethanol (Table 5.4), when aqueous ethanol was used, the selectivity to ethylene shown by the desilicated zeolite (Table 5.7) was significantly higher than that obtained with the parent zeolite (H-Z). The latter catalyst had the tendency to produce more heavier hydrocarbons than ethylene (Table 5.7, 250-275 °C).

5.2.5 MORE ABOUT THE ROLE OF WATER IN THE FEED

Finally, water in the feed may play two roles: diluent of the reacting ethanol (resulting in lower conversion for both catalysts when the feed was aqueous ethanol, see previous section, and Tables 5.4 and 5.7) and rehydrant of the Lewis acid sites including the LAS of type II. Thus steam may be capable

of restoring the BAS II (Bronsted acid sites of Type II) of the H-DZ sample. In fact, it was hypothesized (137) that the massive presence of water in the feed would help, during the first moment of the reaction, by converting the LAS II into the more active BAS II sites.

Table 5.7 Catalytic results for HZ and HDZ catalysts (Feed = aqueous ethanol; contact time, τ = 0.4 h)

Sample	Temperature T (°C)	Total conversion C_t (C atom %)	Product selectivities[1] S_{Et}	S_{DEE}	$S_{OHC's}$
H-Z	200	33.9	13.1	86.8	0.1
	225	35.6	55.4	44.6	0.0
	250	81.7	95.6	0.7	3.7
	275	89.9	87.8	0.9	11.3
H-DZ	200	38.1	63.0	37.0	0.0
	225	43.9	70.4	29.6	0.0
	250	86.0	98.0	1.4	0.6
	275	90.7	95.3	0.8	3.9

[1] Et = Ethylene; DEE = diethylether; OHC's = hydrocarbons higher than Et.

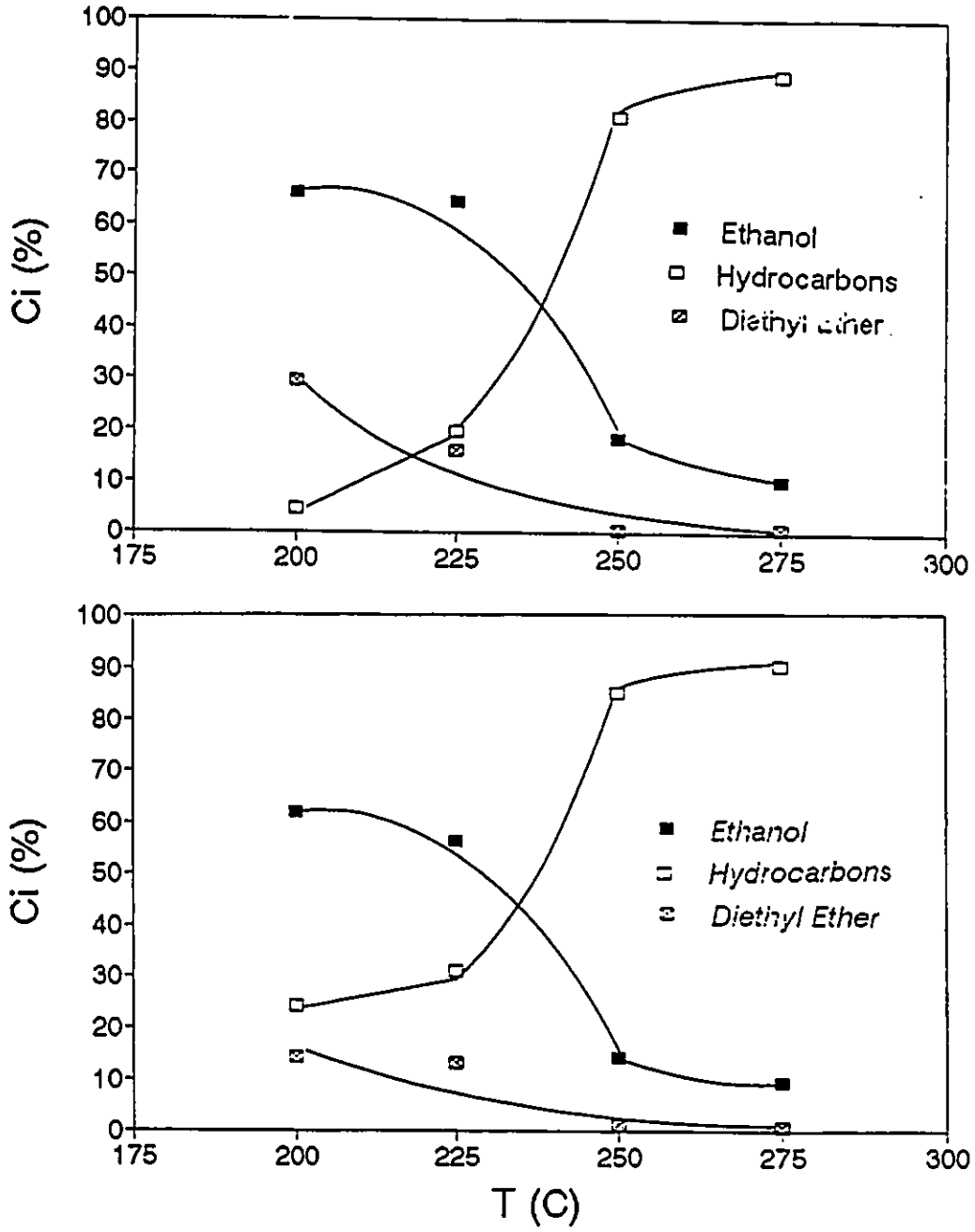

Fig 5.4 Composition of the reactor outstream (C_i) versus reaction temperature, T, (°C) for HZ (top) and HDZ (bottom) in the dehydration of aqueous ethanol (□) hydrocarbons (□) diethyl ether (■) ethanol

This "atmosphere" resulted in the predominant production of ethylene (Table 5.7, case of the H-DZ) while the stronger BAS of type I in the parent zeolite, HZ, led to a higher production of hydrocarbons heavier than ethylene (Table 5.7, case of HZ (137)). This also has the effect of lowering the rate of catalyst deactivation since the formation of coke on ZSM-5 is faster for Lewis acid sites than on Bronsted acid sites (182).

To further verify the hypothesis regarding the rehydrating role of water, the following experiment was performed on the H-DZ(2) sample (Si/Al ratio 14.2 and wt % Na_2O < 0.2 % ; and all other properties were similar to those of HDZ previously used). The sample of HDZ (2) was heated at 275°C for 2 hours in an atmosphere saturated with steam (pumping rate of water = 5ml/hr; flow rate of nitrogen as carrier gas = 12 ml/min) and then left at 225°C under flowing nitrogen overnight to remove the excess water molecules adsorbed onto the surface of the catalyst. This catalyst is referred to as t-H-DZ(2) The same reaction conditions were used to test the activity of this catalyst. Table 5.8 reports activity and product selectivity data for H-DZ(2) and t-H-DZ(2). It is apparent that the steam treatment of H-DZ(2) significantly increased both the total % conversion and selectivity for ethylene. This confirmed the previous hypothesis about the important role of steam as rehydrant of the Type II Lewis acid sites. It is worth noting that the temperature used for the steam treating was much lower compared to those used for zeolite (ultra) stabilization by steaming/dealumination (139).

Table 5.8 Catalytic results obtained with the H-DZ(2) and t- H-DZ(2) (Feed = absolute ethanol ; reaction temperature = 225 ° C ; contact time = 0.12 hr^{-1})

Catalyst	Total conversion, C_t (C atom %)	Product selectivities[1] S_{Et}	S_{DEE}	S_{OHC}'s
t-H-DZ(2)	88.8	90.3	8.9	0.8
H-DZ(2)	85.2	84.2	15.1	0.7

[1] : as in Table 5.4

5.3 CONCLUSION

When compared to the parent ZSM-5 zeolite, desilicated ZSM-5 showed higher values for total conversion and selectivity to ethylene in the dehydration of aqueous ethanol. In terms of reaction pathway, cut-off temperatures for the production of ethylene from absolute ethanol and aqueous ethanol were 200-225 °C and 225-250 °C, respectively.

Steam treatment of the desilicated ZSM-5 zeolite at a relatively low temperature was capable of converting Lewis acid sites of type II to the corresponding Bronsted acid sites, further increasing the conversion and selectivity to ethanol in the dehydration of absolute ethanol to ethylene.

CHAPTER 6

CATALYTIC MULTIPASS REACTOR FOR THE CONVERSION OF BIO ETHANOL INTO ETHYLENE

6.1 INTRODUCTION

The catalytic reactor most commonly used in laboratory microreactor catalytic testing is the plug flow, fixed bed reactor. For reactions which are not extremely exothermic or endothermic and under ideal heat transfer conditions, isothermal behaviour is assumed. In addition to its simplicity in design and high treatment capacity, this reactor permits easy separation of catalyst and product (140). For more demanding reactions, it is necessary to increase operating temperatures in order to achieve higher conversions to the desired products. This usually involves an excessive consumption of energy, or in the case of ethanol dehydration using TFA loaded on ZSM-5 (17), operation at extremes of thermal stability of the catalyst accompanied by high pressures, which is neither economical nor safe. An alternative route for improving conversions or product selectivity is by the forced recycle of unconverted reactants or undesired products. This of course implies an additional expenditure of energy.

Pioneer work on Catalytic Recycle Reactor technology began almost 60 years ago when G.M. Schwab invented a simple device for measuring reaction

rates of solid catalyzed reactions when the reactant is in the vapor phase (141). It consisted of a thermostated tube holding the catalyst particles as a fixed bed with a condenser set at the outlet of the catalyst bed. Fig 6.1 illustrates the basic components of the Schwab reactor which is essentially a round bottomed vaporization flask supporting the vertical reactor chamber containing the catalyst bed. The gaseous effluent is directed into a condenser and sample trap. The gravity assisted recycling of unconverted reactants or undesirable products or the continuous removal of the volatile products can enhance the yield or the (desired) product selectivity. No energy is expended in forcing the reactants to recycle since gravity is the driving force for the reinsertion of the condensable materials into the reaction medium. Schwab studied the decomposition of formic acid, for which he carried out extensive kinetic experiments.

Recent studies on the development of recycle reactor technology aimed at enhancing conversions have been described by among others Carberry (100,101), Berty (102) and Satterfield (103). The first internal recycle reactor was designed by Berty and consisted of a basket into which a variable amount of catalyst could be placed. A magnetically driven blower was used for the internal gas circulation in the reactor. In the spinning basket reactor proposed by Carberry, the catalyst particles are placed in a basket which rotates in an enclosure.

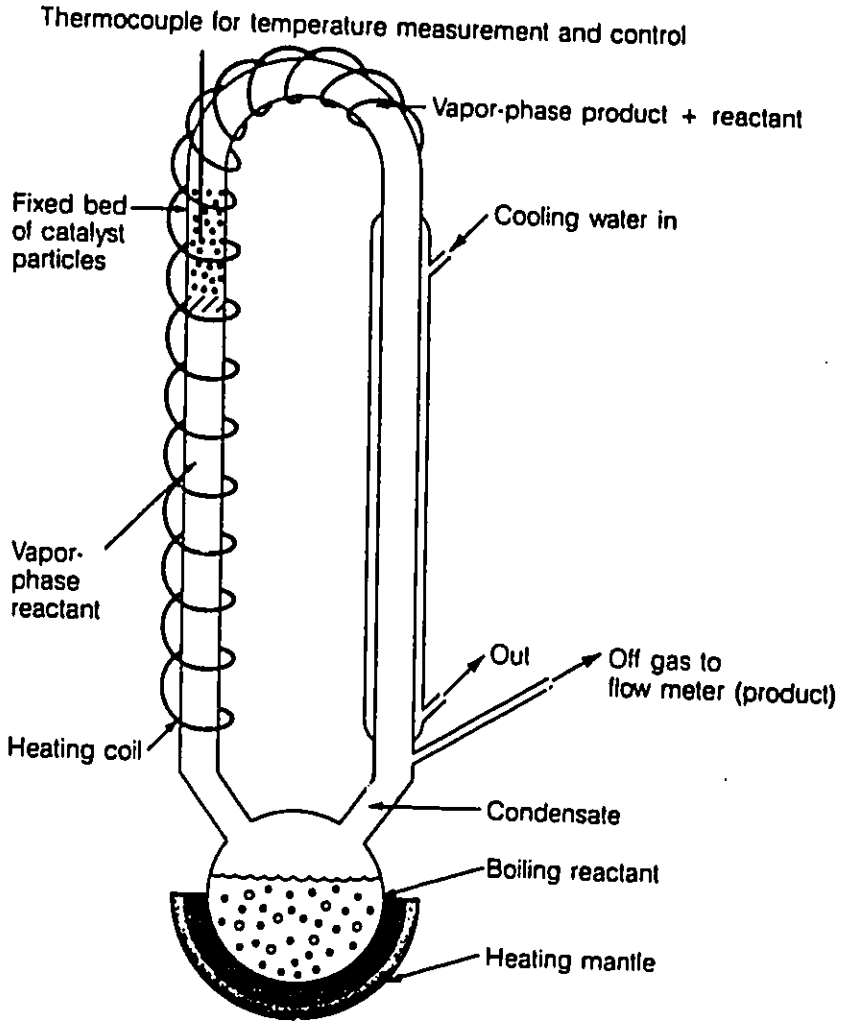

Fig 6.1 Illustration of Schwab Reactor

It is assumed that the rotation of the basket ensures perfectly mixed conditions and high interparticulate transport rates. Another way to approach perfect mixed conditions is by using a packed bed reactor with a recycling of the effluent gas stream (104). In any recycle reactor, a low conversion per pass over the catalyst bed can be maintained, but the overall conversion over the reactor can be large. Many improvements have evolved but many inherent problems still remain with such a design. The reactor cannot be assumed to behave as perfectly mixed and operating under steady state conditions with temperature and concentration gradients having a negligible influence on the experimental data, because parameters such as recycle and feed flow rates, reaction kinetics and heat of the reaction influence the reaction rate (104).

6.2 EXPERIMENTAL

The Catalytic Multipass Reactor (CMR) evolved from a series of modifications to the original horizontal fixed bed reactor first used to study the BETE process. The present design of the CMR operates on the fundamental principle of the Schwab reactor. This design allows the recycling of condensable, unconverted reactant and discharge of undesirable products.

6.2.1 EXPERIMENTAL SET UP AND CATALYST TESTING

The experimental set up of the CMR is illustrated in Fig 6.2. The vaporization chamber is essentially a modified 500 ml round bottomed pyrex flask maintained at approximately 120°C, into which the aqueous ethanol solution is injected at a fixed rate by an infusion pump. The vaporized feed rises into the catalytic reactor chamber which is a cylindrical glass tube positioned vertically above the vaporization chamber. The recycle chamber as shown is positioned over the catalytic reactor and consists of a glass cone with a side arm attached to one outlet of a timer programmed 3-way solenoid valve. The other outlet of the valve is linked back to the vaporization chamber.

The catalyst is loaded onto a ceramic disc at a fixed height and heated by thermo-regulated heating tape. A chromel-alumel thermocouple positioned horizontally and midway in the catalyst bed was used in conjunction with a digital thermometer unit to monitor the temperature of the catalyst bed.

Depending on the time specified by the program, the valve will switch to allow either recycle or discharge of condensed, unconverted feed or products including water. In this way the vaporized effluent from the catalyst chamber enters the recycle chamber from where it can either pass into the condenser and sample trap where it is periodically sampled for GC analysis ; alternatively the condensate can be recycled to pass over the catalyst bed a second time along with fresh feed.

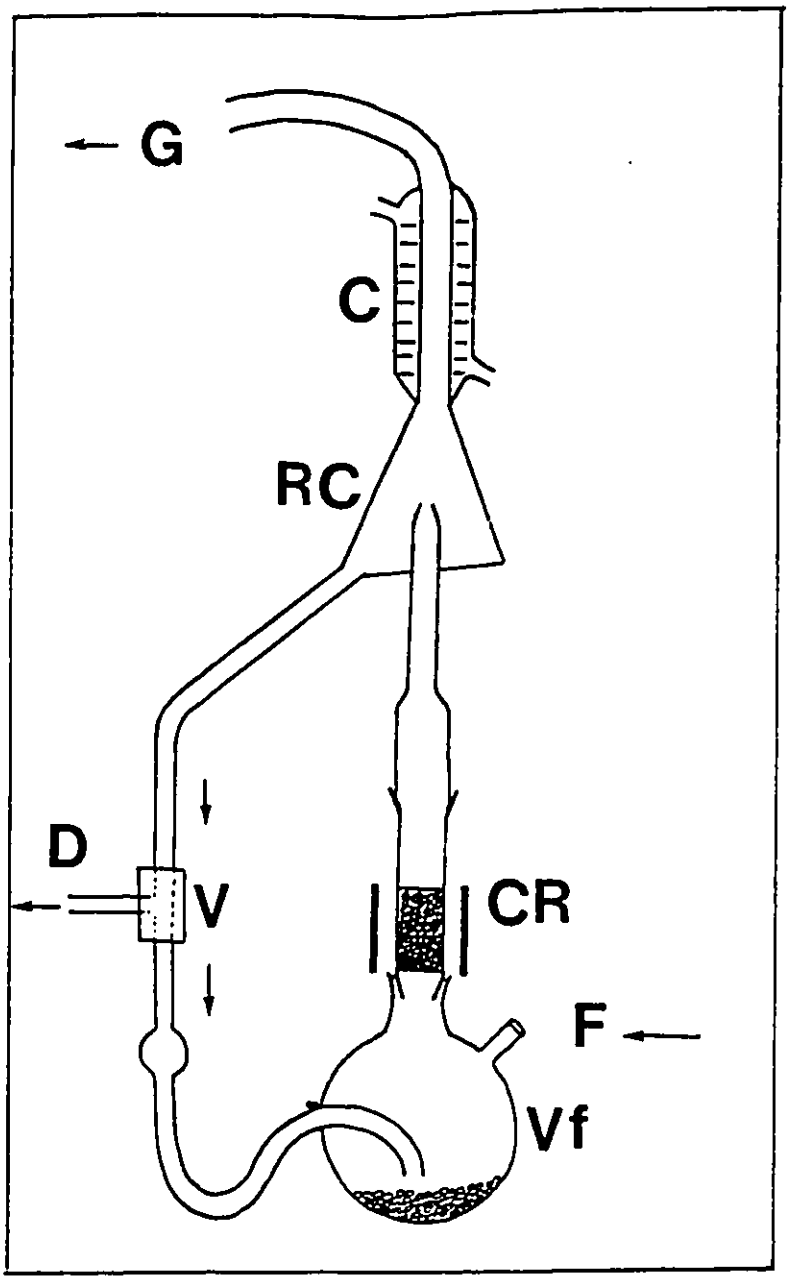

Fig 6.2 Design of the Catalytic Multipass Reactor

Vf : Vaporization flask ; F : Feed ; CR : Catalytic Reactor containing catalyst bed; D : Discharge ; RC : Recycle Chamber : C ; Condenser ; G : Gaseous effluent ; V : 3 way solenoid valve

The gaseous product was analyzed by gas chromatography on a Shimadzu Mini 3 GC (as before) and the liquid product analyzed also by FID on a 50 m PONA capillary column of a HP 5790A GC also as before. The duration of each run was 3 hours. This reactor was capable of operating in the recycle or non recycle mode, the latter corresponding to conditions experienced in the isothermal fixed bed, plug flow reactor or conventional tubular reactor as was used in previous catalytic testing (7-10).

The reported conversion and selectivities are average values obtained during each run and are calculated as defined before.

WHSV = F/W (hr^{-1}) Contact Time, t (hr) = 1/WHSV

The pumping rate of reactant was maintained at 0.085 ml/min during these experiments unless otherwise specified. The ratio of time of recycle: time of discharge of unconverted reactants and/or products, $T_r/T_d = 4$; this value was chosen by taking into consideration the capacity of the vaporization system to completely discharge the amount of liquid accumulated during the time interval of the previous recycle phase.

6.2.2 CATALYST PREPARATION AND CHARACTERIZATION

6.2.2.1 ZSM-5 SYNTHESIS

ZSM-5 zeolite of Si/Al ratio 19.5 was synthesized according to the method of Argauer and Landolt (52). (see Appendix 1)

6.2.2.2 PREPARATION OF HZSM-5

The acidic form of the zeolite ZSM-5 was obtained by repeatedly ion exchanging the Na form of the zeolite obtained from the synthesis, with an aqueous stirred solution of ammonium chloride (5% wt) maintained at 80°C. Each treatment lasted for 1 hour after which the spent solution was decanted and fresh solution added (1g zeolite in 10 ml solution). The procedure was repeated 7-8 times, after which the solid was washed on a filter several times with double deionized water and dried at 120°C (53). The final form was generated by activation in air at 550°C for at least 12 hours and is denoted HZ (19.8) hereafter. The bracketed number refers to the Si/Al ratio.

6.2.2.3 CHARACTERIZATION OF CATALYST

The catalyst was characterized (see Appendix 1) by atomic absorption (analysis for the Na, Al and Si) and X-ray powder diffraction for structural identification and calculation of the degree of crystallinity (DC). BET analysis for nitrogen adsorption was performed to determine the textural properties of surface area and mesopore and micropore volume distribution.

The final form of the catalyst was prepared as before except that the sphagettis after being dried at 120°C for 12 hr. were calcined at 550°C for 12 hr. 4.0g of catalyst extrudates was used for the catalyst testing.

6.3 RESULTS AND DISCUSSION

The various parameters affecting catalytic activity and selectivity for the desired product, ethylene (influence of recycle time, temperature, contact time, water build up) were studied to assess the performance of the reactor under various conditions and in this way optimize the conditions for operation.

6.3.1 PHYSICOCHEMICAL PROPERTIES OF HZSM-5

The chemical and textural properties of HZSM-5 used for catalytic testing are given in Table 6.1.

Table 6.1 Chemical and textural properties of HZSM-5(19.8) catalyst

				%	S.A.(m^2/g)		Vol. N_2	
	% Na_2O	%Al_2O_3	Si/Al	DC	LANG.	BET	Total	MP.
HZ	0.3	4.1	19.8	100	498	374	0.232	0.108

6.3.2 PRELIMINARY EVALUATION OF CMR FOR REPRODUCIBILITY

Table 6.2 reports the results obtained with five runs performed at 150°C. The second and third runs and then the fourth and fifth runs which were carried out under the same recycle conditions, using recycle time: discharge time of 20:5 minutes and 30:7.5 respectively, showed an acceptable reproducibility (about 2 % as experimental error). The first run was performed under non recycle conditions. This data indicates that the use of a recycle mode significantly increased the total conversion of ethanol without noticeably changing the yield in diethyl ether (DEE). This occurred because DEE is the reaction intermediate (Fig 1.3) in the conversion of ethanol into ethylene in this temperature range (9,10). The ether was not condensed and was all found in the vapour phase for this series of experiments. The use of $T_r/T_d = 30/7.5$ achieved a higher total conversion and higher selectivity for ethylene.

6.3.3 INFLUENCE OF THE RECYCLE TIME

The time of recycle, T_r was varied according to the values indicated in Table 6.3 while maintaining $T_r/T_d = 4$, and the conversions of ethanol and product selectivities were determined for each of these experiments. If one considers the build up of liquid which occurred during the recycle period T_r, the total conversion, C_t, at any time during, t_r, of the recycle period could be split into two parts : C_{to}, the conversion to ethanol under non recycle conditions and ΔC_t due to the conversion of the unconverted or recycled ethanol.

Table 6.2 Preliminary runs for evaluating the reproducibility of Data

Ethanol = 10 % WHSV for NRC = 0.13 hr^{-1}

Catalyst = HZSM-5(20) Temperature = 150°C

RC : Recycle and NRC : Non Recycle mode of operation

For run 2 and 3 Recycle operation T_r = 20 mins T_d = 5 mins ; for run 4 and 5 T_r = 30 mins and T_d = 7.5 mins.

	NRC	Recycle(RC)			
		Run2	Run3	Run4	Run5
% Total Conv(C_t)	75.3	82.8	83.7	88.4	90.6
% Conv. to HC	72.8	80.3	80.8	87.0	88.8
% Conv. to DEE	2.5	2.5	3.0	1.4	1.7
Ethylene Yield	72.1	79.5	80.3	85.9	87.6
Product Selectivities (C atom %)					
Ethylene	95.7	96.1	95.9	97.1	96.6
DEE	3.4	3.0	3.5	1.6	1.9
Other HC'S	0.9	0.9	0.6	1.3	1.5

HC : Hydrocarbons

DEE : Diethyl Ether

Table 6.3 Influence of Various Recycle Times (T_r) on Total % Conversion and Yield of Ethylene

Ethanol = 10 % WHSV = 0.13 hr^{-1}

Catalyst = HZSM-5 Temperature = 150°C

T_r (mins)	0	10	20	30	40	50	60
T_d(mins)	-	2.5	5	7.5	10	12.5	15
N[1]	-	14.4	7.2	4.8	3.6	2.9	2.4
% C^2_{total}	75.3	79.1	83.1	89.5	87.5	86.9	81.9
% C^2_{HC}	72.8	76.1	80.5	87.9	85.2	85.0	75.6
% $C^2_{Ethylene}$	72.1	75.8	79.9	79.7	84.8	84.4	75.3
% C^2_{DEE}	2.5	3.0	2.7	1.6	2.4	1.9	6.3

[1] : N = Number of recycles

[2] : Conversion (% Carbon atom)

Thus, $\Delta C_t = C_t - C_{to}$

The unconverted reactant builds up in the vaporization flask and this process of build up depends on C_{to}, recycle time T_r, discharge time, T_d and the number of recycles (cycles). N can be deduced to be $= H/(T_r + T_d)$ where H was the time of reaction, usually 3 hours (ΔC_t was an average value calculated for the entire reaction time H).

Thus

ΔC_t was a function of [$(100-C_{to})$, T_r, T_d and N] (i)

As already mentioned, in this series of tests $T_r/4 = T_d$

Therefore

ΔC_t = function of $(1-C_{to}/100), T_r$ (ii)

Since the contact time, t, is maintained constant, C_{to} is also constant for all the reactions performed in this series, and so C_t depends only on T_r :

A plot of ΔC_t versus T_r is shown in Fig 6.3 which may be represented empirically as a polynomial function :

$$\Delta C_t = 0.3176\ T_r + 0.0087\ T_r^2 - 0.00021\ T_r^3 \quad (r=0.979)$$

Moreover ΔC_t may be considered as due to the recycling of unconverted reactant during the recycle period. Therefore

$$\Delta C_t = 1 / H \,.\, N \,.\, \int f(t_r)\, dt_r \qquad \text{(iv)}$$

It is obvious that $\int f(t_r)dt_r$ increased with T_r. Thus there was a compensating effect between N and this integral as shown in Fig 6.3. This resulted in a maximum which could be calculated by using the following equation obtained from the best fit of the data :

$$d(\Delta C_t)/T_r = 0.3176 + 2 \times 0.0087\, T_r - 3 \times 0.00021 T_r^2 = 0$$

Thus, the positive solution of the equation was 40 mins (T_r for maximum ΔC_t). Testing using the CMR in the recycle mode, was performed using a recycle time of 30 mins, since this was one of the best recycle times.

6.3.4 INFLUENCE OF ETHANOL CONCENTRATION AND CONTACT TIME

Catalytic testing was carried out using a series of various concentrations of ethanol as reactant (Table 6.4) and the conversions and product selectivities are shown. The pumping rate was maintained constant and the contact time, calculated to be the amount of ethanol passing through the catalyst bed which varies according to the concentration of ethanol in the reactant (10 to 100

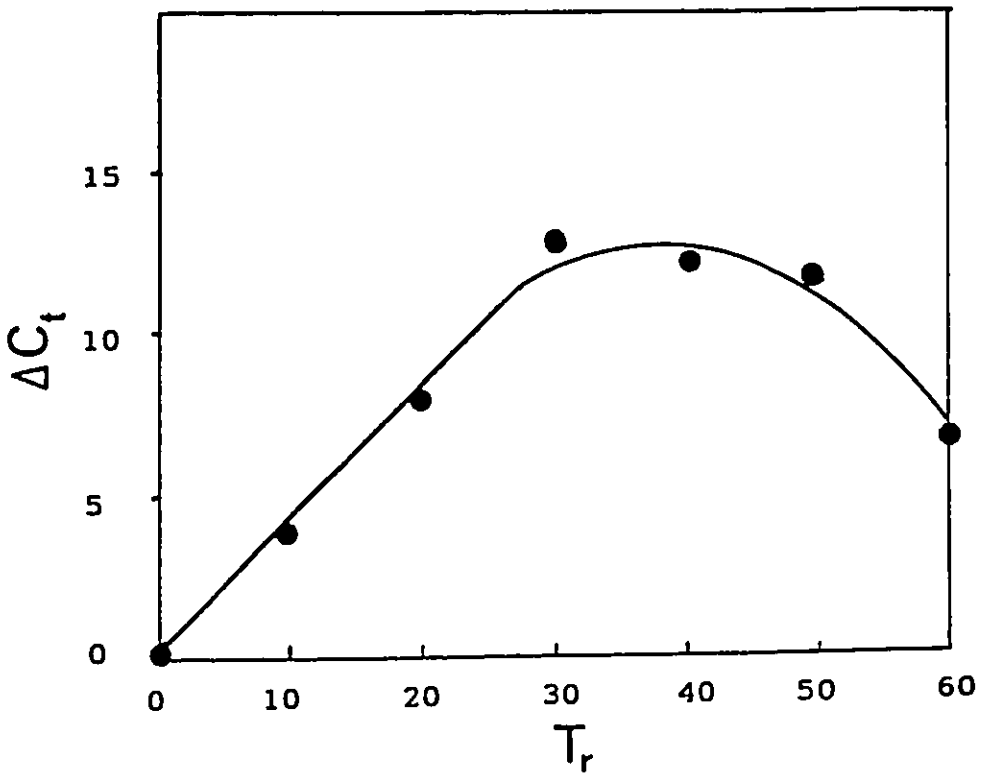

Fig 6.3 Graph of increase in total conversion (%), ΔC_t vs recycle time, T_r (mins)

wt%). Fig 6.4 was obtained by plotting the total % Conversion, C_t and the % conversion to ethylene against the contact time, t. For non-recycle conditions, the conversion to ethylene varied only slightly with contact time, but there was a decrease in the total conversion with increasing contact time. This could be attributed to the increasing water content in the feed with increasing contact time. Moreover, higher ethanol concentrations gave rise to higher conversions to diethyl ether. This is illustrated graphically in Fig 6.5.

On the other hand, the recycle runs allowed a dramatic increase in the total conversion, for which as much as 22% increase in the total conversion was obtained compared to the corresponding reaction performed under non-recycle conditions (Table 6.4 and Fig 6.4). In particular, the conversion to ethylene was practically equal to the total conversion at contact times higher than 3 hr which correlates with water contents in the feed lower than 25 %. Conceivably, the CMR provides the opportunity for conversions and selectivity to a desired product much higher than that achieved with the conventional tubular reactor. Moreover, in the case of the conversion of aqueous ethanol, the concentration range of 10-25 wt %, which gives optimum catalytic results, is actually that of the fermentation broth of ethanol or beer.

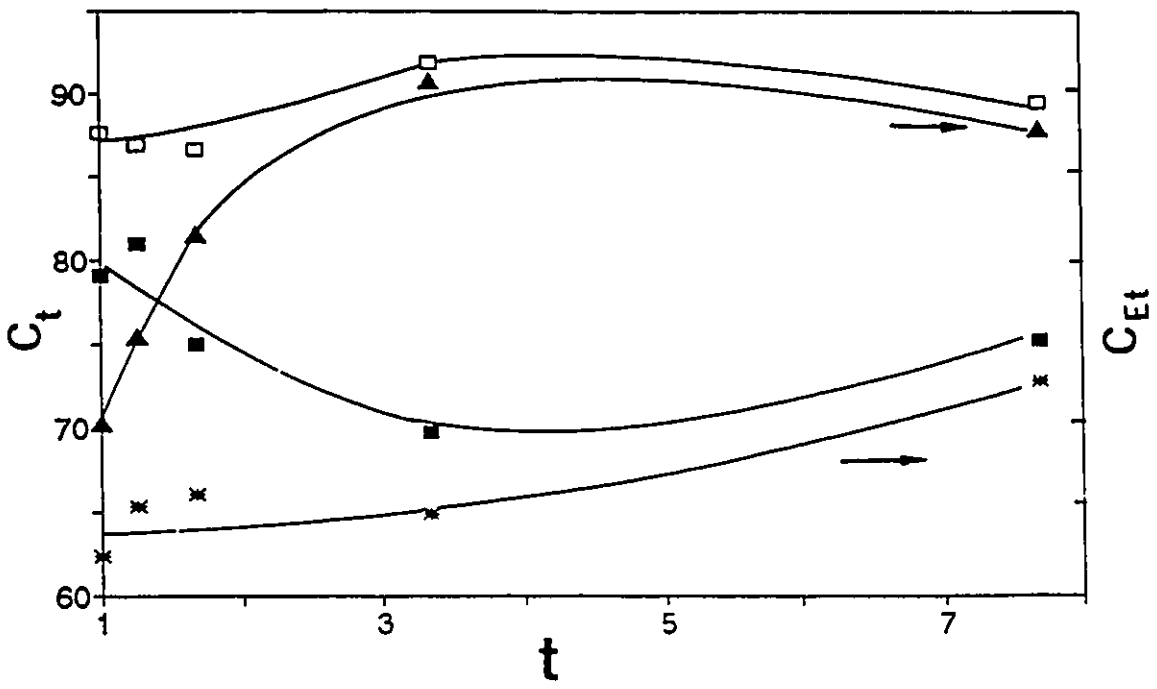

Fig 6.4 Graph of % Total Conversion (C_t) and Conversion to Ethylene (C_{Et}) with contact time for RC versus NRC mode

Non Recycle conditions ■ = C_t and ✱ = $C_{Ethylene}$

Recycle conditions □ = C_t and ▲ = $C_{Ethylene}$

Table 6.4 Influence of the ethanol concentration in the reactant and the reaction contact time t,(hr)

Temperature = 150°C T_r = 30 mins T_d = 7.5 mins

Ethanol Concentration (wt %)	10		25		50		75		100	
W.H.S.V.(hr^{-1})	0.13		0.30		0.60		0.80		1.00	
Contact time(hr)	7.69		3.33		1.67		1.25		1.00	
	NRC	RC	NRC	RC	NRC	RC	NRC	RC	NRC	RC
% C^1_{total}	75.3	89.5	69.8	91.9	75.0	86.7	81.0	86.9	79.1	87.6
% C^1_{HC}	72.8	87.9	64.8	90.8	66.0	81.5	65.3	75.5	62.3	70.3
% $C^1_{Ethylene}$	72.1	86.7	64.3	85.2	65.6	77.1	65.0	74.0	61.6	69.4
% C^1_{DEE}	2.5	1.6	5.0	1.1	9.0	5.2	15.6	11.4	16.8	17.3

[1] : Conversion (% C atom)

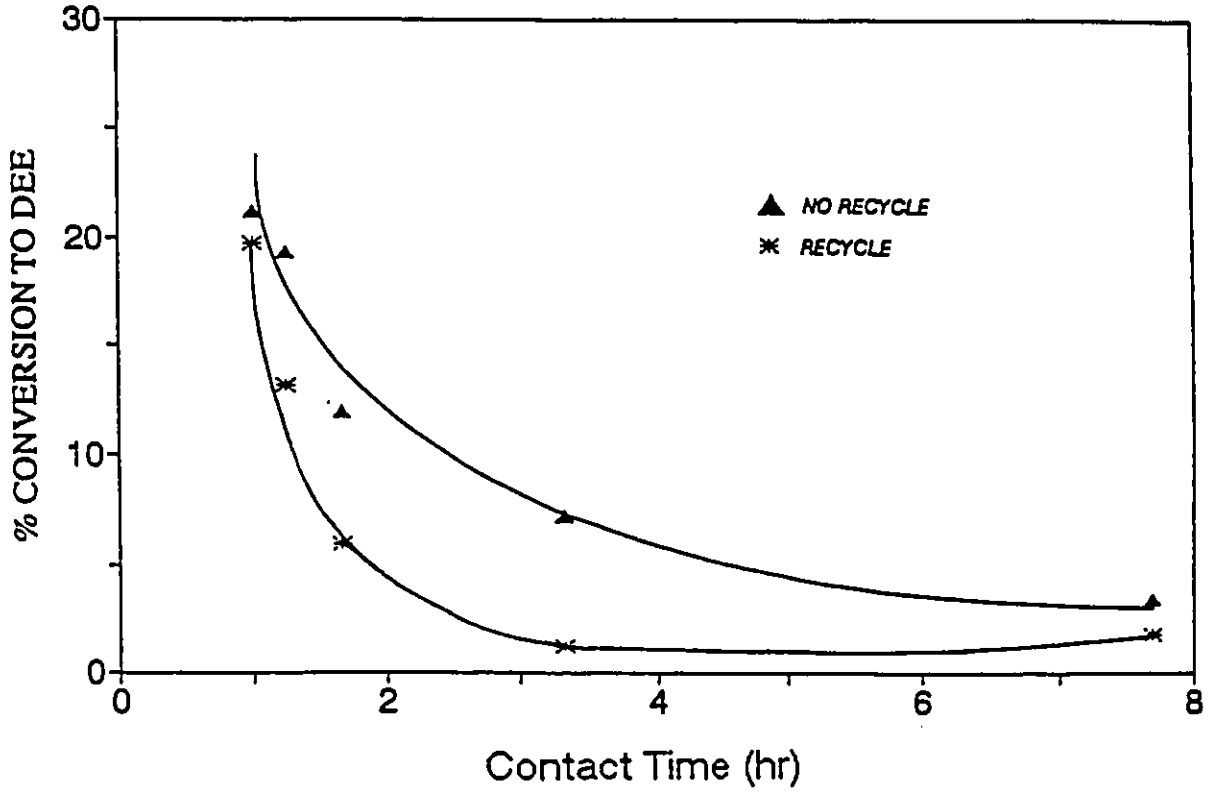

Fig 6.5 Graph of % Conversion to DEE with Contact Time for RC vs NRC mode

6.3.5 INFLUENCE OF TEMPERATURE

Table 6.5 reports the catalytic data obtained when testing in the recycle and non recycle mode was carried out at three different temperatures. T_r was maintained at 30 mins and a 10 wt % ethanol solution was used. It was seen that the difference in total conversion, ΔC_t, and that in the conversion to hydrocarbons, ΔC_{HC}, decreased with increasing temperature. This is understood if one takes into account that the effect of the recycle of unconverted reactant is high when the conversion is low. As expected diethyl ether was formed in higher amounts at lower temperatures. It was also seen that operation of the recycle mode resulted in a significant decrease in the production of DEE. Since the CMR allows the use of lower reaction temperatures to achieve high catalytic performance, it may contribute to preserving the stability and lifetime of some temperature sensitive catalysts which have to operate at the limit of their thermal stability to achieve the desired production performance. Such is the case of our solid superacid catalysts which are fabricated by incorporating an organic superacid (trifluoromethanesulfonic acid: TFSA) into a zeolite structure. As mentioned in Chapter 1 (17), these catalysts are efficient when tested in the conventional tubular reactor in the BETE process for the dehydration of bioethanol to ethylene but the TFSA species begins to decompose at about 245°C.

Table 6.5 Influence of varying the temperature on catalytic activity and product selectivity

Ethanol = 10 % WHSV = 0.13 hr^{-1} Catalyst = HZSM-5

NR = NON RECYCLE RC = RECYCLE 30"/DISCHARGE 7.5"

TEMPERATURE °C	130		150		170	
	NRC	RC	NRC	RC	NRC	RC
% C^1_{total}	43.1	56.4	75.3	89.5	95.9	96.3
% C^1_{HC}	31.1	52.1	72.8	87.9	93.6	95.6
% $C^1_{Ethylene}$	31.2	51.2	72.1	86.7	82.6	83.3
% C^1_{DEE}	12.0	4.4	2.5	1.6	2.3	0.8
ΔC_t	13.3		14.2		0.4	
ΔC_{HC}	21.0		15.1		2.0	

[1] : Conversion (% C atom)

6.3.6 INFLUENCE OF ETHANOL PARTIAL PRESSURE ON CATALYTIC RESULTS

In a typical recycle run, the water accumulating in the reaction system comes from two sources : water in the reactant solution (m_1) and that produced during the catalytic dehydration of ethanol (m_2). At the end of a recycle period, T_r, the amount of water accumulated in the system ready for discharging is equal to

$$M = m_1 + m_2$$

$$m_1 = T_r . V . (1-X)$$

$$m_2 = T_r . V . X . C_t/100$$

where V is the pumping rate of ethanol in g/min and X, the ethanol content in the feed (expressed in wt fraction).

Therefore

$$M = T_r V [1 - X (1 - C_t/100)] \qquad (v)$$

M would increase if X decreased (higher dilution) or if C_t increased (higher conversion).

The relationship between the amount of diethyl ether produced to the partial pressure effect of ethanol can be deduced as follows. In a recycle phase it is obvious that in the presence of higher water contents, the partial pressure of ethanol was lower than in the non recycle mode of operation. Thus, it can

be said that such a partial pressure decreases with increasing M. In the runs performed under non recycle conditions reported in Table 6.4, when the same conditions of temperature, T, and V were used, it is apparent that the higher the ethanol dilution the lower the amount of DEE produced. It is therefore probable that a lower DEE production is associated with a lower ethanol partial pressure. Since the amount of DEE in the recycled liquid phase was perfectly negligible, the difference between the DEE selectivity between the recycle and non recycle mode is ascribed to the lowering of the partial pressure of ethanol due to the water build up during the recycle phase.

To verify this, two runs were performed under non recycle conditions for which the ethanol content and the pumping rate were varied simultaneously but in opposite ways so as to maintain the same WHSV for both runs. These data are reported in Table 6.6. Since the contact time is the same, the total % conversions were practically the same for both runs. However the run in which a higher pumping rate and lower ethanol concentration was used represents an atmosphere of lower partial pressure of ethanol (0.065 atm). In this case a lower production of DEE was observed. The conditions representing a higher ethanol partial pressure (0.115 atm) generated a higher amount of DEE. These data coincide well with the data obtained earlier in Table 6.4 and 6.5 to support the hypothesis that the lowering of the ethanol pressure by the water build up during the recycle mode is concurrent with a lower selectivity for DEE. As a result the yield in hydrocarbons was noticeably increased.

Table 6.6 Influence of ethanol partial pressure a reflected as water build up in the system

Catalyst = HZSM-5 WHSV = 0.30 hr^{-1} Temperature = 150°C

Non Recycle Conditions

Pump rate (ml/min)	.085	.140
Ethanol content,X (x100wt%)	25	15
EtOH PARTIAL PRESSURE(atm)	0.115	.065
Total % Conversion	69.8	69.1
% Conversion to HC	64.8	67.5
% Conversion to DEE	5.0	1.6
% Selectivity for Ethylene	92.0	86.2
% Selectivity for DEE	7.3	2.3
% Selectivity for other HC	0.7	2.3

By using the data in Table 6.6, the estimated partial pressure of ethanol at the beginning, P_o, and at the end, P_f, of the (re)cycle can be calculated.

$$P_o = n_2 / (n_1 + n_2)$$

where n_1 and n_2 are the number of moles of water and ethanol fed per minute respectively. n_1 = .00354 and n_2 = .00046 mole. Thus,

$$P_o = 0.115$$

Using equation (v) to calculate the number of moles of water present in the system at the end of the (re)cycle gives,

M = 30 x 0.085 [1 - 0.25(1-69.8/100)] = 2.357 ml or 0.13097 mole water.

The vaporization rate of this amount of water at the end of any (re)cycle is presumed to be 0.01746 mole/minute since T_d = 7.5 min. Therefore,

$$P_f = 0.00046 / 0.01746 = 0.026$$

However, it can be said that the actual value of P_f is slightly higher than 0.026 since the vaporization rate of aqueous solution including unreacted,

unconverted ethanol (being instantaneously recycled but not yet vaporized) is actually lower than 0.01746 moles/min.

The average value of the ethanol partial pressure during the run under recycle conditions using 25 wt % ethanol, P_{avg}, corresponding to a simulated run under non recycle conditions (Table 6.6, partial pressure 0.065 atm), can be estimated according to the following formulae :

$$P_{avg} = 1/H\ [N \times T_r \times 0.5 \times (P_i + P_f) + (H - N \times T_r)\ P_f] = 0.063$$

This explains the low value of DEE reported in Table 6.4 (25 wt % in ethanol concentration, RC conditions) as compared to that reported in Table 6.6 (second column).

6.4 CONCLUSIONS

Under well defined recycle conditions, the CMR may allow a catalyst to achieve higher catalytic performance in terms of total % conversion of reactant and higher desired selectivity compared to the conventional tubular reactor. This design provides an elegant way to preserve the stability of temperature sensitive catalysts by permitting reaction at a lower temperature. It has been shown to achieve a much higher total conversion and selectivity for ethylene and hydrocarbons in the conversion of aqueous ethanol to ethylene. Evidence indicates that its applicability arises from two factors which occur during the recycle phase, of which the recycle of unconverted reactant is the main factor. The recycling of the solvent which contributes to the further build up of water and the beneficial lowering of the partial pressure of ethanol is of secondary importance.

As was already noted, the reactor performed most efficiently when the concentration of ethanol was similar to that of the fermentation broth of ethanol (10-25 wt %). As was already determined (Chapter 4) the presence of water in the reaction medium has a significant role in directing the dehydration of ethanol reaction. In addition to lowering the partial pressure of ethanol, water accumulation from the condensate had the effect of lowering the temperature inside the vaporization flask requiring the application of compensating heat. Hot spots were observed to arise within the catalyst bed leading to large fluctuations in temperature, probably arising from the variation

in recycle rate. Another major influence was the temperature of the water used for cooling the condensers in series with the recycle chamber. This was an important variable since it directly controlled the volume of liquid condensing at the exit of the recycle chamber and therefore the recycle rate. The use of a "stir cool" apparatus (for cooling flowing liquids) was not sufficient to maintain the temperature constant, since the temperature of the tap water used was known to vary vastly depending on weather. In its present design, the CMR was observed to be only useful for fundamental studies under carefully controlled conditions of temperature. It became extremely difficult to localise the effect of each operational parameter on the reactor's performance and to optimize them because of the number of variables controlling the reactor's performance. The use of experimental design for optimizing the reaction parameters is one option for improving the reactor's performance, but was not considered within the scope of our laboratory facilities because of the complicated nature of such a project.

CHAPTER 7

CONCLUSIONS

The treatment of X, Y and ZSM-5 zeolites with an aqueous solution of sodium carbonate, to which sodium hydroxide was added for adjustment of the pH, resulted in the selective removal of silicon atoms and a significant decrease in the Si/Al ratio. As a general rule, the higher the Si/Al ratio of the zeolite, the less basic the solution needed for treatment.

The original structure, crystallinity and surface area of the materials was generally preserved, although healing processes through activation at high temperatures occurred after silicon removal. These were accompanied by some enlargement of the existing mesopores and the generation of some new micropores. Since all the aluminum atoms remained in the tetrahedral configuration during the treatment, desilication of highly silicious materials provides a novel direct route for increasing the ion exchange capacity or density of proton exchange sites of the materials studied. The utility of such improvements in the cation exchange capacities of desilicated X and Y zeolites (NaDX and NaDY respectively) can be exploited in their activity for the removal of magnesium and calcium ions from water, functioning as less environmentally polluting detergent builders. In particular, the total ion removal rates at ambient temperature increased with the decreased Si/Al ratio zeolites NaDX and NaDY

generated by desilication. Of greatest interest was the case of the NaDX which appeared to be even more effective in the removal of calcium ions at ambient temperatures than the NaA zeolite. It was also shown that the magnesium ion removal rate of the NaA zeolite increased substantially at higher temperatures suggesting that an increase in the diffusion rate of magnesium ions occurs at higher temperatures.

The acidic form of the desilicated ZSM-5 zeolite, HDZ, was shown by the combined techniques of ^{1}H MAS and Broad-line NMR, to have more structural defects and significantly more Bronsted acid sites per unit surface area. The strength of these acidic sites, as determined by the use of an ionization coefficient as an index of acidic strength, were found to be similar to the normal bridging (hydroxyl) Bronsted acid sites in zeolites (BAS I). The origin of this enhancement in Bronsted acidity could be attributed to the generation of new Bronsted acid sites hydrogen bonded to the framework oxygen atoms in the zeolite (BAS II). Some Lewis acid sites, produced by desilication were also detected by ^{1}H MAS NMR during the rehydration phase.

Further characterization of HDZ was effected by techniques such as XPS, the distribution of acidic sites by ammonia TPD, activity testing as a function of total conversion and selectivity for ethylene in the acid catalyzed dehydration of ethanol reaction and poison testing. It was clearly shown from XPS studies that there was an increase in the amount of aluminum upon desilication although it was not certain whether these species were tetrahedral.

The Lewis acid sites detected in the MAS NMR (LAS II) were recognized to be different to the normal Lewis acid sites associated with aluminum in octahedral coordination or tricoordinated aluminum (LAS I). Presumably, the dehydroxylation of the "healed" Bronsted acid sites of the acidic form of the desilicated ZSM-5 zeolite (ie BAS II present in HDZ), resulted in the formation of LAS II through activation at high temperatures.

In the conversion of ethanol into ethylene, the desilicated zeolite catalyst (HDZ) showed a higher total conversion than the parent (HZ). This result which was expected since the HDZ catalyst had a higher density of acid sites, was confirmed from the ammonia TPD curve of the two zeolites. However, in the dehydration of absolute ethanol, the selectivity for ethylene and higher hydrocarbons was slightly lower with HDZ compared to that for the parent at lower reaction temperatures, suggesting that there were less strong acid sites on the desilicated catalyst. This was also demonstrated in the ammonia temperature programmed desorption profiles, in which the HDZ catalyst was seen to possess more weak and medium strength acid sites compared to the parent, HZ. The greater quantity of acidic sites of higher strength in the parent zeolite may be ascribed to its higher Si/Al ratio, which is well known to result in higher acidic strength due to the more isolated Bronsted acid sites. On the other hand, in the dehydration of aqueous ethanol, both the total conversion and the selectivity for ethylene were higher for the desilicated catalyst, HDZ. Steam treatment of the desilicated catalyst, HDZ, was capable of increasing

the conversion and selectivity to ethylene in the dehydration of absolute ethanol. Thus the presence of water as diluent in the reaction medium was demonstrated to be beneficial. Although water competes with reactant molecules and is adsorbed preferentially onto the catalytic active sites, it serves as a rehydrant of all Lewis acid sites, both type I and II.

The rehydration conditions for the unusual Lewis Acid Sites (LAS II) are more demanding than for LAS I, however it was possible to rehydrate those LAS II by steam treatment at a relatively low temperature and thereby convert LAS II into the corresponding Bronsted Acid Sites (BAS II).

In terms of reaction network, cut off temperatures occurred at 200-225°C and 225-250°C for aqueous ethanol and absolute ethanol respectively. The difference is attributed to water dilution of the reactant (ethanol).

From an interest in the BETE process, the catalytic multipass reactor was shown to achieve higher total conversions and selectivities for ethylene than the conventional fixed bed reactor in the conversion of aqueous ethanol. This resulted from the gravity assisted recycle of unconverted reactant and product.

It is recommended that further work be done to improve the acidic properties of the desilicated ZSM-5 zeolite. It is possible that the voids created by desilication were too large for tetrahedral coordination of aluminum, hence this procedure for desilication may actually decrease the probability of aluminum becoming incorporated into the framework of the desilicated material.

REFERENCES

1) D. Klass, *Energy from Biomass and Wastes* (1985).
2) NREL Oxygenated fuels from Biomass, *Biomass Digest*, **Vol 1, No. 1**, Winter (1992).
3) R.J. Schmidt, et al, *Chemtech*, 41, Feb 1993.
4) N. and P. Cheremisinoff and F. Ellerbach, *Biomass Applications, Technology and Production*, Marcel Dekker, NY,10 (1980).
5) J.H.C. van Hooft, J.P. van der Berg, J.P. Wolthuisen and A. Volmer, in Olson and Bisio (editors), *Proc. 6th Intern. Zeolite Conf.*, Butterworth, London, 489 (1984).
6) O.M. Kut, et al., *Catalytic Conversion of Synthesis Gas and Alcohols to Olefins*, Symposium on Catalysis,361 (1981).
7) T.M. Nguyen. M Sc Thesis,1988.
8) R. Le Van Mao, D. Ly and J. Yao, *Chem. Ind.* **46**, edited by L.F. Albright, B.L. Crynes and S. Nowak, M. Dekker, New York,409 (1992).
9) R. Le Van Mao, T.M. Nguyen, and J. Yao, *Appl. Catal.*, **61**,161 (1990).
10) T.M. Nguyen, and R. Le Van Mao, *Appl. Catal.* **58**,119 (1990).
11) E.G. Derouane, J.B. Nagy, P. Dejaifve, J.H.C. Van Hooff, B.P. Spekman, J.C. Vedrine and C. Naccache, *J. Catal.*, **53**, 40 (1978).
12) L. Kniel, O. Winter and K. Stork, *Ethylene : Keystone to the Petrochemical Industry*, Marcel Dekker, NY, 73 (1980).
13) B. Gates, *Catalytic Chemisty*, Wiley and Sons, USA, 397 (1992).
14) D. Jingfa, G. Zhang, et al., *Appl. Catal.*, **41**, 13 (1989).
15) S. K. Saha and S. Sivasanker, *Catal. Lett.*, **15**, 413 (1992).
16) R. Le Van Mao, P. Levesque, G. Mc Laughlin and L.H. Dao, *Appl. Catal.*, **34**, 163 (1987).
17) R. Le Van Mao, T.M. Nguyen and G. Mc Laughlin, *Appl. Catal.*, **48**, 265 (1989).
18) D.E.W. Vaughn, *Chemical Eng. Prog.*, 25 (Feb 1988).
19) W.A. Haag, *Zeolites and related Microporous Materials ;State of the Art 1994, Stud. Surf.Sci. Cat.* **Vol 84**, 1375 (1994).
20) M.E. Davis, *Ind. Eng. Chem. Res.*, **30**, 1675 (1991).
21) J.M. Thomas, *Scientific American*, 112, April 1992.
22) S.M. Scicsery, *Zeolites*, **Vol 4**, 202, July 1984.
23) R.J. Farrauto, R.M. Heck and B.K. Speronello, *Hydrocarbon Proc.*,**71 (6),31**,34 (1992).
24) M. Iwamoto, *Stud. Surf. Sci Cat.*, **Vol 84**,1395 (1994).
25) A.T. Bell et al., *Chem. Eng. Progress*, 26, Feb 1995.
26) S. Ainsworth, *C&EN*, 34, Jan. 24 (1994).
27) J. Armor, *Chemtech*, 557, Sept. 1992.
28) Z. Li, C. Lai and T.E. Mallouk, *Inorg. Chem.*, **28**, 178 (1989).
29) A.J. Lecloux, *Catalysis Science and Technology*, Eds. J.R. Andersen and

M. Boudart, Springer-Verlag, 169 (1981).
30) R. Szostak, *Molecular Sieves: Principles of Synthesis and Identification*, Van Nostrand Reinhold, 6 (1989).
31) W.M. Meier and D.H. Olson, in *Atlas of zeolite structure types*, Butterworth-Heinemann, 3rd Edition, London 138 (1992).
32) C.N Satterfield, *Heterogenous Catalysis in Industrial Practice*, Mc Graw Hill, 240 (1991).
33) R. Le Van Mao, S. Xiao and T.S. Le, *Catal. Lett*, **35**,107 (1995).
34) W.O. Haag, *Heterogenous Catalysis*, Ed. R. Shapiro, Texas A&M University press, 95 (1984).
35) J. Scherzer, *Octane Enhancing Zeolitic FCC Catalysts*, Marcel Dekker, 44 (1990).
36) N.Y. Chen, W.W. Kaeding and F.G. Dwyer, *JACS*, **101**, 6783 (1979).
37) D.W. Breck, *Zeolite Molecular Sieve-Structure, Chemistry and Use*, J. Wiley and Sons, New York ,474 (1974).
38) E. Brunner, K. Beck, M. Koch, H. Pfeifer, B. Staudte and D. Zscherpel, *Zeolites and Related Microporous materials : State of the Art 1994, Stud. Surf. Sci. Catal.*, **84**, 357 (1994).
39) P. Batamack, C. Dormieux Morin, R. Vincent and J. Fraissard, *J. Phys. Chem.*, **97**, 9779 (1993).
40) D. Barthomeuf, *Zeolites*, Vol **14**, 394, July/August 1994.
41) C.G. Hill, *Introduction to Chemical Engineering Kinetics and Reactor Design*, J. Wiley & Sons, Chap 6 (1977).
42) P.B. Weisz and J.N. Miale, *J. Catal.*, **4**, 527 (1965).
43) D.H. Olson, W.O. Hoag and R.M. Lago, *J. Catal.*, **61**, 390 (1980).
44) M.A. Andersen, J. Klinowski and L. Xinsheng, *J. Chem. Soc. Chem. Commun.*, 1596 (1984).
45) E. Oldfield and R.J. Kirkpatrick, *Science*, **227**, 1537 (1985).
46) C.A. Fyfe and R.E. Wasylislen, *in Solid State Chemistry Techniques*, ed. A.K. Cheetham and P. Day, Oxford Scientific, 190 (1988).
47) W. Lowenstein, *Am. Mineral.*, **39**, 92 (1954).
48) R. Le Van Mao, S. Xiao, A. Ramsaran and H.M. Ahmed, Concordia University, unpublished results.
49) R. Le Van Mao and A. Ramsaran, Concordia University, unpublished results.
50) R. Le Van Mao, J. Yao and A. Ramsaran, A., unpublished results.
51) R.M. Barrer, *in Hydrothermal Chemistry of Zeolites*, Academic Press, NY,, 242 (1982).
52) R.L. Argauer and G.R. Landolt, US Pat. 3 702886,1976.
53) R. Le Van Mao, P. Levesque, B. Sjariel and P.H. Bird, *Can. J. Chem. Eng.*, **63**, 3464 (1985).
54) J. Yao, Ph. D. Thesis, 1992.
55) B.M. Lok, B.K. Marcus and C.L. Angell, *Zeolites*, Vol **6**, 185, May 1986.
56) C.V. Hidalgo, H. Itoh, T. Hattori, M. Niwa and Y. Murakami, *J. Catal.*,**85**,

362 (1984).
57) R. Le Van Mao, S. Xiao, A. Ramsaran and J. Yao, *J.Mater. Chem*, **4**(4), 605 (1994).
58) R. Le Van Mao, A. Ramsaran, S. Xiao and V. Semmer, *J. Mater. Chem.*, **5**(3), 533 (1995).
59) G. Lietz, K.H. Schnabel, G. Peuker, W. Storck and J. Volter, *J. Catal.*,**148**, 562 (1994).
60) A. Cizmek, L. Komunjer, B. Subotic, R. Aiello, F. Crea and A. Nastro, *Ninth International Zeolite Conference*, Ed, Higgins, J.B. and Van Ballmoos, R., RP 247 (1992).
61) R.M. Dessau, E.W. Valyocsik and N.H. Goeke, *Zeolites*, **Vol 12**, 776 (1992).
62) D.W. Breck, *Potential Uses of Natural and Synthetic Zeolites in Industry*, Union Carbide Corporation, Brochure, 25 (1979).
63) R. Le Van Mao, N.T. Vu, S. Xiao and A. Ramsaran, *J. Mater. Chem.*, **4**(7), 1143 (1994).
64) C. Dormieux-Morin, A. Ramsaran, et al., *Catal. Lett.*, **34**, 139 (1995).
65) M.W. Andersen, J. Klinokowski and L. Xinsheng, *J. Chem. Soc., Chem. Comm.*, 1596 (1984).
66) R.M. Dessau and G.T. Kerr, *Zeolites*, **Vol 4**, Oct., 315 (1984).
67) Yamagashi, K.,Namba, S.,Yashima, S.,J. Catal., **121**, 1990, 47-55.
68) C.D. Chang, C.T. Chiu, J.N. Miale, R.N. Bridger and J. Calvert, *J. Am. Chem. Soc.*, **106**, 8143 (1984).
69) G.W. Skeels and D.W. Breck, *Proc. 5th International Conference on Zeolites*, 335 (1980).
70) X. Liu, J. Klinokowski and J.M. Thomas, *J. Chem. Soc., Chem. Comm.*, 582 (1986).
71) M. Janicke, D. Kumar, G.D Stucky and B.F. Chmelka, *Zeolites and Related Microporous Materials : State of the Art, Stud. Surf. Sci. and Cat.*, **Vol 84**, 243 (1994).
72) R.M. Lago, W.O. Haag, et al, *Stud. Surf. Sci. Catal.*, **28**, 677 (1986).
73) H. Pfeifer, D. Freude, and M. Hunger, *Zeolites*, **Vol 5**, 274, Sept 1985.
74) Xiao, S., Ph. D. Thesis, 1995.
75) T.W. Solomons, Williamsom reaction, *Organic Chemistry*, John Wiley and Sons (USA), Third ed., 671,685 (1984).
76) S.B. Kulkarni, V.P. Shiralkar, A.N. Kotasthane, R.B. Borade and P. Ratnasamy, *Zeolites*, **Vol 2**, No 4, 392, Oct. 1982.
77) S. Mintova, B. Mihailova, V. Valtchev and L. Konstantinov, *J. Chem. Soc., Chem. Comm.*, 1791 (1994).
78) S. Brunnauer, P.H. Emmett and E. Teller, *J. Am. Chem. Soc.*, **60**, 309 (1938).
79) E. Flanigen and H. Khatami, *Adv. Chem. Ser.*, **101**, 201 (1971).
80) K. Yamagashi, S. Namba and T. Yashima, *Acid-Base Catalysis*, Ed. K. Tanabe, H. Hattori, T. Yamaguchi and T. Tanaka, Sapporo, Kodansha Ltd., 297

(1988).
81) H. Pfeifer, *J. Chem. Soc. Faraday Trans. 1*, **84** (11),3777 (1988).
82) E. Brunner, K. Beck, M. Koch, L. Heeribout and H. G. Karge, *Microporous Mater.*, Aug. 1994.
83) V. L. Zholobenko, L.M. Kustov, V. Y. Borovkov and V.B. Kazansky, *Zeolites*, **8**, 175 (1988).
84) P. Batamack, C. Dormieux Morin, J. Fraissard and D. Freude, *J. Phys. Chem.*, 95, 3790 (1991).
85) L. Heeribout, V. Semmer, P Batamack, C. Dormieux Morin and J. Fraissard, *10th Zeolite Conference Proceedings*, Germany, 1994.
86) K. Arata, *Advances in Catalysis*, Edley. D.D.; Pines, H.; Weisz, P., Eds., **37**, 165 (1990).
87) J.A. Rabo and G.J. Gadja, *Catal. Rev. Sci. Eng.*, **31**(4), 385 (1989-1990).
88) G. Horvath and K. Kawazoe, *J. Chem. Eng. Japan*, **16** (6), 470 (1983).
89) C.D. Wagner, W.M. Riggs and L.E. Davis, *Handbook of X Ray Photoelectron Spectroscopy*, Published by Perkin Elmer Corporation, PhysicalElectronics Division.
90) P.A. Jacobs and C.F. Heylen, *J. Catal.*, **34**, 267 (1974).
91) C. Dormieux Morin, *Part 1, Proceedings of the NATO ASI on Acidity and Basisity: Theory, Assessment and Utility*, J. Fraissard and L. Petrakis ed., Kluwer Acad. Pub., 1993-1994 (in press).
92) T. Barr, *Zeolites*, **Vol 10**, 760 (1990).
93) D.W. Johnson and L. Griffiths, *Zeolites*, **Vol 7**, 484, Sept. 1987.
94) J. Fraissard and T. Ito, *Zeolites*, **Vol 8**, 350, Sept. 1988.
95) S.M. Alexander, J.M. Coddington and R. Howe, *Zeolites*, **Vol 11**, 368, April 1991.
96) R.L. Cotterman, D.A. Hickson, S. Cartlidge, C. Dybowski, et al. *Zeolites*, **Vol 11**, 2734, January 1991.
97) A. Gedeon, J.L. Bonardet, T. Ito and J. Fraissard, *J. Phys. Chem.*, **93**, 2563 (1989).
98) Q. Chen, M.A. Springuel-Huet, J. Fraissard, et al., *J. Phys. Chem.*, **96**, 10914 (1992).
99) H.A. Benesi, *J. Catal.*, **28**, 176 (1973).
100) J.J. Carberry, *Designing Laboratory Catalytic Reactors, Ind. Eng. Chem.*,**56**, 39 (1964).
101) J.J. Carberry, *Chemical Reaction and Reactor Engineering*, Marcel Dekker, Chapter 1.
102) J.M. Berty,Testing Commercial Catalysts in Recycle Reactors, *Catal. Rev. Sci. Eng.*, **20**, 75 (1979).
103) C.N. Satterfield, *Mass Transfer in Heterogenous Catalysis*, Mc Graw Hill,1969.
104) P.C. Borman, A.N.R. Bos and K.R. Westerterp, *AIChE*, 862, **Vol 40**, No 5, May 1994.
105) R. Le Van Mao, N.T.C. Vo, B. Sjariel, L. Lee and G. Denes, *J. Mater.*

Chem., **2**, 595 (1992).
106) R. Le Van Mao, A. Lavigne, B. Sjariel and C. Langford, *J. Mater. Chem.*, **3**, 679 (1993).
107) P.H. Shimitzu, *Soap/Cosmetic/Chemical Specialties*, 33, June 1977.
108) J.D. Sherman, A.F. Denny and A.J. Gioffre,*Soap/Cosmetic/Chemical Specialties*, 33, Dec 1978.
109) S.E. Manahan, in *Environmental Chemistry*, Lewis, Michigan, 59 (1991).
110) R.A. Llenado, *Proc. VI Intern. Conf.*, Rena, USA, D. Olson and A. Bisio, Butterworth, Guildford, 940 (1984).
111) A.F. Denny, A.J. Gioffre and J.D. Sherman, US Patent No. 4,094,778, June 13, 1978.
112) Micromeretics Inst. Corp. *Micropore analysis*, Manual, Norcross, GA, USA, 1993, Appendix c(C15).
113) G.H. Kuhl and H.S. Sherry, *Proc. V Intl. Conf. Zeolites*, Naples, 813, June 1988.
114) S. Xiao, R. Le Van Mao and G. Denes, *J. Mater. Chem.*, 5(8), (1995), 1251.
115) H. Pfeifer, D. Freude and J. Karger, *Catalysis and Adsorption by Zeolites*,eds. G. Ohlmann et al. (Elsevier, Amsterdam, 1991), 255 and references therein.
116) H. Pfeifer, and H.Ernst, *Annual Report on NMR Spectroscopy*, **28**, 91 (1994).
117) P. Batamack, C. Doremieux Morin, R. Vincent and J. Fraissard, *Micropoorous Materials.*, **2**, 515 (1994).
118) L.W. Beck, J.L. White and J.F. Haw, *J. Am. Chem Soc.*, **116**, 9657 (1994).
119) D. Freude, *Chem Phys. Lett.*, submitted.
120) P. Batamack, C. Doremieux Morin and J. Fraissard, *J. Chim. Phys.*,**89**, 423 (1992).
121) M. Hunger,D. Freude and H. Pfeifer, *J. Chem Soc. Faraday Trans.*, **87**, 657 (1991).
122) M.J. Remy, M.J. Genet, P.P. Notte, P. F. Lardinois and G. Ponclet, *Microporous Mater.* **2**, 7 (1993).
123) J.C. Vedrine, *Guidelines for Mastering properties of Molecular Sieves*, D. Barthomeuf (Ed.), 121 (1990).
124) N.Y. Topsoe, K. Pedersen and E.G. Derouane, *J. Catal.*, **70**, 41 (1981).
125) J.C. Oudejans, P.F. Van den Oosterkamp and H. Van Bekkum, J. Catal., **3**, 109 (1982).
126) W.R. Moser, R. W. Thompson, C.C. Chiang and Hao Tong, J. Catal., **117**, 19 (1989).
127) Y. Saito and H. Niiyama, *J. Catal.*, **108**, 329 (1987).
128) H. Knozinger and R. Kohne, *J. Catal.*, **5**, 264 (1966).
129) D.A. Shirley, *Phys. Rev. B*, **5**, 4709 (1972).
130) R. Le Van Mao and G.P. McLaughlin, *Energy & Fuels*, **3**, 620 (1989).

131) Y. Okamoto, M. Ogawa, A. Maezawa and T. Imanaka, *J. Catal.*, 112, 427 (1988).
132) G. Engelhardt and D. Michel, in *High-Resolution Solid-State NMR of Silicates and Zeolites*, J. Wiley & Sons, New York, 216, and refs therein (1987).
133) V.B. Kasansky, *Stud. Surf. Sci. Catal.*, **18**, 61, (1984).
134) D. Barthomeuf, *Mat. Chem. Phys.*, **17**, 49 (1987).
135) R. Le Van Mao, Concordia University, unpublished results.
136) A. Gedeon, unpublished results, Universite de Pierre et Marie Curie, Paris, France.
137) A. Ramsaran, R. Le Van Mao, S. Poulin and L. Reven, *J. Mater. Chem.*, submitted.
138) J.H. de Boer, R.B. Fahim, B.G. Linsen, W.J. Visseren and W.F.N.M. Vleesschuwer, *J. Catal.*, **7**, 163 (1967).
139) Breck, D.W., *Zeolite Molecular Sieve-Structure, Chemistry and Use*, J. Wiley and Sons, New York, 507 (1974).
140) P. Trambouze, H. Van Landeghem and J.P. Wauquier, *Chemical Reactor: Design, Engineering and Operation*, Ed. Technip, Paris, 370 (1988).
141) G.M. Schwab, *Catalysis from the Standpoint of Chemical Kinetics*, Van Nostrand, New York, 1937, cited by Gates, B., reference 13, 189-190 (1992).
142) T. Inui, T. Suzuki, M. Inoue, Y. Murakami and Y. Takegama, *Catalysis by Acids and Bases*, Elsevier, 1984.
143) R. Le Van Mao and T.M. Nguyen, Patent No.4 847 223, 1989.
144) D. Freude, J. Klinowski and H. Hamdan, *Chem Phys. Lett.*, **149**, 355 (1988).
145) D. Freude, T. Frohlich, H. Pfeifer and G. Scheler, *Zeolites*, **Vol 3**, 171, April 1983.
146) V.B. Kazansky, L.M. Kustov and V. Yu. Burovkov, *Zeolites*, **Vol 3**, 79 (1983).
147) G.L Woolery, L.B. Alemany, R.M. Dessau and A.W. Chester, *Zeolites*, **Vol 6**, 14, Jan. 1986.
148) G. Engelhard, H.G. Jerschkewitz, U. Lohse, P. Sarv, A. Samoson and E. Lippmaa, *Zeolites*, **Vol 7**, 289, July 1987.
149) U. Lohse, E. Loffler, M. Hunger, J. Stockner and V. Patzelova, *Zeolites*, **Vol 7**, 11, Jan. 1987.
150) B. Staudte and M. Hunger ; M. Nimz, *Zeolites*, Vol 11, 837, Nov/Dec. 1991.
151) B. Umansky and W.K. Hall, *J. Catal.*, **124**, 97 (1990).
152) B. Umansky, J. Engelhard and W.K. Hall, *J. Catal.*, **127**, 128 (1991).
153) N. Cardona-Martinez and J.A. Dumesic, *J. Catal.*, **127**, 706 (1991).
154) D. and S. Hercules, *J. Chemical Ed.*, **61**(5), 402 (1984)
155) P. Batamack, C. Doremieux Morin and J. Fraissard, *Proceedings on the 10th International Congress on Catalysis*, Budapest, Hungary, 243, July 1992.
156) C. Doremieux Morin, P. Batamack, C. Martin, J.M. Bregeault and J.

Fraissard, *Catal. Lett.*, **9**,403 (1991).
157) P. Batamack, C. Doremieux Morin, R. Vincent and J. Fraissard, *Chem. Phys. Lett.*, **180**,6,545 (1991).
158) D. Freude, *Stud. Surf. Sci. Catal.*, **52**, 169 (1989).
159) XPS: B. Lamontagne, E. Sacher and M.R. Wertheimer, *Appl. Surf. Sci.*, **52, 71** (1991).
160) S. Suib, *Chem. Rev.*, **93**, 803 (1993).
161) A. Ramsaran and R. Le Van Mao, *Catal. Lett.*, submitted.
162) V.R. Choudhary and V.S. Nayak, *Zeolites*, **Vol 5**, 325, Sept. 1985.
163) C.D. Chang, C.W. Chu and R. Socha, *J. Catal.*, **86**, 289 (1984).
164) C.D. Chang and A.J. Silvestre, *J. Catal.*, **47**, 249 (1977).
165) E. M. Flanigen, J.M. Bennett, R.W. Grose, J.P. Cohen, R.L. Patton, R.M. Kirchner and J.V. Smith, *Nature*, **Vol 271**,512 (1978).
166) E. P. Barrett, L.G. Joyner and P. Halenda, **Vol 73**, 373, Jan 1951.
167) S. Xiao and R. Le Van Mao, *Microporous Materials*, **4**, 435 (1995).
168) M.L. Postuma, in *Zeolite Chemistry and Catalysis*, Ed. J.A. Rabo, **ACS Monograph 171**, ACS, Washington DC, 1976.
169) W.S. Borghand, P.T. Reischman and E.W. Sheppard, *J. Catal*, **139**, 19 (1993).
170) M.T. Aronson, R.J. Gorte and W.E. Farneth, *J. Catal.*, **105**, 455 (1987).
171) M.T. Aronson, R.J. Gorte and W.E. Farneth, *J. Catal.*, **98**, 434 (1986).
172) J. Dakta, M. Boczar and P. Rymarowicz, *J. Catal.*, **114**, 368 (1988).
173) R. Le Van Mao, S. Xiao, J. Yao and A. Lavigne, *Microporous Materials*, submitted 1995.
174) D. Breck, *Zeolite Molecular Sieves : Structure, Chemistry and Use*, J. Wiley and Sons, New York, 247 (1974).
175) D. Breck, *Zeolite Molecular Sieves : Structure, Chemistry and Use*, J. Wiley and Sons, New York, p 133,176-177 (1974).
176) Slidewrite Plus, Version 4.00, Advanced Graphics Software, Inc., CA., USA (1990).
177) SIE Ray 112 X ray Diffractometer Automation System Software, Version 2.1, MD., USA.
178) J.Haggin, *C&EN*, 8, Feb 12, 1996.
179) L. Smith, A.K. Cheetham et al.,*Science*, **271**, 799, 1996.
180) G.E. Pake, *J. Chem. Phys.*, 327 (1948).
181) J.R. Goldsmith, *J. Geol.*, **61**, 439 (1953).
182) O.A. Anunziata, O. A. Orio, E.R. Herrero et al., *Appl. Catal.*, **15**, 235 (1985).
183) C.D. Chang, *Hydrocarbons from Methanol*, Chemical Industries Vol 10, Marcel Dekker, Inc., 50 (1983).
184) P.B. Venuto and P.S. Landis, *J. Catal.*, **21**, 330 (1971).

APPENDIX 1

A 1.1 CHEMICALS AND SUPPLIERS

CHEMICAL	Grade	SUPPLIER
Aluminum Chloride $6H_2O$	Reagent	Aldrich
Aluminum Bromide	98 + %	Aldrich
Aluminum Isopropoxide	98 + %	Aldrich
Ammonia (gas)	Anhydrous Liquefied	Linde
Ammonium Chloride	USP	F i s h e r
Ammonium Hexafluoro Aluminate	95 %	Strem
Argon	Ultra High Purity	Air Products
Bentonite	USP	Anachemia
Calcium Chloride	USP	Aldrich
2,6 dimethylpyridine	99 %	Aldrich
Helium	High Purity	Air Products
Hydrochloric acid	Standard	Anachemia
NaZSM-5 zeolite powder		ChemieUetikon,Switzerland
Potassium Bromide	99 + %, FTIR	Aldrich
Pyridine	99.9 %, HPLC	Aldrich
Silica gel	60-200 Mesh	Baker Analyzed
Sodium Aluminate	Technical	Anachemia
Sodium Bromide	99 + %	Aldrich
Sodium Carbonate	Reagent	Fisher

Sodium Carbonate	Reagent	Anachemia
Sodium Hydroxide	Reagent	Aldrich
Sodium Hydroxide	Standard	Anachemia
Tetrapropylammonium Bromide	98 %	Aldrich
Tetrapropyl ammonium hydroxide	1.0 M solution in water	Aldrich

A 1.2 CHARACTERIZATION TECHNIQUES USED IN THIS THESIS

A 1.2.1 ATOMIC ABSORPTION SPECTROMETRY

Atomic absorption Spectrometry is used to determine the chemical composition of the zeolite. The elements of interest are silicon, aluminum and sodium, since the relative quantities of each of these elements will directly affect the catalytic and adsorptive properties of the molecular sieve. From this it is possible to classify zeolites according to the ratio of Si/Al tetrahedra in their frameworks. Ideally the proton exchanged zeolite (H form) should have a sodium content < 0.4 wt % in its role as catalyst.

The method used for analysis of our zeolites consists of heating the sample at 800°C in platinum crucibles for 1 hour for degassing. A fusion mixture comprised of lithium tetraborate and potassium carbonate in a composition ratio of 1:9 respectively was then added, and this was treated at 350°C for 15 minutes before being heated at 800°C to complete the decomposition of the zeolite. The sample was then washed out of the platinum

crucibles by a solution of 10 wt % sulphuric acid and concentrated hydrochloric acid. Hydrogen peroxide (30 %) was added to further decompose any solid material left. The sample solution was diluted and the elemental compositions were obtained using a Perkin Elmer 503 Atomic Absorption Spectrophotometer. External standard solutions of each element were used for determining the concentration of each element from which it is then possible to calculate the Si/Al ratio.

A 1.2.2 X-RAY DIFFRACTION

Since zeolites are crystalline microporous solids whose catalytic properties, such as unique shape selectivity, homogeneity and porosity, depend on their structural integrity and crystallinity, it is necessary that zeolites exist in the form in which they possess their highest crystallinity, chiefly for the purpose of exercising their maximum advantages in shape selective catalytic reactions. X-ray diffraction is performed for the purpose of identifying zeolites based on the unique diffraction pattern generated (31). In addition XRD can detect the presence of a single phase or multiple phases. An amorphous phase in the sample creates pore blockage and thus limits diffusion of reactant and product molecules. Degree of crystallinity has been determined by XRD and recently by Raman Spectroscopy (76). X-ray diffraction spectra arise from the typical scattering of incident X-ray radiation by the particular array of atoms and crystals constituting the zeolite, and the position of their most intense

diffraction signals (d spacing) according to Bragg's equation:

$$n\lambda = 2d\text{Sin}\theta$$

where n is an integer, λ is the wavelength of the incident radiation, d is the value of the interlayer component and spacings and θ is the scattering angle. X Ray analyses are performed using a Cu Kα source on an automated X-ray diffractometer (Philips PW 1050/25, $\lambda = 1.54178$ Å, Ni filter) operating at 40 kV. The sample dried at 120°C, was pressed onto a plexiglass holder, compressed and its X-ray diffractogram was recorded in the region $2\theta = 5$ to 60°. A slow scanning speed of 1°/min was used. Peak intensities were taken as the number of counts recorded by the digital integrating system during a complete scan of the peaks at constant angular velocity. Background correction was applied by subtracting the baseline, using Sietronics software (177). The characteristic pattern for ZSM-5 zeolites lies between $2v = 22.5$ and 25° (52) and the sum of the intensities of the three strongest peaks in this region was used to calculate the DC. The parent ZSM-5 zeolite was used as an external standard. This enabled the calculation of the Degree of Crystallinity of the zeolite by the same technique used by Kulkarmi et al (77).

A 1.2.3 BET NITROGEN AND ARGON

The textural properties of specific surface area, pore volume and pore size distribution were determined from the Brunauer, Emmett and Teller (BET) method (/8). It is also possible to obtain a good estimate of crystallinity from the BET surface area. This method was formulated in 1938 and is based on the variation of multilayer coverage as determined by the volume of nitrogen adsorbed on an exposed surface with variation in the relative pressure (P/P_o) of nitrogen in contact with the surface. In effect multilayer adsorption occurs since each adsorption site in the first layer (monolayer coverage) is assumed to be site available for adsorption of a species in a second layer; species in the second layer provide sites for those in the third layer and so on. The number of probe molecules, each of which occupy a specified area when physically adsorbed on the surface as a monolayer, permit the calculation of the total surface area of the solid.

Assumptions for the range of applicability of the BET model are given below :

1) There is a fixed number of adsorption sites which generate a characteristic isotherm as defined by the porosity of the solid.

2) The surface is assumed to be homogenous and well defined, therefore all the sites have the same energy and can only accommodate one adsorbate molecule.

3) Second and subsequent layers adsorb directly onto the first layer.

4) There are no lateral interactions between the adsorbed molecules

5) The rate of adsorption onto the bare surface is equal to the rate of desorption from the monolayer, then the rate of adsorption onto the monolayer is equal to the rate of desorption from the second layer and so on. ie there is a dynamic equilibrium between the sorbed species and the gas phase.

6) The enthalpy of adsorption to give the second and higher layers (E_L) is equal to the enthalpy of condensation of the adsorbing gas. The enthalpy of adsorption of the first layer E_1 is greater in magnitude.

7) The range of partial pressures (P/P_o) is confined to 0.05 to 0.35. The physical and mathematical treatment of this hypotheses led the BET equation expressed in the following form in order to calculate the specific surface area of a solid :

$$\frac{x}{V(1-x)} = \frac{1}{V_m} + \frac{c-1 \,.\, x}{V_m c}$$

where V = volume of nitrogen adsorbed/unit mass of sorbent

V_m = volume of sorbate just sufficient to cover the unit mass of surface with a complete monolayer (m^3 nitrogen/kg solid at STP)

x = relative pressure P/P_o

c = a constant varying with the adsorbent-adsorbate interactions. This constant is related to the differential heat of adsorption E_1 and the heat of liquefaction

E_L by :

$$c = \exp(E_1 - E_L)/RT.$$

A graph of $y = x/V(1-x)$ versus x for $0.05 < x < 0.35$ will give a BET plot (a straight line) from which V_m and c are determined if the BET model is valid.

$$V_m = 1/(\text{slope} + \text{intercept})$$

The specific surface area can then be calculated since it is directly proportional to V_m :

$$S = \frac{a_m \cdot V_m \cdot N_A \ (m^2/g)}{Vm}$$

N_A = Avogadro's constant

Vm = molar volume of adsorbate ($22.414\ 10^3\ m^3$/mole)

a_m = part of surface occupied by one mole of adsorbate (for nitrogen = $16.2\ 10^{-20}\ m^2$)

For macroporous (pore sizes > 500 Å) and mesoporous (pore sizes within the range 20-500 Å), the BET surface area can be obtained without limitations. However in the presence of large quantities of micropores (pores <20 Å) such as occurs with ZSM-5 zeolite, it becomes more practical to apply the Langmuir isotherm for estimating the Langmuir surface area. Since the size of the adsorbate molecules is of the same order as the pore sizes, a free multilayer adsorption such as occurs in the BET theory does not occur without perturbation by interactions between the walls of the zeolite. Because the

Langmiur treatment gives a more practical assessment of surface area, the Langmuir surface area has also been reported.

BET analyses were performed on an ASAP 2000 instrument from Micromeretics. Samples were degassed for at least 6 hours under vacuum ($< 1x10^{-5}$ mmHg) at 120°C and analysis performed at the temperature of liquid nitrogen (-196°C). Calculations for the BET and Langmuir surface areas were performed using Micromeretics software (ASAPv2.0). Fig A.1 is a plot of the Pore Size Distribution dV/dlog(D) vs Pore Diameter(Å) for ZSM-5.

The micropore size distribution was determined by the adsorption of argon at 87 K using the Micromeretics model ASAP 2000m and the data interpretation model by Horvath Kawazoe (HK)(88).

The micropore size and distribution of the desilicated zeolites used for the optimization of the desilication procedure (58), and all other zeolite samples studied by this technique thereafter in this thesis, were calculated using more suitable values of the interaction parameter (IP). These values were obtained by using parent zeolites of known structures. The new values gave more accurate results than the empirical values used to obtain the average values of the micropore sizes in the first samples studied by this technique (57). Moreover for the measurements of the BET and Langmuir surface area and for micropore size detemination, an outgassing temperature of 150°C was used in order not to favor any advanced healing process which was observed to occur at high temperatures of activation (57).

The interaction parameter as recommended by Horvath Kawazoe was 5.89 x 10^{-43} ergs cm^{-4} for microporous solids (88), and by Micromeretics Corporation for zeolites was 3.19 x 10^{-43} ergs cm^{-4} (112). For ZSM-5 zeolites the best value of the IP was chosen to be 4.22 x 10^{-43}, for the Y zeolite 4.6 x 10^{-43} and for the X zeolite 5.2 x 10^{-43} ergs cm^{-4}.

A 1.2.4 DTA TGA

Differential thermal and thermogravimetric analyses were performed on an PL Thermal STA 1500 DTA/TGA instrument from Thermal Sciences. The samples were heated at a rate of 15°C/min (in an inert atmosphere of flowing nitrogen) from ambient temperature to 900°C and the temperature-weight loss/differential voltage profile monitored. The limit of thermal stability was obtained from these plots.

A 1.2.5 FOURIER TRANSFORM INFRA RED SPECTROSCOPY

Fourier Transform Infra Red Spectroscopy (FTIR) was used to detect any change in the environment of aluminum, such as a variation in the density of framework aluminum sites in the zeolite. FTIR was thereafter used diagnostically to evaluate the effect of desilication on the structure of the zeolite. Spectra (Nicolet Magna IR Spectrometer 500, resolution 2 cm^{-1}) were recorded in the region 400-1400 cm^{-1} using the transmission mode (1 % zeolite in KBR pellets).

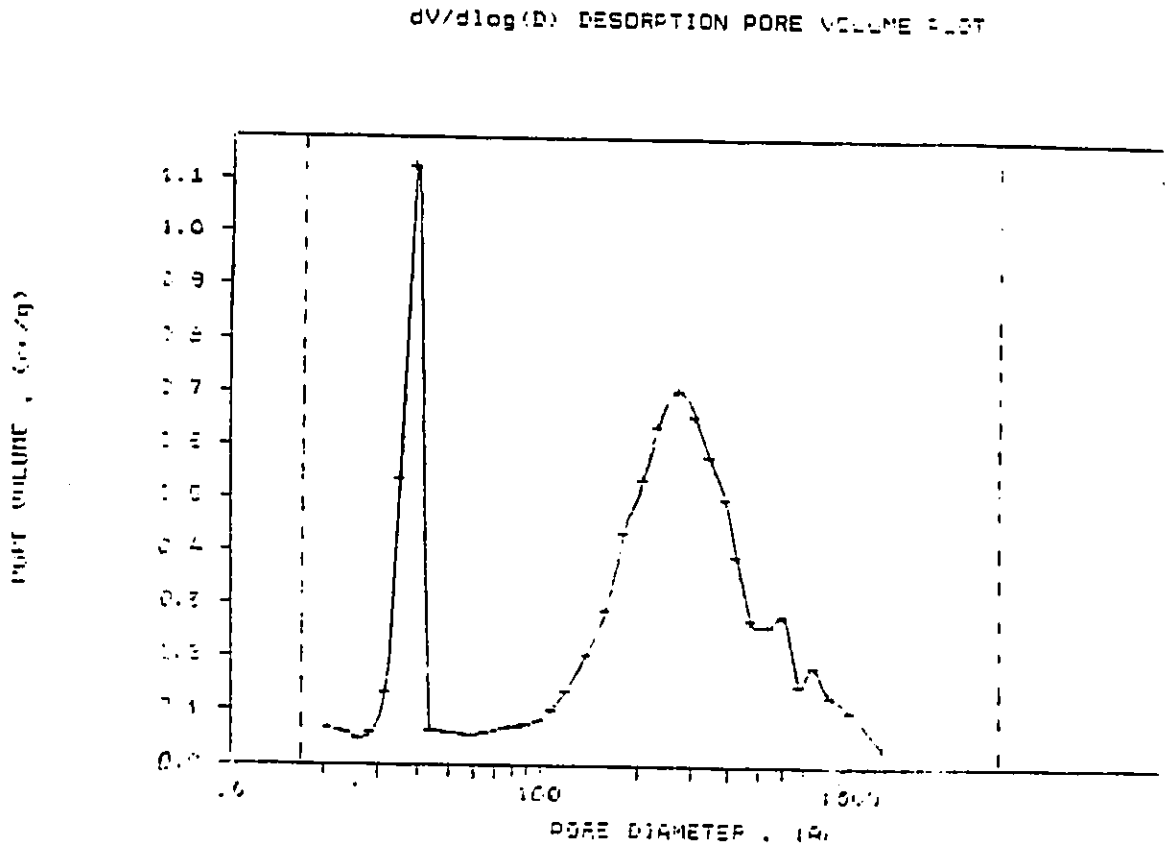

Fig A.1 Plot of the Pore Size Distribution dV/dlog(D) vs Pore Diameter(Å) for ZSM-5 (19.5)

A 1.2.6 GC MSD

The spectrum of aqueous products formed during the dehydration of aqueous ethanol was elucidated from GCMS analysis of the aqueous product fraction, using a HP 5890 GC equipped with a 50 m PONA column coupled to a HP 5970 Mass Spectrometry Detector.

A 1.2.7 ZSM-5 SYNTHESIS

ZSM-5 zeolite of Si/Al ratio 19.5 was synthesized according to the method of Argauer and Landolt (52). Silica gel, dried at 120°C overnight, was added to an aqueous solution of tetrapropylammonium bromide in sodium hydroxide and this slurry mixture was stirred rapidly for 1 hr at 80°C. An aqueous solution of sodium aluminate was then added and this mixture was maintained at 80°C for a further 15 mins with stirring. The contents were then placed in an Hastelloy cylinder of volume capacity 400 ml and this was placed in an autoclave and sealed and heated to 175-180°C under autogenous pressure (approximately 8 atmospheres) and maintained at these conditions for 10 days, after which the autoclave was allowed to cool to room temperature. The solid was washed several times on a filter with deionized water and then dried at 120°C for 12 hours and then calcined in air at 550°C for 12 hours. Table A.1 shows the relative quantities of each component used in the preparation.

Table A.1

The relative amounts of materials for synthesis of ZSM-5 (20)

	Silica Gel	TPBr	Na_2AlO_4	NaOH	Water
Mass(g)	110	110	13.5	7.02	400 ml

APPENDIX 2

A 2.0 INTRODUCTION : ALUMINATION

Catalytic properties arising from acidity of zeolites are strongly dependent on their aluminum content as already discussed in Chapter 1, Section 1.4.8, and it therefore highly desirable to try to increase their aluminum content while retaining the topology and crystallinity of the parent structure.

Several methods have been developed to try to introduce aluminum into zeolite frameworks but the success of tetrahedral insertion has been limited. Pioneer work by Breck (62) and Skeels and Breck (69) more than 15 years ago laid the foundation for a number of subsequent findings. While the "aluminum content" of zeolites can be reduced by heat treatment of their ammonium exchanged forms by ultrastabilization, by acid washing and by using a number of reagents such as ethylene diamine tetraacetic acid, chlorine gas, phosgene or acetylacetone, it has been extremely difficult to increase the aluminum content postsynthetically.

Only when extremely harsh conditions were utilized for alumination was it possible to obtain some indications from ^{27}Al MAS NMR and IR spectroscopy (44) that post synthetic incorporation of aluminum into ZSM-5 may have occurred. Whether aluminum is inserted into tetrahedral or octahedral positions has not been clearly determined. Introducing aluminum or other species into the vacancies of ZSM-5 created by silica removal provides a viable route for

enhancing the acidity since there is an enhanced probability of isomorphous incorporation of aluminum into the zeolite. The use of aluminum halide vapor at high temperature has resulted in the isomorphous substitution of aluminum for silicon into highly siliceous zeolite ZSM-5 (silicalite). However some reports have shown that the substitution has been directed to octahedral intrazeolitic positions associated with Lewis acid activity (65). Presumably Al can be substituted for Si also in the framework sites of high silica zeolites by direct incorporation in the framework using aluminum halide vapors followed by hydrolysis and calcination, since this process has resulted in increase in catalytic activity (66). It has also been reported that not only Bronsted acid sites but Lewis acid sites are generated by such an alumination of highly siliceous zeolites.

On the other hand Yamagashi et al. (67) have proposed that alumination proceeds not through the substitution of silicon, but through the insertion of four coordinate (framework) aluminum into lattice imperfections (defect sites) of the zeolite, and by the introduction of aluminum into non-framework sites as six coordinate species through the reaction of silanol (SiOH) groups on the external surface and/or the non intact Si-O-Si bonds formed from the SiOH groups on the external surface. The authors have discussed mechanisms supporting these processes which effectively discounted alumination by substitution of silicon atoms. Chang et al. have also proposed such a mechanism consistent with alumination by insertion of aluminum into zeolite

frameworks in tetrahedral coordination and chemical reaction with silanol groups, but they maintain that silicon substitution is also possible especially for low silica zeolites treated with aluminum fluoride (68).

A 2.1 INCORPORATION OF ALUMINUM INTO NaDZ

Several methods based on literature procedures were developed for aluminum insertion into the desilicated zeolites. The sample of desilicated zeolite dried at 120°C, was placed in a round bottomed flask containing solutions of varying concentrations of each aluminum compound used, (1g zeolite/10 ml solution). The contents of the flask were swirled at a constant rate (10 rpm) under a mild vacuum at a temperature of 60-65°C for approximately six hours, after which the vacuum was increased and the solution evaporated to dryness. The conditions employed were never as harsh as those used in literature primarily because it was anticipated that the voids created by desilication of the parent zeolite would favor the insertion of tetrahedrally coordinated aluminum and this process would be more exothermic due to the available "unhealed siloxane" functionalities of the desilicated zeolite. The aluminium impregnated desilicated zeolite (AlDZn) was then dried at 120°C overnight. n refers to the various alumination procedures using different compounds.

A 2.1.1 AlDZ1 (AlDZAFA) : Alumination using Ammonium hexafluoro aluminate (AFA) treatment.

Of the solutions of Aluminum compounds studied, AFA was highly insoluble in water (<0.3g AFA/100 ml water; pH 3.5). A solution of 2.2 g of desilicated zeolite was placed in 44 ml of AFA solution, the mixture having a pH 6.0, and treated as outlined above for impregnation of aluminum. This sample (AlDZ1) was calcined at 450°C and washed to remove any residual AFA from the pores of the desilicated zeolite. The pH of the treatment solution was also adjusted to 10.5 using 0.05 M ammonium hydroxide solution and the treatment repeated at higher pH. Atomic absorption analysis and FTIR were performed on both of these samples.

A 2.1.2 HAlDZ2 :

Alumination using Aluminum Chloride ($AlCl_3.6H_2O$)

(i) Initially solutions of 0.01, 0.02 and 0.03 M $AlCl_3$ (1g zeolite/10 ml solution) were used to determine the optimum amount of aluminum that could be loaded onto the desilicated sample according to the number of vacancies created by desilication. Each silicon removed leaves one void which can potentially coordinate as a tetrahedral Aluminum site. The aluminum chloride treated sample is referred to as AlDZ2.

In an attempt to emulate the strongly alkaline conditions used for the hydrothermal synthesis of ZSM-5 zeolite, during which aluminum and silicon

combine in a tetrahedral framework characteristic of the zeolite, 1.5g of AlDZ2 was treated with a mildly aqueous alkaline solution of sodium hydroxide at 100°C (1g/10 or 20 ml solution) under reflux conditions with occasional stirring. These conditions were maintained for 2 hours after which the hot suspension was filtered. The residue on the filter was washed several times with distilled water until the wash water was neutral to alkacid paper. The treatments were repeated three times using varying concentrations of NaOH (0.02 and 0.04 and 0.08 M). The sample treated with the highest concentration of base suffered a dramatic loss [49.6%] in crystallinity as a result of structural decomposition, and no further testing was carried out on this sample. The solid product was dried at 120°C for at least 12 hours and is hereafter referred to as AlDZ2H1 and AlDZ2H2 corresponding to samples treated with 0.02 and 0.04 M NaOH respectively. A sample of AlDZ2 was calcined at 450°C and referred to as AlDZ2C. FTIR Characterization data for these preparations is reported in Table A 2.3.

The acidic form of AlDZ2 was prepared as described before using a 5 wt % solution of ammonium chloride and this sample is referred to as HAlDZ2. Table A 2.1 reports the characterization data of the AFA and $AlCl_3$ treated desilicated samples.

(ii) Calcium ion exchange of aluminated desilicated ZSM-5

Each tetrahedrally coordinated aluminum represents a proton

exchangeable acidic site which will also ion exchange with alkali metal atoms in solution such as calcium. A 5 wt % solution of calcium chloride was used to exchange at the tetrahedrally coordinated aluminum sites. Each Calcium could exchange for 2 positive charges and serve to neutralize two AlO_4^- tetrahedra.

A 2.1.3 HAlDZ3 : $AlBr_3$

The wet impregnation with $AlBr_3$ was carried out in a manner similar to that used before except for the following modifications. A 0.02 M ethanolic basic solution (95 % ethanol) of aluminum bromide (75) was used for the optimum concentration as determined previously with $AlCl_3$. The treatment was repeated and the sample evacuated to dryness and then later dried at 120° C overnight. The aluminum treated sample was then activated in a horizontal fixed bed reactor in which an inert atmosphere was maintained by flowing nitrogen at a low flow rate of 12 ml/min. The sample was heated to 120°C and then to 230-235°C and this temperature was maintained for 1.5 hours during which time the vapor deposition of aluminum bromide was assumed to occur. Finally the sample was heated to 350°C and maintained at this temperature for 2 hrs. This sample was ion exchanged with 5 wt % ammonium chloride solution as described before, filtered, washed until the washing water was neutral, dried at 120°C and activated at 400°C to produce HAlDZ3.

A 2.1.4 AlDZ4 :

An ammonium form of DZ (NH_4DZ) was prepared by a similar ion exchange technique with 5 wt % ammonium chloride but dried at 120 °C overnight. Samples of NH_4DZ zeolite were then treated in the manner of AlDZ2 using 0.02 M aluminum bromide for two successive treatments on the rotor vaporization apparatus, forming $AlNH_4DZ$, which was then activated under inert conditions. The final form HAlDZ4 was obtained by activation at 400°C overnight in a stream of flowing air.

A 2.1.5 HAlDZ5

6.0 g of desilicated NaDZ were added to a solution of 76.8 g of tetrapropyl ammonium hydroxide (10% in water). 0.4 g of sodium bromide and 4.1 g of $Al_2(SO_4)_3$ were dissolved in 150 ml of water and this suspension heated up to 60°C and gently stirred for 1 hour. This slightly alkaline suspension was loaded into a teflon bottle and heated at 95°C for 7 days. The suspension was unloaded and filtered and the solid was washed on the filter with distilled water. After drying at 120°C, the solid obtained was calcined at 550°C overnight (weight = 5.2g). The acidic form was obtained by ion exchange with a 10 wt. % aqueous solution of NH_4Cl, drying at 120°C and activation at 550°C.

A 2.1.6 HAlZ6

7.0 g of NaZ was added to a solution formed with 32 g of tetrapropyl ammonium hydroxide (1.0 M solution in water). 2.0g of $Al_2(SO_4)_3$ and 0.4 g NaBr were dissolved in 170 ml of water and the suspension heated as for HAlDZ5. The same synthesis conditions were also used and the weight of solution activated was 6.0 g. The acidic form of this sample was made as before.

A 2.1.7 HAlDZ7

The same procedure as for the preparation of HAlDZ6 was done using 6.2 g of NaDZ in 1.5 g NaBr, 2.3 g of $Al_2(SO_4)_3$ and 22.5 g of tetrapropyl ammonium hydroxide (1.0 M) dissolved in 200 ml of water. The suspension was heated as before and the weight of solid obtained after activation at 550°C was 6.1 g.

The catalysts HAlDZ2, HAlDZ2H2, HAlDZ3, HAlDZ4, HAlDZ5, HAlZ6 and HAlDZ7 were characterized by atomic absorption, X-ray diffraction, BET nitrogen and argon for pore size distribution and surface area. These data are reported in Tables A 2.1 and 2.2. An FTIR spectrum was obtained for each of these samples to check for changes in the coordination of aluminum. The asymmetric and symmetric stretching frequencies corresponding to the TO bonds (for which downward shifts are accepted as evidence of an increase in

framework aluminum) are reported in Table A 2.3.

Each of these catalysts were further characterized by catalytic activity and selectivity testing in the dehydration of ethanol to ethylene reaction in a fixed bed reactor as described in Chapter 4. Since this reaction is sensitive to medium strength Bronsted acid sites, it gives a good estimate of the content of the amount of tetrahedrally coordinated aluminum atoms arising from alumination subsequent to desilication of the ZSM-5 zeolite. Table A 2.4 reports the data for their catalytic activity and selectivity for ethylene and DEE.

A 2.2 RESULTS AND DISCUSSION

Based on the calcium tests, the desilicated sample treated with 0.02 M aluminum chloride appeared to have the highest concentration of tetrahedrally coordinated aluminum of the three concentrations tested for tetrahedral incorporation of aluminum. This concentration was therefore chosen as the optimum. Similar treatment of the parent zeolite NaZ with a 0.02 M solution of aluminum chloride also showed some increase in the amount of tetrahedrally coordinated aluminum, although Si/Al ratio of this material was higher than that which was desired. The ALDZAFA samples were rejected since based on atomic absorption and FTIR, there did not appear to any significant insertion of framework or other type of Aluminum (Table A 2.1 and 2.3).

As already observed, there is an increase in the size of the mesopores

present in the desilicated ZSM-5 zeolite, which arises from the removal of silicon. This increase in size results in an increase in the volume of nitrogen adsorbed (Table A 2.2). The decrease in the volume of nitrogen adsorbed for HAlDZ2 and HAlDZ4 indicates that the voids are filled by species large enough to be aluminum clusters which may be catalytically active (eg as the classical Lewis acids sites which function as Friedel Crafts catalysts : $AlCl_3$ or $AlBr_3$). FTIR data on these two catalysts did not suggest any framework insertion of aluminum however since there was no significant shift in the asymmetric of symmetric stretching frequencies associates with Si-O of Al-O (resolution ± 2.0 cm^{-1}).

The AlDZ2 samples which were treated with basic solutions under hydrothermal conditions displayed some shift from those of the DZ sample indicating some possible changes in the framework structure of the material. Catalytic testing of this material did not show any improvement in the total conversion but an increase in the selectivity for ethylene was observed compared to the desilicated zeolite.

There was an improvement in the nitrogen adsorption for HAlDZ3 indicating that pores were enlarged. There were some promising shifts in the main stretching frequencies for HAlDZ5, HAlZ6 and HAlDZ7 (FTIR data reported in Table A 2.3).

ACTIVITY STUDIES OF VARIOUS CATALYSTS

Table A 2.4 shows the catalytic activity data of all the catalysts tested at 225°C using absolute ethanol at WHSV of 8.2 hr^{-1}. As discussed, HDZ gave the highest conversion since it has the highest number of Bronsted acid sites per unit surface area, although its selectivity for ethylene was lower than that of the parent HZ. The catalysts for which alumination of DZ was attempted all displayed conversions lower than that of HDZ, and some even lower than that of HZ. The lower catalytic activity probably resulted from the presence of clusters of amorphous aluminum compounds (such as $AlCl_3$, $AlBr_3$, $al(OH)_3$ or Al_2O_3 generated during activation) lowering its catalytic activity per gram of catalyst.

Although these compounds are Lewis acids they have significantly lower acidity than the Bronsted acid sites. In addition the presence of such amorphous compounds in the aluminated NaZ and DZ contributes to pore blockage and restricted diffusion of reactant towards the catalytic sites. This problem is compounded by the fact that the voids created by desilication were too large for incorporation of tetrahedral aluminum but were ideal loci for the accommodation of aluminum cluster compounds.

Table A 2.1 Chemical compositions of parent, desilicated and aluminated zeolites

Sample Treat. (conditions)	$\%Na_2O$	$\%Al_2O_3$	%CaO	$\%SiO_2$	Si/Al
NaZ	1.5	4.1	-	94.4	19.5
DZ	3.9	5.8	-	90.3	13.2
AlDZ (AFA)	2.3	4.7	-	93.0	16.8
DZ[1](Al-0.01)	3.5	5.7	-	90.8	13.5
DZ[1](Al-0.02)	3.5	6.5	-	90.0	11.7
DZ[1](Al-0.034)	3.5	7.0	-	89.5	10.8
DZ[12](Al-0.01/Ca)	0.9	5.8	3.6	89.7	13.1
DZ[12](Al-0.02/Ca)	0.8	6.1	3.7	89.4	12.4
DZ[12](Al-0.034/Ca)	0.9	7.2	2.9	89.0	10.5
NaZ[1](Al-0.02)	1.9	4.8	-	93.3	16.5
NaZ[12](Al-0.02/Ca)	1.0	4.8	4.6	89.6	16.0

[1] refers to the concentration the solution of aluminum chloride used for treatment by alumination : [2] refers to the treatment of the solid with an aqueous solution of calcium chloride for 48 hours at room temperature for ion exchange

Table A 2.2 Physico characterization data for Catalysts studied

Sample	$\%Na_2O$	Si/Al	% DC	SA (m^2/g)	vol N_2 adsorbed meso	micro
HZ	0.3	20.3	100	373	.2412	.1035
HDZ	0.4	13.6	87	405	.4025	.1031
HAlDZ2	0.5	10.3	92	376	.3707	.0991
HAlDZ2H2	0.6	14.2	87	369	.3550	.1021
HAlDZ3	0.3	8.5	86	382	.6559	.0956
HAlDZ4	0.6	13.0	91	402	.3920	.1044
HAlDZ5	0.6	4.8	68	394	.5331	.0889
HAlZ6	0.3	16.1	95	328	.2081	.0921
HAlDZ7	0.4	14.0	81	378	.4734	.0898

Table A 2.3 Frequency shifts for the main FTIR stretching bands of the T-O bonds recorded for the samples prepared

Sample	ν_{asym}/cm^{-1}	$\Delta\nu/cm^{-1}$	ν_{sym}/cm^{-1}	$\Delta\nu cm^{-1}$
NaZ	1102		796	
DZ	1095	7	792	4
AlDZ1	1100	2	794	2
AlDZ2	1095	7	792	4
AlDZ2H1	1094	8	791	5
AlDZ2H2	1093	9	791	5
AlDZ2C	1089	13	792	4
AlDZ3	1093	9	793	3
AlDZ4	1098	4	796	0
AlDZ5	1093	9	792	4
AlZ6	1092	10	791	5
AlDZ7	1089	13	791	5

Table A 2.3 Catalytic Activity and Selectivity of catalysts prepared.

Temperature = 225°C WHSV = 8.2 hr^{-1} Ethanol concentration = 100 % Contact time, T = 0.12 hr

Catalyst	% Total Conversion	Product Selectivity (%)			
		Ethylene	DEE	MeOH	C3-C9^{+}
HZ	79.6	87.15	9.01	0.09	3.75
HDZ	89.7	84.43	15.05	0.03	0.49
HAlDZ2	73.7	49.87	49.99	0.00	0.14
HAlDZ2H1	80.6	90.41	7.91	0.0	1.68
HAlDZ3	78.5	54.11	45.83	0.00	0.06
HAlDZ4	74.1	80.79	18.51	0.00	0.70
HAlDZ5	81.3	67.58	32.29	0.00	0.13
HAlZ6	74.3	36.99	62.96	0.00	0.05
HALDZ7	83.9	86.79	12.74	0.00	0.47

A 2.3 CONCLUSIONS

Presumably, alumination did not occur into tetrahedral positions, which probably agrees with Lowenstein's rule for synthesis of ZSM-5 zeolites whereby two aluminum atoms cannot be nearby in the zeolite framework (13:b,30). The removal of silicon from NaZ results in the creation of voids, resulting in a situation where aluminum ions exert interactions with each other since they are effectively nearer to each other in the DZ framework compared to NaZ. Thus the possibility of aluminum becoming "incorporated" into the framework is lowered.

APPENDIX 3

A 3.0 Program in GWBASIC for calculation of Total % conversion and Product selectivity in C atom %.

```
100 DIM NO$(18),NA$(7),NG$(15)
110 DIM CO(18),CA(7),CG(15)
120 DIM RO(18),RA(7),RG(15)
130 DIM T(18)
140 REM         CORRECTION FACTORS FOR AQUEOUS PHASE
150 DATA DME,.793,MeOH,1.00,DDD,.993,C5-C9alip,.793,BTX,.749,
155 DATA C9+arom,.795,EtOH,.968
160 REM         CORRECTION FACTORS FOR GASEOUS PHASE
170 DATA Methane,1.413,Ethylene,1.534,Ethane,1.481,Propylene,1.482
180 DATA Propane,1.397,iso-Butane,1.252,1-But+iso-but,1.427
185 REM         CORRECTION FACTORS FOR GASEOUS PHASE
190 DATA 1.3-butadiene,1.41,n-butane,1.485,t-2 butene,1.475
200 DATA c-2 butene,1.541,C5+,1.096,benzene,1.090,DEE,1.025,DMB,1.00
210 REM
220 FOR I=1 TO 7
230   READ NA$(I),CA(I)
240 NEXT I
250 FOR I=1 TO 15
260   READ NG$(I),CG(I)
270 NEXT I
280 REM
290 REM Enter experimentals data (area or area%)
300 REM
310 INPUT "catalyst :";C$
320 INPUT "run # : ";R1$
330 INPUT "date performed :";D$
340 INPUT "n2 flow(ml/min) :";F$
350 INPUT "temp. cat. (C.): ";T1$
360 INPUT "ETOH injected (g.)";P
370 INPUT " Enter % of Ethanol : ";ETO
380 INPUT "WHSV (h-1) ";V
400 PRINT
750 REM
760 LPRINT "Catalyst :";C$,"Run # :";R1$,"Date :";D$
770 LPRINT "N2 flow(cc/min):";F$,"Temp. cat.(C.):";T1$
780 LPRINT "WEIGHT OF ETOH SOL. INJ.: ";P;" g."
790 LPRINT "WHSV (h-1) : ";V,
800 LPRINT "ETOH % :" : ETO
```

```
920 LPRINT
965 ETO = ETO / 100
970 LPRINT "AQUEOUS PHASE"
980 INPUT "wt. aq. phase (g.)";Y
990 LPRINT "wt. aq. phase :";Y;" g."
1000 INPUT "VOLUME OF AQUEOUS PHASE(ML)";V
1020 INPUT "conc. std. etoh (C./ml)";U
1030 LPRINT "conc. std etoh :";U;" C./ml."
1040 INPUT "area std. etoh ";Z
1050 LPRINT "area std. etoh :";Z
1060 INPUT  "AREA OF ETOH PEAK IN AQ. PHASE ";AQET
1070 LPRINT "area of etoh peak in aq. phase :";AQET
1072 LPRINT
1073 PRINT
1075 PRINT "enter the area (not area %)"
1076 PRINT
1080 FOR I=1 TO 6
1090   PRINT NA$(I);
1100   INPUT RA(I)
1110   T(I) =RA(I)*CA(I)
1120 NEXT I
1130 PRINT
1140 PRINT
1150 FOR I=1 TO 6
1160   PRINT NA$(I),RA(I)
1170 NEXT I
1175 LPRINT "TOTAL C ATOMS IN LIQUID PRODUCTS"
1180 INPUT "area ok (y or n) ";A$
1190 IF A$ = "n" THEN GOTO 1075
1200 LPRINT "COMPOUND","AREA","No. of C atoms"
1220 FOR I=1 TO 6
1230   T(I)=((T(I)*U)/Z)*V
1240   LPRINT NA$(I),RA(I),T(I)
1250   RA(I)=T(I)
1260 NEXT I
1261 SA=0
1262 FOR I=1 TO 6
1263   SA = SA + T(I)
1264 NEXT I
1360 LPRINT "TOTAL C. ATOMS IN AQ. PHASE";SA
1410 PRINT
1420 LPRINT
1430 PRINT "Gas Phase"
1440 PRINT "Enter average area %"
1460 FOR I=1 TO 15
1470   PRINT NG$(I);
1480   INPUT RG(I)
1490   T(I) = RG(I) * CG(I)
1510 NEXT I
1520 PRINT
1560 PRINT "area % ok ( y or n )";
1570 INPUT A$
1580 IF A$ = "n" THEN GOTO 1420
```

```
1620 PRINT
1630 LPRINT "GAS PHASE"
1635 LPRINT "COMPOUND","AREA %","CORRECTION","C. ATOM"
1640 V1=21.5
1650 D=4.518E-05
1680 D=D/V1
1690 INPUT "run time :";T1
1730 INPUT "enter average flow rate (in ml/min) :";V3
1740 FOR I=1 TO 14
1750 T = T1 * V3
1760    T(I) = T * D * T(I) / RG(15)
1770 NEXT I
1790 LPRINT
1800 LPRINT "COMPOUND","AREA %","CORRECTION ","C. ATOM"
1805 S=0
1810 FOR I = 1 TO 14
1820   S = S + T(I)
1830 NEXT I
1840 FOR I=1 TO 14
1850   LPRINT NG$(I),RG(I),CG(I),T(I)
1860 NEXT I
1870 LPRINT NG$(15),RG(15)
1880 LPRINT "TOTAL C. ATOMS IN GASEOUS PHASE"; S
1930 M8=Y*ETO*AQET/(Z*23.035)
1935 LPRINT
2005 P=P*ETO/23.035
2010 LPRINT "% conversion total based on weight : ";((P-M8)/P)*100;'
2100 TOTAL = S + SA
2110 LPRINT "TOTAL C. ATOMS "; TOTAL
2120 LPRINT
2130 LPRINT "% PRODUCT SELECTIVITY"
2150 LPRINT
2160 FOR I=1 TO 14
2165   RG(I)=T(I)
2170 NEXT I
2175 DEE=RG(14)+RA(3)
2180 LPRINT "COMPOUNDS","%  PRODUCT SELECTIVITY"
2190 LPRINT NG$(2),RG(2)*100/(TOTAL)
2200 LPRINT NG$(4),RG(4)*100/(TOTAL)
2210 Z=RG(7)+RG(8)+RG(10)+RG(11)
2220 LPRINT "Butene",Z*100/(TOTAL)
2230 Z=RG(1)+RG(3)+RG(5)+RG(6)+RG(9)
2240 LPRINT "C1-C4(others)",Z*100/(TOTAL)
2260 LPRINT "C5-C9(alip)",RG(12)*100/(TOTAL)
2270 LPRINT NG$(13),RG(13)*100/(TOTAL)
2295 LPRINT "TOTAL "NG$(14),DEE*100/(TOTAL)
2296 LPRINT NA$(1),RA(1)*100/(TOTAL)
2297 LPRINT NA$(2),RA(2)*100/(TOTAL)
2299 LPRINT NA$(4)"AQ",RA(4)*100/(TOTAL)
2370 STOP
```